ENERGY-BASED MODELING OF DOWEL-TYPE CONNECTIONS IN WOOD-PLASTIC COMPOSITE HOLLOW SECTIONS

By

WILLIAM ROSSE PARSONS

A thesis submitted in partial fulfillment of
the requirements for the degree of

MASTER OF SCIENCE IN CIVIL ENGINEERING

WASHINGTON STATE UNIVERSITY
Department of Civil and Environmental Engineering

August 2001

To the Faculty of Washington State University:

The members of the Committee appointed to examine the thesis of WILLIAM ROSSE PARSONS find it satisfactory and recommend that it be accepted.

_____

Chair

_____

_____

_____

ACKNOWLEDGMENTS

First of all I would like to thank my advisor, Don Bender, for all his time, advise, and mentorship throughout my graduate work and the start of my engineering career. I would also like to thank the members of my committee, Mike Wolcott, Dave Pollock, and John Hermanson for providing their unique prospectives and devoting many hours to this project. I would also like to thank Office of Naval Research for providing the project funding.

I would also like to thank the entire staff of the Wood Materials and Engineering Laboratory; everyone at the lab had a part in helping me complete this project. I would especially like to thank Dave Dostal and Scott Lewis for their help extruding the wood-plastic composite material. Thanks also to Bob Duncan and Scott Lewis for helping with sample preparation, testing, and constantly moving my wobbly pallets of material. I would also like to thank all the WSU structural graduate students for their hours of consultation and entertainment. Specifically, Jeff Linville and Vikram Yadama for their tutelage on basic wood science concepts and Brian Tucker for his constant advise, snowboarding trips, golf outings, and late-night concerts. I would also like to thank Chris Brandt, Kristin Meyers, Casey McNeese, Melissa Verwest, and Sara Minier for being a constant source of distraction and great friends.

Finally, I would like to thank my parents, Roger and Rose Marie Parsons, for their moral and financial support. Dad, thanks for all the hours of working extra math problems that provided me with the math skills needed to conduct this research and be an engineer. Mom, thank you for all care packages and for always making sure we did not miss "the Sunday phone call." I would also like to thank my brothers, Brian and Ben. Brian, thank you for always providing me with an interesting story to tell and a little bit of home when I needed it. Ben, thank you for always keeping the phone calls short by talking as little as possible.

ENERGY-BASED MODELING OF DOWEL-TYPE CONNECTIONS

IN WOOD-PLASTIC COMPOSITE HOLLOW SECTIONS

Abstract

by William Rosse Parsons, M.S.
Washington State University
August 2001

Chair: Donald A. Bender

The goal of this research was to develop a rational method of designing dowel-type connections for hollow wood-plastic composite sections. Additionally, a method of predicting the load-displacement behavior of a connection with hollow members was developed for use in energy-based design and deformation calculations.

A yield model consisting of six controlling yield modes was found to govern the hollow section connection behavior. A model for predicting load-displacement behavior of connections with hollow members was derived for the six controlling modes of the hollow section yield model. The models were validated with double-shear unconstrained bolted connection tests using two wood-plastic composite formulations, three wall thicknesses, and three dowel diameters. Input parameters were also quantified through dowel bearing tests and bending yield strength tests. Dowel bearing tests were completed for each combination of WPC formulation, wall thickness, and dowel diameter. Significant variation in dowel bearing strength with dowel diameter and wall thickness was observed.

The hollow section yield model performed well when using a maximum load basis; the average percent difference between the theoretical maximum load and tested maximum load was 5.7%. The maximum connection loads were compared to the theoretical load calculated by entering the dowel bearing strength based on maximum load and a bending yield strength based on the stress in the dowel at the displacement of maximum connection load. Design for WPC hollow section connection maximum loads was based on maximum dowel bearing strength and the 5% diameter offset bending yield strength.

The load-displacement behavior model was validated by comparing the predicted and actual work done by the connections to a displacement of 0.11 inches. The Mode I_m work prediction was 4.7% less than the actual value. The Mode IV and Mode III_s equations under-predicted the actual work by an average of 7.6% and 13.2 %, respectively. All Mode III_s and Mode IV predicted curves were sensitive to the location parameters of the dowel rotation and dowel yielding.

TABLE OF CONTENTS

LIST OF TABLES

LIST OF FIGURES

CHAPTER 1: INTRODUCTION

In 1949, Johansen published the basis for the European Yield Model (EYM), which is the current yield model used for dowel-type connection design in wood structures in the U.S., Canada, and Europe. Since the development of the EYM, other methods of modeling bolted connections have been researched ranging from a beam on an elastic foundation model (Kuenzi, 1955) to three-dimensional finite element models (Patton-Mallory et al., 1998). These models either provide crude approximations of connection behavior (beam on elastic foundation models) or more accurate connection behavior but a process that may not be practical for design engineers (finite element models). The EYM represents a reasonable compromise between complexity and accuracy for use by design professionals.

Over the years, the EYM has gone through several revisions and interpretations; however, the basic concepts remain the same. Connection yield strength is based on the geometry of its components (dowel and members), the dowel bearing strength of the member material, and the bending yield strength of the dowel. Experimental research has shown the EYM to be sufficient for the design of timber connections (e.g. Wilkinson, 1978; Soltis and Wilkinson, 1987; McLain and Thangjitham, 1983; Aune and Patton-Mallory, 1986b). Balma (1999) validated the EYM for the design of wood-plastic composite (WPC) members with solid cross-sections.

In timber engineering, the majority of structural components have solid cross-sections. However, many WPC members are extruded in hollow cross-sections, and dowel-type connections may be used to fasten these members. While a majority of WPC products are used as decking, structural framing members will be used in the future and are currently being developed. Another example of hollow sections are structural insulated panels (SIPs) that

consist of a foam core sandwiched between two oriented strand board sheets. SIPs may be considered a hollow cross-section for lateral connection design if the bearing strength of the foam is ignored. The current dowel-type connection yield model (EYM) was developed for members with solid cross-sections. The EYM needs to be modified to accommodate hollow sections.

Objectives

The overall goal of this research was to develop rational design procedures for dowel connections using members consisting of wood-plastic composite hollow sections. This goal was achieved by meeting the following objectives:

- Develop a method to predict connection capacity for hollow sections using similar assumptions and derivation procedures as the existing EYM.
- Develop a method to predict the entire load-displacement curve for dowel-type connections in hollow WPC sections
- Validate the yield model and load-displacement model through laboratory testing of bolted connections over a range of WPC formulations, bolt diameters, and wall thicknesses.

CHAPTER 2: LITERATURE REVIEW

Connection Design Models

In 1949, Johansen published the basis for the yield model that is used today to design laterally loaded timber connections in North America and Europe. Over the years, this model has gone through several revisions and interpretations; however, the basic concepts remain the same. Connection yield strength is based on the geometry of its components (dowel and members), the dowel bearing strength of the member material, and the bending yield strength of the dowel. This model is commonly referred to as the European Yield Model (EYM). Experimental research has shown the EYM to be sufficient for the design of timber connections (e.g. Wilkinson, 1978; Soltis and Wilkinson, 1987; McLain and Thangjitham, 1983; Aune and Patton-Mallory, 1986b). Balma (1999) validated the EYM for the design of WPC members with solid cross-sections.

The 1991 National Design Specification for Wood Construction (NDS) was the first NDS edition to include the EYM. Prior to 1991, connection design methods were empirically based. The EYM equation solutions are now arranged in design tables that allow engineers to quickly design common connection configurations. ASTM D5456-98a Annex A2 discusses determination of the design strength of a structural composite lumber connection using the NDS tables. The method described is commonly referred to as the *equivalent specific gravity* (ESG) method. The equivalent specific gravity method uses the original EYM equations to compute connection strength. Dowel bearing tests are used to compute an equivalent specific gravity. The equivalent specific gravity is then used to design the connection as if it were made of the common material that it most closely resembles. The ESG method is a simplified procedure that enables designers to easily design structural composites using the NDS tables. Johnson and

Woeste (1999) demonstrated several examples that apply this concept to design problems. Bilunas (2000) used a similar procedure to design screw connections in structural insulated panels. The ESG method still relies on a yield model based on solid cross-sections, and does not apply to connecting members with hollow cross-sections.

Several papers have outlined the derivation procedures for the development of the EYM. The American Forest and Paper Association (1999) published Technical Report 12 (TR12) which discusses the static equilibrium-based derivation of the EYM equations. An energy-based derivation of the EYM was developed by Aune and Patton-Mallory (1986a) using the method of virtual displacement to develop connection yield equations. Peyer (1995) expanded the model to include a gap between members at the shear plane. The equations derived produce the same yield load as the equations derived by the static equilibrium-based approach in TR12.

Other methods have also been used to model connection behavior. In an early model, a dowel was modeled as a beam on a finite elastic foundation (Kuenzi, 1955). Wilkinson (1971 and 1972) further refined the modeling equations found by Kuenzi. Wilkinson's simplifications enabled the beam on elastic foundation concepts to be used by design engineers. However, the connection yield point was still defined empirically. The proportional limit slip of a connection was determined through testing to occur at approximately 0.011 inches (Wilkinson, 1971). However, the load-displacement behavior for most timber connections is nonlinear. Therefore, the beam on elastic foundation equations are only useful for predicting the initial stiffness of a connection (Foschi, 1974).

Three-dimensional finite element models have also been used to model connection behavior (Patton-Mallory et al., 1998). After the finite element model was verified, a maximum stress failure criterion was used to investigate the distribution of critical stress along the dowel in

a connection (Patton-Mallory et al., 1998). However, this type of analysis has not been applied to connection design.

Load-Displacement Behavior Modeling

The load-displacement behavior of a connection is important because connection rigidity may contribute significantly to the overall deformation of the structure (Foschi and Bonac, 1977). Researchers have used an empirical model to describe load-displacement behavior in nailed connections (Pellicane et al., 1991; Sá Ribeiro and Pellicane, 1992). Foschi and Bonac (1977) used a finite element approximation of the load displacement behavior of nailed connections with limited success. Aune and Patton-Mallory (1986a) and Peyer (1995)used the general form of the virtual displacement method equation and a fourth-root curve to predict the load displacement behavior of nailed connections.

Dowel Bearing Testing

Dowel bearing strengths of most timber species used in construction have been established (Wilkinson, 1991; AF&PA, 1997). Dowel bearing test procedures are outlined in ASTM D5764-97. Balma (1999) found a significant rate of load effect when conducting dowel bearing tests on two formulations of WPCs made from low- and high-density polyethylenes. Presently, no modifications to ASTM D5764-97 have been made for wood-plastic composites. Therefore, it was important to take special care to ensure that the testing procedures used in this research recognize the load rate effect found in WPC.

Several studies have shown that dowel bearing strength is dependent on dowel diameter. Research by Wilkinson (1991) has shown for bolts that in solid cross-sections of timber members the dowel diameter affects the dowel bearing strength in perpendicular to the grain loading.

Balma (1999) found that in two WPC formulations orientation with respect to the extruded direction did not significantly affect dowel bearing strength using 0.5-inch diameter bolts.

Defining Yield

In North America, the standard technique for defining the yield point of connection tests, dowel bearing tests, and bending yield strength is the 5% diameter offset method (ASTM D1575, ASTM D5764, and ASTM D5652). A line is fit to the initial linear region of the load-displacement curve of a test. The line is then offset by 5% of the dowel diameter in the positive displacement direction. The yield point is defined as the intersection of the offset line and the load-displacement curve. In some WPC formulations and nailed timber connections, the 5% offset method become cumbersome because there is no definite initial linear region (Balma, 1999; Theilen et al., 1998). When common methods of defining yield prove ineffective, Balma (1999) worked from a basis of maximum load when comparing WPC connection tests with EYM predicted loads.

CHAPTER 3: MODEL DEVELOPMENT

Several design methodologies were investigated. Two models were derived for members with hollow sections. One model predicts the yield point, and is formulated for the allowable stress design of laterally loaded connections with hollow members. The other model predicts the entire load-displacement behavior of laterally loaded connections with hollow members, and will be useful for energy-based design approaches and structural deformation calculations.

Equivalent Specific Gravity

The equivalent specific gravity (ESG) method is a simplified procedure that enables designers to easily design connections in structural composites using the NDS tables. The first step of the ESG method is to conduct several dowel bearing tests on a structural composite. Next, the average dowel bearing strength is computed. Then, the equivalent specific gravity is found using the appropriate formula. For bolts, the following equations are used for parallel-to-grain loading and perpendicular-to-grain loading respectively:

$$ESG_{\parallel} = \frac{F_{e\parallel}}{11200} \qquad \text{Equation 3-1}$$

$$ESG_{\perp} = \left(\frac{F_{e\perp}\sqrt{D}}{6100} \right)^{0.6897} \qquad \text{Equation 3-2}$$

Next, the NDS dowel bearing strength tables are consulted (e.g. NDS Table 8A for bolted connections). A timber species grouping is found that has a specific gravity less than or equal to the equivalent specific gravity of the structural composite. Connections are then designed assuming that the structural composite has the same dowel bearing strength as the assumed timber species grouping. Because of the hollow geometries of the cross-sections used in this research, the NDS tables were not directly applicable. Therefore, an equivalent specific gravity was *not* found. Instead, the EYM equations were evaluated using the average dowel bearing

strength. By evaluating the equations instead of using the NDS tables, the yield mode was also identified.

EYM-Based Yield Model for Allowable Stress Design

In connections with members with a solid cross-section, the dowel is supported continuously throughout the connection. In a connection with hollow members, the dowel is supported only at the walls which limits the potential locations of dowel rotation and dowel yielding; thus, the number of possible yield modes is increased. In this research, only hollow sections with two walls will be investigated.

Prior to deriving a yield model for hollow sections, the current design model for timber connections, the European Yield Model (EYM), derivation was examined. Two previous modeling approaches were investigated: a static equilibrium-based approach in AF&PA (1999) and an energy-based approach in Aune and Patton-Mallory (1986a). Both papers only included partial derivations. Therefore, the EYM was rederived using the guidelines set forth by the previous work. The complete derivation of the EYM using the static equilibrium-based approach is given in APPENDIX A. The energy-based derivation of the EYM is given in APPENDIX B. Although the two derivations are similar, the energy-based approach is more straightforward and enables the derivation of entire load-displacement curves. Therefore, an energy-based derivation method was chosen to derive the hollow section yield model.

Several simplifying assumptions were deemed necessary for hollow sections. First, members are assumed to have two walls with equal wall thickness and dowel bearing strength (Figure 3-1). The side member and main member can have different wall thicknesses and dowel bearing strengths, but the wall properties are constant within members. Also, identically to the EYM, double shear connections must be symmetric (identical side members).

End fixity of the dowel, tension forces in the dowel, and friction between members are conservatively ignored. Dowel loading is assumed to be uniformly distributed and perpendicular to the axis of the dowel. All materials are assumed to exhibit perfect elastic/plastic behavior.

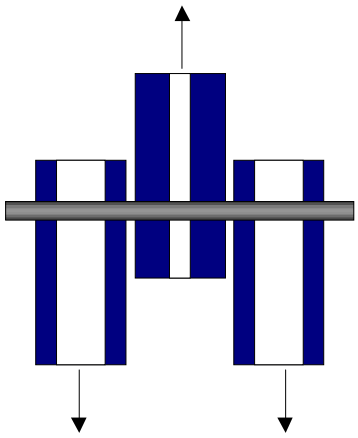

Figure 3-1: Double shear connection. Side member and main member have different wall thicknesses. However, the walls are uniform within the individual members.

Like the EYM, the input parameters into the hollow section yield model are size of the connection components, dowel bearing strength of the members, and the bending yield strength of the dowel. For the derivation of equations, the dowel bearing strength is converted to dowel bearing resistance (a line load) by multiplying by the dowel diameter and the bending yield strength is converted to the moment resistance of the dowel (a moment) by multiplying by the plastic section modulus.

The energy-based derivation procedures use the virtual displacement method. External work and internal work are set equal to each other as a connection undergoes a unit deformation. The general equation for this energy balance is Equation 3-3.

$$W = F \cdot 1 = \int f_e \cdot \eta \cdot d\xi + \sum \left(M_y \theta \right) \qquad \text{Equation 3-3}$$

where :

$F = yield\ load, lb$

$F_e = dowel\ bearing\ strength,\ psi$

$F_{yb} = bending\ yield\ strength\ of\ dowel,\ psi$

$D = dowel\ diameter, in$

$f_e = F_e D = dowel\ bearing\ resistance, lb/in$

$M_y = F_{yb}\left(\frac{D^3}{6}\right) = moment\ resistance\ of\ the\ dowel, lb-in$

$\theta = angle\ of\ rotation\ of\ the\ dowel$

$\eta, \xi = integration\ variables\ for\ the\ area\ crushed\ by\ the\ dowel$

The general equation can be simplified to Equation 3-4.

$$F = \sum\left(f_e \cdot A\right) + \sum\left(\frac{M_y}{a}\right) \qquad \text{Equation 3-4}$$

where :

$A = area\ of\ material\ crushed, in^2$

$a = distance\ from\ the\ point\ of\ dowel\ rotation\ or\ dowel\ yielding\ in\ the\ side\ member\ (x_s)$
$to\ the\ point\ of\ dowel\ rotation\ or\ dowel\ yielding\ in\ the\ main\ member\ (x_m)$
$= x_s + x_m = \frac{1}{\tan\theta} = \frac{1}{\theta} \quad (small\ rotation\ assumed)$

The simplified equation is now evaluated in the following manner to determine the yield equations for the hollow section model:

1. The dowel and member in a single-shear connection after undergoing the unit displacement are drawn (Figure 3-2). Note: the dimensions defined in Figure 3-2 apply to every yield mode. Wall thickness is defined as *t* and the void width is defined as *v*. The subscript identifies if the variable corresponds to a dimension in the main or side member.

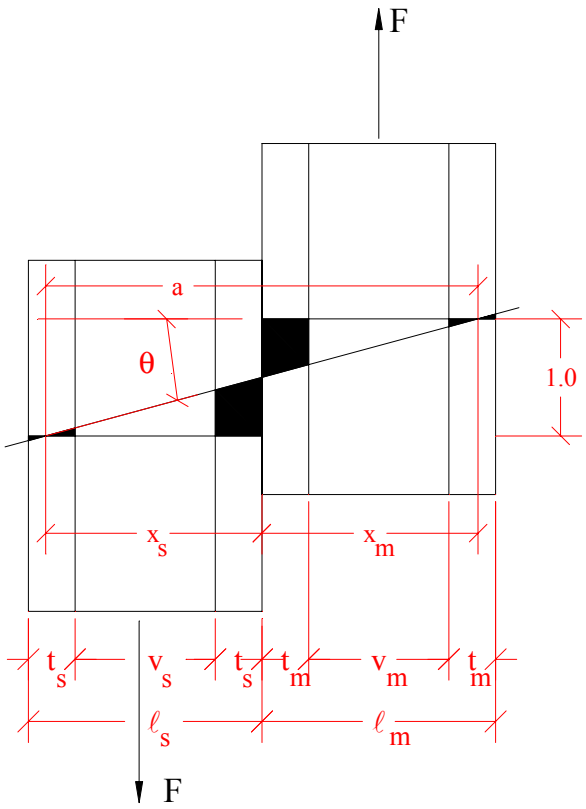

Figure 3-2: Diagram used to develop Mode II - Case 3-3 equation
by the virtual displacement method.

The EYM assumes six yield modes in this step. For the hollow section model, the same six yield modes were assumed. Two of the yield modes involve crushing of the entire main or side member so the equations are the same as the EYM equations. However, due to the void space in a hollow section, in Modes II, III_s, III_m, and IV there are several locations where dowel rotation or dowel yielding can occur in each member. Each scenario is given a different case name. Case 1 is when the dowel rotation or yielding occurs in the wall adjacent to the shear plane. Case 2 is when the dowel rotation or yielding occurs in the void space. Note, Case 2 cannot occur unless the void has negligible dowel bearing strength. Case 3 is when the dowel rotation or yielding occurs in the wall farthest from the shear plane. The combinations result in eighteen possible yield modes (Figure 3-3). The subscript on the yield mode number describes which member is being crushed – *s* for side member and *m* for

main member. For example, the yield mode where the dowel rotation occurs in the wall farthest from the shear plane in the side member and dowel yields in the wall closest to the shear plane in the main member is termed Mode III_s: Case 3-1.

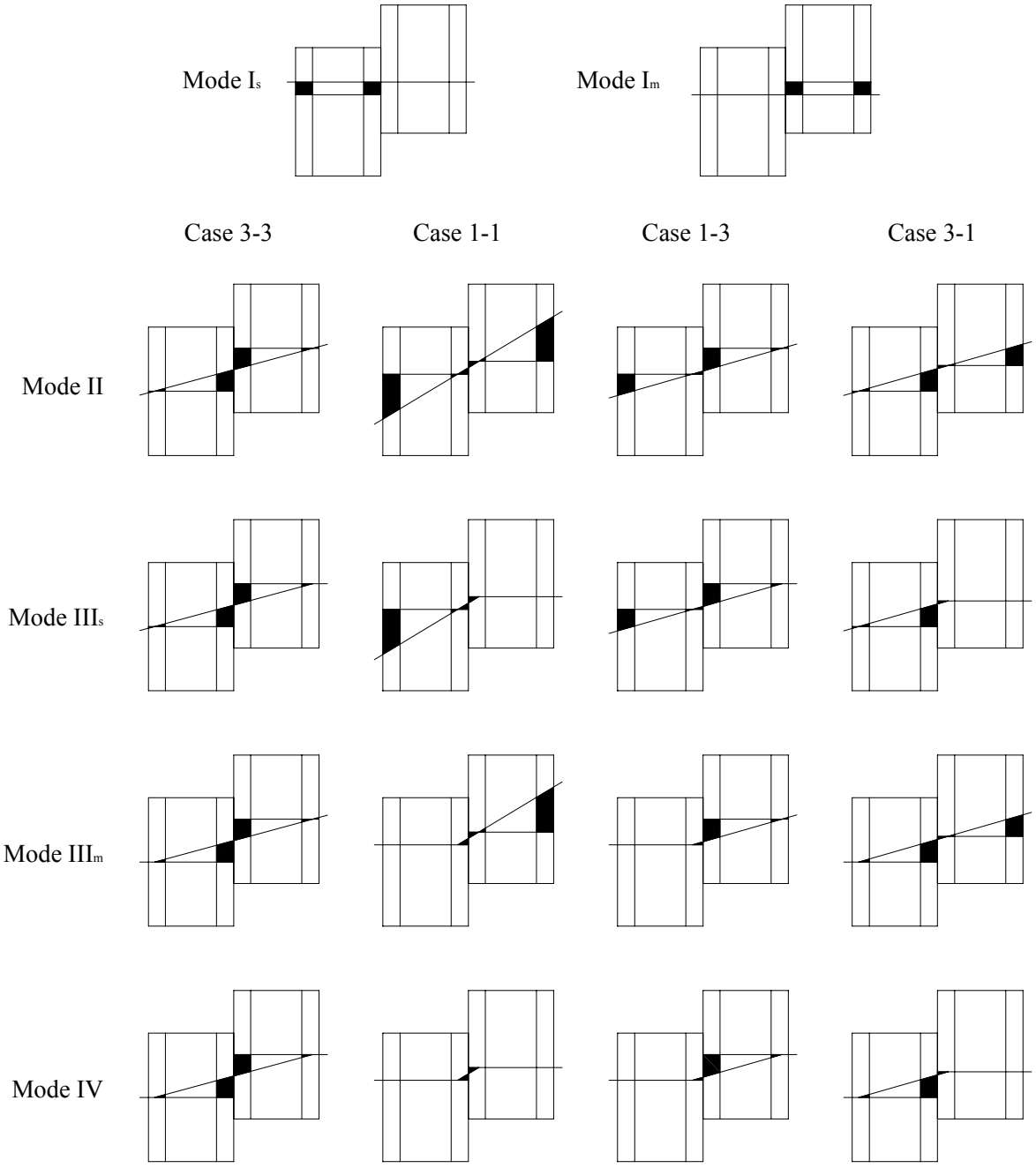

Figure 3-3: Assumed yield modes for hollow section yield model. The left member is the side member and the right member is the main member. The shaded region indicates a location of material crushing.

2. Expressions for A and *a* are written in terms of the connection dimensions. In all cases, $a = x_s + x_m$. The terms x_s and x_m define the location of dowel rotation or bending, and they are the only unknown distances in the problem. An expression for the area crushed by the dowel must be found in terms of the horizontal distances only. The crushed area of material is either triangular or trapezoidal in shape.
3. Next, an expression for the embedment stress distribution is written and used to relate the dimensions of the side and main members. It should now be possible to write a function for the yield load, *F*, that is only a function of one unknown variable (x_s). This unknown is the location of dowel rotation in Mode II and Mode III connections or the location of the hinge in Mode III and Mode IV connections.
4. The derivative of *F* with respect to the unknown variable *x* is now computed and set to zero. The variable x_s is solved for and thus the location where the energy is minimized is located.
5. Finally, the expression for x_s is now substituted back into the function for *F*. The resulting equation is the yield equation in terms of the connection dimensions and dowel bearing strengths only. The equation is then reduced to a design format.

This procedure was completed for all eighteen yield modes. The equations were further simplified for use with the quadratic formula. Additionally, four double shear yield modes due to symmetry were included. However, these yield modes could not control connection design because the imposed boundary conditions only increased the energy from the assumed yield modes. The complete derivation of the hollow section yield model can be found in APPENDIX C.

A computer program was written to evaluate the yield equations over the complete range of reasonable property values and connection geometries. The program involves a series of

nested loops that evaluated all eighteen equations for the connection properties of that iteration and records the governing yield mode and case. APPENDIX D lists the ranges of properties included and other details of the computer program used.

The program verified that only six equations controlled connection behavior; therefore, the other twelve equations could be eliminated from the model. The resulting yield modes are Mode I_s, Mode I_m, Mode II : Case 3-3, Mode III_s: Case 3-1, Mode III_m: Case 1-3, and Mode IV: Case 1-1 (Figure 3-4). The controlling yield equations are shown in Table 3-1. A pattern in the controlling cases was observed as all rotation of the dowel occurs about a point in the wall(s) farthest from the shear plane and all dowel yielding occurs in the wall(s) next to the shear plane.

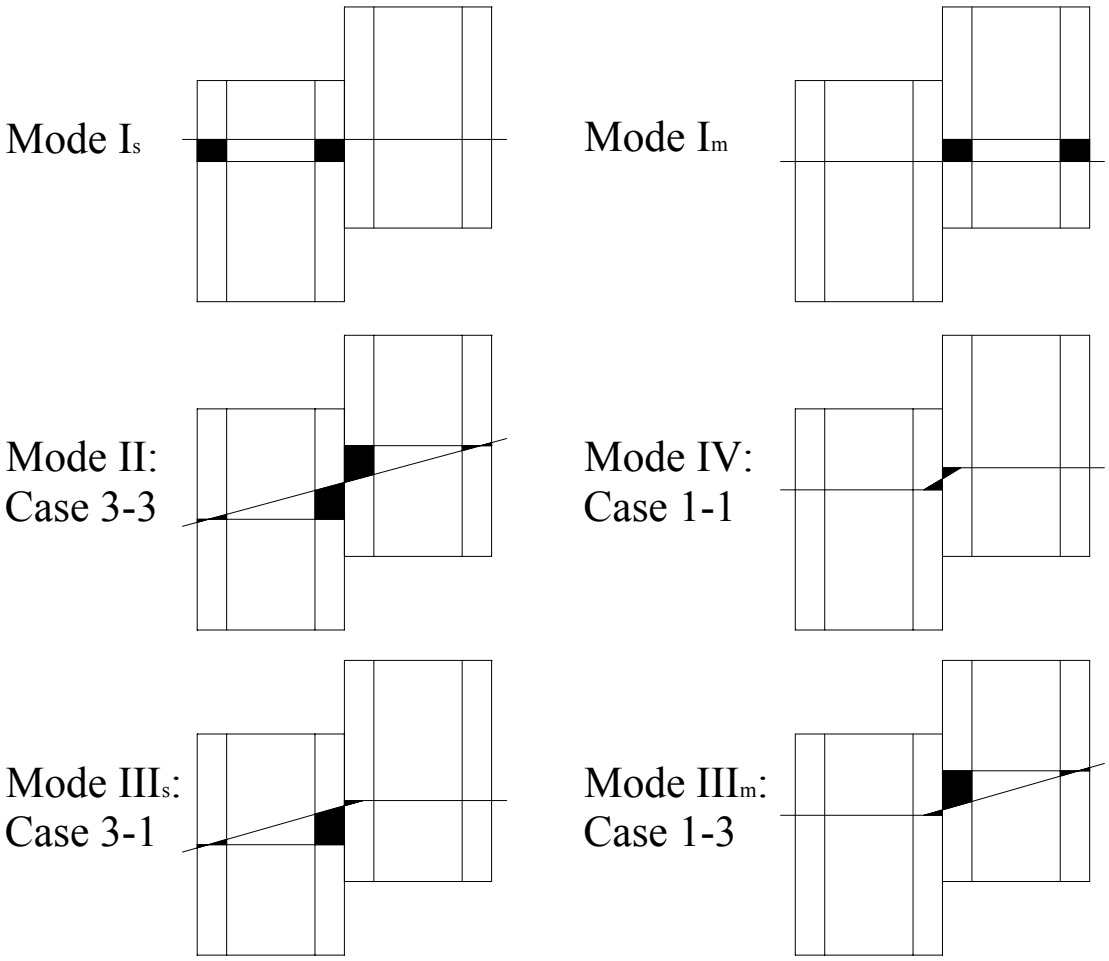

Figure 3-4: Controlling yield modes for hollow section yield model.

Table 3-1: Controlling Hollow Section Yield Mode Equations

Yield Mode	Single Shear	Double Shear
I_m	$F = 2 \cdot t_m \cdot f_{em}$	$F = 2 \cdot t_m \cdot f_{em}$
I_s	$F = 2 \cdot t_s \cdot f_{es}$	$F = 4 \cdot t_s \cdot f_{es}$
II-IV	$F = \frac{-B + \sqrt{B^2 - 4 \cdot A \cdot C}}{2 \cdot A}$	$F = \frac{-B + \sqrt{B^2 - 4 \cdot A \cdot C}}{A}$

Coefficients for Mode II-IV Equations				
Mode	Case	A	B	C
Mode II	3-3	$\frac{1}{4 \cdot f_{em}} + \frac{1}{4 \cdot f_{es}}$	$t_s + v_s + t_m + v_m$	$-\left[f_{es} \cdot t_s \cdot \left(t_s + v_s\right) + f_{em} \cdot t_m \cdot \left(t_m + v_m\right)\right]$
Mode III_m	1-3	$\frac{1}{4 \cdot f_{em}} + \frac{1}{2 \cdot f_{es}}$	$t_m + v_m$	$-\left[f_{em} \cdot t_m \cdot \left(t_m + v_m\right) + M_y\right]$
Mode III_s	3-1	$\frac{1}{2 \cdot f_{em}} + \frac{1}{4 \cdot f_{es}}$	$t_s + v_s$	$-\left[f_{es} \cdot t_s \cdot \left(t_s + v_s\right) + M_y\right]$
Mode IV	1-1	$\frac{1}{4 \cdot f_{em}} + \frac{1}{4 \cdot f_{es}}$	0	$-M_y$

See Table C-1 and Table C-2 for the definitions of the individual terms. Recall that $f_e = F_e D$.

The Mode I equations are evaluated directly. The Mode II, Mode III, and Mode IV equations utilize the quadratic formula where each mode has different coefficients.

One check of the hollow section yield model is that when the void width equals zero, the equations produce identical results to the EYM. The model was further verified by testing double shear connections and comparing the results.

Load-Displacement Curve Model for Energy-Based Design

The load-displacement curve of a connection provides information useful to energy-based design and can be incorporated into predictions of the overall deformation of a structure. The derivation techniques of the load-displacement method are identical to the methods used to develop the design model. The modeling relies on the virtual displacement method (Equation 3-3). The difference between the two derivations is that instead of displacing a connection yield mode one unit, a yield mode is displaced by the displacement, δ. The term δ is no longer mathematically removed from the equations. Rather, the final expression for the yield load, F, is a function of the connection displacement, δ. The load-displacement model only includes the six controlling modes and cases found during the development of the design yield model. Complete details of the load-displacement model derivation can be found in APPENDIX E.

One advantage of a model that predicts the entire load-displacement behavior of a connection is that the model output no longer relies on ambiguous yield points from the dowel bearing strength and bending yield strength curves. Instead, the strength of the connection materials are entered as curves fit to the dowel bearing or bending yield test data. For this research, sixth-order polynomials (restricted to pass through the origin) were fit to all the dowel bearing tests and bending yield tests conducted. The general form of the fitted curves is shown in Equation 3-5.

$$F = C_1\delta + C_2\delta^2 + C_3\delta^3 + C_4\delta^4 + C_5\delta^5 + C_6\delta^6 \qquad \text{Equation 3-5}$$

Similarly to the hollow section yield model, the load-displacement model uses the strength properties converted to line loads and moments. The load from the dowel bearing tests was divided by the sum of the wall thicknesses to produce dowel bearing resistance. Curves fit to the dowel bearing resistance versus displacement curves for the side members are given the

coefficients of A through F. Curves fit to the dowel bearing resistance versus displacement curves for the main members are given the coefficients of L through Q. For the bending yield strength tests, the load versus displacement curve must be changed to a bending moment versus displacement curve by multiplying the load by one-fourth the span. The displacement of the bending yield test must be converted to the connection test displacement using the angle of rotation of the dowel at midspan prior to entering the bending moment curve into the load-displacement model. Curves fit to the bending moment versus displacement at midspan are given the coefficients of A_m through F_m.

The Mode I_s and I_m load-displacement model equations are simply the curves fit to the dowel resistance data multiplied by the sum of the wall thicknesses. Modes II, III, and IV utilize the method of virtual displacement. The external energy consists of the yield load, F, times the displacement, δ. The internal energy depends on the yield mode and is a combination of dowel rotation and dowel yielding. Five contributions of internal energy have been defined (Figure 3-5). E1, E2, E3, and E4 relate to energy of material crushing. E1, E2, and E3 relate to energy of material crushing when the dowel rotates about a point in the wall farthest from the shear plane. E4 relates to energy of material crushing when a hinge forms within the wall closest to the shear plane. E5 corresponds to the energy of forming a hinge in the dowel. Table 3-2 defines the types of internal energy present in each yield mode. The total internal energy is the sum of all the applicable E-terms to the side and main members. For example, for Mode III_s: Case 3-1, the internal energy equals $E_{1s}+E_{2s}+E_{3s}+E_{4m}+E_{5m}$.

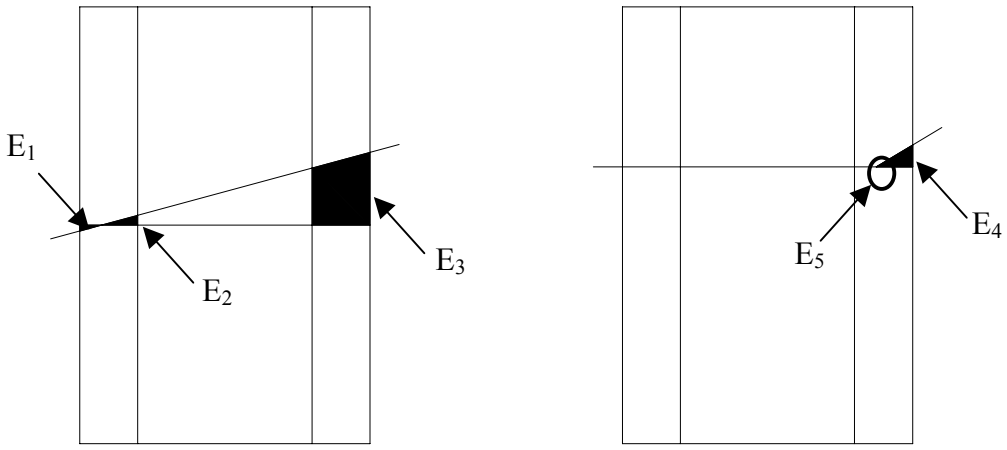

Figure 3-5: General internal energy conditions

Table 3-2: Energy Terms by Mode

Yield Mode	Applicable Internal Energy Terms	
	Side Member	Main Member
Mode II: Case 3-3	E_1, E_2, E_3	E_1, E_2, E_3
Mode III_m: Case 1-3	E_4, E_5	E_1, E_2, E_3
Mode III_s: Case 3-1	E_1, E_2, E_3	E_4, E_5
Mode IV: Case 1-1	E_4, E_5	E_4, E_5

Predicting an entire load-displacement curve is mathematically intensive and hence a spreadsheet was used. Derived equations are evaluated at specific displacements to produce ordered pairs of displacement and load. In order to utilize a spreadsheet more effectively, separate equations were developed for each component of the internal energy. A general equation has been identified for the internal energy due to material crushing (E_1, E_2, E_3, and E_4) (Equation 3-6).

$$E_{1,2,3,\,or\,4} = \frac{\delta}{840a^7}\begin{bmatrix} 280C_1a^5\left(i^3 - j^3\right)\delta + 210C_2a^4\left(i^4 - j^4\right)\delta^2 + \\ 168C_3a^3\left(i^5 - j^5\right)\delta^3 + 140C_4a^2\left(i^6 - j^6\right)\delta^4 + \\ 120C_5a\left(i^7 - j^7\right)\delta^5 + 105C_6\left(i^8 - j^8\right)\delta^6 \end{bmatrix} \qquad \text{Equation 3-6}$$

where:

$a = x_s + x_m$

$C_1, C_2, C_3, C_4, C_5, and\ C_6$ *are the coefficients from the fit dowel resistance curves*

i and j depend on the type of energy (Table 3 - 3)

Table 3-3: Coefficients for Equation 3-6

Internal Energy Type	i	j
E_1	$2t+v-x$	0
E_2	$x-t-v$	0
E_3	x	$x-t$
E_4	x	0
Note: x will either be x_s or x_m depending on the mode and member being considered		

Equation 3-7 gives the expression for energy associated with dowel yielding (E_5).

$$E_5 = \frac{M_y(\delta)}{x_s + x_y} \qquad \text{Equation 3-7}$$

As stated earlier, a sixth-order polynomial curve was fit to the bending yield strength load-displacement data (Equation 3-8). This fitted curve cannot be used directly in the E_5 equation because the displacement in the bending yield test is different than the displacement in a connection test. The angle of rotation of the dowel was used to relate the two tests and produce Equation 3-9.

$$M_y(\Delta) = A_m\Delta + B_m\Delta^2 + C_m\Delta^3 + D_m\Delta^4 + E_m\Delta^5 + F_m\Delta^6 \qquad \text{Equation 3-8}$$

$$M_y(\delta) = A_m\left[2\tan\left(\frac{\delta}{2(x_s+x_m)}\right)\right] + B_m\left[2\tan\left(\frac{\delta}{2(x_s+x_m)}\right)\right]^2 + C_m\left[2\tan\left(\frac{\delta}{2(x_s+x_m)}\right)\right]^3 + D_m\left[2\tan\left(\frac{\delta}{2(x_s+x_m)}\right)\right]^4 + E_m\left[2\tan\left(\frac{\delta}{2(x_s+x_m)}\right)\right]^5 + F_m\left[2\tan\left(\frac{\delta}{2(x_s+x_m)}\right)\right]^6 \qquad \text{Equation 3-9}$$

where :

Δ = *displacement in bending yield strength test*

δ = *displacement in connection test*

Table 3-4 summarizes the load-displacement predicting equations for single shear connections. The double shear equations are produced by multiplying the single shear equations

by two; except in Mode I_m where the single shear and double shear equations are identical. Only the Mode I_m, Mode III_s, and Mode IV equations were compared to test data.

Table 3-4: Load-Displacement Equations for Single Shear Connections

Mode	Load-Displacement Equation
I_s	$F(\delta) = 2t_s\left(A\delta + B\delta^2 + C\delta^3 + D\delta^4 + E\delta^5 + F\delta^6\right)$
I_m	$F(\delta) = 2t_m\left(L\delta + M\delta^2 + N\delta^3 + O\delta^4 + P\delta^5 + Q\delta^6\right)$
II: Case 3-3	$F(\delta) = \left(E_{1s} + E_{2s} + E_{3s} + E_{1m} + E_{2m} + E_{3m}\right)/\delta$
III_s: Case 3-1	$F(\delta) = \left(E_{1s} + E_{2s} + E_{3s} + E_{4m} + E_5\right)/\delta$
III_m: Case 1-3	$F(\delta) = \left(E_{4s} + E_5 + E_{1m} + E_{2m} + E_{3m}\right)/\delta$
IV: Case 1-1	$F(\delta) = \left(E_{4s} + E_5 + E_{4m} + E_5\right)/\delta$

The equations for Mode II, III, and IV shown in Table 3-4 assume that the locations of dowel yielding and/or dowel rotation are known (i.e. x_s and x_m). In the hollow section yield model these terms were solved for directly by taking the derivative of the yield load expression, setting it to zero, and solving for x. In the derivation of the load-displacement equations, this approach is not practical due to the increased number of terms. Therefore, x_s and x_m must either be assumed or found by other means in order to evaluate the load-displacement equations. Assuming the values of x_s and x_m remain constant during connection deformation, approximate values may be obtained using the expressions for x_s and x_m found during the development of the yield model (APPENDIX C).

In the Mode IV connections used in this research, the side member and the main member are made of the same material. Therefore, only one set of coefficients are needed and the Mode IV equation may be simplified to Equation 3-10.

$$F(\delta) = \sqrt{\left[M_y(\delta)\right]\left[\frac{2}{3}A\delta + \frac{1}{4}B\delta^2 + \frac{1}{10}C\delta^3 + \frac{1}{24}D\delta^4 + \frac{1}{56}E\delta^5 + \frac{1}{128}F\delta^6\right]} \qquad \text{Equation 3-10}$$

CHAPTER 4: EXPERIMENTAL METHODS

The predicted connection capacities were validated with the laboratory tests. The tests consisted of double shear bolted connection tests. The testing was limited to connections where the main and side members were loaded parallel to their extruded directions. The model was validated through testing Mode I_m, Mode III_s, and Mode IV connections. Prior to connection testing, dowel bearing tests and bolt yielding tests were conducted. The testing utilized three wall thicknesses and three dowel sizes.

The experimental data were collected and analyzed as outlined in the appropriate ASTM standard (discussed individually below). All tests used the 5% diameter offset method to determine yield points. In cases where the 5% diameter offset intersected the load-displacement curve after the maximum load is reached, the maximum load was used as the yield load.

Wood-Plastic Composite Material

The wood-plastic composite materials used in this research were produced with a parallel counter-rotating, twin-screw extruder (Cincinnati Milacron Atlas 93) with a stranding die at the Wood Materials and Engineering Laboratory. In order to bracket the current range of WPC stiffness, two WPC formulations were used. One formulation consists of 50% Ponderosa Pine flour (AWF #4020) and 50% polyvinyl chloride compound (Georgia Gulf: 3014 nat 00) (PVC formulation). The other formulation consists of 66% Maple flour (AWF #4010), 31% high density polyethylene (Equistar: LB 0100 00), 2% zinc stearate (Ferro Chemicals Synpro DLG-20B) and 1% EBS wax (GE Specialty) (HDPE formulation). Three different cross-sections were used to achieve the necessary yield modes to validate the models. The test specimens consisted of triple-box sections shown in Figure 4-1. The outside dimensions of the triple box section remained constant; however, the average wall thickness varied from 0.2 inches, 0.3 inches, and

0.4 inches, which in turn changes the void distance. The connection members were formed by cutting the WPC material into pieces twenty-inches in length. There were two holes of three-quarter-inch diameter to attach the test members to the testing machine and one hole with a diameter equal to the dowel diameter at the location of the connection being studied. The locations of the holes are shown in Figure 4-2.

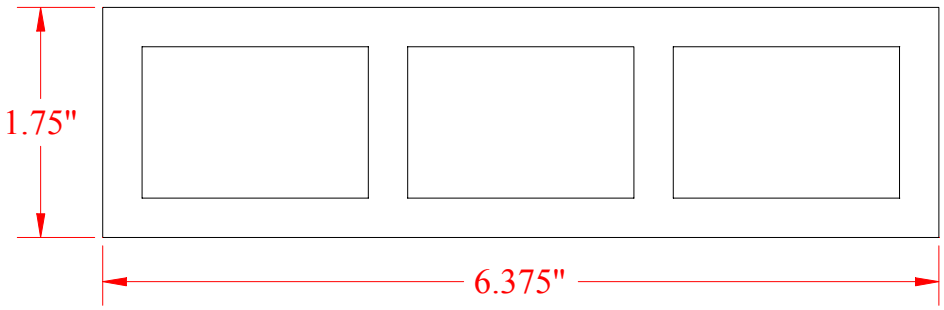

Figure 4-1: Triple-box section. Outside dimensions remain constant. However, wall thickness varies between 0.2 inches, 0.3 inches, and 0.4 inches.

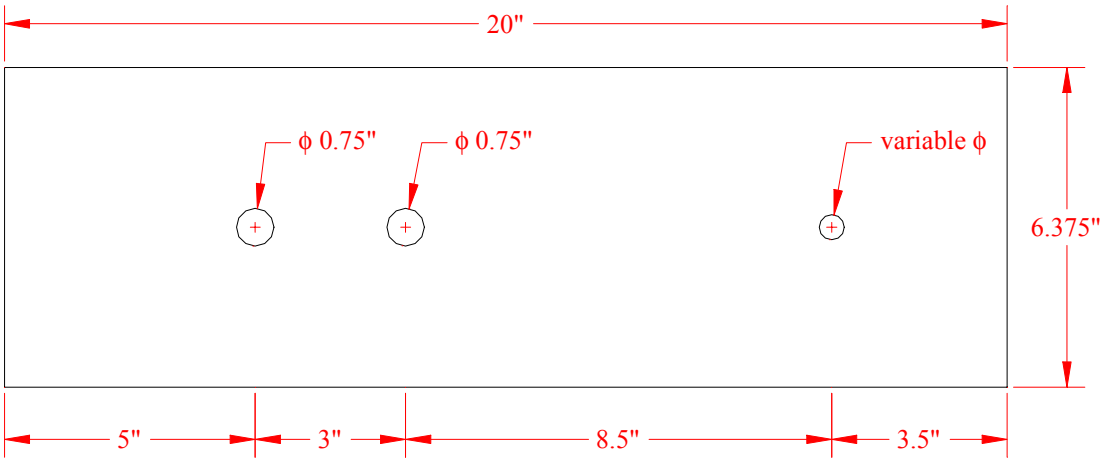

Figure 4-2: Connection member with dimensions.

ASTM 5652-95 Section 8.1 discusses sample conditioning and states that wood and wood based products for bolted connection tests should be conditioned to meet the objectives of

the testing. ASTM 1761-88 Section 27.1 suggests that wood should be conditioned at a temperature of 68 ± 6°F and a relative humidity of 65 ± 3%. ASTM D618-96 deals with conditioning plastics for testing and suggests that the material should be stored at a temperature of 73.4 ± 3.6°F and a relative humidity of 50 ± 5%. For this research, the WPC samples were conditioned in the lab environment where testing occurred. That was at approximately 73°F and 30% relative humidity.

Steel Dowels

Three dowel sizes were used in this research with nominal diameters of 3/8", 1/4", and 3/16". The 3/8" and 1/4" diameter samples consisted of zinc-plated A307 bolts obtained from local hardware vendors. To reduce variability, the bolts of each diameter were selected from the same manufacturing lot. The 3/16" dowels consisted of mild steel welding rod that was cut into six-inch pieces from an original length of three-feet. Ten three-foot rods were purchased at the same time and location.

Dowel Bearing Strength, F_e

The test methods outlined in ASTM D5764-97 were used for the dowel bearing tests. A dowel bearing test involves compressing a dowel into a specimen (Figure 4-3). The dowel is placed in a semicircular hole created by first drilling a hole and then cutting the member in half at the location of the hole. The dowel bearing strength is found by using Equation 4-1. The yield load is commonly found using the 5% diameter offset method.

$$F_e = \frac{Yield\ Load}{\left[\sum (Wall\ Thicknesses)\right]\left[Dowel\ Diameter\right]} \qquad \text{Equation 4-1}$$

There is no dowel bearing test standard that specifically addresses hollow sections. ASTM D5764-97 calls for minimum specimen dimensions based on the diameter of the fastener being embedded. Since WPC are extruded from a die with fixed cross-sectional dimensions,

only the specimen length is variable. However, the outside dimensions of the cross-sections used in this research are large enough to meet the dimension requirements of ASTM D5764-97. The length of the dowel bearing samples was 3.5 inches. This same block size was used for all the cross-sections being studied. The dowel bearing samples were removed from the end of the connection test samples (Figure 4-4).

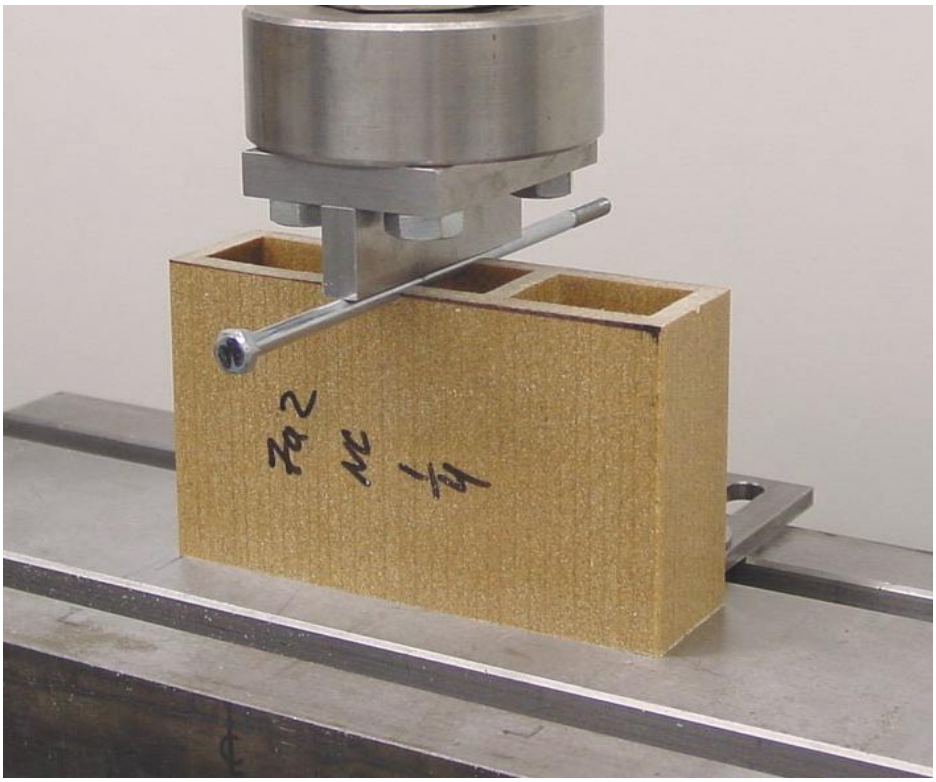

Figure 4-3: Dowel bearing test

ASTM D5764-97 suggests a displacement rate that results in maximum load in one to ten minutes. Balma (1999) showed that dowel bearing strengths of two WPC formulations vary while testing in this large displacement rate range. For this research, all dowel bearing tests were conducted at a constant crosshead displacement of 0.04 inches per minute which resulted in reaching maximum load in about three minutes for most test groups.

Table 4-1 lists the number of dowel bearing tests conducted for this research. The test matrix is larger than necessary to validate the connection model. Several additional groups were added to determine if the dowel bearing strength varied with bolt diameter. The only deviation from ASTM D5764-97 procedures was that the hole drilled in the member was not oversized to be consistent with the connection tests.

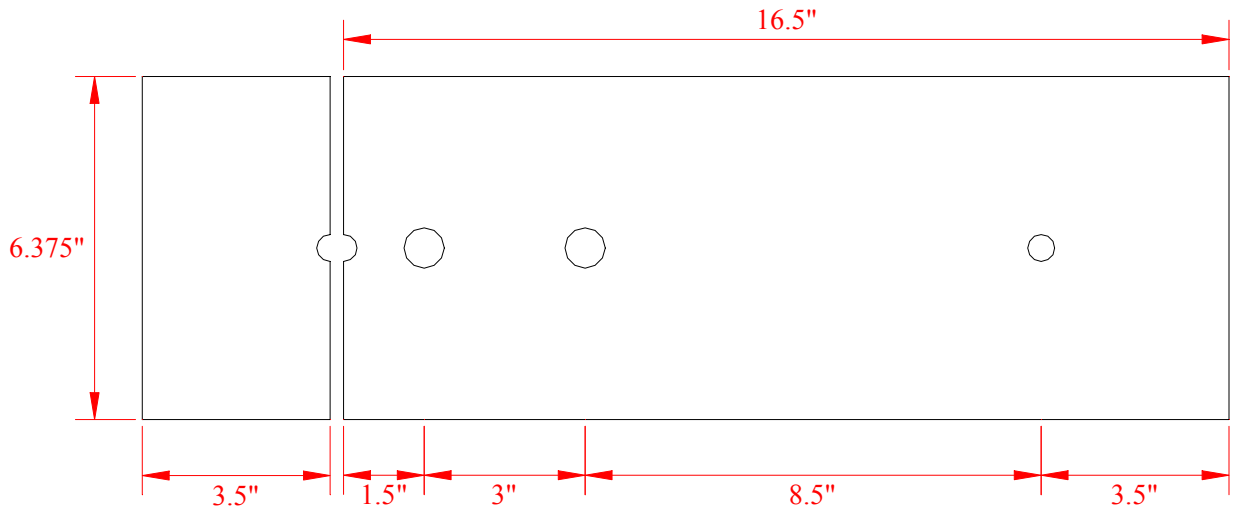

Figure 4-4: The dowel bearing samples were cut from the members after connection testing.

Table 4-1: Number of Dowel Bearing Tests Conducted

Dowel Diameter	HDPE			PVC		
	0.2" wall	0.3" wall	0.4" wall	0.2" wall	0.3" wall	0.4" wall
3/8"	6	9	10	14	10	10
1/4"	13	10	12	5	8	16
3/16"	0*	0*	16	0*	0*	0*

* Dowel bearing tests only required on HDPE 0.4" wall thickness with 3/16" dowel to enable validation of HDPE Mode IV connection tests.

Bending Yield Strength, F_{yb}

The average bending yield strength of the three diameters of bolts used in the connection testing were measured and used as a model inputs. ASTM F1575-95 outlines the determination of the bending yield strength of nails. There is no ASTM standard specifying procedures for

determining the bending yield strength of bolts. Therefore, ASTM F1575 was utilized as a guideline for determining the bending yield strength of the bolts in this research. A displacement rate of 0.25 inches per minute was used.

Figure 4-5 shows a typical bending yield strength test. The test apparatus consists of two-3/4"diameter high-strength steel dowels spaced at a span of four inches on center that support the test specimen. Another 3/4" diameter high-strength steel dowel is used to load the test specimen at midspan. The beam formula for a simply-supported beam with a point load at midspan is used to calculate the moment in the dowel. The bending yield stress is then found by dividing the moment in the dowel at yield by the plastic section modulus of the dowel (Equation 4-2). The yield load is commonly found using the 5% diameter offset method.

$$F_{yb} = \frac{3}{2}\frac{(Yield\ Load)(Span)}{(DowelDiameter)^3}$$ Equation 4-2

Fifteen bending yield tests were conducted for the 1/4" diameter bolts. For the 3/8" bolts, 24 bending yield tests were conducted. The increased sample size was required to study the variability of the bending yield strengths between several boxes of bolts. This extra check was to insure that indeed all the bolts had the same bending yield strength. A different procedure had to be performed on the 3/16" dowels since they were purchased in three-foot lengths. The rods were cut into six-inch pieces. The original rod number was carefully marked on each piece. Bending yield strength tests were then conducted on four of the six-inch pieces. The five weakest rods were used in the connection tests because they would be most likely to form plastic hinges.

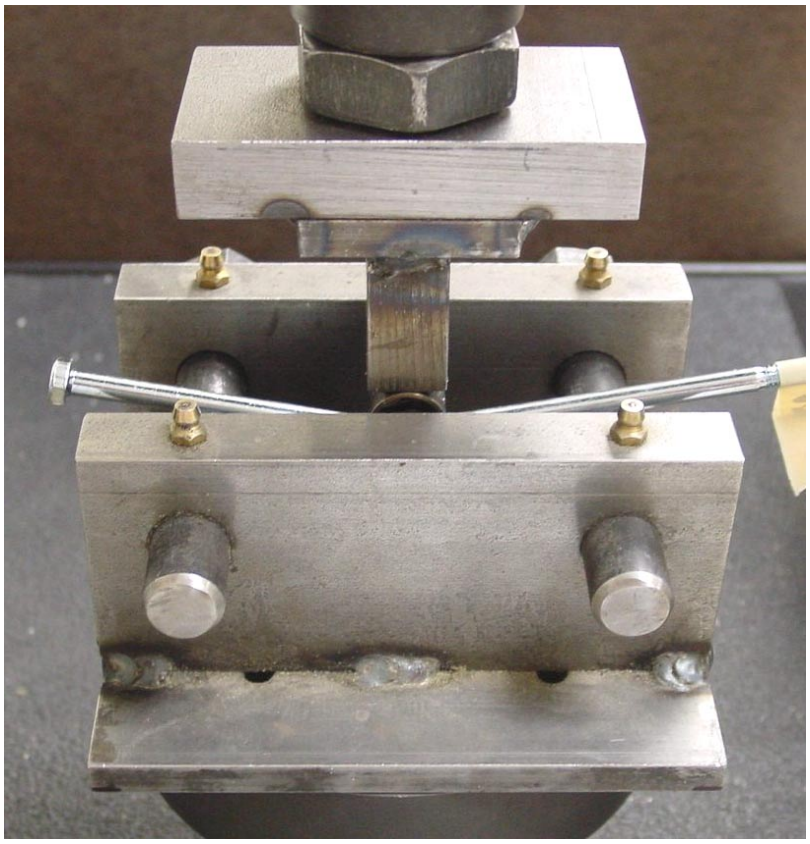

Figure 4-5: Bending yield test

Connection Testing

Double shear connections were tested in tension to validate the theoretical models. The typical connection configuration is shown in Figure 4-6. During all the connection tests, load and displacements measurements were recorded. The load was read using a 5-kip load cell with a resolution of ± 1%. Displacement was measured using two LVDTs with a resolution of ± 0.001 inches mounted on either side of the connection being studied (Figure 4-7). Readings from the two LVDTs were averaged for use in the subsequent data analysis.

ASTM D1761-88 and ASTM D5652-95 specify bolted connection testing for solid timber members. Both standards suggest similar testing procedures and sample sizes of five to ten specimens. For this research, a sample size of five was used for the Mode I_m connections. A sample size of ten was used for Mode III_s and Mode IV connections. The small sample size is

justified because preliminary testing has indicated a coefficient of variation (COV) lower than the assumed COV for timber connections (ASTM D1761-Note 6). Using Equation 1 in ASTM D2915, a sample size of ten pertains to a 95% confidence interval and a COV of less than or equal to 7%. For a sample size of five, the COV must be less than or equal to 3%. Table 4-2 contains the test matrix for the connection tests.

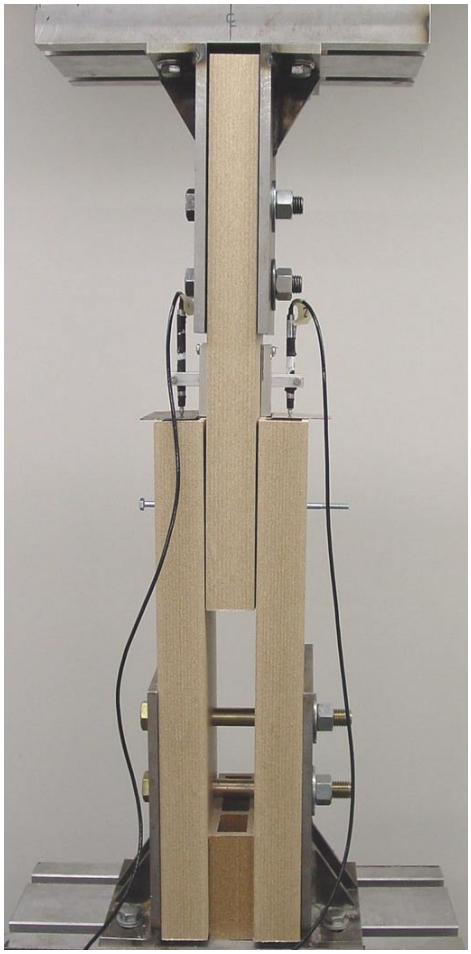

Figure 4-6: Connection test prior to loading. The two LVDTs measure only the displacement of the connection being studied.

Figure 4-7: LVDTs measured the displacement of the connection only.

Table 4-2: Connection Configuration

WPC Formulation	Mode	Sample Size	Dowel Diameter	Main Member Wall Thickness	Side Member Wall Thickness
HDPE	I_m	5	3/8”	0.2”	0.3”
	III_s	10	1/4”	0.4”	0.2”
	IV	10	3/16”	0.4”	0.4”
PVC	I_m	5	3/8”	0.2”	0.3”
	III_s	10	3/8”	0.4”	0.2”
	IV	10	1/4”	0.4”	0.4”

The displacement rate for the connection tests was 0.04 inches per minute. This displacement rate was consistent with displacement rates specified in timber connection test standards (ASTM D1761-88; ASTM D5652-95) and previous WPC connection testing (Balma, 1999). The HDPE formulation used in this research was comprised of a majority of wood flour. However, there was still a large percentage of plastic in the HPDE formulation and the PVC formulation was comprised of half plastic. Plastic standards have been consulted to verify that displacement rates specified do not affect test results because of the high plastic content. ASTM D6117-97 deals with mechanical fastener testing in plastic lumber, but bolted connections are not covered. ASTM D953-95 discusses determination of bearing strength in plastics and

suggests a displacement rate of 0.05 ± 0.01 inches per minute. Therefore, a displacement rate of 0.04 inches per minute was acceptable for the dowel bearing tests and the connection tests. ASTM D5652-95 Section 9.5 states that maximum load should be reached in not less than five minutes and not more than twenty minutes. This criterion was satisfied using the 0.04 inches per minute displacement rate.

The connection models being validated only take into account bolt embedment, bolt rotation, and bolt yielding. Other factors like friction between the members and tensile forces developed in the bolt are not modeled. Therefore, nuts and washers were not used to constrain the bolt at the location of the hole being studied (Figure 4-6).

ASTM D1761 Note 7 states that all holes in a connection member should be oversized. The 3/4" diameter apparatus holes were oversized as specified by 1/16 of an inch to allow members to fit the test apparatus correctly. However, oversizing the test hole did not meet the parameters of this research. The yield models do not account for hole oversizing. When a hole is oversized in thin-walled member, dowel rotation may occur in the wall farthest from the shear plane without any material crushing. When the hole is drilled the same size as the dowel, any rotation or yielding of the dowel must involve yielding of the member material under the dowel.

CHAPTER 5: RESULTS AND DISCUSSION

Dowel Bearing Strength Tests

A total of thirteen test groups were included in the dowel bearing testing. Seven test groups for the HDPE formulation and six groups for the PVC formulation. A majority of the test configurations were needed as input for validating the yield models. Additional test groups were added to facilitate the investigation of the dependence of dowel bearing strength on dowel diameter and wall thickness.

ANOVA analysis was conducted using SAS and verified that significant differences in mean dowel bearing strengths existed between test groups at a significance level of 5%. Dowel bearing strengths increased as the dowel diameters decreased. The dowel bearing strength also increased within a WPC formulation as the dowel diameter was held constant and the wall thickness increased. The dowel bearing test results found using the 5% offset method to define the yield point are in Table 5-1. The COV of each test group was between 1.1% and 4.1%. The low COVs justifies the small samples sizes as predicted prior to testing and meets the sample size requirements of ASTM D2915.

Table 5-1: Dowel Bearing Strength Data (yield based on 5% offset)

Formulation	Wall Thickness	Dowel Diameter	Sample Size	Average	COV	Minimum	Maximum
-	(inches)	(inches)	-	(psi)	(%)	(psi)	(psi)
HDPE	0.2	1/4	13	4680	2.7	4430	4830
		3/8	8	4250	3.1	4020	4420
	0.3	1/4	10	5090	2.1	4940	5280
		3/8	9	4690	1.1	4590	4740
	0.4	3/16	16	6310	2.5	6060	6660
		1/4	12	5310	2.6	5060	5510
		3/8	10	4960	1.8	4810	5140
PVC	0.2	1/4	5	16800	3.4	16100	17400
		3/8	14	13800	4.1	13000	14900
	0.3	1/4	8	18800	1.0	18500	19100
		3/8	10	17000	1.5	16600	17300
	0.4	1/4	16	20100	2.6	19100	21000
		3/8	10	18600	1.4	18300	18900

The dowel bearing strength of the PVC formulation was an average of 3.6 times higher than the dowel bearing strength of the HDPE formulation. The failure modes of the two materials was different. The PVC formulation failed brittlely and crumbled as failure progressed (Figure 5-1). The HDPE formation deformed ductilely out of plane (Figure 5-2). These phenomena can also be seen in the load-displacement curves. The PVC formulation takes load rapidly, but as failure occurs, the load drops off quickly as the material crumbles (Figure 5-3). In the HDPE formulation, behavior is more ductile; load is gained and lost at a slower rate. After the sample reaches failure at the maximum load, the load decreases gradually until the test is concluded (Figure 5-4).

Careful sample preparation was critical to producing satisfactory dowel bearing results. Any skew between the hole being loaded and the load head would cause one wall to be loaded before the other wall. When one wall yielded prematurely, the load-displacement curve became non-linear when the wall yielded, and the maximum load was much lower than the samples loaded ideally. Tests that had a wall fail prematurely were not included in the final results because those samples did not truly measure the dowel bearing strength. For members with a solid cross-section, the reducing the amount of skew is important, but the dowel is supported continually so the effect is less dramatic.

As seen in Figure 5-3 and Figure 5-4 when using the 5% offset method to predict yield, the intersection load was either near the maximum load or after the maximum load had already occurred. Common practice is that if the maximum load occurs before the intersection load, the maximum load is used as the yield load. When this dowel bearing strength is then used to predict connection capacity, the model input is really based on maximum load rather than yield load. In order to validate the yield models on a maximum load basis, the dowel bearing strengths

using maximum load instead of the 5% offset load were computed (Table 5-2). The HDPE dowel bearing strengths increase slightly from the 5% offset based strengths. The PVC dowel bearing strengths remain the same as the 5% offset based strengths because the intersection load always occurred after the maximum load had been reached.

Table 5-2: Dowel Bearing Strength Data (based on maximum load)

Formulation	Wall Thickness	Dowel Diameter	Sample Size	Average	COV	Minimum	Maximum
-	(inches)	(inches)	-	(psi)	(%)	(psi)	(psi)
HDPE	0.2	1/4	13	4680	2.7	4450	4830
		3/8	8	4250	3.1	4020	4420
	0.3	1/4	10	5170	1.9	5010	5340
		3/8	9	4700	1.1	4590	4760
	0.4	3/16	16	6800	2.2	6620	7230
		1/4	12	5620	2.7	5290	5860
		3/8	10	5050	1.7	4940	5230
PVC	0.2	1/4	5	16800	3.4	16100	17400
		3/8	14	13800	4.1	13000	14900
	0.3	1/4	8	18800	1.0	18500	19100
		3/8	10	17000	1.5	16600	17300
	0.4	1/4	16	20100	2.6	19100	21000
		3/8	10	18600	1.4	18300	18900

Dowel bearing strength increased as wall thickness increased within a given WPC formulation which was likely due to production parameters and the change in boundary conditions between wall thicknesses. The increase of dowel bearing strength by decreasing the dowel diameter was expected. This type of behavior is common in timber design in the dowel bearing strengths for bolt perpendicular to the grain (AF&PA, 1997). Although insignificant in timber design for small diameters (Wilkinson, 1991), there does appear to be a diameter effect in the WPC hollow sections and dowel sizes studied. The average increase in dowel bearing strength by decreasing the bolt diameter from 3/8" to 1/4" was 11%. A designer cannot assume that the dowel bearing strength will be constant for a formulation. The dowel bearing strength will clearly vary for different cross-sections of the same formulation and when using different dowel diameters within a single cross-section.

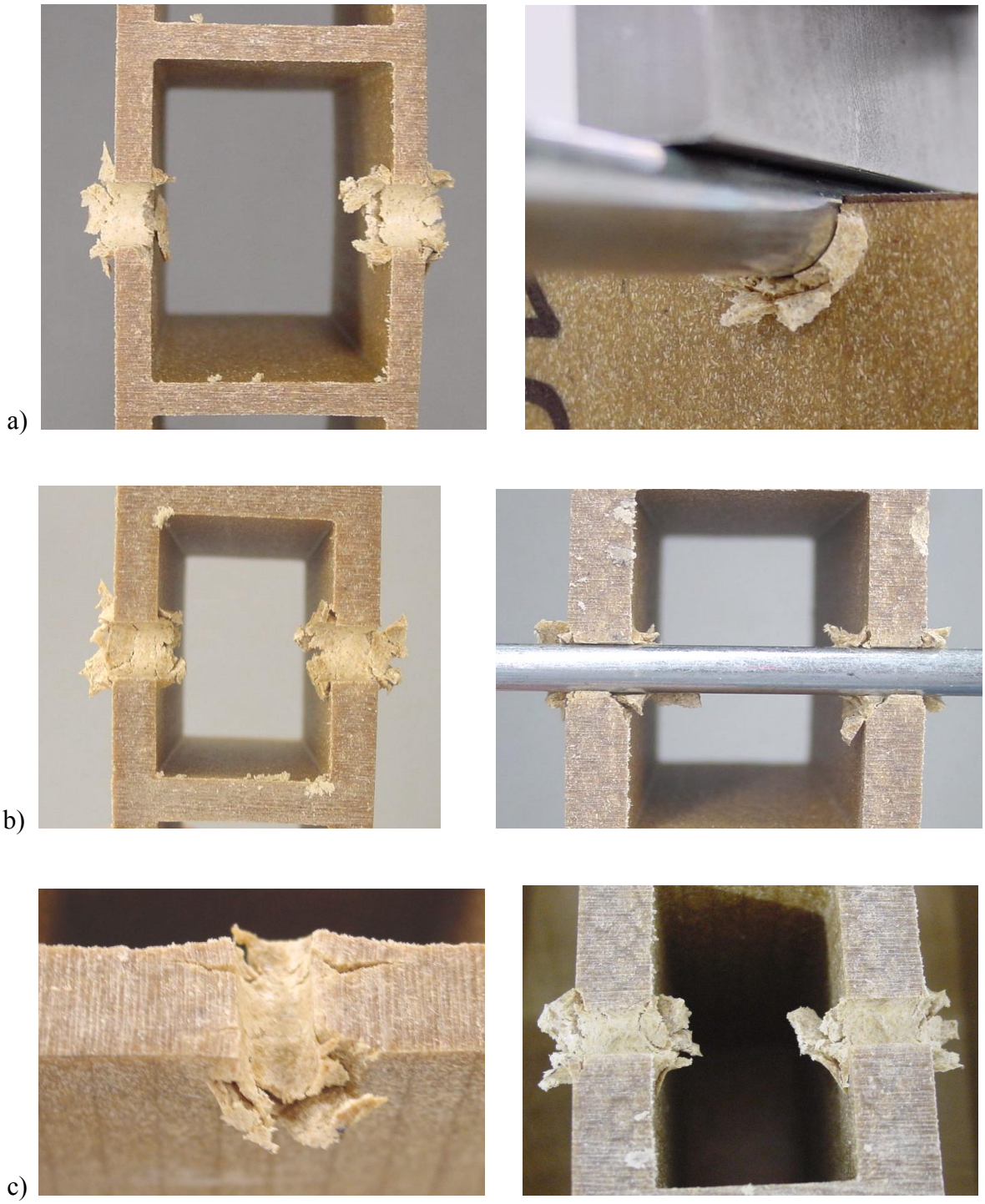

Figure 5-1: Typical PVC dowel bearing failures: a) 0.2" wall b) 0.3" wall c) 0.4" wall

a)

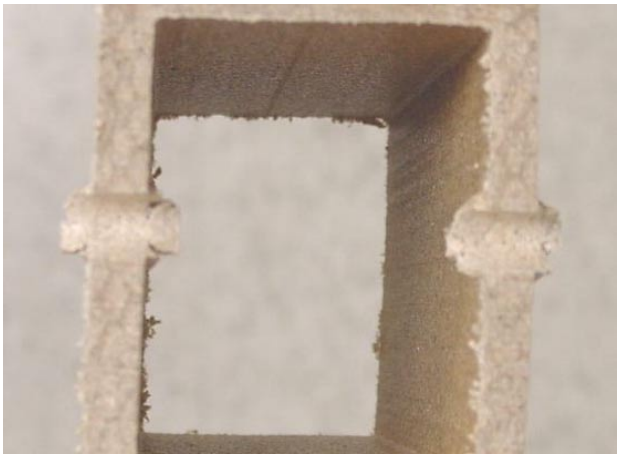

b)

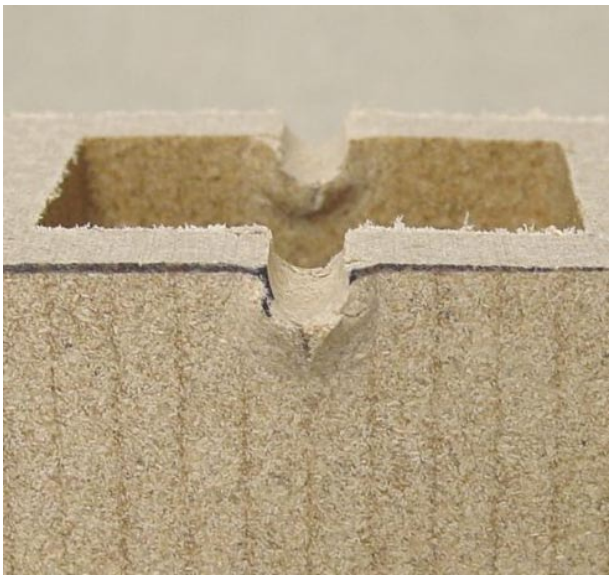

c)

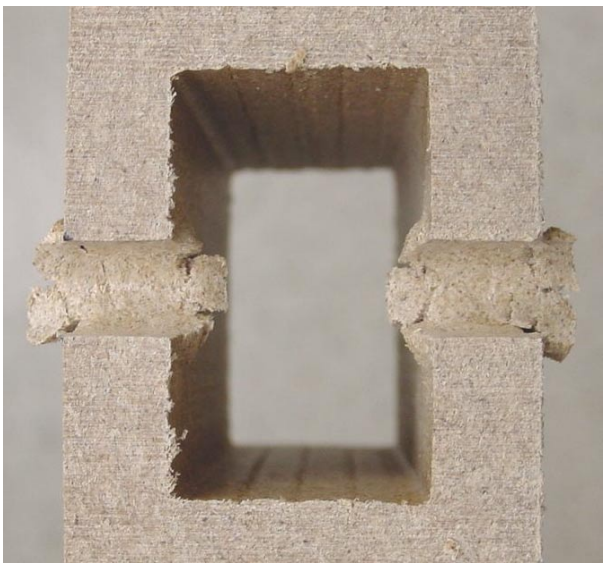

Figure 5-2: Typical HDPE dowel bearing failures: a) 0.2" wall b) 0.3" wall c) 0.4" wall

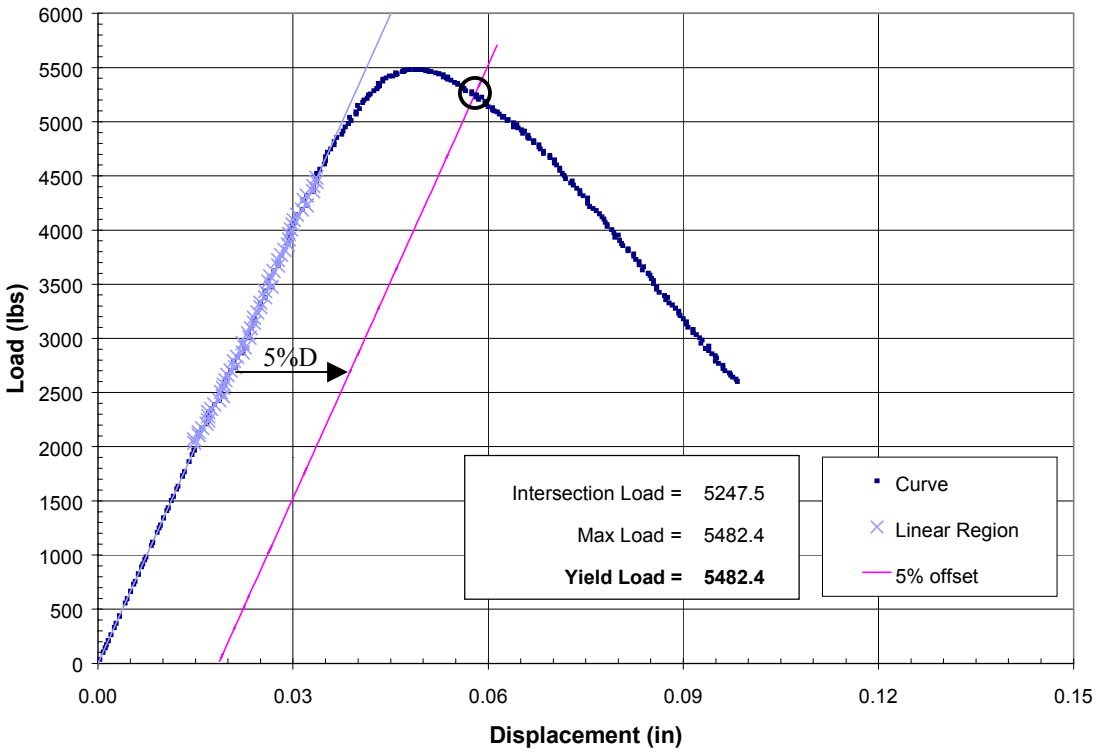

Figure 5-3: Load-displacement curve of PVC 0.4" sample with 3/8" diameter dowel

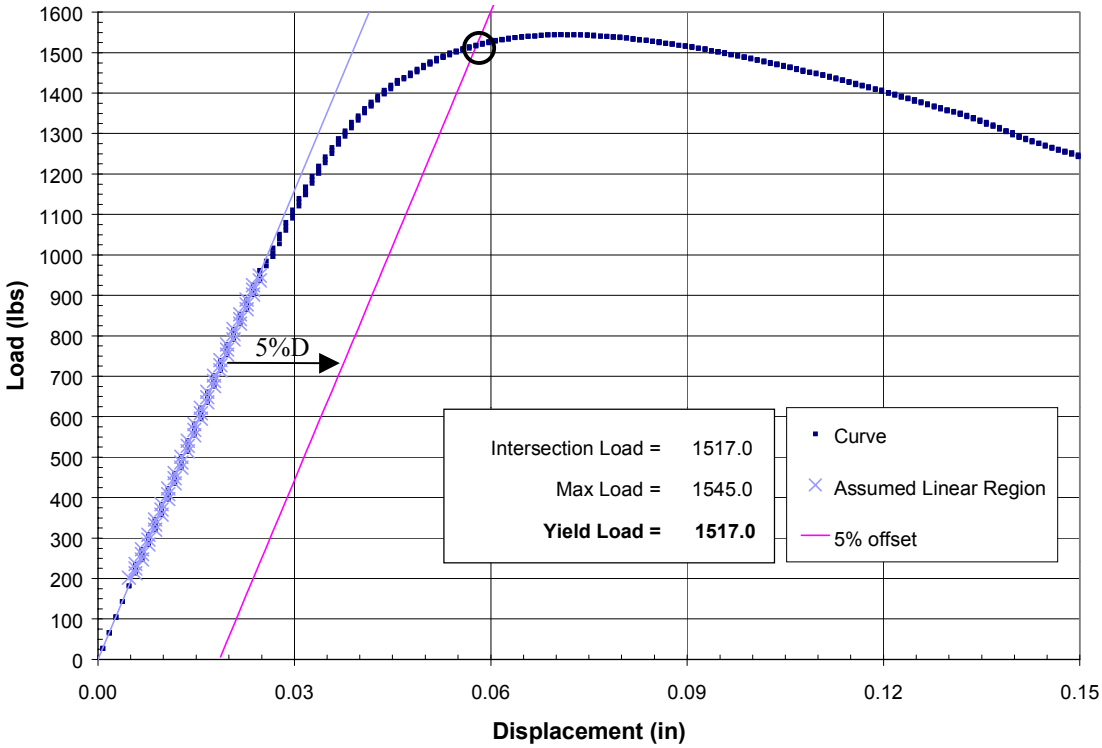

Figure 5-4: Load-displacement curve of HDPE 0.4" sample with 3/8" diameter dowel

Bending Yield Strength Tests

The bending yield strength of three dowel diameters (3/8", 1/4", and 3/16") was determined. The 3/8" and 1/4" diameter dowels were commercially available bolts and the 3/16" diameter dowels were cut from mild steel welding rods. The bending yield strength was found using the 5% diameter offset method (Table 5-3). Low COVs were obtained for the 3/8" and 1/4" diameter bolts because the bolts were purchased from the same manufacturing lot. The relatively high COV of the rod group is because five different rods were used. The COV was lower for each individual rod (Table 5-4). Rod type 5 had a significantly lower yield strength that resulted in the higher than expected group COV. A typical load-displacement curve is shown if Figure 5-5.

Table 5-3: Bending Yield Strength Based on 5% Offset

Dowel Type	Sample Size	Average Diameter	Average F_{yb}	COV	Minimum	Maximum
-	-	(inches)	(psi)	(%)	(psi)	(psi)
A307 3/8	23	0.371	87400	1.1	85100	90000
A307 1/4	15	0.247	86800	2.1	83700	89700
rod 3/16	20	0.186	55800	6.4	48300	60200

Table 5-4: Bending Yield Strength of Individual Rod Groups

Dowel Type	Rod Type	Sample Size	Average F_{yb}	COV	Minimum	Maximum
-	-	-	(psi)	(%)	(psi)	(psi)
rod 3/16	2	4	57400	2.9	55500	58900
	4	4	57300	1.7	57100	58300
	5	4	49800	3.2	48700	51700
	6	4	59400	1.7	58000	60200
	9	4	55400	2.5	54200	57300

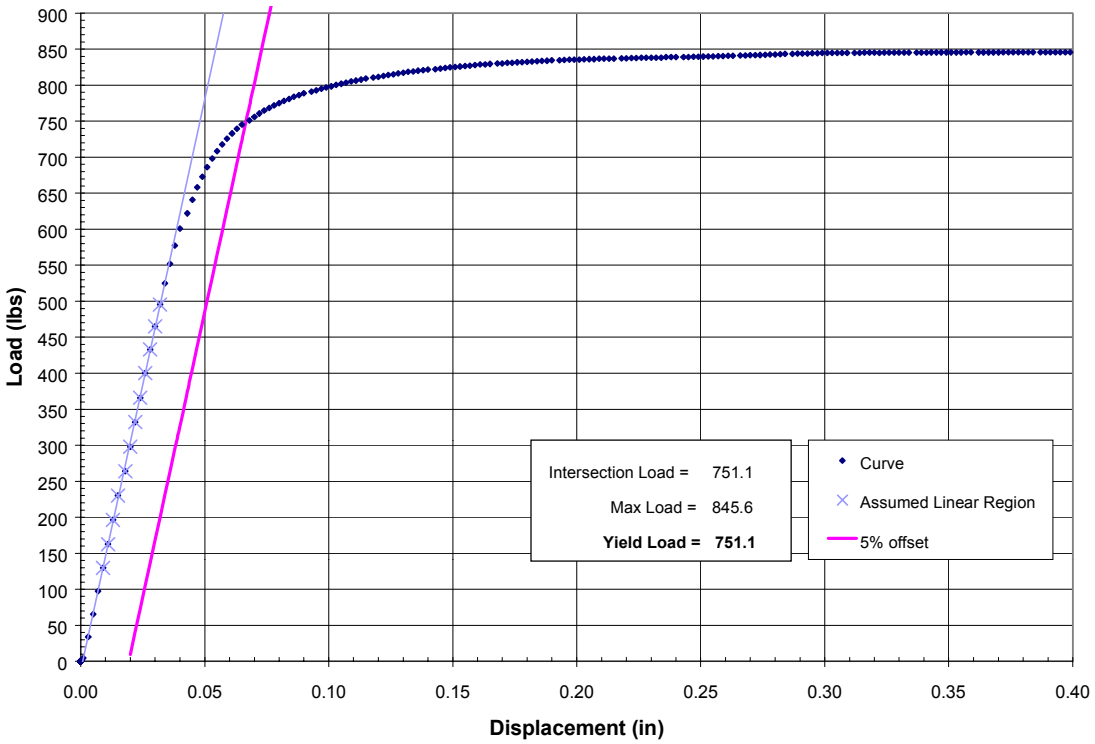

Figure 5-5: Typical bending yield strength test (3/8" diameter)

Due to the problems defining a yield point in the dowel bearing tests noted above, maximum connection loads were be compared predicted maximum loads. Bending yield strength was recalculated on a maximum load basis (Table 5-5). The COV of the 3/16" rods improved dramatically since nearly all the rods approached the same load at a large displacement. However, Table 5-5 is misleading because the maximum loads are extremely arbitrary. The maximum load was always the last point recorded from testing and solely depended on when data collection was terminated.

Table 5-5 : Bending Yield Strength Based on Maximum Load

Dowel Type	Sample Size	Average Diameter	Average F_{yb}	COV	Minimum	Maximum
-	-	(inches)	(psi)	(%)	(psi)	(psi)
A307 3/8	23	0.371	100800	3.0	97800	107300
A307 1/4	15	0.247	105200	1.2	103900	107500
rod 3/16	20	0.186	77100	1.8	74400	79900

To determine the bending yield strength that relates to the maximum load in the connection tests, the stress in the dowel must be computed when the connection is at maximum load. The two tests can be related by matching the angle of rotation of the dowel in the connection test with the corresponding displacement in the bending yield test. This is done in the following manner:

1) The displacement, δ, at the location of maximum load was found for each connection test. The average was computed for each of the connection tests groups.
2) An expression that related the angle for rotation to the displacement of the connection was used during the theoretical development of the hollow section yield theory (Equation 5-1). Equation 5-1 is used here to calculate the angle of rotation of the dowel, θ, at maximum load. The theoretical expressions for x_s and x_m from APPENDIX C were used in the calculation.

$$\tan(\theta) = \theta = \frac{\delta}{x_s + x_m} \qquad \text{(small displacement assumed)} \qquad \text{Equation 5-1}$$

3) Now knowing the angle of rotation of the dowel in the connection test, the displacement of the dowel, Δ, required to produce this rotation in the bending yield strength test is back calculated. Equation 5-2 was developed based on the geometry of the bending yield test setup (Figure 5-6).

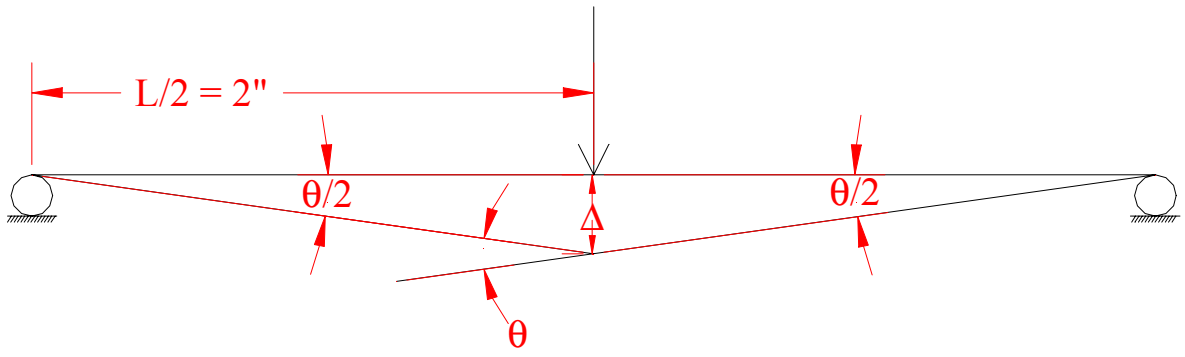

Figure 5-6: Bending yield test diagram

$$\Delta = 2\tan\left(\frac{\theta}{2}\right)$$ Equation 5-2

4) The sixth-root polynomial fit to each group of bending yield strength tests was used to determine the load at the computed displacement, Δ.

5) Equation 4-2 was used to calculate the bending yield strength from the load found in Step 4.

The results of each step are given in Table 5-6.

Table 5-6: Bending Yield Strength Based on Displacement of the Max Load of Connection Test

Dowel Type	Connection Test			F_{yb} Test		Average F_{yb}*
	Connection Type	Displacement at maximum load	Angle of Dowel Rotaion	Corresponding Displacement	Load on Curve	
-	-	(inches)	(radians)	(inches)	(lbs)	(psi)
A307 3/8	PVC - Mode III_s	0.065	0.034	0.034	534	62800
A307 1/4	HDPE - Mode III_s	0.157	0.079	0.079	230	91800
	PVC - Mode IV	0.092	0.155	0.156	252	100600
rod 3/16	HDPE - Mode IV	0.244	0.381	0.386	14266	77100

* For HDPE - Mode IV, the F_{yb} displacement was larger than fit data. Therefore, the maximum load was used to calculate F_{yb}.

This analysis procedure worked for three of the four connection test groups. In the HDPE - Mode IV connections, the maximum load occurred when data collection was terminated. The large angle of rotation of the dowel at maximum connection load corresponded with a displacement in the bending yield test that was out of the range of the bending yield test and the line fit to those tests. The maximum load based bending yield strength (Table 5-5) was used to predict maximum connection capacity for the 3/16" diameter rods only. For connections with 3/8" and 1/4" diameter dowels the Table 5-6 bending yield strength was used to predict maximum connection capacity.

Connection Tests

Six connection configurations were tested – three yield modes in two wood-plastic composite formulations (Table 4-2). The results are tabulated in Table 5-7. The expected yield mode was observed in all the test groups. COVs ranged from 2.3% to 4.5% and are much lower than other WPC connection research (Balma, 1999). Typical curves load-displacement curves are shown in Figure 5-7 through Figure 5-12. All the load-displacement curves can be found later in "Model Validation" section of this chapter.

Table 5-7: Connection Test Data Based on 5% Offset Method

Formulation	Connection Type	Sample Size	Average	COV	Minimum	Maximum
-	-	-	(lbs.)	(%)	(lbs.)	(lbs.)
HDPE	Mode I_m	4	656	2.7	635	674
	Mode III_s	9	504	2.3	481	521
	Mode IV	10	617	2.9	594	640
PVC	Mode I_m	4	1992	3.9	1882	2055
	Mode III_s	10	2330	4.5	2170	2485
	Mode IV	10	2570	2.5	2503	2674

A connection that yields in Mode I_m is similar to a dowel bearing test in that the yielding occurs in only one member. No deformation was observed in the side members in either the PVC or the HDPE Mode I_m tests. Therefore, the load-displacement curve of the connection tests should be similar to the load-displacement curve of the dowel bearing test. In the HDPE Mode I_m connections, the initial slope was higher than the slope in the dowel bearing tests. In the PVC Mode I_m connections, initial slope was lower than the dowel bearing tests and the load did not drop off rapidly after the maximum load is reached as it did in the dowel bearing tests. A more ductile behavior was observed. Also, the load was not maintained smoothly due to brittleness of the PVC. It is speculated that additional load was sustained due to the confinement of the material caused by the side members. Even though no nuts were included on the end of the

bolts, the side members remained in contact with the main member throughout the tests. As the main member yielded, the out of plane deformation was restricted by the side members and thus the yield behavior of the member was altered. In Figure 5-13, confinement in both HDPE and PVC is clearly visible.

The Mode III_s and Mode IV tests produced expected results. The observed yield modes were Mode IIIs: Case 3-1 and Mode IV: Case 1-1. For Mode IIIs: Case 3-1, dowel rotation occurred in the side members in the walls farthest from the shear plane and dowel yielding occurred in the main member in the walls closest to the shear plane (Figure 5-15). For Mode IV: Case 1-1, dowel yielding occurred in the main and side members in the walls closest to the shear plane (Figure 5-16 and Figure 5-17). Determinations of the exact locations of dowel rotation and dowel yield were impossible due to the small displacement of the connection when yield occurred. All connection test pictures presented were taken at large displacements (> 0.4") and do not reflect connection behavior at yield. Additional dowel deformation within the void space and separation of the members occurred after maximum load was reached.

Maximum connection load data has been tabulated to enable the comparison of predicted maximum loads (Table 5-8).

Table 5-8: Connection Test Data Based on Maximum Load

Formulation	Connection Type	Sample Size	Average	COV	Minimum	Maximum
-	-	-	(lbs.)	(%)	(lbs.)	(lbs.)
HDPE	Mode I_m	4	669	1.9	652	679
	Mode III_s	9	635	1.9	618	653
	Mode IV	10	864	1.6	833	880
PVC	Mode I_m	4	1997	4.0	1884	2055
	Mode III_s	10	2394	1.9	2334	2485
	Mode IV	10	2858	2.4	2764	2960

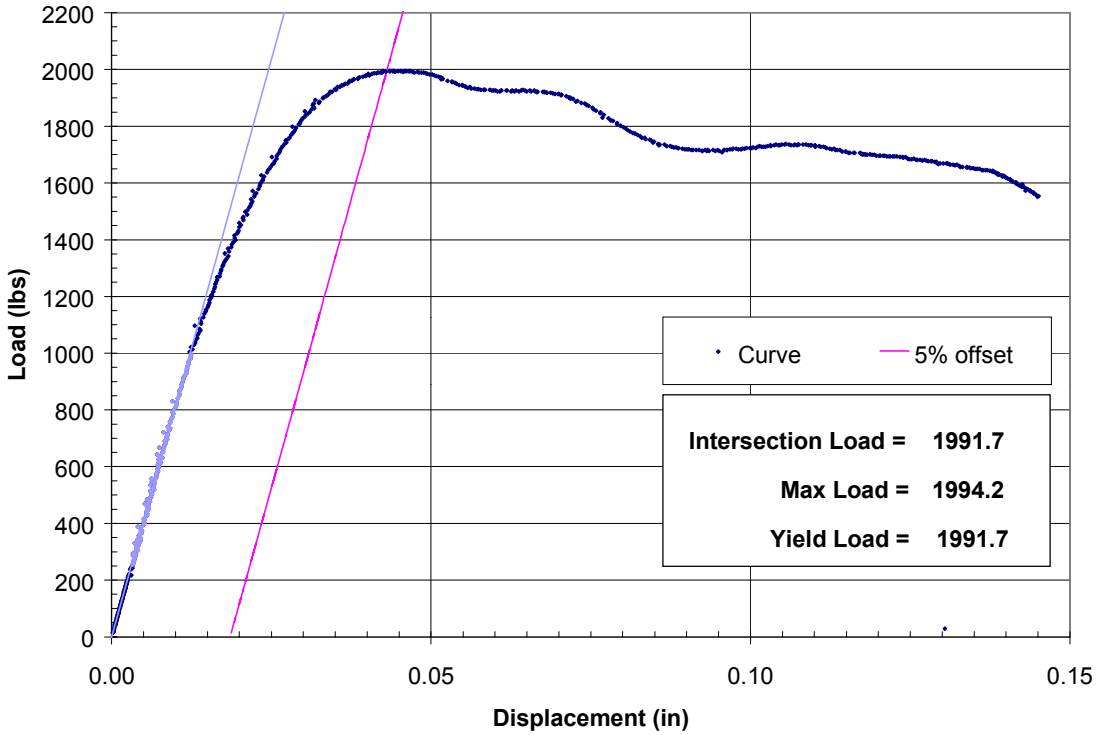

Figure 5-7: Typical load-displacement curve of Mode I_m connection test - PVC

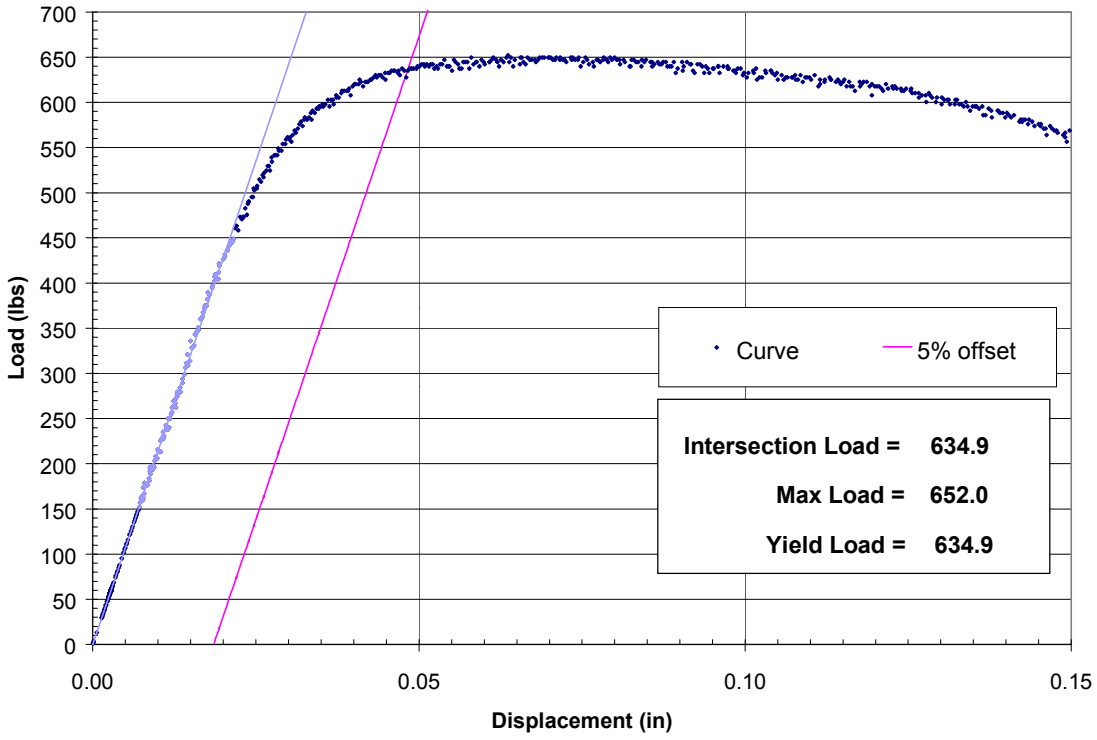

Figure 5-8: Typical load-displacement curve of Mode I_m connection test - HDPE

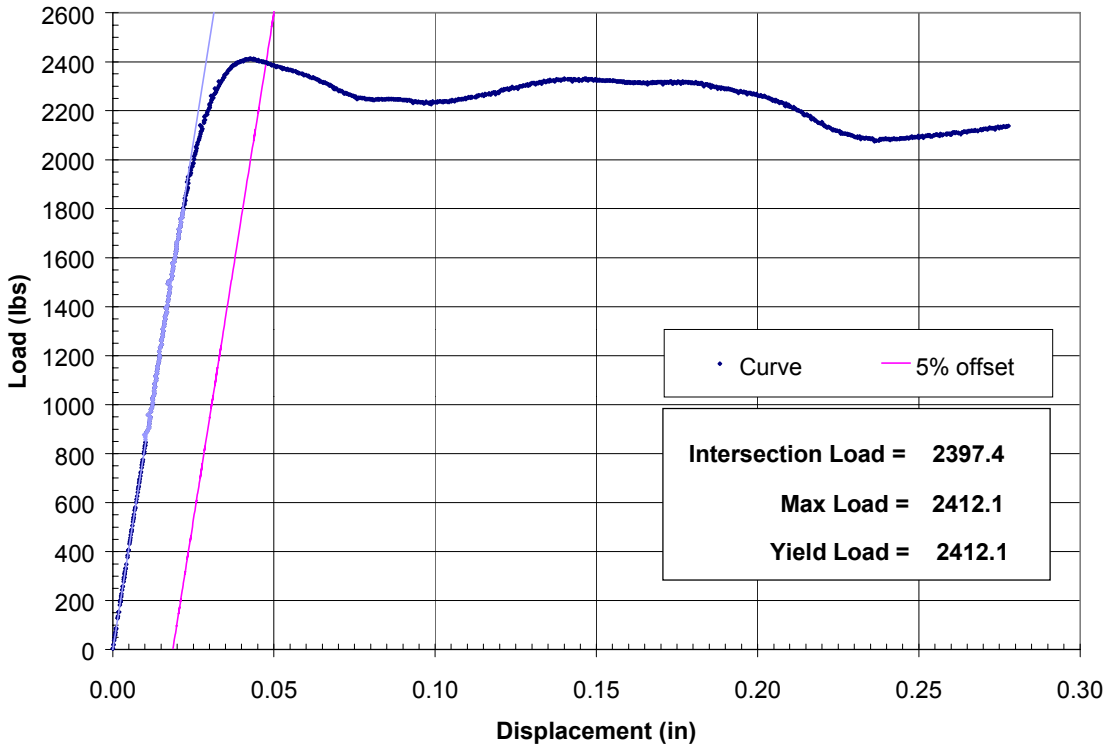

Figure 5-9: Typical load-displacement curve of Mode III_s connection test - PVC

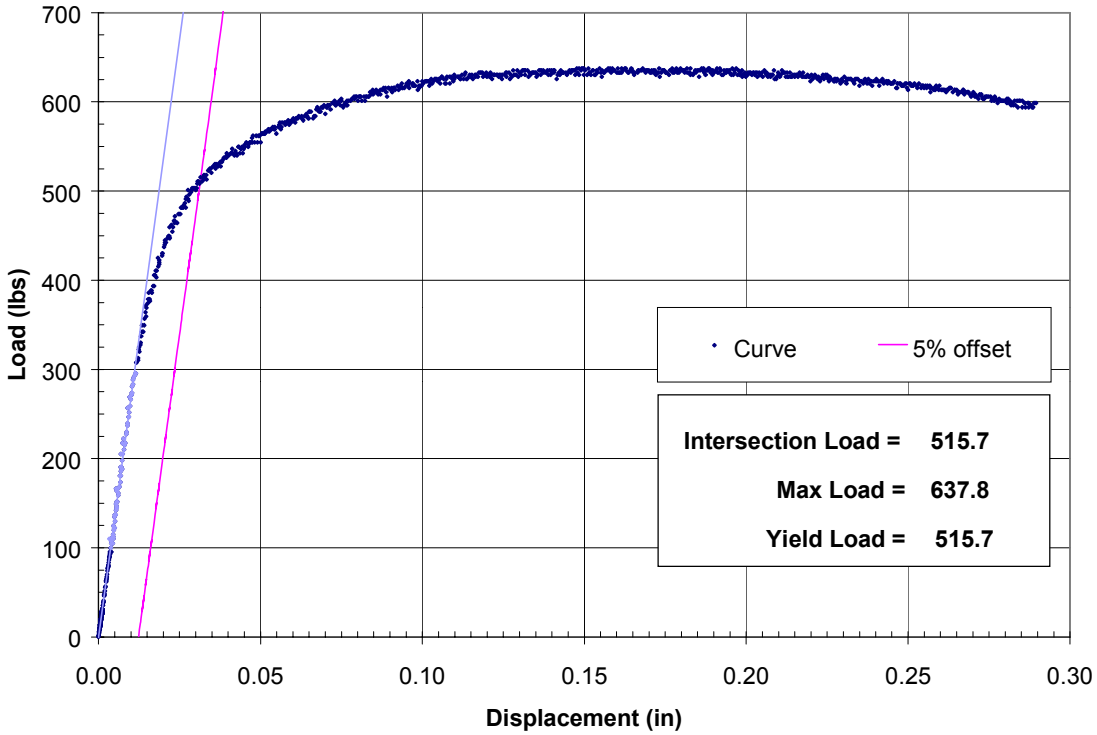

Figure 5-10: Typical load-displacement curve of Mode III_s connection test - HDPE

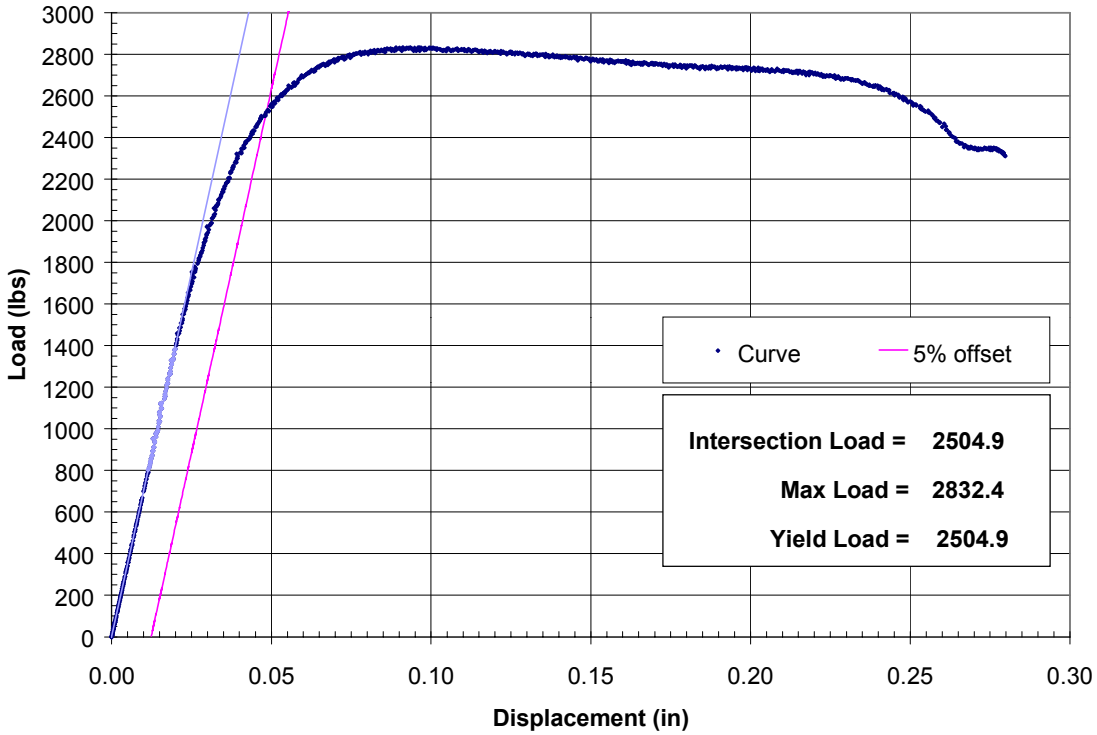

Figure 5-11: Typical load-displacement curve of Mode IV connection test – PVC

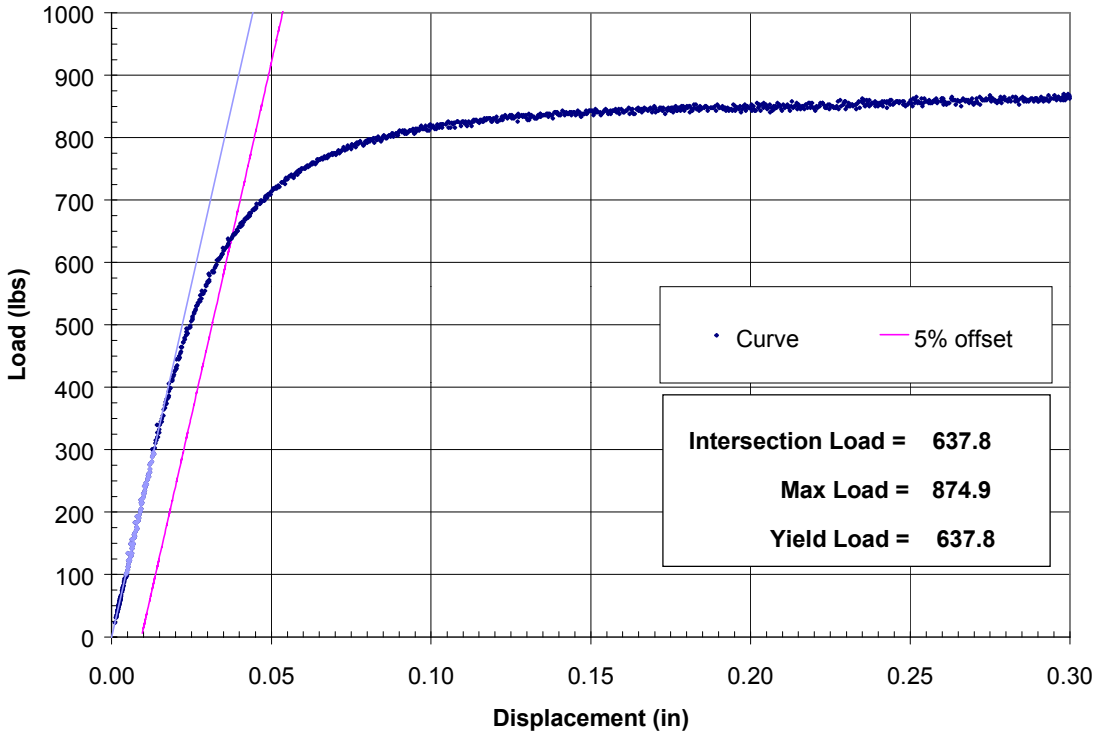

Figure 5-12: Typical load-displacement curve of Mode IV connection test – HDPE

a)  b) 

Figure 5-13: Confinement in Mode I_m connection tests a) HPDE b) PVC

a) 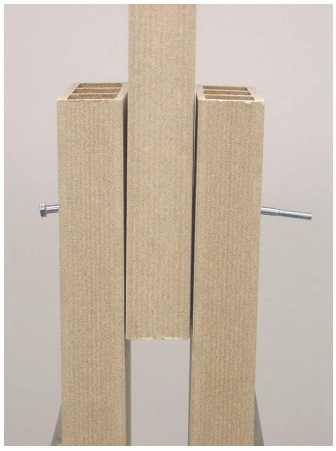 b) 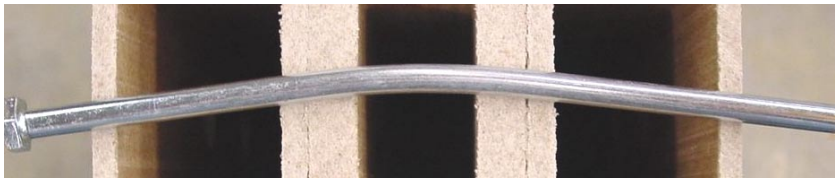

Figure 5-14: HDPE Mode III_s connections a) Entire connection
b) Approximate location of dowel and walls during testing

a) 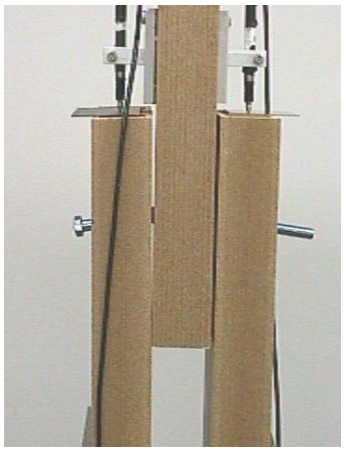 b) 

Figure 5-15: PVC Mode III_s connections a) Entire connection
b) Approximate location of dowel and walls during testing

a) 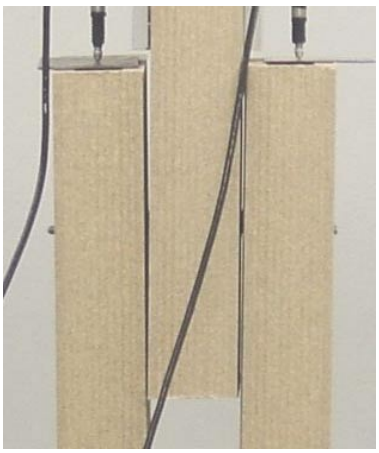 b) 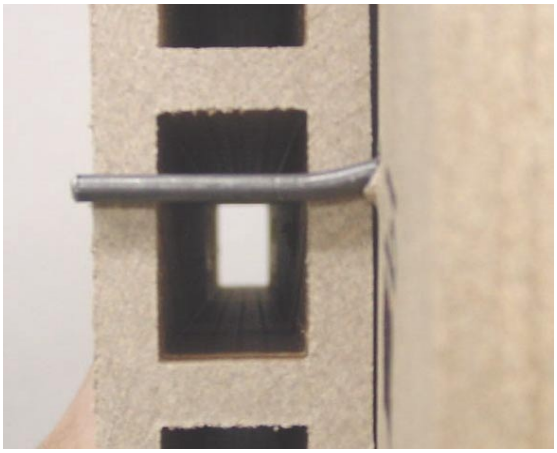

c) 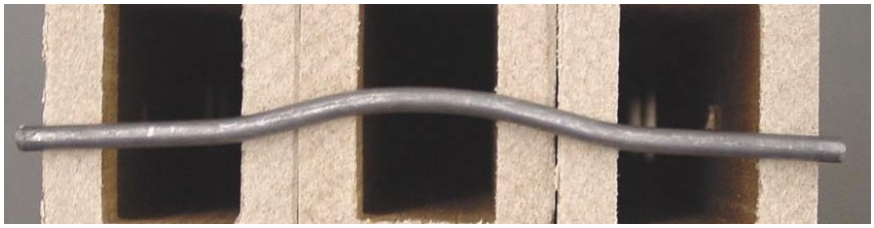

Figure 5-16: HDPE Mode IV connections a) Entire connection b) Location of dowel yielding in side member c) Approximate location of dowel and walls during testing

a) 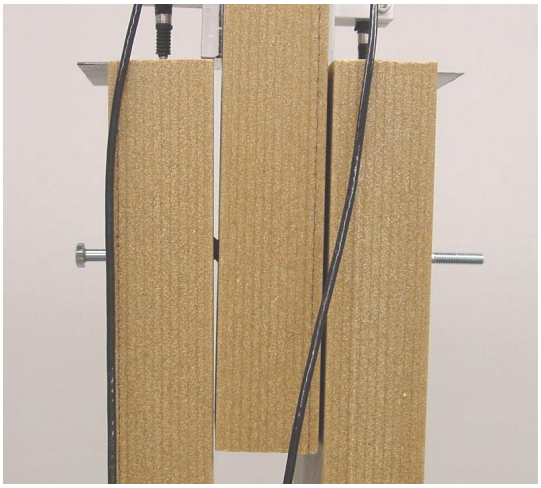 b) 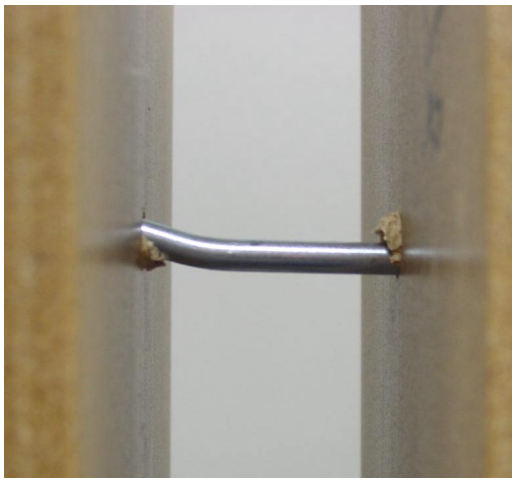

c) 

Figure 5-17: PVC Mode IV connections a) Entire connection b) Dowel yielding in side member c) Approximate location of dowel and walls during testing

Model Validation

Several approaches were used to validate the connection models developed in CHAPTER 3. First, the hollow section yield model was evaluated using the 5% diameter offset method to predict the yield point of the input parameters and the connection tests. Then, the maximum load of the input curves was used to predict maximum connection load. Finally, the load-displacement predicting equations were evaluated for Mode I_m, Mode III_s, and Mode IV.

Hollow Section Yield Model

When the hollow section yield model was evaluated on a 5% offset basis, the model prediction differed from the tested connection 5% offset value by an average of 14.7% (Table 5-9). The dowel bearing values from Table 5-1 and the bending yield strength values from Table 5-3 were used as model inputs. The HDPE Mode I_m 5% offset connection load was under-predicted. Whereas, the remainder of the 5% offset connection loads were over-predicted. The increase in the HDPE Mode I_m connection load has been attributed to confinement from the side members. The PVC Mode I_m connection results were not increased, but the shape of the load-displacement curve was modified. As noted earlier, the 5% offset method did not truly identify the yield point of the dowel bearing tests. Therefore, using the 5% offset method to define the yield point is not a correct assessment of validity of the hollow section yield model.

Table 5-9: Connection Test Results and Predicted Yield (5% offset based)

Yield Mode	HDPE			PVC		
	Predicted	Tested	Difference*	Predicted	Tested	Difference*
-	(lbs)	(lbs)	(%)	(lbs)	(lbs)	(%)
I_m	630	656	-3.9	2046	1992	2.7
III_s	654	504	29.7	2699	2330	15.8
IV	752	617	21.9	2936	2570	14.2
	HDPE average =		18.5	PVC average =		10.9

* Difference calculated by subtracting the predicted value from the test value and then dividing by the test value.

A maximum load basis is more appropriate as an unbiased method of validating the yield model for the WPC material used in this research. As noted earlier, the maximum load of the bending yield strength was defined as the stress in the dowel at maximum connection load. When the bending yield strength based on deflection at maximum connection load (Table 5-6) and maximum dowel bearing strength (Table 5-2) are used as input into the hollow section yield model, the predicted values differ from the maximum connection load values by an average of only 5.7% (Table 5-10).

Table 5-10: Connection Test Results and Predicted Yield (maximum load based dowel bearing strength and bending yield strength based on displacement at maximum connection load)

Yield Mode	HDPE			PVC		
	Predicted	Tested	Difference*	Predicted	Tested	Difference*
-	(lbs)	(lbs)	(%)	(lbs)	(lbs)	(%)
I_m	630	669	-5.9	2046	1997	2.4
III_s	669	635	5.3	2480	2394	3.6
IV	917	864	6.2	3161	2858	10.6
	HDPE average =		5.8	PVC average =		5.5

* Difference calculated by subtracting the predicted value from the test value and then dividing by the test value.

The difference between the predicted values and the tested values can be mainly attributed to variation of input parameters and testing anomalies. One model assumption that has not been accounted for is that the dowel loading is uniform along the length of the dowel. It is probable that this assumption is violated in actual connections and that the force on the dowel in the wall closest to the shear plane is higher than the force in the outside wall. This would explain why the yield model over-predicted the actual connection capacity in nearly every case. If the interior wall was carrying more load, then the yield load would be lower. However, the assumption that the dowel loading is uniform simplifies the model and allows for a close approximation of connection behavior.

Another model assumption violation that contributed to the difference between the predicted and actual connection loads was the assumption of perfect elastic/plastic materials. The load-displacement curves clearly show that neither the dowel bearing tests nor the bending yield tests behave as assumed. A derivative of the elastic/plastic material behavior assumption is that both the dowel and the members yield at the same time. This assumption was violated in the PVC connections. The brittle PVC formulation yielded much sooner than the dowels. A load-displacement model is one way of overcoming the elastic/plastic material behavior assumption.

The amount of error between the predicted and tested values of the hollow section yield is well within the range reported by Aune and Patton-Mallory (1986b) in their study of nailed connections. In that work, predicted loads and the Mode III connection loads varied by 6.5% and the Mode IV connection loads varied by 13%. McLain and Thangjitham (1984) evaluated several large data sets of bolted connection tests to validate their modification of the EYM. However, the performance of the unmodified EYM was also evaluated; the ratio of actual load to predicted load ranged from 0.90 to 1.32. When Balma (1999) validated the EYM for use in solid cross-sections of WPC, the EYM over-predicted connection capacity by an average of 14% using the 5% diameter offset to predict load. Using a maximum load basis, the EYM under-predicted connection capacity by an average of 5%.

Load-Displacement Yield Model

The load-displacement model inputs are curves fit to the dowel bearing resistance tests and the dowel bending yield tests. The dowel bearing resistance curves were fit over a displacement range of zero to 0.11 inches. The bending yield strength tests were fit over a displacement range of zero to 0.2 inches. Plots of all the dowel bearing resistance curves and the bending yield strength tests are located in APPENDIX F. The coefficients of the fit curves used in this research are given in Table 5-12.

A summary of the difference between the predicted load-displacement curve and the average of the connection tests was found using two methods (Table 5-11). An analysis was completed based on the absolute value of the percent error between the curves and another was based on the work done to a displacement of 0.11 inches. The percent error was calculated by computing the absolute value of the difference between the average connection load and the predicted load at each displacement (every 0.0005 inches) and then dividing by the average connection load at that displacement; the overall average for the entire curve was then calculated. The percent error method is a measure of how well the shape of the curves matched. The work done by the actual connection curves and predicted connection curves was calculated by finding the areas under the curves using the trapezoidal method at a width of 0.0005 inches. The connection work is relevant since the load-displacement behavior predicting equations could be used in energy-based design. Mode I_m equations under-predicted the work by an average of 4.7%, and the Mode IV and Mode III_s equations under-predicted the work by 7.6% and 13.2%, respectively.

Table 5-11: Difference between Connection Tests and Load-Displacement Model

Formulation	Connection Type	Absolute Percent Error	Work to a displacement of 0.11 inches		
			Actual	Predicted	Difference
-	-	(%)	(in-lbs)	(in-lbs)	(%)
HDPE	Mode I_m	18.8	537	532	-1.0
	Mode III_s	14.1	546	477	-12.6
	Mode IV	5.7	662	634	-4.1
PVC	Mode I_m	13.7	1724	1580	-8.4
	Mode III_s	16.3	2153	1857	-13.7
	Mode IV	13.0	2459	2189	-11.0
Average =		13.6			-8.5

The PVC Mode I_m prediction agreed well with the connection test curves (Figure 5-18). After the maximum load, the connection tests sustained higher loads than predicted. As stated earlier, this increase was probably due to the confinement effect of the side members. The

HDPE Mode I_m prediction varied significantly from the connection tests (Figure 5-19). The main difference was that the predicted curve had a higher slope than the connection tests. Another difference between the test data and predicted curve was the aforementioned behavior after maximum load was reached; the HDPE samples also demonstrated an increased ability to sustain load.

In the Mode III_s connections, the predicted load-displacement curves under-predicted the tests curves, but captured the shape of the curves well (Figure 5-20 and Figure 5-21). The same is true of the Mode IV results in the HDPE material only (Figure 5-23). The Mode IV PVC curve was incorrectly predicted (Figure 5-22). The initial slope is correctly predicted, but the predicted curve did not yield the same as the tested connections. In the predicted PVC Mode IV curve, the internal energy was heavily weighted toward the behavior of the dowel and only a small contribution was from the brittle PVC behavior causing the difference in yield prediction.

The predicted curves were sensitive to the locations of dowel yielding and dowel rotation (x_s and x_m). The equations for x_s and x_m from the yield model were used to produce the predicted curves found in Figure 5-20, Figure 5-21, Figure 5-22, and Figure 5-23 (Table 5-13). Excluding the PVC Mode IV tests, nearly exact predictions of the test data can be produced by varying the values of x_s and x_m from the theoretical values by a few hundredths of an inch. The model predictions, even with the simplifying assumptions, must have been close to the locations of dowel yielding and dowel rotation that occurred during connection testing.

The Mode IV connections were the only test groups that possessed a theoretical closed-form solution for the load-displacement relationship. However, due to the method used to enter the entire load-displacement behavior of the bending yield tests (Equation 3-9), no closed-form solution was found. The location of dowel yielding is needed to calculate the bending yield

moment at each point. Perhaps, if an alternative function was fit to the test data, a closed-form solution may be determined.

Table 5-12: Coefficients of Fitted Curves

Material Property		a (x^1)	b (x^2)	c (x^3)	d (x^4)	e (x^5)	f (x^6)
Bending Yield Strength	3/16" diameter	1213	14441	-535880	5301137	-22553205	35638685
	1/4" diameter	3328	70355	-1958282	17575455	-70005907	105108240
	3/8" diameter	16474	131273	-6447049	67910008	-299526836	485602196
HDPE Dowel Bearing	0.2"wall - 3/8"	68459	920060	-90879442	1730243488	-13616864344	39302347608
	0.2" wall - 1/4"	56619	384634	-64068237	1313230298	-10797582528	32209094319
	0.4" wall - 1/4"	42510	799332	-52486029	892993302	-6613914480	18389401291
	0.4" wall - 3/16"	37523	878236	-53685873	918546956	-6910183992	19608872585
PVC Dowel Bearing	0.2"wall - 3/8"	126180	5056329	-209742898	2442816519	-10460103167	10233129694
	0.4" wall - 3/8"	144381	5049568	-144743672	591130636	6739670299	-43400820401
	0.4" wall - 1/4"	105162	644097	38579662	-2098284246	24679590411	-89389626203

Table 5-13: Locations used to validate load-displacement model

Connection Type	xs	xm
-	(inches)	(inches)
Mode IIIs (HDPE)	1.74	0.25
Mode IIIs (PVC)	1.73	0.2
Mode IV (HDPE)	0.32	0.32
Mode IV (PVC)	0.296	0.296

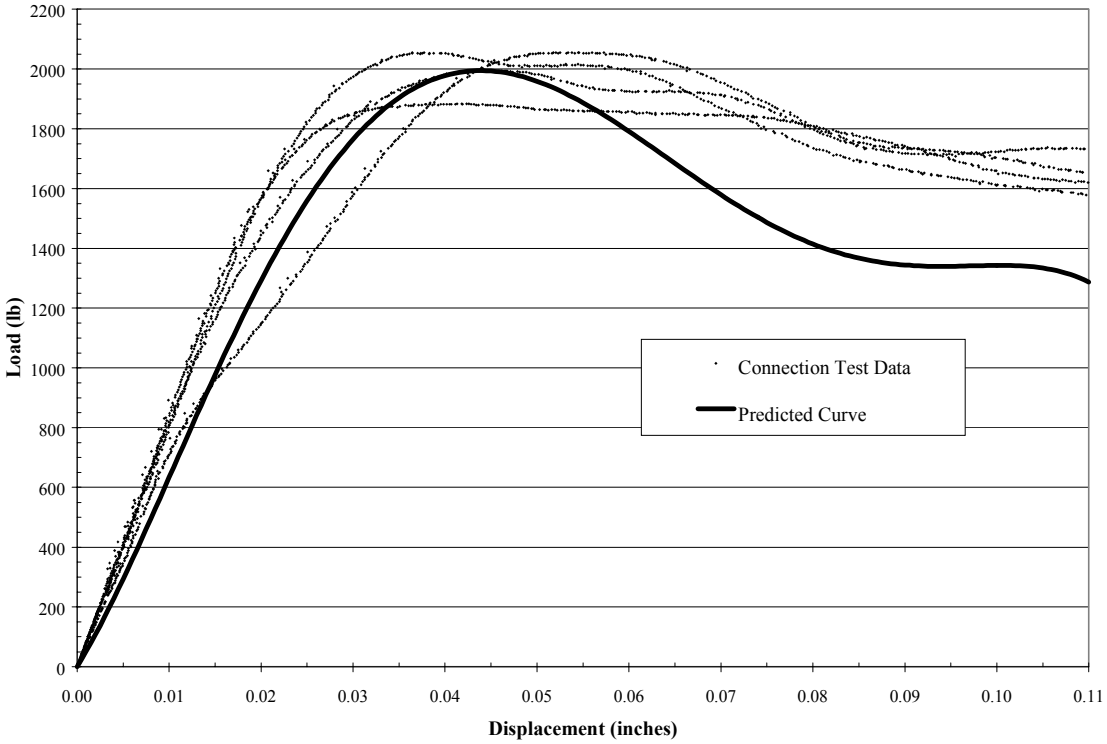

Figure 5-18: PVC Mode I_m Connection Tests with Predicted Curve

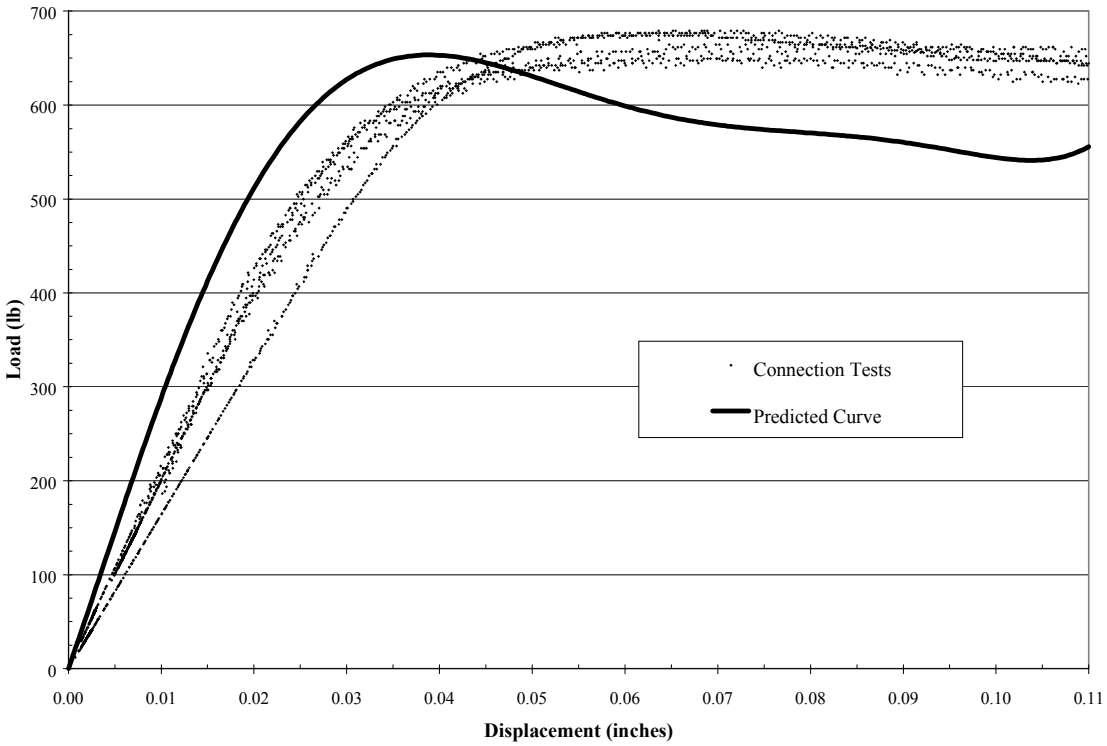

Figure 5-19: HDPE Mode I_m Connection Tests with Predicted Curve

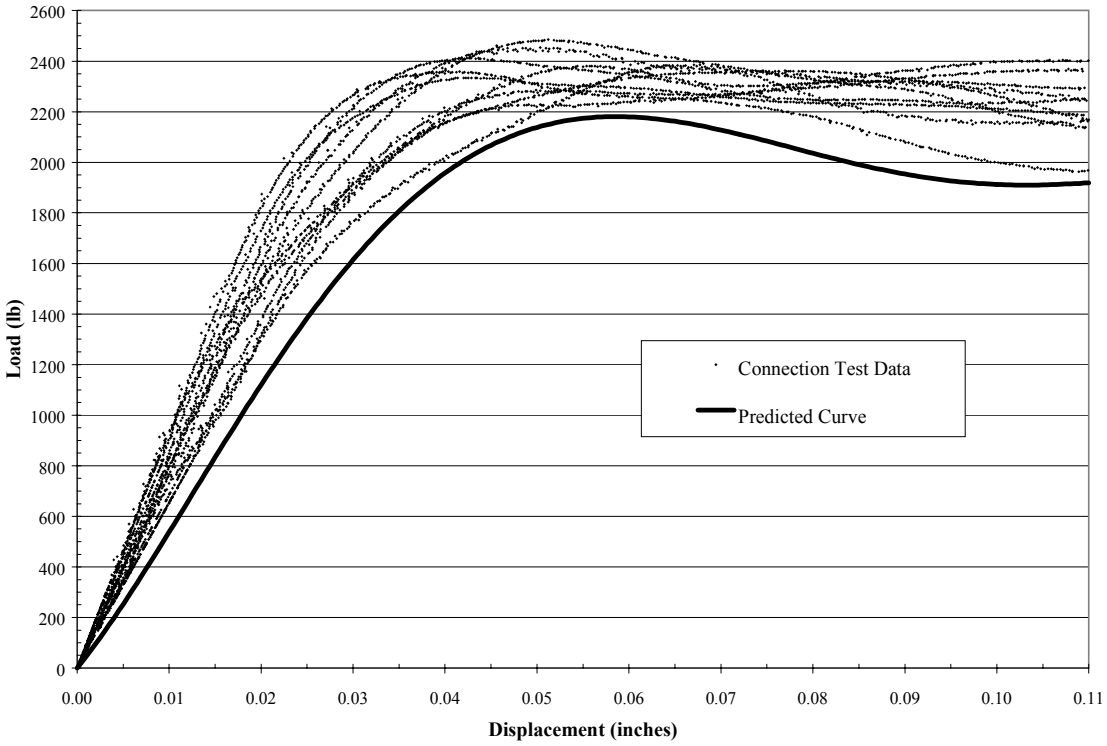

Figure 5-20: PVC Mode III_s Connection Tests with Predicted Curve

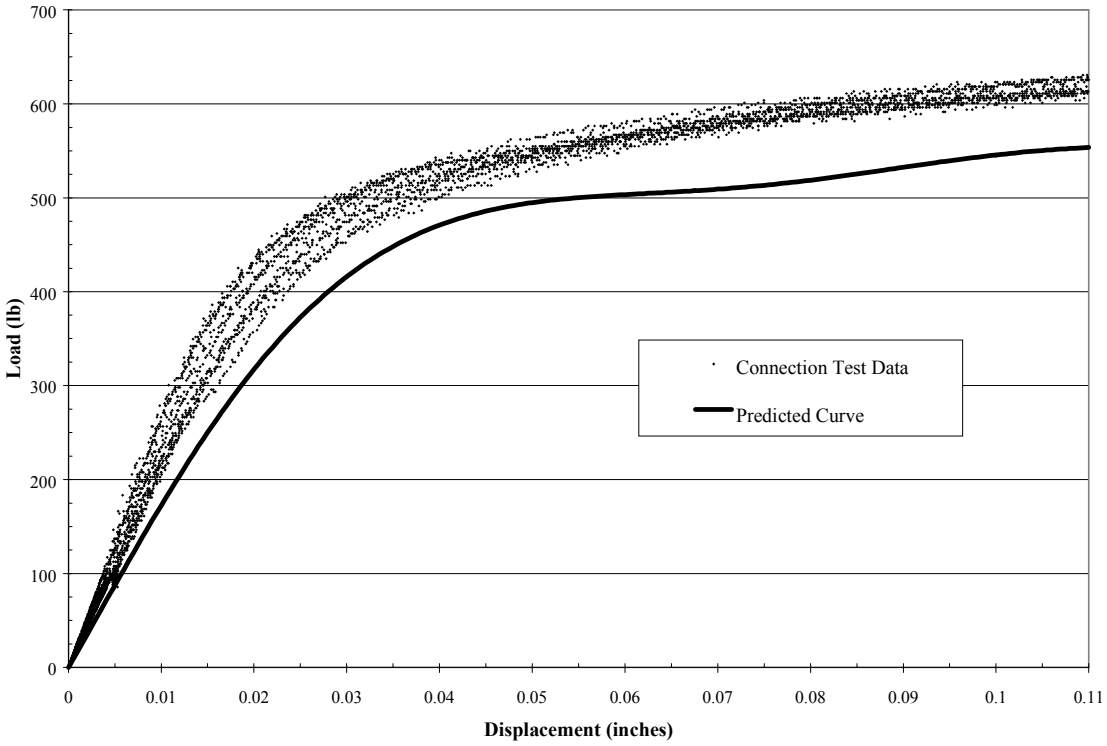

Figure 5-21: HDPE Mode III_s Connection Tests with Predicted Curve

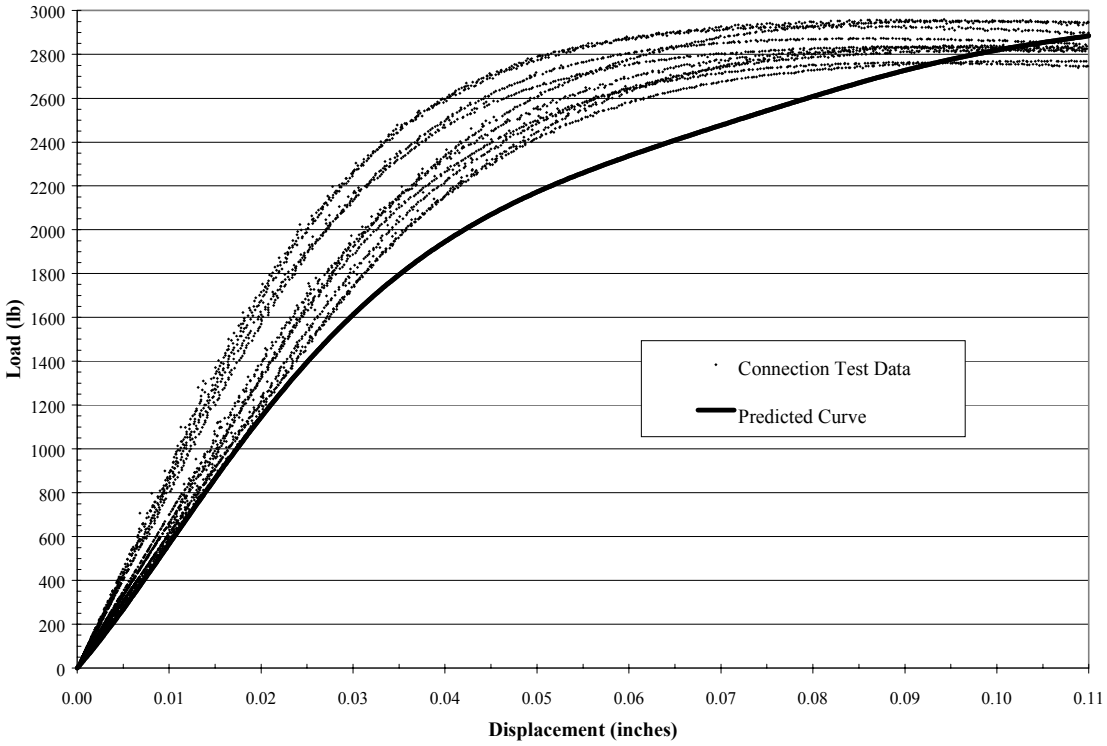

Figure 5-22: PVC Mode IV Connection Tests with Predicted Curves

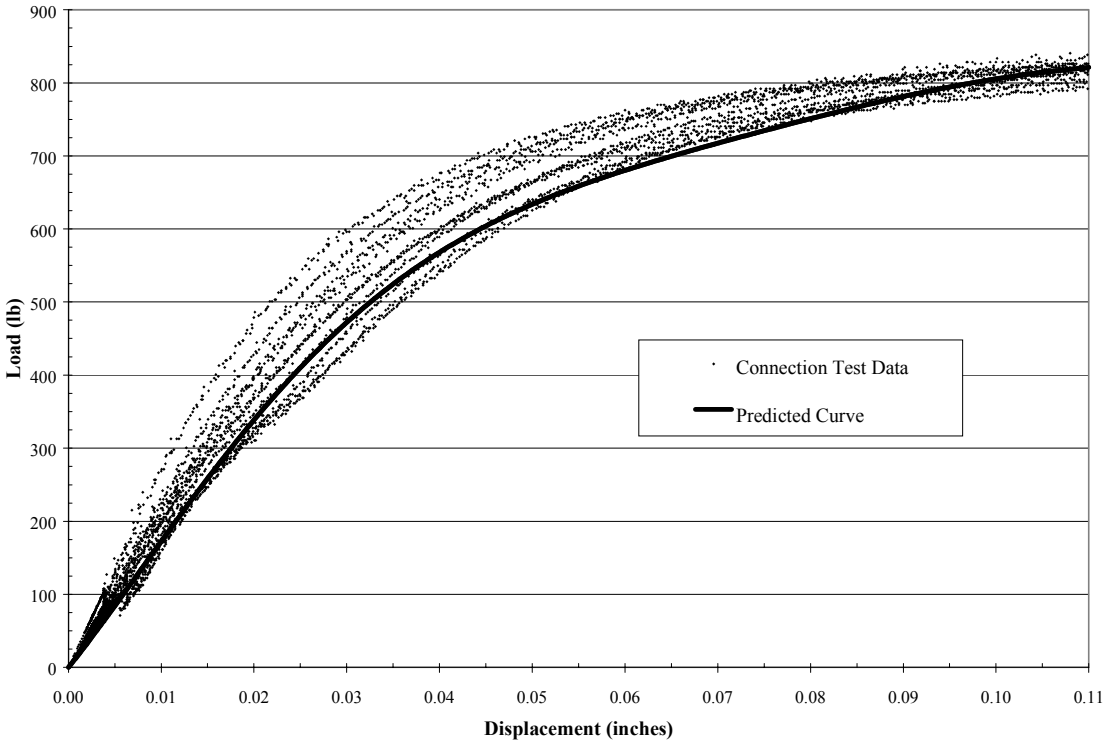

Figure 5-23: HDPE Mode IV Connection Tests with Predicted Curves

Load-Displacement Model Sensitivity

The sensitivities of the Mode III_s and Mode IV load-displacement equations were studied by varying the input parameters. The three input parameters are the bearing resistance of the main and side members and the bending yield strength for the dowel. Each parameter was systematically varied to determine their effect on the load-displacement predictions while the remaining input parameters were held constant. The results of model sensitivity study are given in Table 5-14; the tabulated percent difference values is the percent difference between the original predicted curves and the curve predicted with the increased parameter. Any manipulation of the coefficients of the fit curves results in a linear change in the error. The results of increasing the coefficients by 10% are shown.

The Mode III_s results were as expected – i.e., changing the dowel bearing strength of the side member had the most effect on the load-displacement behavior, followed by the bending strength of the dowel, and the strength of the main member. Changing the main member dowel bearing strength had little effect on the load-displacement behavior. Also, the dowel bearing strengths of the members had less effect in the stronger, stiffer PVC formulation than it did in the more ductile HDPE formulation.

For the Mode IV sensitivity study, the connections with the same side member and main member were used. Therefore, only one set of dowel resistance coefficients was used and the location of dowel rotation (x) is the same in both members. As expected, the load-displacement model is more sensitive to strength of the bending yield strength than the bearing resistance of the members. Also, similar to the Mode III_s, the bending yield strength had more of effect in the stiffer PVC formulation than the ductile HDPE formulation.

Table 5-14: Results of Model Sensitivity Study

Yield Mode	Formulation	Material Property	Increase in Property	Difference from Unmodified Predicted Curve	
				Absolute Error Based	Work Based
-	-	-	(%)	(%)	(%)
Mode III_s	HDPE	f_{es}	10	7.6	7.4
		f_{em}	10	0.14	0.15
		M_y	10	2.3	2.5
	PVC	f_{es}	10	7.4	7.3
		f_{em}	10	0.08	0.08
		M_y	10	2.5	2.6
Mode IV	HDPE	f_e	10	3.4	3.6
		M_y	10	6.6	6.4
	PVC	f_e	10	2.9	3.2
		M_y	10	7.1	6.8

The sensitivity of the load-displacement equations to the locations of dowel yielding and dowel rotation (x_s and x_m) was also investigated using the formulations and cross-sections of this research (Table 5-15, Table 5-16, and Table 5-17). The entire range of valid values for x_s and x_m in each yield mode were investigated. For Mode III_s: Case 3-1, decreasing x_s and x_m from the theoretical value resulted in increasing the connection work. Increasing x_s and x_m from the theoretical value resulted in a decrease in connection work. Additionally, the movement of x_m had a larger effect than the movement of x_s. The same results were observed in both the HDPE and the PVC formulation. For Mode IV: Case 1-1, decreasing the location of yielding, x, resulted in an increase in the work. Decreasing x by 30% results in a increase in work of nearly 100% in HDPE and nearly 75% in PVC. Predicting the location of dowel yield and dowel rotation is critical to predicting the correct load-displacement behavior.

Table 5-15: Sensitivity of Mode III_s to the location of dowel rotation (x_s)

Formulation	x_s	Change in x_s	Difference from Unmodified Predicted Curve	
			Absolute Error Based	Work Based
-	(inches)	(%)	(%)	(%)
HDPE: theoretical x_s = 1.74"	1.60	-8.0	2.7	3.3
	1.65	-5.2	1.3	1.7
	1.70	-2.3	0.4	0.6
	1.75	0.6	-0.1	-0.1
	1.80	3.4	-0.2	-0.4
PVC: theoretical x_s = 1.73"	1.60	-7.5	2.7	3.1
	1.65	-4.6	1.4	1.6
	1.70	-1.7	0.4	0.5
	1.75	1.2	-0.2	-0.3
	1.80	4.0	-0.6	-0.7

Table 5-16: Sensitivity of Mode III_s to the location of dowel yielding (x_m)

Formulation	x_m	Change in x_m	Difference from Unmodified Predicted Curve	
			Absolute Error Based	Work Based
-	(inches)	(%)	(%)	(%)
HDPE: theoretical x_m = 0.25	0.00	-100.0	18.2	16.5
	0.10	-60.0	9.7	8.8
	0.20	-20.0	2.8	2.5
	0.30	20.0	-2.4	-2.1
	0.40	60.0	-5.8	-4.8
PVC: theoretical x_m = 0.20"	0.00	-100.0	14.2	12.2
	0.10	-50.0	6.4	5.4
	0.20	0.0	0.0	0.0
	0.30	50.0	-4.6	-3.8
	0.40	100.0	-7.3	-5.7

Table 5-17: Sensitivity of Mode IV to the location of dowel yielding (x)

Formulation	x	Change in x	Difference from Unmodified Predicted Curve	
			Absolute Error Based	Work Based
-	(inches)	(%)	(%)	(%)
HDPE: theoretical x = 0.32"	0.10	-68.8	86784.9	117838.6
	0.20	-37.5	93.4	98.6
	0.30	-6.3	4.2	3.2
	0.40	25.0	-9.8	-7.3
PVC: theoretical x = 0.296"	0.10	-66.2	66224.8	91352.9
	0.20	-32.4	72.6	74.0
	0.30	1.4	-0.9	-0.7
	0.40	35.1	6.0	9.5

Design Procedures for Connections with Hollow Members

The hollow section yield model was validated using a maximum load basis that included the theoretical stress in the dowel at maximum connection load. This procedure was necessary to demonstrate the validity of the yield model, however it is impractical for design use. Design engineers will not know the displacement at maximum connection load. Therefore, for use in design, the 5% diameter offset method was used to define yield in the bending yield strength tests. The bending yield strengths codified for use in timber design could be utilized in the design of hollow sections. WPC hollow section design would differ from timber design in that the design basis would be maximum connection load rather than 5% offset yield load. This basis was necessary because of the difficulty defining yield in WPC dowel bearing tests. Any additional offset method used to determine yield was arbitrary and specific to a WPC formulation. Working on a maximum load basis was an unbiased method of quantifying dowel bearing strength. For the connections in this research, the predicted maximum load calculated using the 5% diameter offset method to calculate the bending yield strength and the maximum dowel bearing strength differed from the actual maximum connection capacity by an average of 6.1% (Table 5-18).

Table 5-18: Connection Test Results and Predicted Yield (maximum load based dowel bearing strength and bending yield strength based on 5% diameter offset method)

Yield Mode	HDPE			PVC		
	Predicted	Tested	Difference*	Predicted	Tested	Difference*
-	(lbs)	(lbs)	(%)	(lbs)	(lbs)	(%)
I_m	630	669	-5.9	2046	1997	2.4
III_s	657	635	3.3	2699	2394	12.7
IV	781	864	-9.6	2936	2858	2.7
	HDPE average =		6.3	PVC average =		6.0

* Difference calculated by subtracting the predicted value from the test value and then dividing by the test value.

CHAPTER 6: SUMMARY AND CONCLUSIONS

Summary

Current timber connection design in the U.S. is based on the European Yield Model (EYM). The basis of the EYM was published by Johansen in 1949 and has been codified in the U.S. since 1991 for timber connections with members of solid cross-section. Many wood-plastic composite members are extruded in hollow cross-sections. No design methodology exists for connections with hollow members. The goal of this research was to develop an EYM-based method of predicting connection capacity in hollow sections and validate with experimental testing. Additionally, a method of predicting the entire load-displacement behavior of a connection with hollow members was desired for use in energy-based design and deformation calculations.

Expressions for the yield load of lateral connections in single and double shear were derived using the virtual work concept. Each member was assumed to have two walls of equal thickness and dowel bearing strength, separated by voids. A hollow section yield model, consisting of 18 single-shear equations, was derived by considering all the possible locations of dowel hinge formation and dowel rotation. A computer program was used to evaluate the equations over a reasonable range of input parameters and cross-section geometries. Only six single-shear equations were found to govern the connection behavior, and they reduced into a practical design format.

The model for predicting load-displacement behavior of connections with hollow members was derived for the six controlling modes and cases of the hollow section yield model. The Mode I_s and I_m load-displacement model equations are simply the curves fit to the dowel resistance data multiplied by the sum of the wall thicknesses. Modes II, III, and IV utilize the

method of virtual displacements. A closed-form of the solution was impractical due to the number of terms introduced by the hollow members. Therefore, the load-displacement equations require the calculation of the locations of dowel yielding and dowel rotation based on expressions from the hollow section yield model. Five general contributions to internal energy were defined and equations were derived for each energy component. A general expression was developed for the energy associated with the four types of material crushing. The load-displacement behavior of the predicted yield mode of a connection was found by adding the relevant internal energy terms and dividing by the connection displacement.

The models were validated by conducting double-shear unconstrained bolted connection tests using two wood-plastic composite formulations, three wall thicknesses, and three dowel diameters. Input parameters were quantified through dowel bearing tests and bending yield strength tests for each combination of WPC formulation, wall thickness, and dowel diameter. The dowel bearing strength of the members, bending yield strength of the dowel, and the connection dimensions were need as input for the hollow section yield model. Sixth-order polynomial functions (restricted to pass through the origin) were fit to the dowel resistance curves and bending yield strength data as input for the load-displacement behavior model.

The COVs of all the test groups were low due to the uniformity of the WPC material and all the dowels originated from the same manufacturing lot. The COV of the connection tests ranged from 1.6% to 4.5%. The COV of the dowel bearing tests ranged from 1.0% to 4.1%. The COV of the bending yield strength tests ranged from 1.1% to 6.4%. The relatively higher COV of the bending yield strength data was due to the 3/16” diameter dowels being cut from more than one steel rod.

The hollow section yield model was evaluated using several methods of interpreting the test data. The standard timber method of defining yield using the 5% offset produced an average percent difference between the yield point of the connection test and the predicted yield load of 14.7%. However, the dowel bearing deformation behavior of the WPC material was such that yield point from the 5% offset method did not coincide with the sample yielding. The hollow section yield model was then evaluated on a maximum load basis. The maximum connection loads were compared to the theoretical load calculated by entering the dowel bearing strength based on maximum load and a bending yield strength based on the stress in the dowel at the displacement of maximum connection load. Using this maximum load basis, the average percent difference between the theoretical maximum load and tested maximum load was 5.7%.

The load-displacement behavior model was validated by comparing the percent difference between the predicted curve and the average of the connection tests and by comparing the work of the connections to a displacement of 0.11 inches. A work analysis was deemed more useful since a primary use of the load-displacement model would be energy design. The Mode I_m prediction performed best by under-predicting the work by an average of 4.7%. The Mode IV and Mode III_s equations under-predicted the work by an average of 7.6% and 13.2 %, respectively.

The Mode I_m load-displacement curve predictions should have been nearly identical to the average of the dowel bearing tests. The major difference in the HDPE Mode I_m was the poor prediction of the initial slope. Both the HDPE and PVC connection showed an improved ability to sustain load after reaching maximum; this is likely due to the material confinement caused by the side members.

Both the HDPE and PVC Mode III_s predicted load-displacement curves under-predicted the tests curves, but captured the shape of the curves well. The HDPE Mode IV predicted the test curves well by both capturing the initial slope and general curve shape. The PVC Mode IV test curves were predicted poorly. All Mode III_s and Mode IV predicted curves were sensitive to the location of the dowel rotation and dowel yielding that was input. Every Mode III_s and Mode IV predicted curve could be fit to the test curves by slightly modifying the location of dowel rotation and dowel yielding. The theoretical location of the dowel rotation and dowel yielding may not have occurred during the connection testing due to the violation of the model assumptions or experimental error.

For design purposes, using the maximum dowel bearing strength and 5% offset bending yield strength to predict maximum connection capacity achieved satisfactory results by predicting the maximum load within an average of 6%.

Conclusions

1. A hollow section yield model was derived, reduced to a usable allowable stress design format, and validated through the laboratory testing of Mode I_m, Mode III_s, and Mode IV connections in two wood-plastic composite formulations.
    - The predictions of the hollow section yield model differed from the connection test data by an average of 5.7% (maximum load basis).
    - The 5% offset method was an inappropriate method of defining yield in the two WPC formulation studied. Therefore, maximum dowel bearing strength should be used in design for maximum connection capacity.
    - The 5% diameter offset method should be used to design for maximum connection capacity instead of the maximum bending yield strength.

- Confinement of the member material resulted the Mode I_m connections performing more ductilely than the dowel bearing tests.

2. A method of predicting the load-displacement behavior of dowel-type connections using hollow sections was developed, reduced to a usable format, and validated through the laboratory testing of Mode I_m, Mode III_s, and Mode IV connections in two wood-plastic composite formulations.
   - The work done by the connection tests was under-predicted by an average of 8.5%.
   - The shapes of the predicted curves were similar to the connection tests curves. The average percent difference between the curves was 13.6%.
   - The load-displacement model is sensitive to the locations of dowel rotation and dowel yielding.
   - The virtual displacement model provides a straightforward derivation method for the load-displacement behavior of connections that could be used in energy-based design methods.
3. Dowel bearing strength tests should be conducted on each WPC formulation and cross-section geometry before evaluating connection performance.
   - Dowel bearing strength varied significantly within a wood-plastic composite formulation as the wall thickness changed.
   - Dowel bearing strength varied significantly within each wall thickness as the dowel diameter changed.

Suggestions for Further Research

1. Validate the hollow section yield model with additional materials and cross-sections. Include connections where the main and side member have substantially different dowel bearing behaviors and additional types of structural composites (more formulations and traditional timber composites like oriented strand board). Conduct connection tests of connections between hollow members and solid members (i.e. structural insulated panels). Conduct tests and evaluate the models with other types of fasteners such as screws and nails.
2. Rederive hollow section yield model and load-displacement model using alternative function types fit to dowel bearing tests and bending yield tests. Other types of functions may enable prediction of the load-displacement curve to a larger displacement or produce a closed-form solution.
3. Predict the load-displacement behavior of timber connections (solid cross-section) using the concepts utilized in this research.
4. Change the initial assumptions of the hollow section problem and derive an expanded hollow section yield model. Incorporate more than two walls and vary the dowel bearing strength of the walls.
5. Investigate the variability in dowel bearing strength over a large range of dowel diameters.
6. Evaluate hollow sections for such parameters as end spacing, edge spacing, and multiple fasteners.

REFERENCES

American Forest & Paper Association. 1999. General dowel equations for calculating lateral connection values. Technical Report 12. Washington, D.C.

American Forest & Paper Association. 1997. National design specification for wood construction. AF&PA. Washington, D.C.

American Society for Testing and Materials. 1997. Standard practice for conditioning plastics for testing. ASTM D618-96. ASTM. Philadelphia, PA.

American Society for Testing and Materials. 1997. Standard test method for bearing strength of plastics. ASTM D953-95. ASTM. Philadelphia, PA.

American Society for Testing and Materials. 1997. Standard test method for determining bending yield moment of nails. ASTM D1575-95. ASTM. Philadelphia, PA.

American Society for Testing and Materials. 1997. Standard test methods for mechanical fasteners in wood. ASTM D1761-88. ASTM. Philadelphia, PA.

American Society for Testing and Materials. 1997. Standard Practice for evaluating allowable properties for grades of structural lumber. ASTM D2915-94. ASTM. Philadelphia, PA.

American Society for Testing and Materials. 1999. Standard specification for evaluation of structural composite lumber products. ASTM D5456-98a. ASTM. Philadelphia, PA.

American Society for Testing and Materials. 1997. Standard test methods for bolted connections in wood and wood-base products. ASTM D5652-97. ASTM. Philadelphia, PA.

American Society for Testing and Materials. 1997. Standard test method for evaluating dowel-bearing strength of wood and wood-base products. ASTM D5764-97. ASTM. Philadelphia, PA.

American Society for Testing and Materials. 1997. Standard test methods for mechanical fasteners in plastic lumber and shapes. ASTM D6117-97. ASTM. Philadelphia, PA.

Aune, P. and M. Patton-Mallory. 1986a. Lateral load-bearing capacity of nailed joints based on the yield theory: theoretical development. Research Paper FPL 469. USDA, Forest Service, Forest Products Laboratory, Madison, WI.

Aune, P. and M. Patton-Mallory. 1986b. Lateral load-bearing capacity of nailed joints based on the yield theory: experimental verification. Research Paper FPL 470. USDA, Forest Service, Forest Products Laboratory, Madison, WI.

Balma, D. A. 1999. Evaluation of bolted connections in wood plastic composites. Masters Thesis, Washington State University. Pullman, WA.

Bilunas, N. J. 2000. Diaphragm behavior of structural insulated panels. Masters Thesis, Washington State University. Pullman, WA.

Foschi, R.O. 1974. Load-slip characteristics of nails. Wood Science. 7(1):69-76.

Foschi, R.O. and T. Bonac. 1977. Load-slip characteristics of connections with common nails. Wood Science. 9(3):118-123.

Johansen, K. W. 1949. Theory of timber connections. International Association for Bridge and Structural Engineering 9:249-262. Zurich, Switzerland.

Johnson, E. and F. Woeste. 1999. Connection design methodology for structural composite lumber. Wood Design Focus. Winter 1999.

Kuenzi, E.W. 1955. Theoretical design of a nailed or bolted joint under lateral load. Report 1951, Forest Products Lab, Madison, WI.

McLain, T.E. and S. Thangjitham. 1983. Bolted wood-joint yield model. ASCE Journal of Structural Engineering. 109(8):1820-1835.

Patton-Mallory, M., F.W. Smith, and P.J. Pellicane. 1998. Modeling bolted connections in wood: a three-dimensional finite-element approach. Journal of Testing and Evaluation. 26(2):115-124.

Patton-Mallory, M., P.J. Pellicane, and F.W. Smith. 1998. Qualitative assessment of failure in bolted connections: maximum stress criterion. Journal of Testing and Evaluation. 26(5):498-505.

Pellicane, P.J., J.L. Stone, and M.D. Vanderbilt. 1991. Generalized model for lateral load slip of nailed joints. Journal of Materials in Civil Engineering. 3(1):60-77.

Peyer, S.M. 1995. Lateral resistance of a plywood-to-wood nailed connection at elevated temperatures. Masters Thesis, University of Wisconsin, Madison, WI.

Soltis, L.A. and T.L. Wilkinson. 1987. Bolted connection design. General Technical Report FPL-GTR-54. U.S. Department of Agriculture. Forest Service. Forest Products Laboratory, Madison, WI.

Sá Ribeiro, R.A. and P.J. Pellicane. 1992. Modeling load-slip behavior of nailed joints. Journal of Materials in Civil Engineering. 4(4):385-397.

Theilen, R.D., D.A. Bender, D.G. Pollock, and S.G. Winistorfer. 1998. Lateral resistance of ring-shank nail connections in southern pine lumber. Transactions of the ASAE 41(2):465-472.

Wilkinson, T.L. 1971. Theoretical lateral resistance of nailed joints. Journal of the Structural Division-Proceedings of ASCE. 97(5):1381-1398.

Wilkinson, T.L. 1972. Analysis of nailed joints with dissimilar members. Journal of the Structural Division-Proceedings of ASCE. 98(9):20005-2013.

Wilkinson, T.L. 1978. Strength of bolted wood joints with various ratios of member thicknesses. Research Paper FPL 314. U.S. Department of Agriculture. Forest Service. Forest Products Laboratory, Madison, WI.

Wilkinson, T.L. 1991. Dowel bearing strength. Research Paper FPL-RP-505. U.S. Department of Agriculture. Forest Service. Forest Products Laboratory, Madison, WI.

APPENDIX A: DERIVATION OF EYM EQUATIONS – STATIC EQUILIBRIUM BASED

Overview

This appendix outlines the static equilibrium-based derivation of the European Yield Model (EYM). A partial derivation using these same procedures is outlined in American Forest & Paper Association's Technical Report 12 (1999). The EYM equations predict connection yield load based on its geometry, dowel bearing strength, and bending yield strength. The EYM uses six possible yield modes for single shear connections and four yield modes for double shear connections. The connection yield load is reached when either the compressive yield load of the member under the dowel is reached or when one or more plastic hinges forms in the dowel. Using simplifying assumptions and static equilibrium of the dowel, a general expression of the lateral yield load of each mode was derived. For a specific connection, the general equation with the lowest value controls the design.

Description of Modes

Table A-1: Yield modes

Yield Mode	Description of Failure	Applicable Connection Type
I_m	Main member bearing	Both single and double shear
I_s	Side member bearing	Both single and double shear
II	Main and side member bearing	Only single shear
III_m	Main member bearing, Dowel yielding in side member	Only single shear
III_s	Side member bearing, Dowel yielding in main member	Both single and double shear
IV	Dowel yielding in main and side member	Both single and double shear

Assumptions

- End fixity of the dowel is ignored.
- Tension forces in the dowel are ignored.
- Friction between the members is ignored

- Dowel loading is assumed to be uniformly distributed and perpendicular to the axis of the dowel.
- Perfect elastic/plastic behavior of all materials is assumed.

Input Parameters

The only necessary input parameters deal with connection geometry and material strengths as follows:

Table A-2: Input Parameters

Parameter	Description
l_s	Side member dowel bearing length, in
l_m	Main member dowel bearing length, in
g	Gap between members, in
D	Dowel diameter, in
F_{es}	Side member dowel-bearing strength, psi
F_{em}	Main member dowel-bearing strength, psi
F_b	Dowel bending strength, psi

The input parameters are used to calculate distributed loads and moments on the dowel:

Table A-3: Derivation Parameters

Parameter	Description
q_s	Side member dowel-bearing resistance, lbs/in
q_m	Main member dowel-bearing resistance, lbs/in
M_s	Side member dowel moment resistance, in-lbs
M_m	Main member dowel moment resistance, in-lbs
D_s	Dowel diameter at max. stress in side member, in
D_m	Dowel diameter at max. stress in main member, in

The above parameters can be calculated in the following manner:

$$q_s = F_{es}D \qquad q_m = F_{em}D$$

$$M_s = F_b\left(\frac{D_s^3}{6}\right) \qquad M_m = F_b\left(\frac{D_m^3}{6}\right)$$

General Dowel Loading Conditions

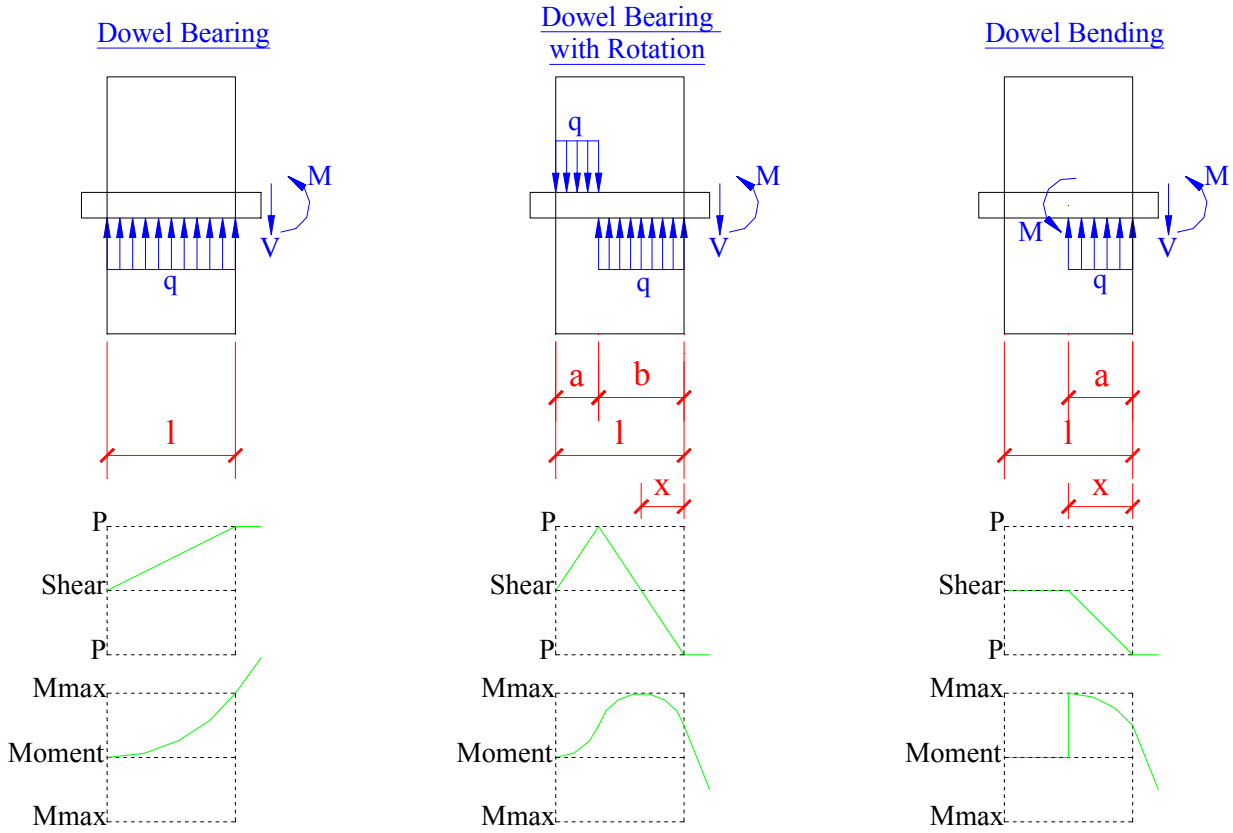

Figure A-1: General dowel loading conditions

The following expressions are found from the shear and bending moment diagrams:

Dowel Bearing:

$P = V = ql$

$M_{max} = ql2/2$

Dowel Bearing with Rotation:

$P = V = qx$

$M_{max} = qa2$

Dowel Bending:

$P = V = qx$

$M_{max} = M_{dowel}$

Next, using the three general dowel loading conditions, connection models are developed.

Note:
The "m" subscript indicates main member bearing.
The "s" subscript indicates side member bearing.

Additional Expressions – Dowel Bearing with Rotation Only

In the following brief derivation, a useful expression for the location "a" is developed for the case of dowel bearing with rotation.

From the shear and bending moment diagram:

$$M_{max} = q \cdot a^2$$

Location of zero shear is defined as x:

$$x = l - 2 \cdot a$$ Note: x = a and l = 3a

Solve for a:

$$a = \frac{l - x}{2}$$

Substitute into moment expression:

$$M_{max} = q \cdot \left(\frac{l - x}{2} \right)^2$$

Also, P=qx or P=qa:

$$x = \frac{P}{q} \qquad a = \frac{P}{q}$$

Substituting:

$$M_{max} = q \cdot \left(\frac{l \cdot q - P}{2 \cdot q} \right)^2$$

Now express moment in terms of "a" and solve:

$$q \cdot a^2 = q \cdot \left(\frac{l \cdot q - P}{2 \cdot q} \right)^2$$

$$a = \frac{l \cdot q - P}{2 \cdot q}$$

In terms of the side and main member, this expression is:

$$a_s = \frac{l_s \cdot q_s - P}{2 \cdot q_s} \qquad a_m = \frac{l_m \cdot q_m - P}{2 \cdot q_m}$$

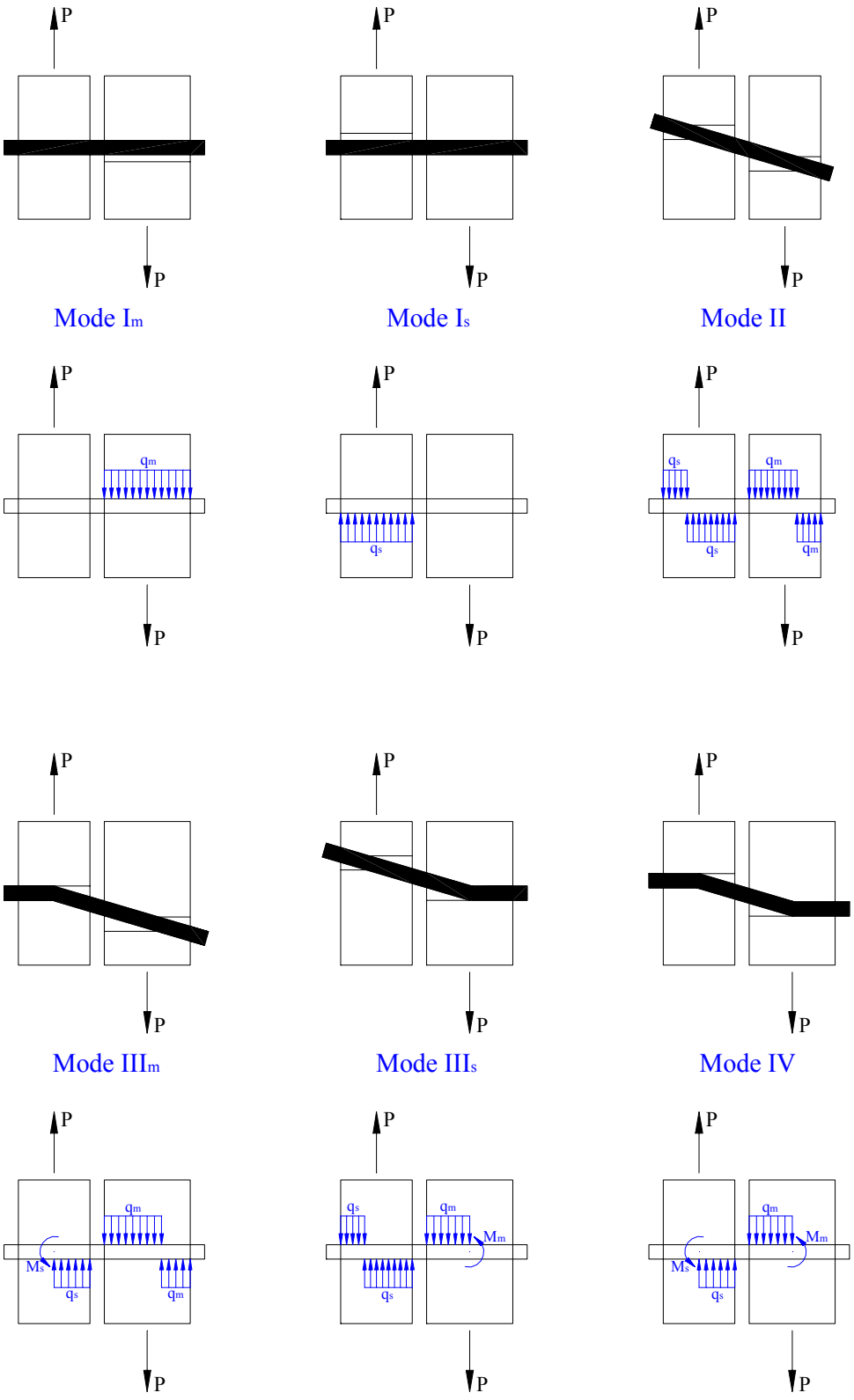

Figure A-2: Single shear connection models

Double Shear Connection Models

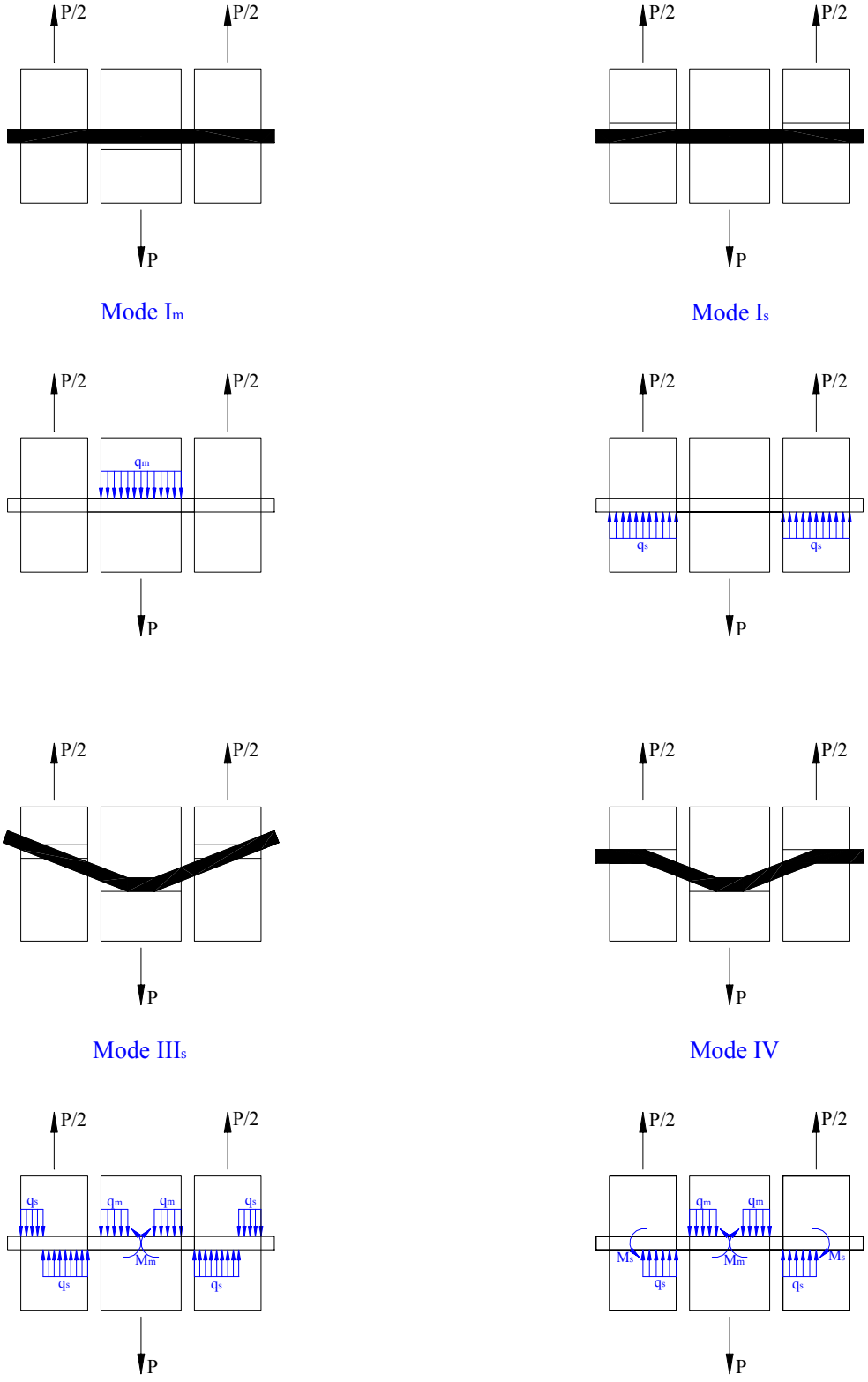

Figure A-3: Double shear connection models

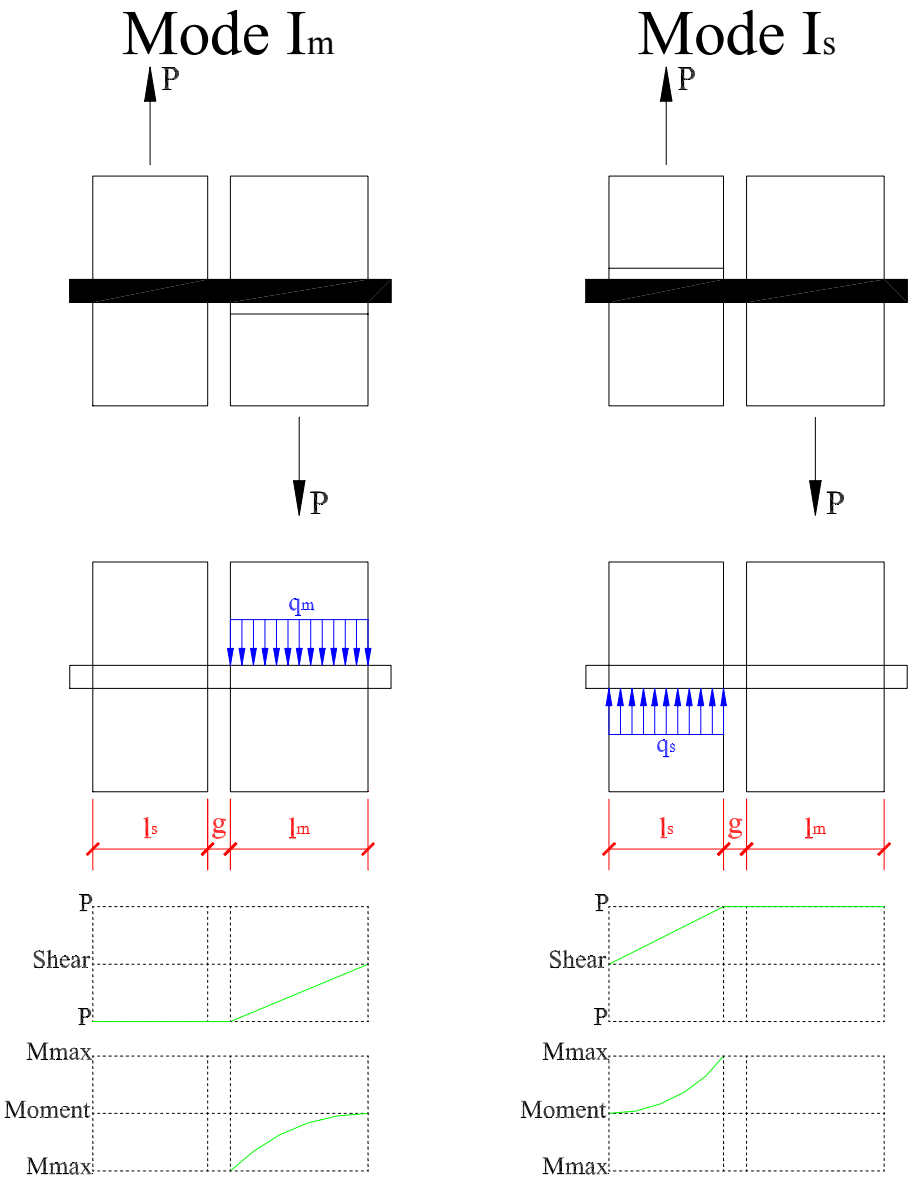

Figure A-4: Mode I_m and Mode I_s connection models

Derivation of Mode I_m and Mode I_s – Single Shear

Note: The Mode I_m failure is produced by the main member crushing under the dowel. The Mode I_s failure is produced by the side member crushing under the dowel. In both cases, the load causing this failure is P. Therefore, the equation governing this type of failure is the dowel bearing resistance multiplied by the member bearing length.

Mode I_m:

$$P = q_m \cdot l_m$$

Mode I_s:

$$P = q_s \cdot l_s$$

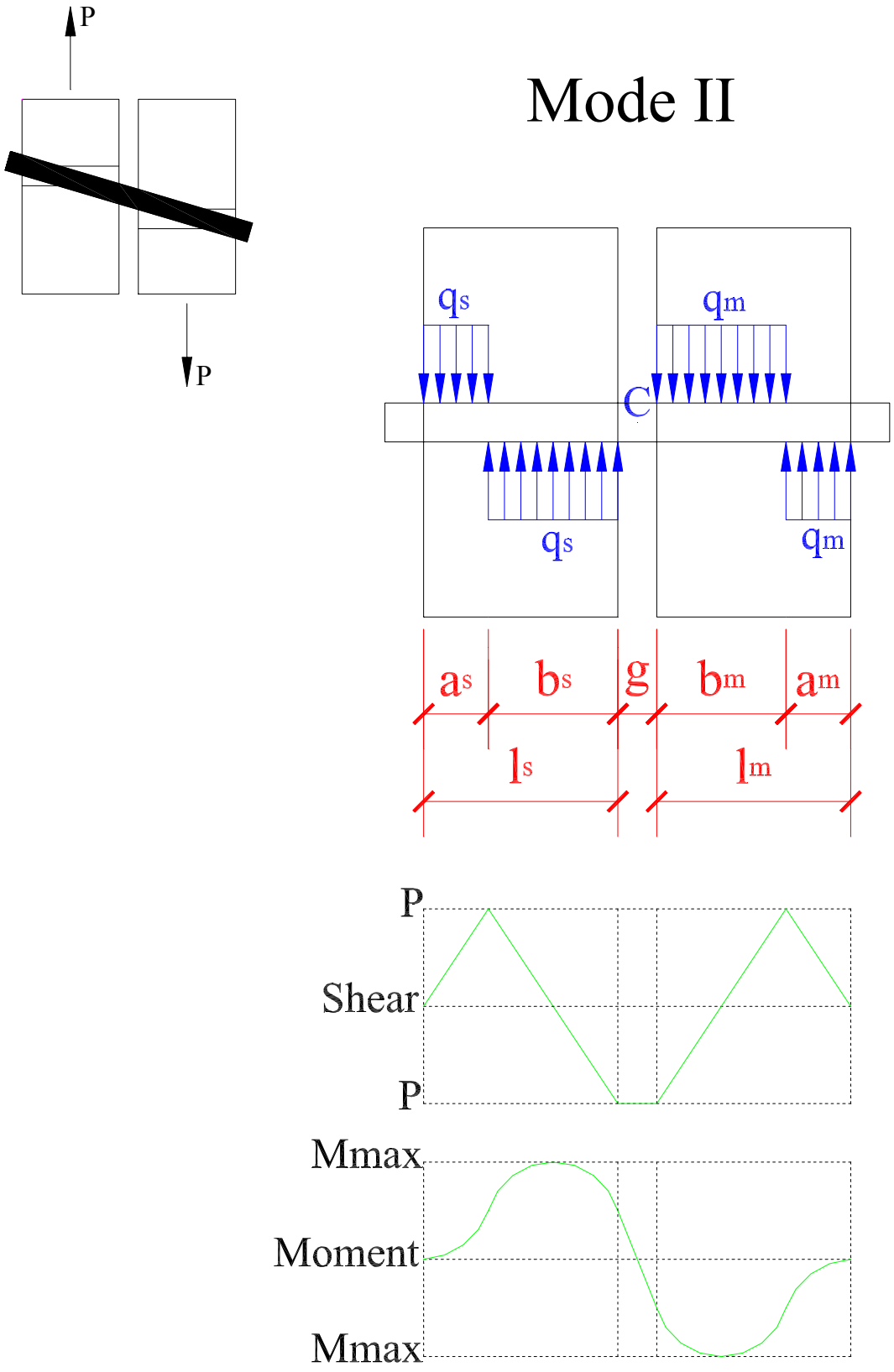

Figure A-5: Mode II connection model

Derivation of Mode II

Equilibrium equation found by summing moments at point C and setting equal to zero:

$$-\left(\frac{g}{2}+b_s+\frac{a_s}{2}\right)\cdot q_s\cdot a_s+\left(\frac{g}{2}+\frac{b_s}{2}\right)\cdot q_s\cdot b_s+\left(\frac{g}{2}+\frac{b_m}{2}\right)\cdot q_m\cdot b_m-\left(\frac{g}{2}+b_m+\frac{a_m}{2}\right)\cdot q_m\cdot a_m=0$$

First, the equilibrium equation is simplified using expressions relating model variables.

Substituting $b_s = \left(2\cdot a_s\right)$ and $b_m = \left(2\cdot a_m\right)$. Then, simplifying:

$$\frac{1}{2}\cdot q_s\cdot a_s\cdot g-\frac{1}{2}\cdot q_s\cdot a_s^{\,2}+\frac{1}{2}\cdot q_m\cdot a_m\cdot g-\frac{1}{2}\cdot q_m\cdot a_m^{\,2}=0$$

Substituting $P = \left(q_s\cdot a_s\right)$ and $P = \left(q_m\cdot a_m\right)$ into the "g" terms:

$$\frac{1}{2}\cdot P\cdot g-\frac{1}{2}\cdot q_s\cdot a_s^{\,2}+\frac{1}{2}\cdot P\cdot g-\frac{1}{2}\cdot q_m\cdot a_m^{\,2}=0$$

Combining the "g" terms:

$$P\cdot g-\frac{1}{2}\cdot q_s\cdot a_s^{\,2}-\frac{1}{2}\cdot q_m\cdot a_m^{\,2}=0$$

Next, using the previously derived expression for "a," the above equation is expressed as a quadratic in P.

Substituting $a_s = \left(\frac{l_s\cdot q_s - P}{2\cdot q_s}\right)$ and $a_m = \left(\frac{l_m\cdot q_m - P}{2\cdot q_m}\right)$. Then, simplifying:

$$P\cdot g-\frac{1}{8}\cdot q_s\cdot l_s^{\,2}+\frac{1}{4}\cdot l_s\cdot P-\frac{1}{\left(8\cdot q_s\right)}\cdot P^2-\frac{1}{8}\cdot q_m\cdot l_m^{\,2}+\frac{1}{4}\cdot l_m\cdot P-\frac{1}{\left(8\cdot q_m\right)}\cdot P^2=0$$

Grouping the "P" terms:

$$\left[\frac{-1}{\left(8\cdot q_s\right)}-\frac{1}{\left(8\cdot q_m\right)}\right]\cdot P^2+\left(\frac{1}{4}\cdot l_s+g+\frac{1}{4}\cdot l_m\right)\cdot P-\frac{1}{8}\cdot q_m\cdot l_m^{\,2}-\frac{1}{8}\cdot q_s\cdot l_s^{\,2}=0$$

Multiplying both sides by 2:

$$\left[\frac{-1}{\left(4\cdot q_s\right)}-\frac{1}{\left(4\cdot q_m\right)}\right]\cdot P^2+\left(\frac{1}{2}\cdot l_m+2\cdot g+\frac{1}{2}\cdot l_s\right)\cdot P-\frac{1}{4}\cdot q_m\cdot l_m^{\,2}-\frac{1}{4}\cdot q_s\cdot l_s^{\,2}=0$$

Now, the expression is in the correct general form. However, the coefficients of the P^2 and P terms differ from the TR12 equation. The equation is now manipulated to produce the correct coefficients.

Separating a "Pg" term:

$$\left[\frac{-1}{(4\cdot q_s)}-\frac{1}{(4\cdot q_m)}\right]\cdot P^2+\left(\frac{1}{2}\cdot l_m+g+\frac{1}{2}\cdot l_s\right)\cdot P-\frac{1}{4}\cdot q_m\cdot l_m^{\,2}-\frac{1}{4}\cdot q_s\cdot l_s^{\,2}+P\cdot g = 0$$

Substituting $g = \frac{1}{2}a_s+\frac{1}{2}a_m$: (See Technical Note #1)

$$\left[\frac{-1}{(4\cdot q_s)}-\frac{1}{(4\cdot q_m)}\right]\cdot P^2+\left(\frac{1}{2}\cdot l_m+g+\frac{1}{2}\cdot l_s\right)\cdot P-\frac{1}{4}\cdot q_m\cdot l_m^{\,2}-\frac{1}{4}\cdot q_s\cdot l_s^{\,2}+P\cdot\left(\frac{1}{2}a_s+\frac{1}{2}a_m\right) = 0$$

Substituting $a_s = \frac{P}{q_s}$ and $a_m = \frac{P}{q_m}$:

$$\left[\frac{-1}{(4\cdot q_s)}-\frac{1}{(4\cdot q_m)}\right]\cdot P^2+\left(\frac{1}{2}\cdot l_m+g+\frac{1}{2}\cdot l_s\right)\cdot P-\frac{1}{4}\cdot q_m\cdot l_m^{\,2}-\frac{1}{4}\cdot q_s\cdot l_s^{\,2}+P\cdot\left(\frac{1}{2}\frac{P}{q_s}+\frac{1}{2}\frac{P}{q_m}\right) = 0$$

Regrouping "P" terms:

$$\left[\frac{1}{(4\cdot q_s)}+\frac{1}{(4\cdot q_m)}\right]\cdot P^2+\left(\frac{1}{2}\cdot l_m+g+\frac{1}{2}\cdot l_s\right)\cdot P-\frac{1}{4}\cdot q_m\cdot l_m^{\,2}-\frac{1}{4}\cdot q_s\cdot l_s^{\,2} = 0$$

Technical Note #1

Where did $g = \frac{1}{2} a_s + \frac{1}{2} a_m$ come from?

An expression for "g" is developed using the Mode II shear and bending moment diagram. The moment at a point on the moment diagram is equal to the area under the shear diagram up to that point.

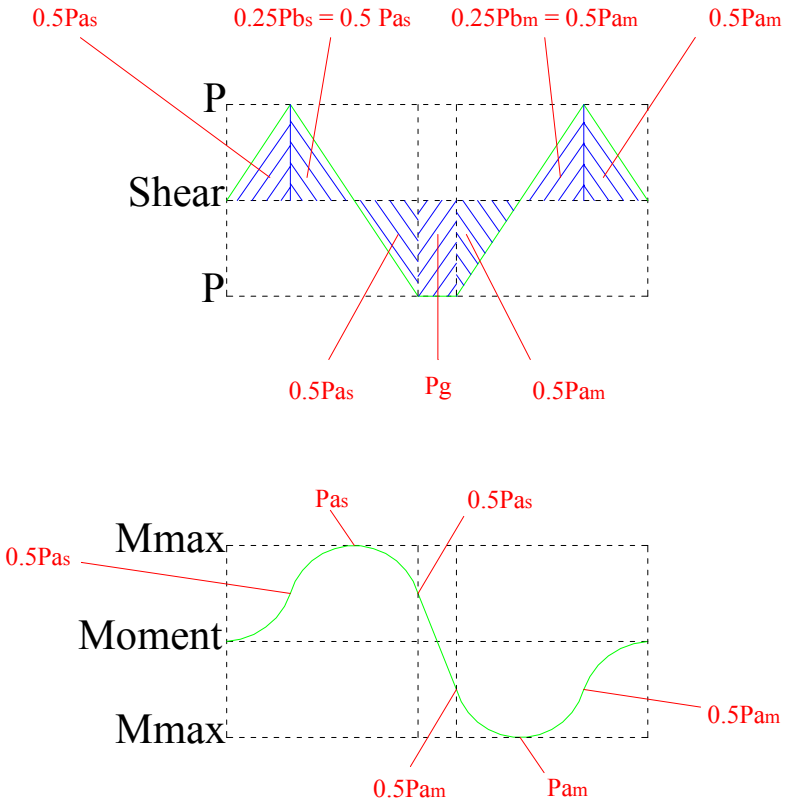

Figure A-6: Detailed Mode II shear and bending moment diagram

From the gap region:

$$\frac{1}{2} \cdot P \cdot a_s - P \cdot g = \frac{-1}{2} \cdot P \cdot a_m$$

$$\frac{1}{2} \cdot P \cdot a_s + \frac{1}{2} \cdot P \cdot a_m = P \cdot g$$

$$g = \frac{1}{2} a_s + \frac{1}{2} a_m$$

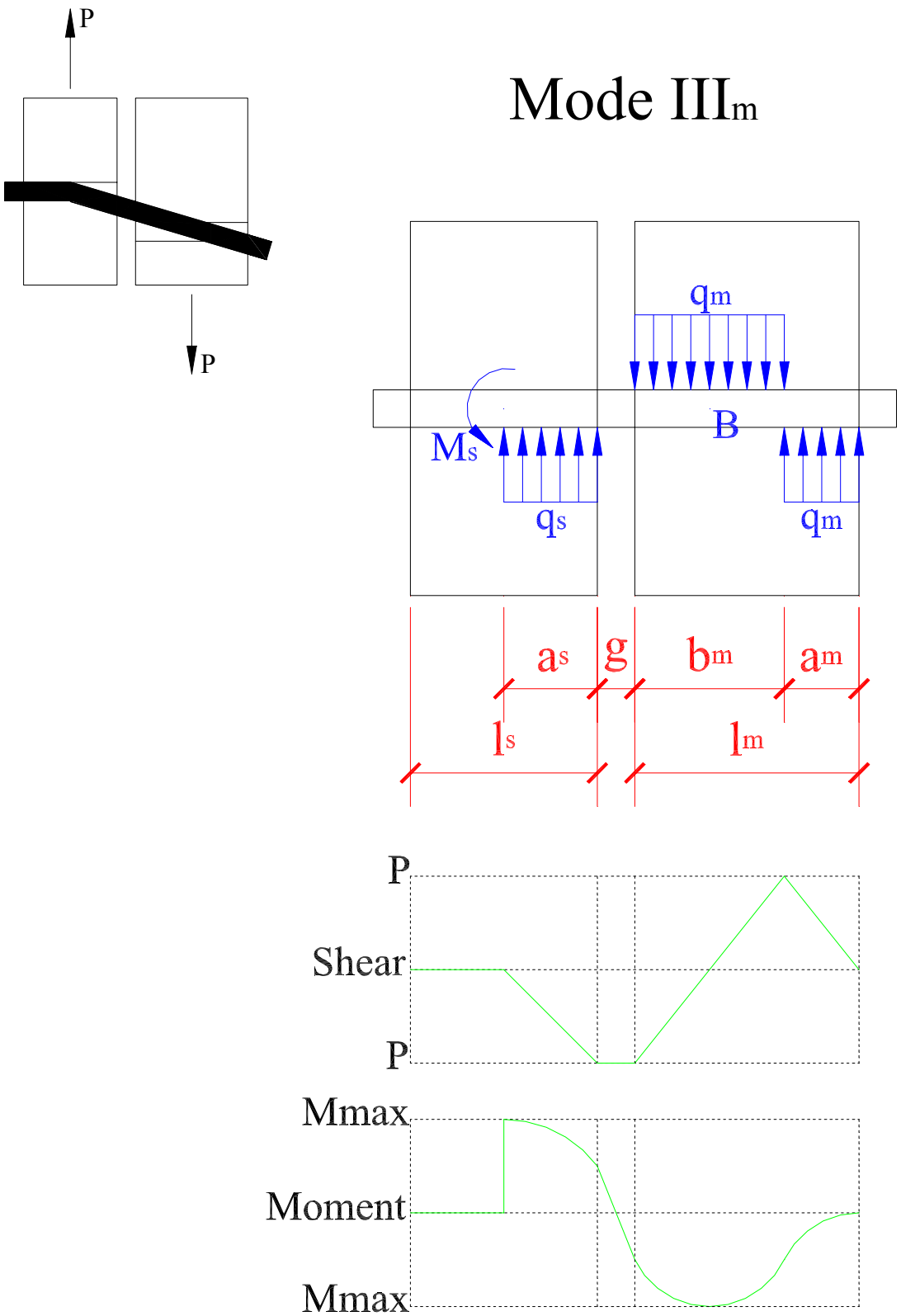

Figure A-7: Mode III_m connection model

Derivation of Mode III_m

Equilibrium equation found by summing moments at point B and setting equal to zero:

$$-M_s - \left(\frac{a_m}{2} + \frac{b_m}{2}\right)\cdot q_m \cdot a_m + \left(\frac{a_s}{2} + g + \frac{b_m}{2}\right)\cdot q_s \cdot a_s = 0$$

First, the equilibrium equation is simplified using expressions relating model variables.

Substituting $b_m = \left(2 \cdot a_m\right)$:

$$-M_s - \frac{3}{2}\cdot a_m^{\,2}\cdot q_m + \left(\frac{1}{2}\cdot a_s + g + a_m\right)\cdot q_s \cdot a_s = 0$$

Substituting $P = \left(q_s \cdot a_s\right)$ and $P = \left(q_m \cdot a_m\right)$:

$$-M_s - \frac{3}{2}\cdot a_m \cdot P + \left(\frac{1}{2}\cdot a_s + g + a_m\right)\cdot P = 0$$

Substituting $a_s = \left(\frac{P}{q_s}\right)$:

$$-M_s - \frac{3}{2}\cdot a_m \cdot P + \left(\frac{1}{2}\cdot\frac{P}{q_s} + g + a_m\right)\cdot P = 0$$

Next, using the previously derived expression for "a," the above equation is expressed as a quadratic in P.

Substituting $a_m = \left(\frac{l_m \cdot q_m - P}{2 \cdot q_m}\right)$:

$$-M_s - \frac{3}{4}\cdot\frac{\left(l_m \cdot q_m - P\right)}{q_m}\cdot P + \left[\frac{1}{2}\cdot\frac{P}{q_s} + g + \frac{1}{2}\cdot\frac{\left(l_m \cdot q_m - P\right)}{q_m}\right]\cdot P = 0$$

Collecting "P" terms:

$$\left[\frac{1}{\left(4 \cdot q_m\right)} + \frac{1}{\left(2 \cdot q_s\right)}\right]\cdot P^2 + \left(\frac{-1}{4}\cdot l_m + g\right)\cdot P - M_s = 0$$

Now, the expression is in the correct general form. However, the constant term and the coefficient of the P term differ from the TR12 equation.

Using a simple mathematical approach, the correct coefficient of the P term is produced.

Adding and Subtracting $\frac{l_m \cdot P}{2}$:

$$\left[\frac{1}{(4 \cdot q_m)} + \frac{1}{(2 \cdot q_s)}\right] \cdot P^2 + \left(\frac{-1}{4} \cdot l_m + g\right) \cdot P - M_s + \frac{l_m \cdot P}{2} - \frac{l_m \cdot P}{2} = 0$$

Combining "$l_m P$" terms:

$$\left[\frac{1}{(4 \cdot q_m)} + \frac{1}{(2 \cdot q_s)}\right] \cdot P^2 + \left(\frac{1}{2} \cdot l_m + g\right) \cdot P - M_s - \frac{3\, l_m \cdot P}{4} = 0$$

The constant term for each equation involving dowel bearing with rotation should be a function of the member length squared. This is done by relating the load, the member bearing resistance, and the member length.

$$P = q_m \cdot a_m$$

$$l_m = 3 \cdot a_m$$

$$P = \left(\frac{l_m \cdot q_m}{3}\right)$$

This expression can now be used to produce the TR12 equation.

Substituting $P = \left(\frac{l_m \cdot q_m}{3}\right)$:

$$\left[\frac{1}{(4 \cdot q_m)} + \frac{1}{(2 \cdot q_s)}\right] \cdot P^2 + \left(\frac{1}{2} \cdot l_m + g\right) \cdot P - M_s - \frac{l_m^2 \cdot q_m}{4} = 0$$

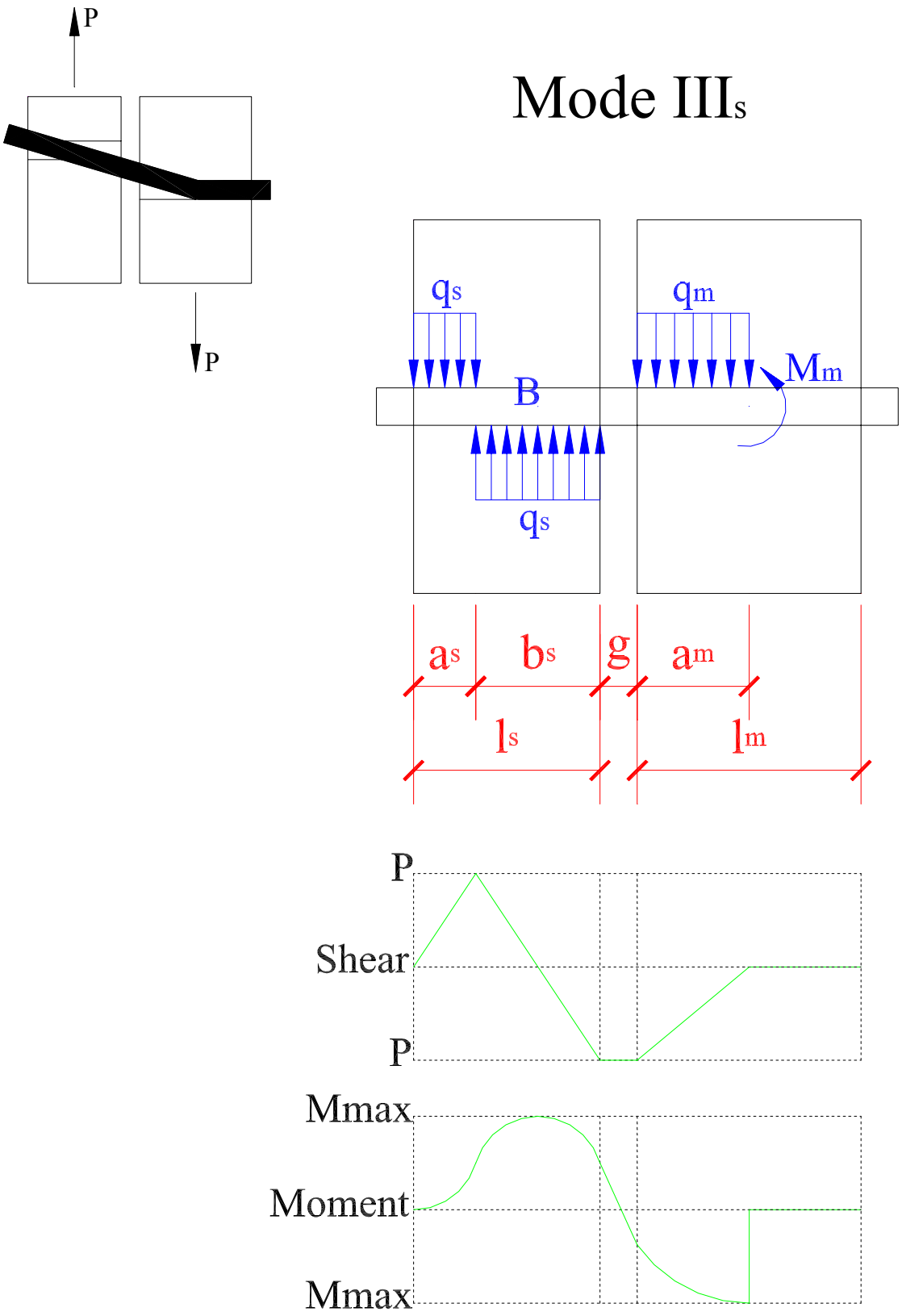

Figure A-8: Mode IIIs connection model

Derivation of Mode III$_s$ – Single Shear

Equilibrium equation found by summing moments at point B and setting equal to zero:

$$-M_m - \left(\frac{a_s}{2} + \frac{b_s}{2}\right)\cdot q_s \cdot a_s + \left(\frac{a_m}{2} + g + \frac{b_s}{2}\right)\cdot q_m \cdot a_m = 0$$

First, the equilibrium equation is simplified using expressions relating model variables.

Substituting $b_s = (2\cdot a_s)$:

$$-M_m - \left(\frac{a_s}{2} + \frac{b_s}{2}\right)\cdot q_s \cdot a_s + \left(\frac{a_m}{2} + g + \frac{b_s}{2}\right)\cdot q_m \cdot a_m = 0$$

Substituting $P = (q_s \cdot a_s)$ and $P = (q_m \cdot a_m)$:

$$-M_m - \frac{3}{2}\cdot a_s \cdot P + \left(\frac{1}{2}\cdot a_m + g + a_s\right)\cdot P = 0$$

Substituting $a_m = \left(\frac{P}{q_m}\right)$:

$$-M_m - \frac{3}{2}\cdot a_s \cdot P + \left(\frac{1}{2}\cdot\frac{P}{q_m} + g + a_s\right)\cdot P = 0$$

Next, using the previously derived expression for "a," the above equation is expressed as a quadratic in P.

Substituting $a_s = \left(\frac{l_s \cdot q_s - P}{2\cdot q_s}\right)$:

$$-M_m - \frac{3}{4}\cdot\frac{(l_s \cdot q_s - P)}{q_s}\cdot P + \left[\frac{1}{2}\cdot\frac{P}{q_m} + g + \frac{1}{2}\cdot\frac{(l_s \cdot q_s - P)}{q_s}\right]\cdot P = 0$$

Collecting "P" terms:

$$\left[\frac{1}{(4\cdot q_s)} + \frac{1}{(2\cdot q_m)}\right]\cdot P^2 + \left(\frac{-1}{4}\cdot l_s + g\right)\cdot P - M_m = 0$$

Now, the expression is in the correct general form. However, the constant term and the coefficient of the P term differ from the TR12 equation.

Using a simple mathematical approach, the correct coefficient of the P term is produced.

Adding and Subtracting $\frac{l_s \cdot P}{2}$:

$$\left[\frac{1}{(4 \cdot q_s)} + \frac{1}{(2 \cdot q_m)}\right] \cdot P^2 + \left(\frac{-1}{4} \cdot l_s + g\right) \cdot P - M_m + \frac{l_s \cdot P}{2} - \frac{l_s \cdot P}{2} = 0$$

Combining "$l_s P$" terms:

$$\left[\frac{1}{(4 \cdot q_s)} + \frac{1}{(2 \cdot q_m)}\right] \cdot P^2 + \left(\frac{1}{2} \cdot l_s + g\right) \cdot P - M_m - \frac{3 \cdot l_s \cdot P}{4} = 0$$

The constant term for each equation involving dowel bearing with rotation should be a function of the member length squared. This is done by relating the load, the member bearing resistance, and the member length.

$$P = q_s \cdot a_s$$

$$l_s = 3 \cdot a_s$$

$$P = \frac{l_s \cdot q_s}{3}$$

This expression can now be used to produce the TR12 equation.

Substituting $P = \frac{l_s \cdot q_s}{3}$:

$$\left[\frac{1}{(4 \cdot q_s)} + \frac{1}{(2 \cdot q_m)}\right] \cdot P^2 + \left(\frac{1}{2} \cdot l_s + g\right) \cdot P - M_m - \frac{l_s^2 \cdot q_s}{4} = 0$$

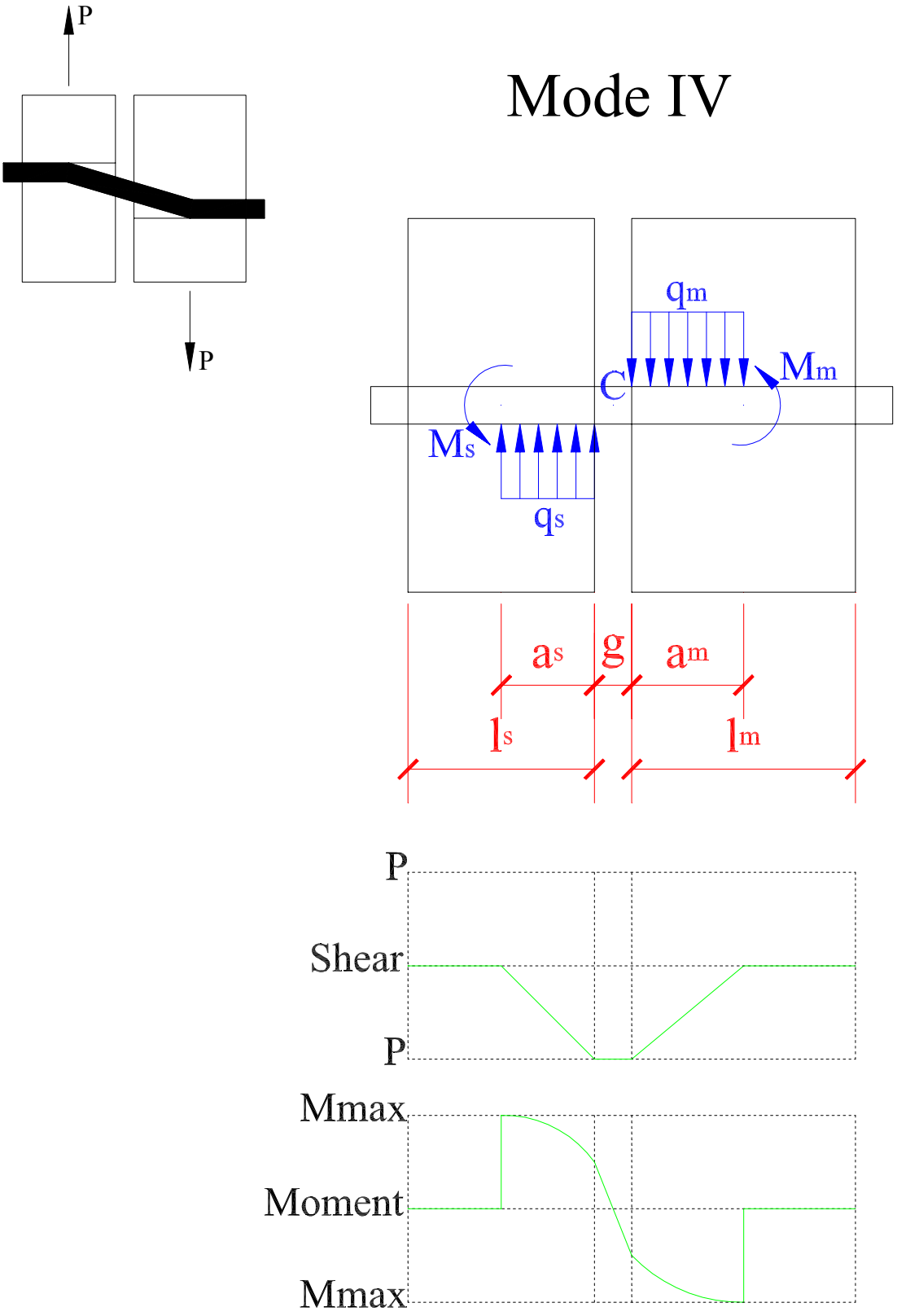

Figure A-9: Mode IV connection model

Derivation of Mode IV – Single Shear

Equilibrium Equation found by summing moments at point C and setting equal to zero:

$$-\left(M_s + M_m\right) + \left(\frac{a_m}{2} + \frac{g}{2}\right)\cdot q_m \cdot a_m + \left(\frac{a_s}{2} + \frac{g}{2}\right)\cdot q_s \cdot a_s = 0$$

The derivation of the Mode IV equation only involves one substitution to produce the required quadatic form.

Expanding:

$$-M_s - M_m + \frac{1}{2}\cdot q_m \cdot a_m^2 + \frac{1}{2}\cdot q_m \cdot a_m \cdot g + \frac{1}{2}\cdot q_s \cdot a_s^2 + \frac{1}{2}\cdot q_s \cdot a_s \cdot g = 0$$

Substituting $a_s = \left(\frac{P}{q_s}\right)$ and $a_m = \left(\frac{P}{q_m}\right)$:

$$-M_s - M_m + \frac{1}{\left(2\cdot q_m\right)}\cdot P^2 + g\cdot P + \frac{1}{\left(2\cdot q_s\right)}\cdot P^2 = 0$$

Grouping P terms:

$$\left[\frac{1}{\left(2\cdot q_m\right)} + \frac{1}{\left(2\cdot q_s\right)}\right]\cdot P^2 + g\cdot P - M_s - M_m = 0$$

Double Shear Connections

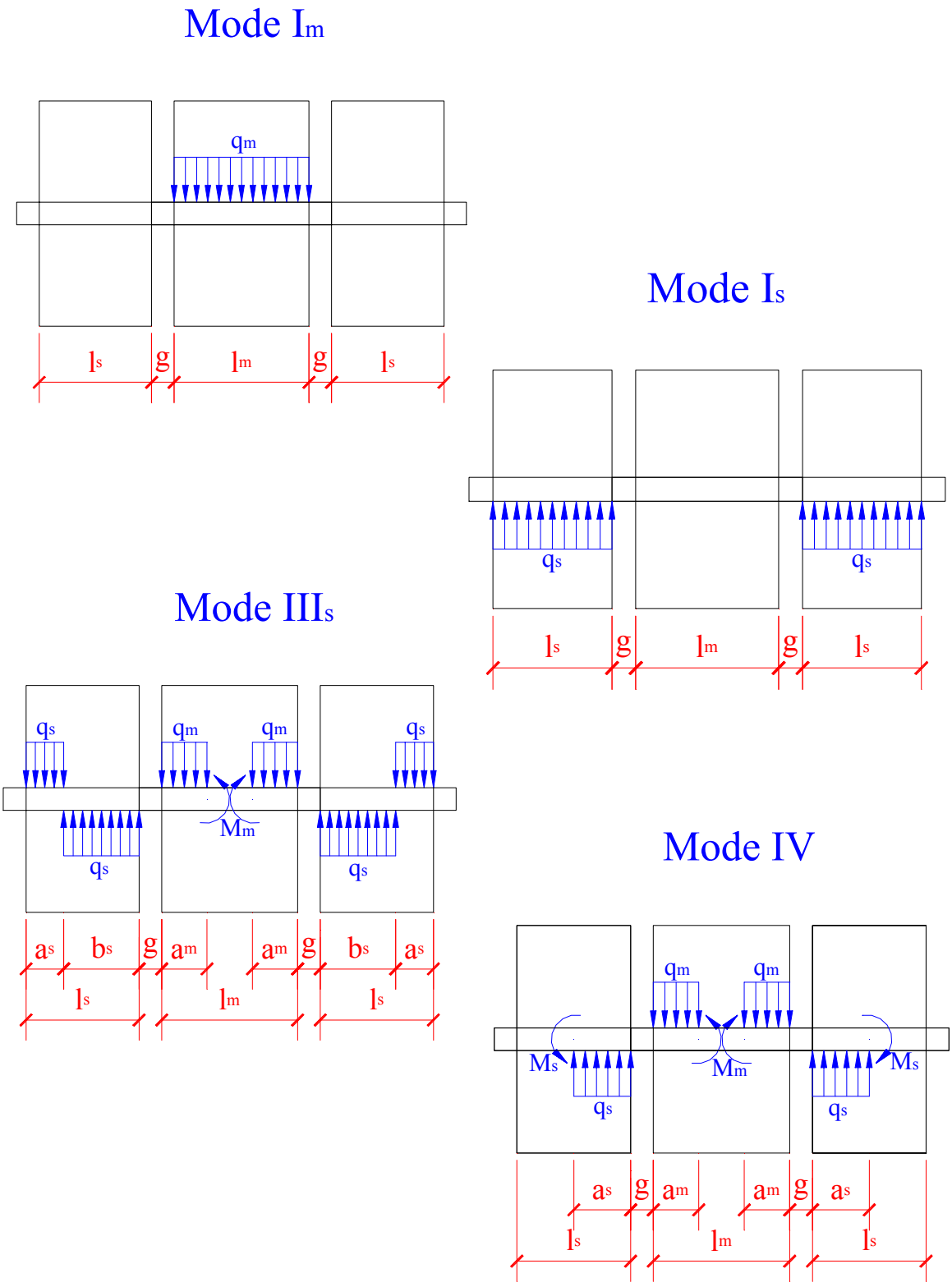

Figure A-10: Double shear connection free-body diagrams

Derivation of Double Shear Equations

Note: Each double shear connection consists of two single shear connections. Each single shear connection transfers a load of P/2. The double shear connection equations are derived by using the single shear connection equations and replacing the load, P, with P/2.

Mode I_m:

Note: In the case of main member crushing, the total load causing failure is still P. Half the load (P/2) comes from each side member.

Single Shear Equation:

$$P = q_m \cdot l_m$$

Double Shear Equation:

$$P = q_m \cdot l_m$$

Mode I_s:

Single Shear Equation:

$$P = q_s \cdot l_s$$

Double Shear Equation:

$$P = 2 \cdot q_s \cdot l_s$$

Mode III_s:

Single Shear Equation:

$$\left[\frac{1}{(4 \cdot q_s)} + \frac{1}{(2 \cdot q_m)}\right] \cdot P^2 + \left(\frac{1}{2} \cdot l_s + g\right) \cdot P - M_m - \frac{l_s^2 \cdot q_s}{4} = 0$$

Double Shear Equation:

$$\left[\frac{1}{(4 \cdot q_s)} + \frac{1}{(2 \cdot q_m)}\right] \cdot \frac{P^2}{4} + \left(\frac{1}{2} \cdot l_s + g\right) \cdot \frac{P}{2} - M_m - \frac{l_s^2 \cdot q_s}{4} = 0$$

Mode IV:

Single Shear Equation:

$$\left[\frac{1}{(2 \cdot q_m)} + \frac{1}{(2 \cdot q_s)}\right] \cdot P^2 + g \cdot P - M_s - M_m = 0$$

Double Shear Equation:

$$\left[\frac{1}{(2 \cdot q_m)} + \frac{1}{(2 \cdot q_s)}\right] \cdot \frac{P^2}{4} + g \cdot \frac{P}{2} - M_s - M_m = 0$$

Summary of Derived EYM Equations

Table A-4: European Yield Model equations

Yield Mode	Single Shear	Double Shear
I_m	$P = q_m l_m$	$P = q_m l_m$
I_s	$P = q_s l_s$	$P = 2 q_s l_s$
II-IV	$P = \frac{-B + \sqrt{B^2 - 4AC}}{2A}$	$P = \frac{-B + \sqrt{B^2 - 4AC}}{A}$

Table A-5: Factors for European Yield Model equations

Yield Mode	A	B	C
II	$\frac{1}{4q_s} + \frac{1}{4q_m}$	$\frac{l_s}{2} + g + \frac{l_m}{2}$	$-\frac{q_s l_s^2}{4} - \frac{q_m l_m^2}{4}$
III_m	$\frac{1}{2q_s} + \frac{1}{4q_m}$	$g + \frac{l_m}{2}$	$-M_s - \frac{q_m l_m^2}{4}$
III_s	$\frac{1}{4q_s} + \frac{1}{2q_m}$	$\frac{l_s}{2} + g$	$-\frac{q_s l_s^2}{4} - M_m$
IV	$\frac{1}{2q_s} + \frac{1}{2q_m}$	g	$-M_s - M_m$

APPENDIX B: DERIVATION OF EYM EQUATIONS – ENERGY BASED

Overview

This appendix outlines the energy-based derivation of the European Yield Model (EYM). This method of deriving the EYM is described in Aune and Patton-Mallory (1986). In that paper, the derivation was outlined briefly. Here, all the general dowel equations will be derived. The virtual displacement method provides a more systematic approach to the derivation than the static equilibrium-based approach (APPENDIX A). The method used in the derivation was the method of virtual displacements and was outlined in CHAPTER 3.

Description of Modes

Table B-1: Yield Modes

Yield Mode	Description of Failure	Applicable Connection Type
I_m	Main member bearing	Both single and double shear
I_s	Side member bearing	Both single and double shear
II	Main and side member bearing	Only single shear
III_m	Main member bearing, Dowel yielding in side member	Only single shear
III_s	Side member bearing, Dowel yielding in main member	Both single and double shear
IV	Dowel yielding in main and side member	Both single and double shear

Assumptions

- End fixity of the dowel is ignored.
- Tension forces in the dowel are ignored.
- Friction between the members is ignored
- Dowel loading is assumed to be uniformly distributed and perpendicular to the axis of the dowel.
- Perfect elastic/plastic behavior of all materials is assumed.

Input Parameters

The only necessary input parameters deal with connection geometry and strength properties as follows:

Table B-2: Input Parameters

Parameter	Description
ℓ_s	Side member dowel bearing length, in
ℓ_m	Main member dowel bearing length, in
D	Dowel diameter, in
F_{es}	Side member dowel bearing strength, psi
F_{em}	Main member dowel bearing strength, psi
F_b	Dowel bending strength, psi

The derivation parameters are used in the yield model to incorporate the input parameters:

Table B-3: Derivation Parameters

Parameter	Description
f_{es}	Side member dowel bearing resistance, lbs/in
f_{em}	Main member dowel bearing resistance, lbs/in
M_y	Moment resistance, in-lbs

The above parameters can be calculated in the following manner:

$$f_{es} = F_{es} D \qquad f_{em} = F_{em} D$$

$$M_y = F_b \left(\frac{D^3}{6} \right)$$

Single Shear Connection Models

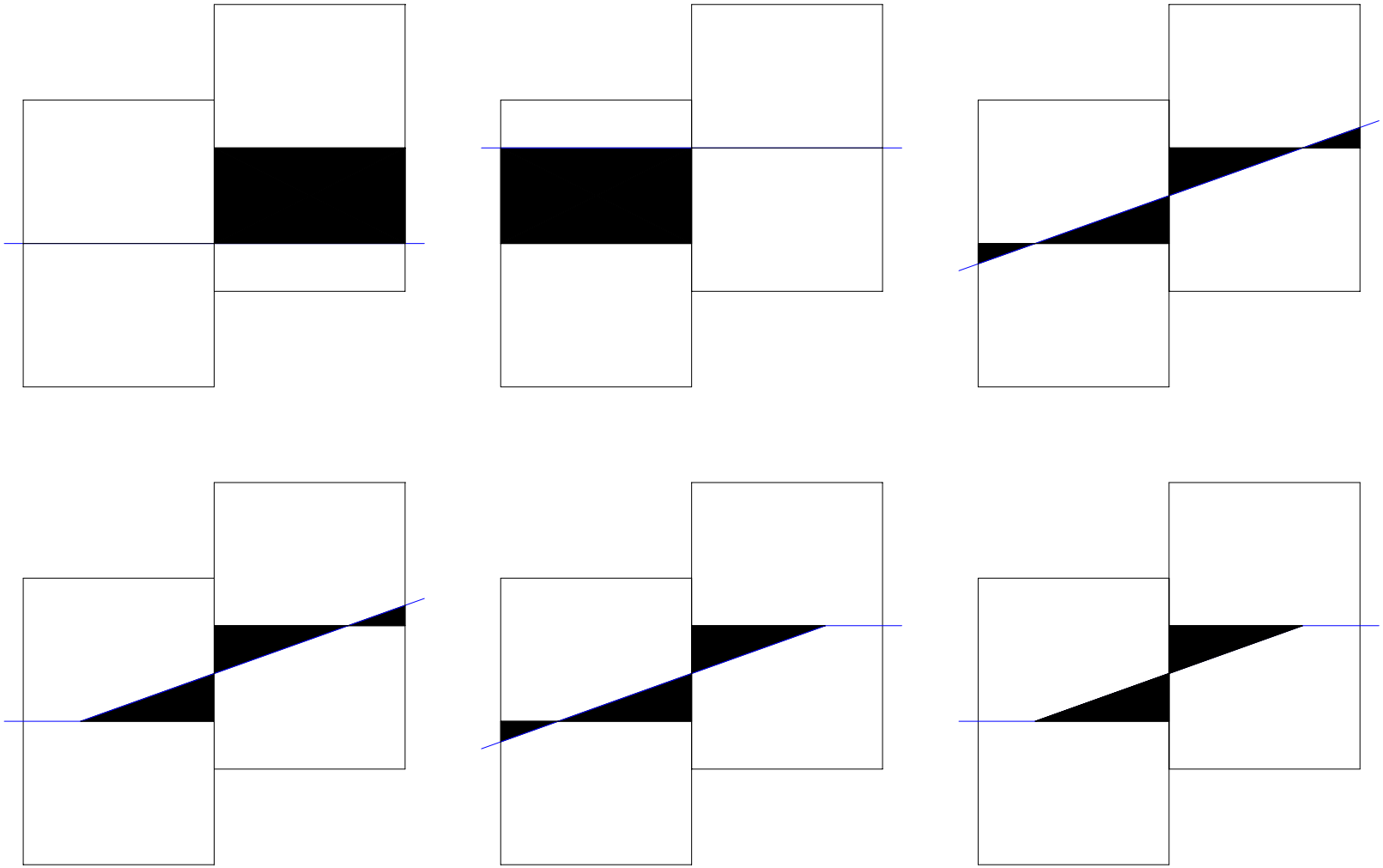

Figure B-1 : Single shear connection models

Mode I

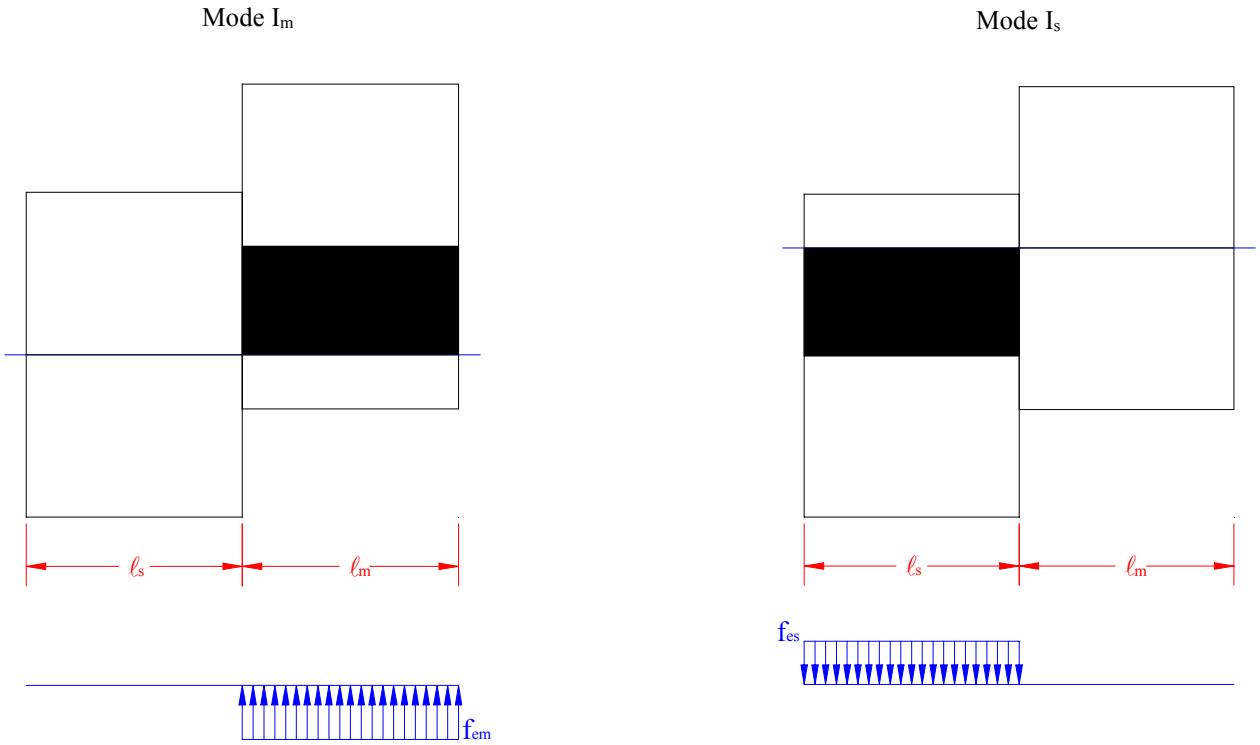

Figure B-2: Mode I_m and I_s connection models

The Mode I_m failure is produced by the main member crushing under the dowel. The Mode I_s failure is produced by the side member crushing under the dowel. In both cases, the load causing this failure is F. Therefore, the equation governing this type of failure is the dowel bearing resistance multiplied by the member bearing length.

Mode I_m:

$$F = f_{em} \cdot l_m$$

Mode I_s:

$$F = f_{es} \cdot l_s$$

Mode II

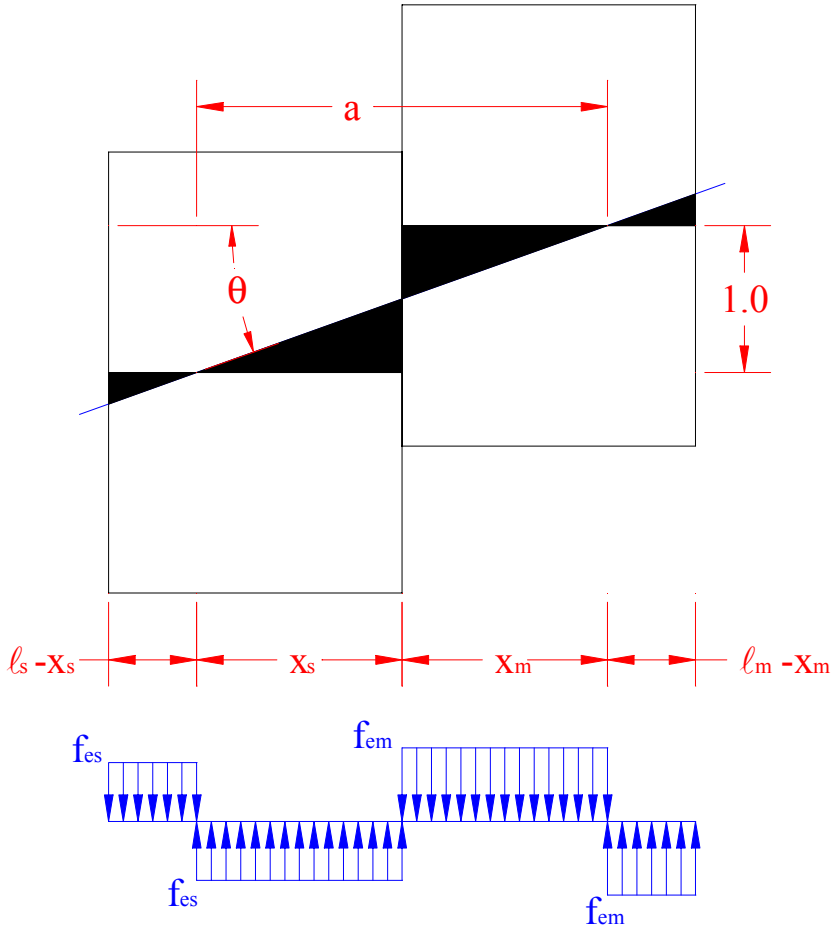

Figure B-3: Mode II connection model

General Equation:

$$W = \Sigma \left(f_e \cdot A\right) + \Sigma \left(M_y \cdot \theta\right)$$

Small displacements assumed:

$$\tan(\theta) = \frac{l}{a} = \theta$$

$$a = x_s + x_m$$

$\Sigma \left(M_y \cdot \theta\right)$ term:

For Mode II there is no yielding in the bolt. Therefore, M_y equals 0.

$\Sigma \left(f_e \cdot A\right)$ term:

$$\Sigma \left(f_e \cdot A\right) = \frac{f_{es}}{2 \cdot a} \cdot \left[\left(l_s - x_s\right)^2 + x_s^2\right] + \frac{f_{em}}{2 \cdot a} \cdot \left[\left(l_m - x_m\right)^2 + x_m^2\right]$$

Substituting into the general equation:

$$W = \Sigma \left(f_e \cdot A\right) + \Sigma \left(M_y \cdot \theta\right)$$

$$W = F \cdot 1 = \frac{f_{es}}{2 \cdot a} \cdot \left[\left(l_s - x_s\right)^2 + x_s^2\right] + \frac{f_{em}}{2 \cdot a} \cdot \left[\left(l_m - x_m\right)^2 + x_m^2\right]$$

Substituting for a:

$$F = \frac{f_{es}}{2 \cdot \left(x_s + x_m\right)} \cdot \left[\left(l_s - x_s\right)^2 + x_s^2\right] + \frac{f_{em}}{2 \cdot \left(x_s + x_m\right)} \cdot \left[\left(l_m - x_m\right)^2 + x_m^2\right]$$

At this point, the general equation is in terms of two unknown variables, x_s and x_m. An equation relating x_s and x_m is found using a diagram of the bearing stress.

By considering equilibrium in the vertical direction ($\Sigma F_y = 0$), the following expression is obtained:

$$f_{es} \cdot \left(l_s - x_s\right) + f_{em} \cdot x_m = f_{es} \cdot x_s + f_{em} \cdot \left(l_m - x_m\right)$$

Solve for x_m:

$$x_m = \frac{1}{2}\cdot\frac{\left(-f_{es}\cdot l_s + 2\cdot f_{es}\cdot x_s + f_{em}\cdot l_m\right)}{f_{em}}$$

Substituting x_m into the expression for F and simplifying:

$$F = \frac{1}{2}\cdot\frac{\left(2\cdot f_{em}\cdot f_{es}\cdot l_s^{\,2} - 4\cdot x_s\cdot f_{em}\cdot f_{es}\cdot l_s + 4\cdot x_s^{\,2}\cdot f_{em}\cdot f_{es} + f_{em}^{\,2}\cdot l_m^{\,2} + f_{es}^{\,2}\cdot l_s^{\,2} - 4\cdot f_{es}^{\,2}\cdot l_s\cdot x_s + 4\cdot f_{es}^{\,2}\cdot x_s^{\,2}\right)}{\left(2\cdot x_s\cdot f_{em} - f_{es}\cdot l_s + 2\cdot f_{es}\cdot x_s + f_{em}\cdot l_m\right)}$$

This results in an equation with one unknown variable, x_s. The expression is minimized by finding the derivative with respect to x_s and setting it equal to zero. An expression for x_s in terms of the known variables can then be found.

Evaluating $\frac{d}{dx_s}(F) = F' = 0$:

$$\frac{d}{dx_s}(F) = 0 = \frac{-\left[\left(f_{em} + f_{es}\right)\cdot\left(-f_{es}^{\,2}\cdot l_s^{\,2} + 4\cdot f_{es}^{\,2}\cdot l_s\cdot x_s - 4\cdot f_{es}^{\,2}\cdot x_s^{\,2} - 4\cdot f_{es}\cdot x_s\cdot f_{em}\cdot l_m - 4\cdot f_{es}\cdot x_s^{\,2}\cdot f_{em} + 2\cdot f_{es}\cdot f_{em}\cdot l_s^{\,2} + 2\cdot f_{es}\cdot l_s\cdot f_{em}\cdot l_m + f_{em}^{\,2}\cdot l_m^{\,2}\right)\right]}{\left(2\cdot x_s\cdot f_{em} - f_{es}\cdot l_s + 2\cdot f_{es}\cdot x_s + f_{em}\cdot l_m\right)^2}$$

Solving for x_s and simplifying:

$$x_s = \begin{bmatrix} \frac{-1}{2}\cdot\frac{\left[f_{es}\cdot\left(l_m\cdot f_{em} - l_s\cdot f_{es}\right) + \sqrt{f_{em}\cdot f_{es}\cdot\left(2\cdot f_{em}\cdot l_m^{\,2}\cdot f_{es} + f_{es}^{\,2}\cdot l_s^{\,2} + 2\cdot f_{es}\cdot l_s\cdot f_{em}\cdot l_m + 2\cdot f_{em}\cdot f_{es}\cdot l_s^{\,2} + f_{em}^{\,2}\cdot l_m^{\,2}\right)}\right]}{\left[f_{es}\cdot\left(f_{em} + f_{es}\right)\right]} \\ \frac{-1}{2}\cdot\frac{\left[f_{es}\cdot\left(l_m\cdot f_{em} - l_s\cdot f_{es}\right) - \sqrt{f_{em}\cdot f_{es}\cdot\left(2\cdot f_{em}\cdot l_m^{\,2}\cdot f_{es} + f_{es}^{\,2}\cdot l_s^{\,2} + 2\cdot f_{es}\cdot l_s\cdot f_{em}\cdot l_m + 2\cdot f_{em}\cdot f_{es}\cdot l_s^{\,2} + f_{em}^{\,2}\cdot l_m^{\,2}\right)}\right]}{\left[f_{es}\cdot\left(f_{em} + f_{es}\right)\right]} \end{bmatrix}$$

To pick which root to use, look at the second derivative. The second derivative must be greater than zero for a minimum.

Taking the second derivative of F and simplifying:

$$\frac{d}{dx_s}(F') = \frac{\left(4\cdot f_{em} + 4\cdot f_{es}\right)\cdot f_{em}\cdot\left(2\cdot f_{em}\cdot l_m^{\,2}\cdot f_{es} + f_{es}^{\,2}\cdot l_s^{\,2} + 2\cdot f_{es}\cdot l_s\cdot f_{em}\cdot l_m + 2\cdot f_{em}\cdot f_{es}\cdot l_s^{\,2} + f_{em}^{\,2}\cdot l_m^{\,2}\right)}{\left[\left(2\cdot f_{em} + 2\cdot f_{es}\right)\cdot x_s - f_{es}\cdot l_s + f_{em}\cdot l_m\right]^3}$$

x_s must be greater than zero (i.e. use the x_s expression with the positive root.)

Take the positive x_s:

$$x_s = \frac{-1}{2}\cdot\frac{\left[f_{es}\cdot\left(l_m\cdot f_{em}-l_s\cdot f_{es}\right)-\sqrt{f_{em}\cdot f_{es}\cdot\left(2\cdot f_{em}\cdot l_m^{\,2}\cdot f_{es}+f_{es}^{\,2}\cdot l_s^{\,2}+2\cdot f_{es}\cdot l_s\cdot f_{em}\cdot l_m+2\cdot f_{em}\cdot f_{es}\cdot l_s^{\,2}+f_{em}^{\,2}\cdot l_m^{\,2}\right)}\right]}{\left[f_{es}\cdot\left(f_{em}+f_{es}\right)\right]}$$

Let $R = \sqrt{f_{em}\cdot f_{es}\cdot\left(2\cdot f_{em}\cdot l_m^{\,2}\cdot f_{es}+f_{es}^{\,2}\cdot l_s^{\,2}+2\cdot f_{es}\cdot l_s\cdot f_{em}\cdot l_m+2\cdot f_{em}\cdot f_{es}\cdot l_s^{\,2}+f_{em}^{\,2}\cdot l_m^{\,2}\right)}$:

$$x_s = \frac{-1}{2}\cdot\frac{\left[f_{es}\cdot\left(l_m\cdot f_{em}-l_s\cdot f_{es}\right)-R\right]}{\left[f_{es}\cdot\left(f_{em}+f_{es}\right)\right]}$$

Substituting x_s into the expression for F and reducing:

$$F = \frac{1}{2}\cdot\frac{\left(2\cdot f_{em}\cdot f_{es}\cdot l_s^{\,2}-4\cdot x_s\cdot f_{em}\cdot f_{es}\cdot l_s+4\cdot x_s^{\,2}\cdot f_{em}\cdot f_{es}+f_{em}^{\,2}\cdot l_m^{\,2}+f_{es}^{\,2}\cdot l_s^{\,2}-4\cdot f_{es}^{\,2}\cdot l_s\cdot x_s+4\cdot f_{es}^{\,2}\cdot x_s^{\,2}\right)}{\left(2\cdot x_s\cdot f_{em}-f_{es}\cdot l_s+2\cdot f_{es}\cdot x_s+f_{em}\cdot l_m\right)}$$

$$F = \frac{1}{2}\cdot\frac{\left(l_m^{\,2}\cdot f_{es}\cdot f_{em}^{\,3}+2\cdot f_{em}^{\,2}\cdot f_{es}^{\,2}\cdot l_s^{\,2}+2\cdot f_{em}^{\,2}\cdot l_s\cdot f_{es}^{\,2}\cdot l_m+2\cdot f_{es}^{\,2}\cdot l_m^{\,2}\cdot f_{em}^{\,2}+f_{em}\cdot f_{es}^{\,3}\cdot l_s^{\,2}-2\cdot f_{es}\cdot l_m\cdot f_{em}\cdot R-2\cdot f_{em}\cdot l_s\cdot f_{es}\cdot R+R^2\right)}{\left[\left(f_{em}+f_{es}\right)\cdot R\right]}$$

$$F = \frac{1}{\left[2\cdot\left(f_{em}+f_{es}\right)\right]}\cdot R+\frac{1}{2}\cdot\frac{\left(-2\cdot f_{es}\cdot l_m\cdot f_{em}-2\cdot f_{em}\cdot l_s\cdot f_{es}\right)}{\left(f_{em}+f_{es}\right)}+\frac{1}{2}\cdot\frac{\left(l_m^{\,2}\cdot f_{es}\cdot f_{em}^{\,3}+2\cdot f_{em}^{\,2}\cdot f_{es}^{\,2}\cdot l_s^{\,2}+2\cdot f_{em}^{\,2}\cdot l_s\cdot f_{es}^{\,2}\cdot l_m+2\cdot f_{es}^{\,2}\cdot l_m^{\,2}\cdot f_{em}^{\,2}+f_{em}\cdot f_{es}^{\,3}\cdot l_s^{\,2}\right)}{\left[\left(f_{em}+f_{es}\right)\cdot R\right]}$$

$$F = \frac{1}{\left[2\cdot\left(f_{em}+f_{es}\right)\right]}\cdot R+\frac{1}{2}\cdot\frac{\left[-2\cdot f_{em}\cdot f_{es}\cdot\left(l_m+l_s\right)\right]}{\left(f_{em}+f_{es}\right)}+\frac{1}{2}\cdot\frac{\left[f_{em}\cdot f_{es}\cdot\left(f_{em}^{\,2}\cdot l_m^{\,2}+2\cdot f_{em}\cdot f_{es}\cdot l_s^{\,2}+2\cdot f_{es}\cdot f_{em}\cdot l_s\cdot l_m+2\cdot f_{es}\cdot f_{em}\cdot l_m^{\,2}+f_{es}^{\,2}\cdot l_s^{\,2}\right)\right]}{\left[\left(f_{em}+f_{es}\right)\cdot R\right]}$$

$$F = \frac{1}{\left[2\cdot\left(f_{em}+f_{es}\right)\right]}\cdot R+\frac{1}{2}\cdot\frac{\left[-2\cdot f_{em}\cdot f_{es}\cdot\left(l_m+l_s\right)\right]}{\left(f_{em}+f_{es}\right)}+\frac{1}{2}\cdot\frac{R^2}{\left[\left(f_{em}+f_{es}\right)\cdot R\right]}$$

$$F = \frac{R}{f_{em}+f_{es}} - \frac{f_{em}\cdot f_{es}\cdot\left(l_m+l_s\right)}{f_{em}+f_{es}}$$

$$F = \frac{1}{f_{em}+f_{es}}\cdot\left[\frac{-f_{em}\cdot f_{es}\cdot\left(l_m+l_s\right)}{f_{em}+f_{es}} + R\right]$$

$$F = \frac{1}{f_{em}+f_{es}}\cdot\left[-f_{em}\cdot f_{es}\cdot\left(l_m+l_s\right) + \sqrt{f_{em}\cdot f_{es}\cdot\left(2\cdot f_{em}\cdot l_m{}^2\cdot f_{es} + f_{es}{}^2\cdot l_s{}^2 + 2\cdot f_{es}\cdot l_s\cdot f_{em}\cdot l_m + 2\cdot f_{em}\cdot f_{es}\cdot l_s{}^2 + f_{em}{}^2\cdot l_m{}^2\right)}\right]$$

$$F = \frac{1}{f_{em}+f_{es}}\cdot\left[-f_{em}\cdot f_{es}\cdot\left(l_m+l_s\right) + \sqrt{f_{em}\cdot f_{es}\cdot\left[f_{em}{}^2\cdot l_m{}^2 + f_{es}{}^2\cdot l_s{}^2 + \left(2\cdot l_m{}^2 + 2\cdot l_s\cdot l_m + 2\cdot l_s{}^2\right)\cdot f_{em}\cdot f_{es}\right]}\right]$$

A simpler method to evaluate this formula would be to use the quadratic formula: $F = \frac{-B+\sqrt{B^2-4\cdot A\cdot C}}{2\cdot A}$

Terms A and B can be found by inspection:

$$A = \frac{\left(f_{em}+f_{es}\right)}{2} \qquad B = f_{em}\cdot f_{es}\cdot\left(l_m+l_s\right)$$

Using the previously defined R to represent the radical:

$$R = \sqrt{B^2-4\cdot A\cdot C}$$

$$0 = B^2 - 4\cdot A\cdot C - R^2$$

$$C = \frac{1}{4}\cdot\frac{\left(B^2-R^2\right)}{A}$$

Substituting and simplifying produces:

$$C = \frac{-1}{2}\cdot\left(l_s{}^2\cdot f_{es} + f_{em}\cdot l_m{}^2\right)\cdot f_{em}\cdot f_{es}$$

The terms A, B, and C can now be reduced further. Since $A\cdot P^2 + B\cdot P + C = 0$

The results of this last simplification will be shown in the equation summary.

Mode III$_m$

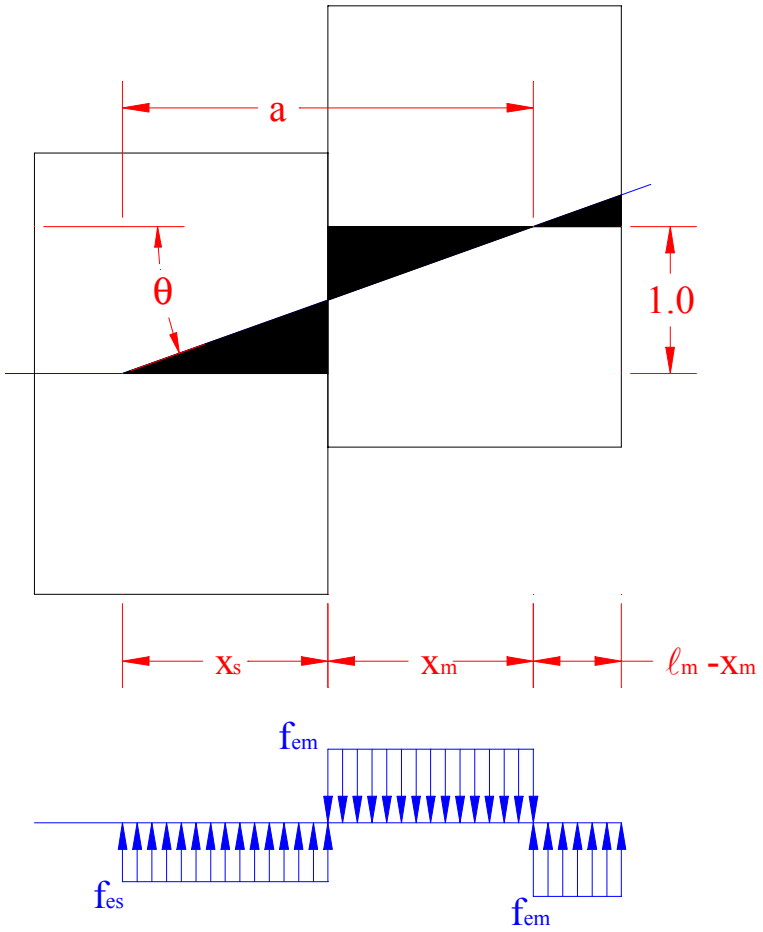

Figure B-4: Mode III$_m$ connection model

General Equation:

$$W = \Sigma\left(f_e \cdot A\right) + \Sigma\left(M_y \cdot \theta\right)$$

Small displacements assumed:

$$\tan(\theta) = \frac{l}{a} = \theta$$

$$a = x_s + x_m$$

$\Sigma\left(M_y \cdot \theta\right)$ term:

$$\Sigma\left(M_y \cdot \theta\right) = \frac{M_y}{a}$$

$\Sigma\left(f_e \cdot A\right)$ term:

$$\Sigma\left(f_e \cdot A\right) = \frac{f_{em}}{2 \cdot a} \cdot \left[\left(l_m - x_m\right)^2 + x_m^2\right] + \frac{f_{es}}{2 \cdot a} \cdot \left(x_s^2\right)$$

Substituting into the general equation:

$$W = \Sigma\left(f_e \cdot A\right) + \Sigma\left(M_y \cdot \theta\right)$$

$$W = F \cdot 1 = \frac{f_{em}}{2 \cdot a} \cdot \left[\left(l_m - x_m\right)^2 + x_m^2\right] + \frac{f_{es}}{2 \cdot a} \cdot \left(x_s^2\right) + \frac{M_y}{a}$$

Substituting for a:

$$F = \frac{f_{em}}{2 \cdot \left(x_s + x_m\right)} \cdot \left[\left(l_m - x_m\right)^2 + x_m^2\right] + \frac{f_{es}}{2 \cdot \left(x_s + x_m\right)} \cdot \left(x_s^2\right) + \frac{M_y}{x_s + x_m}$$

At this point, the general equation is in terms of two unknown variables, x_s and x_m. An equation relating x_s and x_m is found using a diagram of the bearing stress.

By considering equilibrium in the vertical direction ($\Sigma F_y = 0$), the following expression is obtained:

$$f_{em} \cdot \left(l_m - x_m\right) + f_{es} \cdot x_s = f_{em} \cdot x_m$$

Solve for x_s:

$$x_s = -f_{em}\cdot\frac{\left(l_m - 2\cdot x_m\right)}{f_{es}}$$

Substituting for x_m into the expression for F and simplifying:

$$F = \frac{1}{2}\cdot\frac{\left(f_{em}\cdot f_{es}\cdot l_m^{\,2} - 2\cdot f_{em}\cdot f_{es}\cdot l_m\cdot x_m + 2\cdot f_{em}\cdot f_{es}\cdot x_m^{\,2} + f_{em}^{\,2}\cdot l_m^{\,2} - 4\cdot f_{em}^{\,2}\cdot l_m\cdot x_m + 4\cdot f_{em}^{\,2}\cdot x_m^{\,2} + 2\cdot M_y\cdot f_{es}\right)}{\left(x_m\cdot f_{es} - f_{em}\cdot l_m + 2\cdot f_{em}\cdot x_m\right)}$$

This results in an equation with one unknown variable, x_m. The expression is minimized by finding the derivative with respect to x_m and setting it equal to zero. An expression for x_m in terms of the known variables can then be found .

Evaluating $\frac{d}{dx_m}(F) = F' = 0$:

$$\frac{d}{dx_m}(F) = 0 = \frac{1}{2}\cdot\frac{\left[\left(f_{es} + 2\cdot f_{em}\right)\cdot\left(2\cdot f_{es}\cdot f_{em}\cdot x_m^{\,2} - f_{es}\cdot f_{em}\cdot l_m^{\,2} - 2\cdot M_y\cdot f_{es} + 4\cdot f_{em}^{\,2}\cdot x_m^{\,2} + f_{em}^{\,2}\cdot l_m^{\,2} - 4\cdot f_{em}^{\,2}\cdot l_m\cdot x_m\right)\right]}{\left(x_m\cdot f_{es} - f_{em}\cdot l_m + 2\cdot f_{em}\cdot x_m\right)^2}$$

Solving for $x_m$and simplifying:

$$x_m = \left[\begin{array}{l} \frac{1}{2}\cdot\frac{\left[2\cdot f_{em}^{\,2}\cdot l_m - \sqrt{2\cdot f_{es}\cdot f_{em}\cdot\left(f_{em}^{\,2}\cdot l_m^{\,2} + f_{es}\cdot f_{em}\cdot l_m^{\,2} + 2\cdot M_y\cdot f_{es} + 4\cdot M_y\cdot f_{em}\right)}\right]}{\left[f_{em}\cdot\left(f_{es} + 2\cdot f_{em}\right)\right]} \\ \frac{1}{2}\cdot\frac{\left[2\cdot f_{em}^{\,2}\cdot l_m + \sqrt{2\cdot f_{es}\cdot f_{em}\cdot\left(f_{em}^{\,2}\cdot l_m^{\,2} + f_{es}\cdot f_{em}\cdot l_m^{\,2} + 2\cdot M_y\cdot f_{es} + 4\cdot M_y\cdot f_{em}\right)}\right]}{\left[f_{em}\cdot\left(f_{es} + 2\cdot f_{em}\right)\right]} \end{array}\right]$$

To pick which root to use, look at the second derivative. The second derivative must be greater than zero for a minimum.

Taking the second derivative of F and simplifying:

$$\frac{d}{dx_m}(F') = \frac{\left(f_{es} + 2\cdot f_{em}\right)\cdot f_{es}\cdot\left(f_{em}^{\,2}\cdot l_m^{\,2} + f_{es}\cdot f_{em}\cdot l_m^{\,2} + 2\cdot M_y\cdot f_{es} + 4\cdot M_y\cdot f_{em}\right)}{\left[\left(f_{es} + 2\cdot f_{em}\right)\cdot x_m - f_{em}\cdot l_m\right]^3}$$

x_m must be greater than zero (i.e. use the x_m expression with the positive root.).

Take the positive x_m:

$$x_s = \frac{1}{2}\cdot\frac{\left[2\cdot f_{em}^{2}\cdot l_m + \sqrt{2\cdot f_{es}\cdot f_{em}\cdot\left(f_{em}^{2}\cdot l_m^{2} + f_{es}\cdot f_{em}\cdot l_m^{2} + 2\cdot M_y\cdot f_{es} + 4\cdot M_y\cdot f_{em}\right)}\right]}{\left[f_{em}\cdot\left(f_{es} + 2\cdot f_{em}\right)\right]}$$

Let $R = \sqrt{2\cdot f_{es}\cdot f_{em}\cdot\left(f_{em}^{2}\cdot l_m^{2} + f_{es}\cdot f_{em}\cdot l_m^{2} + 2\cdot M_y\cdot f_{es} + 4\cdot M_y\cdot f_{em}\right)}$:

$$x_m = \frac{1}{2}\cdot\frac{\left(2\cdot f_{em}^{2}\cdot l_m + R\right)}{\left[f_{em}\cdot\left(f_{es} + 2\cdot f_{em}\right)\right]}$$

Substituting x_m into the expression for F and reducing:

$$F = \frac{1}{2}\cdot\frac{\left(f_{em}\cdot f_{es}\cdot l_m^{2} - 2\cdot f_{em}\cdot f_{es}\cdot l_m\cdot x_m + 2\cdot f_{em}\cdot f_{es}\cdot x_m^{2} + f_{em}^{2}\cdot l_m^{2} - 4\cdot f_{em}^{2}\cdot l_m\cdot x_m + 4\cdot f_{em}^{2}\cdot x_m^{2} + 2\cdot M_y\cdot f_{es}\right)}{\left(x_m\cdot f_{es} - f_{em}\cdot l_m + 2\cdot f_{em}\cdot x_m\right)}$$

$$F = \frac{1}{2}\cdot\frac{\left(2\cdot f_{em}^{2}\cdot f_{es}^{2}\cdot l_m^{2} + 4\cdot f_{es}^{2}\cdot f_{em}\cdot M_y - 2\cdot f_{em}\cdot f_{es}\cdot l_m\cdot R + 8\cdot f_{em}^{2}\cdot M_y\cdot f_{es} + 2\cdot f_{es}\cdot f_{em}^{3}\cdot l_m^{2} + R^{2}\right)}{\left[\left(f_{es} + 2\cdot f_{em}\right)\cdot R\right]}$$

$$F = \frac{1}{\left[2\cdot\left(f_{es} + 2\cdot f_{em}\right)\right]}\cdot R - \frac{f_{em}\cdot f_{es}\cdot l_m}{f_{es} + 2\cdot f_{em}} + \frac{1}{2}\cdot\frac{\left(2\cdot f_{em}^{2}\cdot f_{es}^{2}\cdot l_m^{2} + 4\cdot f_{es}^{2}\cdot f_{em}\cdot M_y + 8\cdot f_{em}^{2}\cdot M_y\cdot f_{es} + 2\cdot f_{es}\cdot f_{em}^{3}\cdot l_m^{2}\right)}{\left[\left(f_{es} + 2\cdot f_{em}\right)\cdot R\right]}$$

$$F = \frac{1}{\left[2\cdot\left(f_{es} + 2\cdot f_{em}\right)\right]}\cdot R - \frac{f_{em}\cdot f_{es}\cdot l_m}{f_{es} + 2\cdot f_{em}} + \frac{1}{2}\cdot\frac{\left[2\cdot f_{em}\cdot f_{es}\cdot\left(f_{em}^{2}\cdot l_m^{2} + f_{em}\cdot f_{es}\cdot l_m^{2} + 4\cdot f_{em}\cdot M_y + 2\cdot M_y\cdot f_{es}\right)\right]}{\left[\left(f_{es} + 2\cdot f_{em}\right)\cdot R\right]}$$

$$F = \frac{1}{\left[2\cdot\left(f_{es}+2\cdot f_{em}\right)\right]}\cdot R - \frac{f_{em}\cdot f_{es}\cdot l_m}{f_{es}+2\cdot f_{em}} + \frac{1}{2}\cdot\frac{R^2}{\left[\left(f_{es}+2\cdot f_{em}\right)\cdot R\right]}$$

$$F = \frac{-f_{em}\cdot f_{es}\cdot l_m + R}{\left(f_{es}+2\cdot f_{em}\right)}$$

$$F = \frac{1}{\left(f_{es}+2\cdot f_{em}\right)}\cdot\left[-f_{em}\cdot f_{es}\cdot l_m + \sqrt{2\cdot f_{em}\cdot f_{es}\cdot\left(f_{em}^{2}\cdot l_m^{2} + f_{em}\cdot f_{es}\cdot l_m^{2} + 4\cdot f_{em}\cdot M_y + 2\cdot M_y\cdot f_{es}\right)}\right]$$

$$F = \frac{1}{\left(f_{es}+2\cdot f_{em}\right)}\cdot\left[-f_{em}\cdot f_{es}\cdot l_m + \sqrt{2\cdot f_{em}\cdot f_{es}\cdot\left[f_{em}^{2}\cdot l_m^{2} + f_{em}\cdot f_{es}\cdot l_m^{2} + \left(2\cdot f_{es}+4\cdot f_{em}\right)\cdot M_y\right]}\right]$$

$$F = \frac{1}{\left(f_{es}+2\cdot f_{em}\right)}\cdot\left[-f_{em}\cdot f_{es}\cdot l_m + \sqrt{2\cdot f_{em}\cdot f_{es}\cdot\left[f_{em}\cdot l_m^{2}\cdot\left(f_{em}+f_{es}\right) + 2\cdot M_y\cdot\left(f_{es}+2\cdot f_{em}\right)\right]}\right]$$

A simpler method to evaluate this formula would be to use the quadratic formula:

$$F = \frac{-B+\sqrt{B^2-4\cdot A\cdot C}}{2\cdot A}$$

Terms A and B can be found by inspection:

$$A = \frac{\left(f_{es}+2\cdot f_{em}\right)}{2} \qquad B = f_{em}\cdot f_{es}\cdot l_m$$

Using the procedure outlined in the Mode II derivation:

$$C = \frac{-1}{2}\cdot\left(f_{em}\cdot l_m^{2} + 4\cdot M_y\right)\cdot f_{em}\cdot f_{es}$$

The terms A, B, and C can now be reduced further. Since $A\cdot P^2 + B\cdot P + C = 0$

The results of this last simplification will be shown in the equation summary.

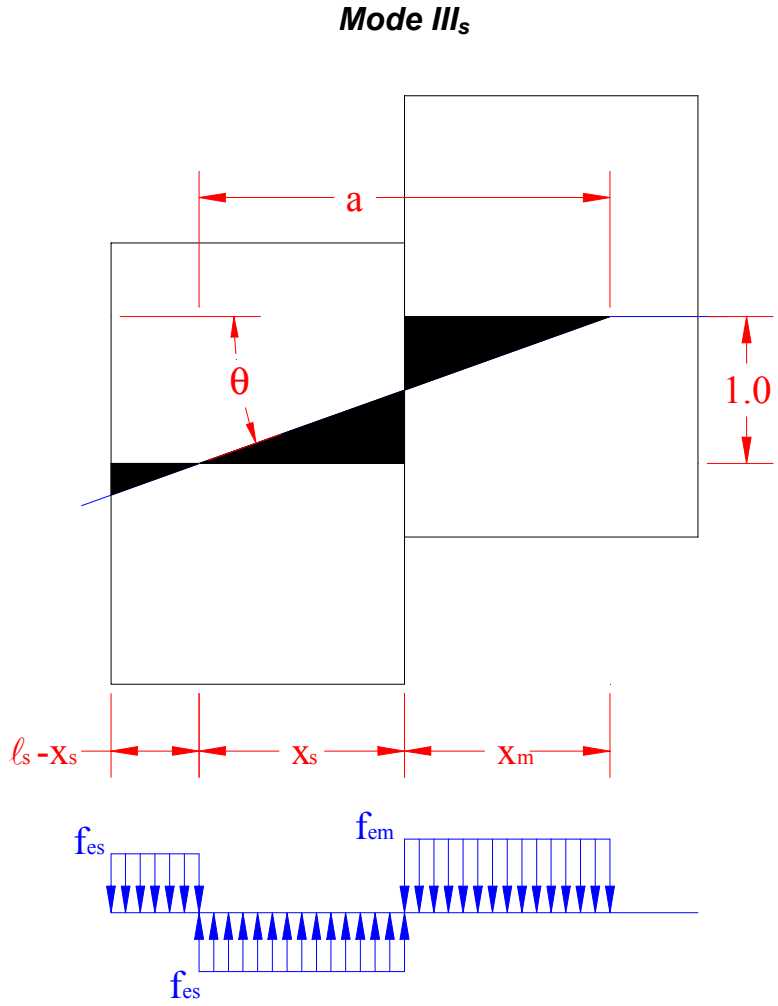

Figure B-5: Mode III_s connection model

General Equation:

$$W = \Sigma\left(f_e \cdot A\right) + \Sigma\left(M_y \cdot \theta\right)$$

Small displacements assumed:

$$\tan(\theta) = \frac{l}{a} = \theta$$

$$a = x_s + x_m$$

$\Sigma\left(M_y \cdot \theta\right)$ term:

$$\Sigma\left(M_y \cdot \theta\right) = \frac{M_y}{a}$$

$\Sigma\left(f_e \cdot A\right)$ term:

$$\Sigma\left(f_e \cdot A\right) = \frac{f_{es}}{2 \cdot a} \cdot \left[\left(l_s - x_s\right)^2 + x_s^2\right] + \frac{f_{em}}{2 \cdot a} \cdot \left(x_m^2\right)$$

Substituting into the general equation:

$$W = \Sigma\left(f_e \cdot A\right) + \Sigma\left(M_y \cdot \theta\right)$$

$$W = F \cdot 1 = \frac{f_{es}}{2 \cdot a} \cdot \left[\left(l_s - x_s\right)^2 + x_s^2\right] + \frac{f_{em}}{2 \cdot a} \cdot \left(x_m^2\right) + \frac{M_y}{a}$$

Substituting for a:

$$F = \frac{f_{es}}{2 \cdot \left(x_s + x_m\right)} \cdot \left[\left(l_s - x_s\right)^2 + x_s^2\right] + \frac{f_{em}}{2 \cdot \left(x_s + x_m\right)} \cdot \left(x_m^2\right) + \frac{M_y}{x_s + x_m}$$

At this point, the general equation is in terms of two unknown variables, x_s and x_m. An equation relating x_s and x_m is found using a diagram of the bearing stress.

By considering equilibrium in the vertical direction ($\Sigma F_y = 0$), the following expression is obtained:

$$f_{es} \cdot \left(l_s - x_s\right) + f_{em} \cdot x_m = f_{es} \cdot x_s$$

Solve for x_m:

$$x_m = -f_{es} \cdot \frac{\left(l_s - 2 \cdot x_s\right)}{f_{em}}$$

Substituting for x_m into the expression for F and simplifying:

$$F = \frac{1}{2} \cdot \frac{\left(f_{em} \cdot f_{es} \cdot l_s^{\,2} - 2 \cdot f_{em} \cdot f_{es} \cdot l_s \cdot x_s + 2 \cdot f_{em} \cdot f_{es} \cdot x_s^{\,2} + f_{es}^{\,2} \cdot l_s^{\,2} - 4 \cdot f_{es}^{\,2} \cdot l_s \cdot x_s + 4 \cdot f_{es}^{\,2} \cdot x_s^{\,2} + 2 \cdot M_y \cdot f_{em}\right)}{\left(x_s \cdot f_{em} - f_{es} \cdot l_s + 2 \cdot f_{es} \cdot x_s\right)}$$

This results in an equation with one unknown variable, x_s. The expression is minimized by finding the derivative with respect to x_s and setting it equal to zero. An expression for x_s in terms of the known variables can then be found .

Evaluating $\frac{d}{dx_s}(F) = F' = 0$:

$$\frac{d}{dx_s}(F) = 0 = \frac{1}{2} \cdot \frac{\left[\left(f_{em} + 2 \cdot f_{es}\right) \cdot \left(2 \cdot f_{em} \cdot f_{es} \cdot x_s^{\,2} - f_{em} \cdot f_{es} \cdot l_s^{\,2} - 2 \cdot M_y \cdot f_{em} + 4 \cdot f_{es}^{\,2} \cdot x_s^{\,2} + f_{es}^{\,2} \cdot l_s^{\,2} - 4 \cdot f_{es}^{\,2} \cdot l_s \cdot x_s\right)\right]}{\left(x_s \cdot f_{em} - f_{es} \cdot l_s + 2 \cdot f_{es} \cdot x_s\right)^2}$$

Solving for $x_s$and simplifying:

$$x_s = \begin{bmatrix} \frac{1}{2} \cdot \frac{\left[2 \cdot f_{es}^{\,2} \cdot l_s - \sqrt{2 \cdot f_{em} \cdot f_{es} \cdot \left(f_{es}^{\,2} \cdot l_s^{\,2} + f_{em} \cdot f_{es} \cdot l_s^{\,2} + 2 \cdot M_y \cdot f_{em} + 4 \cdot M_y \cdot f_{es}\right)}\right]}{\left[f_{es} \cdot \left(f_{em} + 2 \cdot f_{es}\right)\right]} \\ \frac{1}{2} \cdot \frac{\left[2 \cdot f_{es}^{\,2} \cdot l_s + \sqrt{2 \cdot f_{em} \cdot f_{es} \cdot \left(f_{es}^{\,2} \cdot l_s^{\,2} + f_{em} \cdot f_{es} \cdot l_s^{\,2} + 2 \cdot M_y \cdot f_{em} + 4 \cdot M_y \cdot f_{es}\right)}\right]}{\left[f_{es} \cdot \left(f_{em} + 2 \cdot f_{es}\right)\right]} \end{bmatrix}$$

To pick which root to use, look at the second derivative. The second derivative must be greater than zero for a minimum.

Taking the second derivative of F and simplifying:

$$\frac{d}{dx_s}(F') = \frac{\left(f_{em} + 2 \cdot f_{es}\right) \cdot f_{em} \cdot \left(f_{es}^{\,2} \cdot l_s^{\,2} + f_{em} \cdot f_{es} \cdot l_s^{\,2} + 2 \cdot M_y \cdot f_{em} + 4 \cdot M_y \cdot f_{es}\right)}{\left[\left(f_{em} + 2 \cdot f_{es}\right) \cdot x_s - f_{es} \cdot l_s\right]^3}$$

x_s must be greater than zero (i.e. use the x_s expression with the positive root.).

Take the positive x_s:

$$x_s = \frac{1}{2}\cdot\frac{\left[2\cdot f_{es}^{\,2}\cdot l_s + \sqrt{2\cdot f_{em}\cdot f_{es}\cdot\left(f_{es}^{\,2}\cdot l_s^{\,2} + f_{em}\cdot f_{es}\cdot l_s^{\,2} + 2\cdot M_y\cdot f_{em} + 4\cdot M_y\cdot f_{es}\right)}\right]}{\left[f_{es}\cdot\left(f_{em} + 2\cdot f_{es}\right)\right]}$$

Let $R = \sqrt{2\cdot f_{em}\cdot f_{es}\cdot\left(f_{es}^{\,2}\cdot l_s^{\,2} + f_{em}\cdot f_{es}\cdot l_s^{\,2} + 2\cdot M_y\cdot f_{em} + 4\cdot M_y\cdot f_{es}\right)}$:

$$x_s = \frac{1}{2}\cdot\frac{\left(2\cdot f_{es}^{\,2}\cdot l_s + R\right)}{\left[f_{es}\cdot\left(f_{em} + 2\cdot f_{es}\right)\right]}$$

Substituting x_s into the expression for F and reducing:

$$F = \frac{1}{2}\cdot\frac{\left(f_{em}\cdot f_{es}\cdot l_s^{\,2} - 2\cdot f_{em}\cdot f_{es}\cdot l_s\cdot x_s + 2\cdot f_{em}\cdot f_{es}\cdot x_s^{\,2} + f_{es}^{\,2}\cdot l_s^{\,2} - 4\cdot f_{es}^{\,2}\cdot l_s\cdot x_s + 4\cdot f_{es}^{\,2}\cdot x_s^{\,2} + 2\cdot M_y\cdot f_{em}\right)}{\left(x_s\cdot f_{em} - f_{es}\cdot l_s + 2\cdot f_{es}\cdot x_s\right)}$$

$$F = \frac{1}{2}\cdot\frac{\left(2\cdot f_{em}^{\,2}\cdot f_{es}^{\,2}\cdot l_s^{\,2} + 4\cdot f_{em}^{\,2}\cdot f_{es}\cdot M_y - 2\cdot f_{em}\cdot f_{es}\cdot l_s\cdot R + 8\cdot f_{es}^{\,2}\cdot M_y\cdot f_{em} + 2\cdot f_{em}\cdot f_{es}^{\,3}\cdot l_s^{\,2} + R^2\right)}{\left[\left(f_{em} + 2\cdot f_{es}\right)\cdot R\right]}$$

$$F = \frac{1}{\left[2\cdot\left(f_{em} + 2\cdot f_{es}\right)\right]}\cdot R - \frac{f_{em}\cdot f_{es}\cdot l_s}{f_{em} + 2\cdot f_{es}} + \frac{1}{2}\cdot\frac{\left(2\cdot f_{em}^{\,2}\cdot f_{es}^{\,2}\cdot l_s^{\,2} + 4\cdot f_{em}^{\,2}\cdot f_{es}\cdot M_y + 8\cdot f_{es}^{\,2}\cdot M_y\cdot f_{em} + 2\cdot f_{em}\cdot f_{es}^{\,3}\cdot l_s^{\,2}\right)}{\left[\left(f_{em} + 2\cdot f_{es}\right)\cdot R\right]}$$

$$F = \frac{1}{\left[2\cdot\left(f_{em} + 2\cdot f_{es}\right)\right]}\cdot R - \frac{f_{em}\cdot f_{es}\cdot l_s}{f_{em} + 2\cdot f_{es}} + \frac{1}{2}\cdot\frac{\left[2\cdot f_{em}\cdot f_{es}\cdot\left(f_{es}^{\,2}\cdot l_s^{\,2} + f_{em}\cdot f_{es}\cdot l_s^{\,2} + 4\cdot f_{es}\cdot M_y + 2\cdot M_y\cdot f_{em}\right)\right]}{\left[\left(f_{em} + 2\cdot f_{es}\right)\cdot R\right]}$$

$$F = \frac{1}{\left[2\cdot\left(f_{em}+2\cdot f_{es}\right)\right]}\cdot R - \frac{f_{em}\cdot f_{es}\cdot l_s}{f_{em}+2\cdot f_{es}} + \frac{1}{2}\cdot\frac{R^2}{\left[\left(f_{em}+2\cdot f_{es}\right)\cdot R\right]}$$

$$F = \frac{-f_{em}\cdot f_{es}\cdot l_s + R}{\left(f_{em}+2\cdot f_{es}\right)}$$

$$F = \frac{1}{\left(f_{em}+2\cdot f_{es}\right)}\cdot\left[-f_{em}\cdot f_{es}\cdot l_s + \sqrt{2\cdot f_{em}\cdot f_{es}\cdot\left(f_{es}^{\,2}\cdot l_s^{\,2} + f_{em}\cdot f_{es}\cdot l_s^{\,2} + 2\cdot M_y\cdot f_{em} + 4\cdot M_y\cdot f_{es}\right)}\right]$$

$$F = \frac{1}{\left(f_{em}+2\cdot f_{es}\right)}\cdot\left[-f_{em}\cdot f_{es}\cdot l_s + \sqrt{2\cdot f_{em}\cdot f_{es}\cdot\left[f_{es}^{\,2}\cdot l_s^{\,2} + f_{em}\cdot f_{es}\cdot l_s^{\,2} + 2\cdot M_y\cdot\left(f_{em}+2\cdot f_{es}\right)\right]}\right]$$

$$F = \frac{1}{\left(f_{em}+2\cdot f_{es}\right)}\cdot\left[-f_{em}\cdot f_{es}\cdot l_s + \sqrt{2\cdot f_{em}\cdot f_{es}\cdot\left[f_{es}\cdot l_s^{\,2}\cdot\left(f_{es}+f_{em}\right) + 2\cdot M_y\cdot\left(f_{em}+2\cdot f_{es}\right)\right]}\right]$$

A simpler method to evaluate this formula would be to use the quadratic formula:

$$F = \frac{-B+\sqrt{B^2-4\cdot A\cdot C}}{2\cdot A}$$

Terms A and B can be found by inspection:

$$A = \frac{\left(f_{em}+2\cdot f_{es}\right)}{2} \qquad B = f_{em}\cdot f_{es}\cdot l_s$$

Using the procedure outlined in the Mode II derivation:

$$C = \frac{-1}{2}\cdot\left(f_{es}\cdot l_s^{\,2} + 4\cdot M_y\right)\cdot f_{em}\cdot f_{es}$$

The terms A, B, and C can now be reduced further. Since $A\cdot P^2 + B\cdot P + C = 0$

The results of this last simplification will be shown in the equation summary.

Mode IV

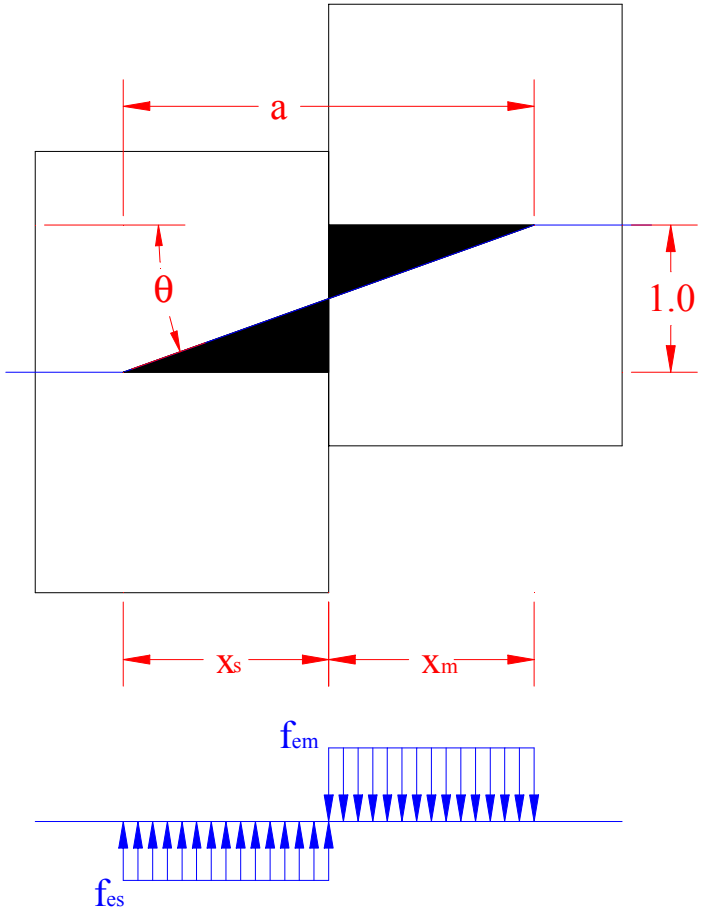

Figure B-6: Mode IV connection model

General Equation:

$$W = \Sigma\left(f_e \cdot A\right) + \Sigma\left(M_y \cdot \theta\right)$$

Small displacements assumed:

$$\tan(\theta) = \frac{1}{a} = \theta$$

$$a = x_s + x_m$$

$\Sigma\left(M_y \cdot \theta\right)$ term:

$$\Sigma\left(M_y \cdot \theta\right) = \frac{2 \cdot M_y}{a}$$

$\Sigma\left(f_e \cdot A\right)$ term:

$$\Sigma\left(f_e \cdot A\right) = \frac{f_{es}}{2 \cdot a} \cdot \left(x_s^2\right) + \frac{f_{em}}{2 \cdot a} \cdot \left(x_m^2\right)$$

Substituting into the general equation:

$$W = \Sigma\left(f_e \cdot A\right) + \Sigma\left(M_y \cdot \theta\right)$$

$$W = F \cdot 1 = \frac{f_{es}}{2 \cdot a} \cdot \left(x_s^2\right) + \frac{f_{em}}{2 \cdot a} \cdot \left(x_m^2\right) + \frac{2 \cdot M_y}{a}$$

Substituting for a:

$$F = \frac{f_{es}}{2 \cdot \left(x_s + x_m\right)} \cdot \left(x_s^2\right) + \frac{f_{em}}{2 \cdot \left(x_s + x_m\right)} \cdot \left(x_m^2\right) + \frac{2 \cdot M_y}{x_s + x_m}$$

At this point, the general equation is in terms of two unknown variables, x_s and x_m. An equation relating x_s and x_m is found using a diagram of the bearing stress.

By considering equilibrium in the vertical direction ($\Sigma F_y = 0$), the following expression is obtained:

$$f_{es} \cdot x_s = f_{em} \cdot x_m$$

Solve for x_m:

$$x_m = \frac{f_{es} \cdot x_s}{f_{em}}$$

Substituting for x_m into the expression for F and simplifying:

$$F = \frac{1}{2} \cdot \frac{\left(f_{es} \cdot f_{em} \cdot x_s^{\,2} + f_{es}^{\,2} \cdot x_s^{\,2} + 4 \cdot M_y \cdot f_{em}\right)}{\left[x_s \cdot \left(f_{em} + f_{es}\right)\right]}$$

This results in an equation with one unknown variable, x_s. The expression is minimized by finding the derivative with respect to x_s and setting it equal to zero. An expression for x_s in terms of the known variables can then be found .

Evaluating $\frac{d}{dx_s}(F) = F' = 0$:

$$\frac{d}{dx_s}(F) = 0 = \frac{1}{2} \cdot \frac{\left(f_{es} \cdot f_{em} \cdot x_s^{\,2} + f_{es}^{\,2} \cdot x_s^{\,2} - 4 \cdot M_y \cdot f_{em}\right)}{\left[x_s^{\,2} \cdot \left(f_{em} + f_{es}\right)\right]}$$

Solving for $x_s$and simplifying:

$$x_s = \begin{bmatrix} 2 \cdot \frac{\sqrt{f_{es} \cdot \left(f_{em} + f_{es}\right) \cdot M_y \cdot f_{em}}}{\left[f_{es} \cdot \left(f_{em} + f_{es}\right)\right]} \\ -2 \cdot \frac{\sqrt{f_{es} \cdot \left(f_{em} + f_{es}\right) \cdot M_y \cdot f_{em}}}{\left[f_{es} \cdot \left(f_{em} + f_{es}\right)\right]} \end{bmatrix}$$

To pick which root to use, look at the second derivative. The second derivative must be greater than zero for a minimum.

Taking the second derivative of F and simplifying:

$$\frac{d}{dx_s}(F') = \frac{4 \cdot M_y \cdot f_{em}}{x_s^{\,3} \cdot \left(f_{em} + f_{es}\right)}$$

x_s must be greater than zero (i.e. use the x_s expression with the positive root.)

Take the positive x_s:

$$x_s = 2 \cdot \frac{\sqrt{f_{es} \cdot (f_{em} + f_{es}) \cdot M_y \cdot f_{em}}}{\left[f_{es} \cdot (f_{em} + f_{es}) \right]}$$

Subsituting x_s into the expression for F and reducing:

$$F = \frac{1}{2} \cdot \frac{\left(f_{es} \cdot f_{em} \cdot x_s^{\,2} + f_{es}^{\,2} \cdot x_s^{\,2} + 4 \cdot M_y \cdot f_{em} \right)}{\left[x_s \cdot (f_{em} + f_{es}) \right]}$$

$$F = \frac{2 \cdot M_y \cdot f_{em} \cdot f_{es}}{\sqrt{(f_{em} + f_{es}) \cdot M_y \cdot f_{em} \cdot f_{es}}}$$

$$F = \sqrt{\frac{4 \cdot M_y \cdot f_{em} \cdot f_{es}}{f_{em} + f_{es}}}$$

A simpler method to evaluate this formula would be to use the quadratic formula:

$$F = \frac{-B + \sqrt{B^2 - 4 \cdot A \cdot C}}{2 \cdot A}$$

The B term can be found by inspection:

$$B = 0$$

Leaving:

$$F = \frac{\sqrt{-4 \cdot A \cdot C}}{2 \cdot A} = \sqrt{\frac{-C}{A}}$$

Therefore:

$$A = f_{em} + f_{es} \qquad C = -4 \cdot M_y \cdot f_{em} \cdot f_{es}$$

The simplified form of the terms A, B, and C will be shown in the equation summary.

Summary of Single Shear Equations

Mode I_m:

$$F = f_{em} \cdot l_m$$

Mode I_s:

$$F = f_{es} \cdot l_s$$

Mode II:

$$F = \frac{1}{f_{em} + f_{es}} \cdot \left[-f_{em} \cdot f_{es} \cdot \left(l_m + l_s \right) + \sqrt{f_{em} \cdot f_{es} \cdot \left[f_{em}^{2} \cdot l_m^{2} + f_{es}^{2} \cdot l_s^{2} + \left(2 \cdot l_m^{2} + 2 \cdot l_s \cdot l_m + 2 \cdot l_s^{2} \right) \cdot f_{em} \cdot f_{es} \right]} \right]$$

Mode III_m:

$$F = \frac{1}{\left(f_{es} + 2 \cdot f_{em} \right)} \cdot \left[-f_{em} \cdot f_{es} \cdot l_m + \sqrt{2 \cdot f_{em} \cdot f_{es} \cdot \left[f_{em} \cdot l_m^{2} \cdot \left(f_{em} + f_{es} \right) + 2 \cdot M_y \cdot \left(f_{es} + 2 \cdot f_{em} \right) \right]} \right]$$

Mode III_s:

$$F = \frac{1}{\left(f_{em} + 2 \cdot f_{es} \right)} \cdot \left[-f_{em} \cdot f_{es} \cdot l_s + \sqrt{2 \cdot f_{em} \cdot f_{es} \cdot \left[f_{es} \cdot l_s^{2} \cdot \left(f_{es} + f_{em} \right) + 2 \cdot M_y \cdot \left(f_{em} + 2 \cdot f_{es} \right) \right]} \right]$$

Mode IV:

$$F = \sqrt{\frac{4 \cdot M_y \cdot f_{em} \cdot f_{es}}{f_{em} + f_{es}}}$$

Summary of Double Shear Equations

The double shear equations are obtained by using the single shear equations where half the load, F, is applied per shear plane. The only exception is Mode I_m where the load in the main member remains F.

Mode I_m:

$$F = f_{em} \cdot l_m$$

Mode I_s:

$$F = 2 \cdot f_{es} \cdot l_s$$

Mode II:

$$F = \frac{2}{f_{em} + f_{es}} \cdot \left[-f_{em} \cdot f_{es} \cdot \left(l_m + l_s \right) + \sqrt{f_{em} \cdot f_{es} \cdot \left[f_{em}^{2} \cdot l_m^{2} + f_{es}^{2} \cdot l_s^{2} + \left(2 \cdot l_m^{2} + 2 \cdot l_s \cdot l_m + 2 \cdot l_s^{2} \right) \cdot f_{em} \cdot f_{es} \right]} \right]$$

Mode III_m:

$$F = \frac{2}{\left(f_{es} + 2 \cdot f_{em} \right)} \cdot \left[-f_{em} \cdot f_{es} \cdot l_m + \sqrt{2 \cdot f_{em} \cdot f_{es} \cdot \left[f_{em} \cdot l_m^{2} \cdot \left(f_{em} + f_{es} \right) + 2 \cdot M_y \cdot \left(f_{es} + 2 \cdot f_{em} \right) \right]} \right]$$

Mode III_s:

$$F = \frac{2}{\left(f_{em} + 2 \cdot f_{es} \right)} \cdot \left[-f_{em} \cdot f_{es} \cdot l_s + \sqrt{2 \cdot f_{em} \cdot f_{es} \cdot \left[f_{es} \cdot l_s^{2} \cdot \left(f_{es} + f_{em} \right) + 2 \cdot M_y \cdot \left(f_{em} + 2 \cdot f_{es} \right) \right]} \right]$$

Mode IV:

$$F = \sqrt{\frac{16 \cdot M_y \cdot f_{em} \cdot f_{es}}{f_{em} + f_{es}}}$$

Summary of Equations for Use with Quadratic Equation

Table B-4: European Yield Model equations

Yield Mode	Single Shear	Double Shear
I_m	$F = f_{em} \cdot l_m$	$F = f_{em} \cdot l_m$
I_s	$F = f_{es} \cdot l_s$	$F = 2 \cdot f_{es} \cdot l_s$
II-IV	$F = \frac{-B + \sqrt{B^2 - 4 \cdot A \cdot C}}{2 \cdot A}$	$F = \frac{-B + \sqrt{B^2 - 4 \cdot A \cdot C}}{A}$

Table B-5: Factors for European Yield Model equations

Yield Mode	A	B	C
II	$\frac{1}{2 \cdot f_{es}} + \frac{1}{2 \cdot f_{em}}$	$l_m + l_s$	$\frac{-1}{2} \cdot \left(f_{es} \cdot l_s^2 + f_{em} \cdot l_m^2 \right)$
III_m	$\frac{1}{2 \cdot f_{em}} + \frac{1}{f_{es}}$	l_m	$\frac{-1}{2} \cdot \left(f_{em} \cdot l_m^2 + 4 \cdot M_y \right)$
III_s	$\frac{1}{f_{em}} + \frac{1}{2 \cdot f_{es}}$	l_s	$\frac{-1}{2} \cdot \left(f_{es} \cdot l_s^2 + 4 \cdot M_y \right)$
IV	$\frac{1}{f_{em}} + \frac{1}{f_{es}}$	0	$-4 \cdot M_y$

APPENDIX C: DERIVATION OF HOLLOW SECTION YIELD MODEL

Overview

This appendix outlines the energy-based derivation of the hollow section yield model (HSYM). The method of virtual displacements was used to develop the equations and the general procedures were outlined in CHAPTER 3. The entire HSYM includes 18 equations. Only the derivation of the six controlling equations will be shown in this appendix. The derivation of the other 12 equations used the identical procedures as those presented here. Recall, that this yield model only applies to sections with two identical walls and a void in the middle (Figure 3-1).

Due to the length of the equations of some intermediate steps of the derivation, the equations were wrapped to fit on the page. The software used has several rules it uses when wrapping equations. Figure C-1 shows several algebraic expressions and how they would be wrapped. In general, the sign shown at the end of the first line only pertains to the first term of the wrapped portion of the equation; the negative sign is *not* distributed to the entire wrapped portion.

$a + b + c$	$a - b + c$	$a - b - c$
$a + \blacksquare \ldots$ $+ b + c$	$a - \blacksquare \ldots$ $+ b + c$	$a - \blacksquare \ldots$ $+ b - c$

Figure C-1: Wrapping Examples

Input Parameters

The only necessary input parameters deal with connection geometry and strength properties as follows:

Table C-1: Input Parameters

Parameter	Description
t_s	Average thickness of walls in side member, inches
t_m	Average thickness of walls in main member, inches
v_s	Width of void in side member, inches
v_m	Width of void in main member, inches
ℓ_s	Total width of side member ($\ell_s = 2t_s + v_s$), inches
ℓ_m	Total width of main member ($\ell_m = 2t_m + v_m$), inches
D	Dowel diameter, inches
F_{es}	Side member dowel bearing strength, psi
F_{em}	Main member dowel bearing strength, psi
F_{yb}	Dowel bending strength, psi

The derivation parameters are used in the yield model to incorporate the input parameters:

Table C-2: Derivation Parameters

Parameter	Description
f_{es}	Side member dowel bearing resistance, lbs./in.
f_{em}	Main member dowel bearing resistance, lbs./in.
M_y	Moment resistance, in-lbs.

The above parameters can be calculated in the following manner:

$$f_{es} = F_{es} D \qquad f_{em} = F_{em} D$$

$$M_y = F_{yb}\left(\frac{D^3}{6}\right)$$

Finding Area of Crushed Material

For each derivation, the area crushed by the dowel must be found. This area is either triangular or trapezoidal in shape. The general procedures to find the areas are summarized below. In all cases, the area crushed will be similar to the a triangle of unit height and base "a".

From the figure on the right and connection yield modes:

$$\tan\theta = \frac{1}{a}$$

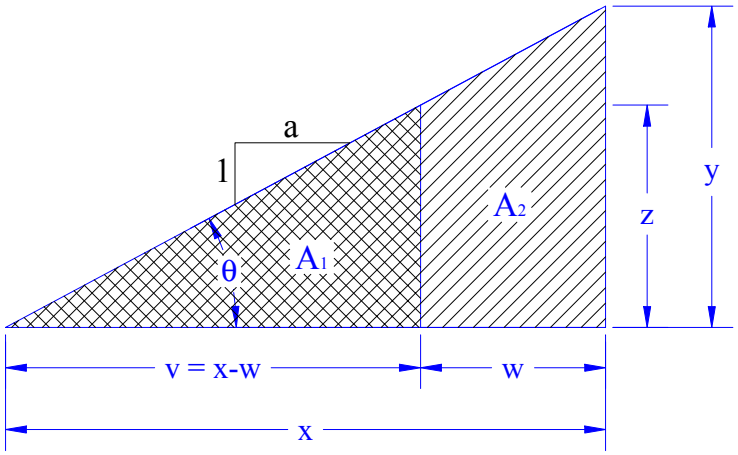

A_1 (for triangular areas):

From drawing on the right:

$$\tan\theta = \frac{z}{v}$$

An expression for z in terms of v is needed.

By similar triangles:

$$\frac{1}{a} = \frac{z}{v}$$

$$z = \frac{v}{a}$$

Find the area of the triangle:

$$\text{Area} = \frac{1}{2}\cdot v \cdot z = \frac{v^2}{2\cdot a}$$

In all the NSYM derivations, the triangular areas crushed are found in this manner. The triangular area is always equal to the base of the triangle squared divided by the quantity 2 times a.

A_2 (for trapezoidal areas):

From drawing above:

$$\tan\theta = \frac{y}{x} = \frac{z}{x - w}$$

An expression for y and z in terms of x and w is needed.

By similar triangles:

$$\frac{1}{a} = \frac{y}{x} = \frac{z}{x - w}$$

$$y = \frac{x}{a} \qquad z = \frac{x - w}{a}$$

Find the area of the trapezoid:

$$\text{Area} = \frac{z + y}{2}\cdot x = \frac{(x - w) + x}{2\cdot a}\cdot w = \frac{(2\,x - w)\cdot w}{2\cdot a}$$

In all the NSYM derivations, the trapezoidal areas crushed are found in this manner.

Single Shear Connection Models

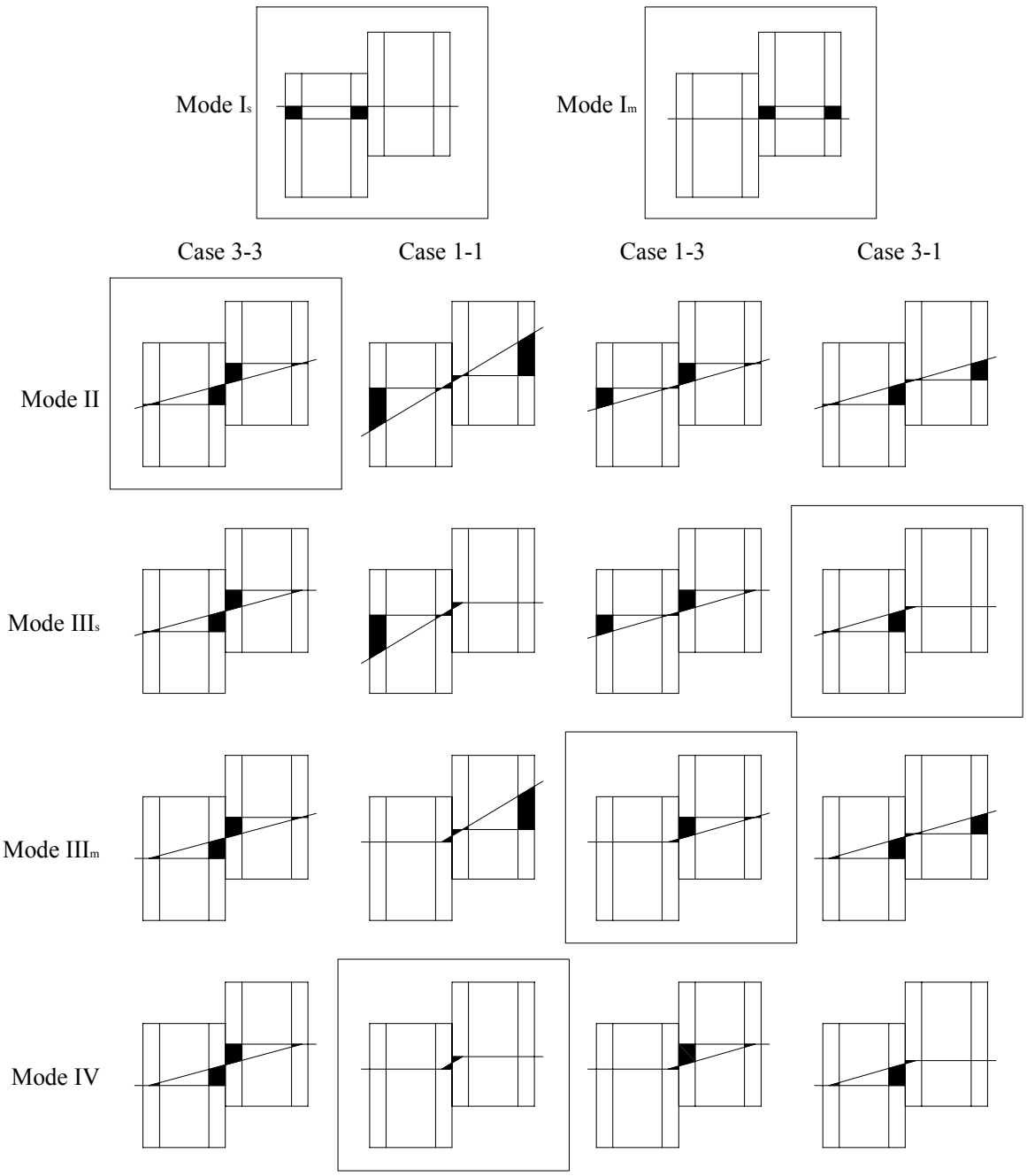

Figure C-2: Single shear connection models. Boxes highlight controlling yield modes. Only the controlling yield modes will be derived in this appendix.

Mode I_s and Mode I_m

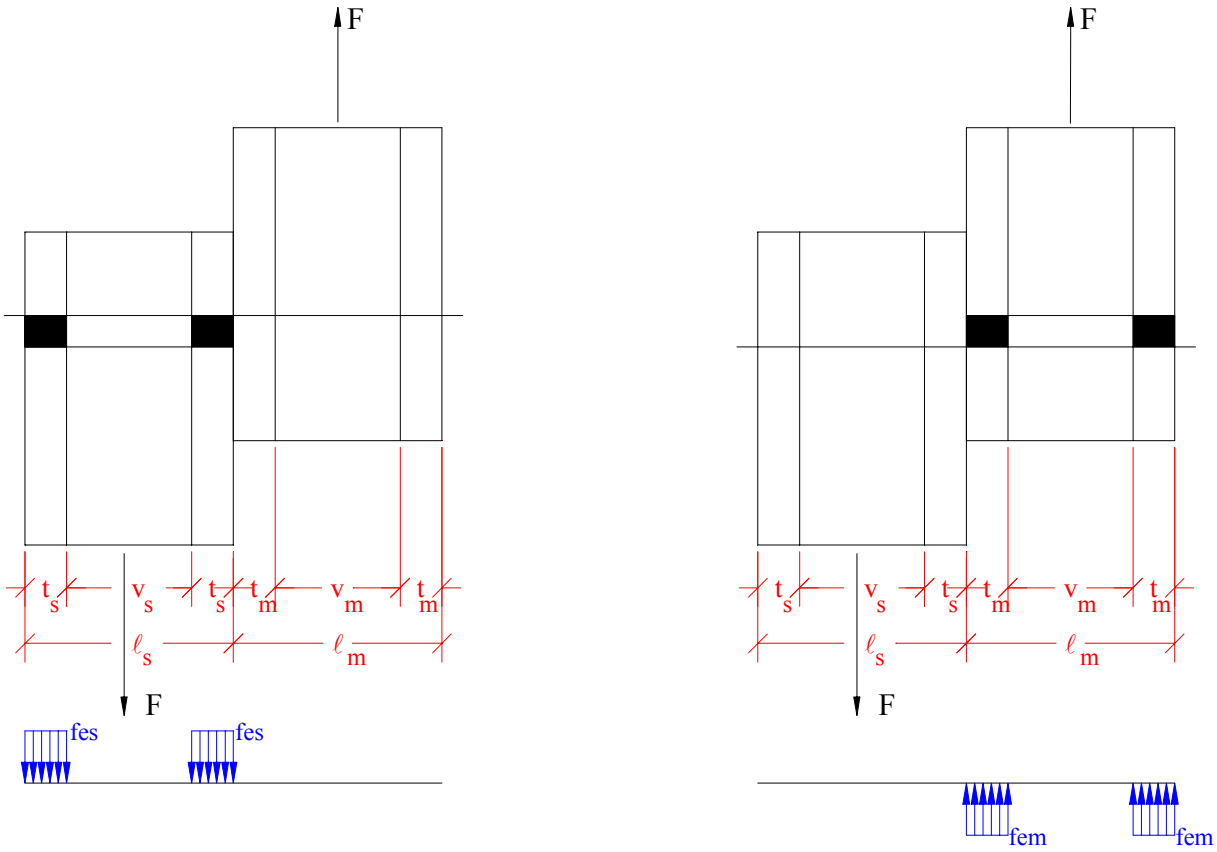

Figure C-3: Mode I_s and Mode I_m connection model

The Mode I_m failure is produced by the main member crushing under the dowel. The Mode I_s failure is produced by the side member crushing under the dowel. In both cases, the load causing this failure is F. Therefore, the equation governing this type of failure is the dowel bearing resistance multiplied by sum of wall thicknesses.

Mode I_m:

$$F = 2 \cdot t_s \cdot f_{es}$$

Mode I_s:

$$F = 2 \cdot t_m \cdot f_{em}$$

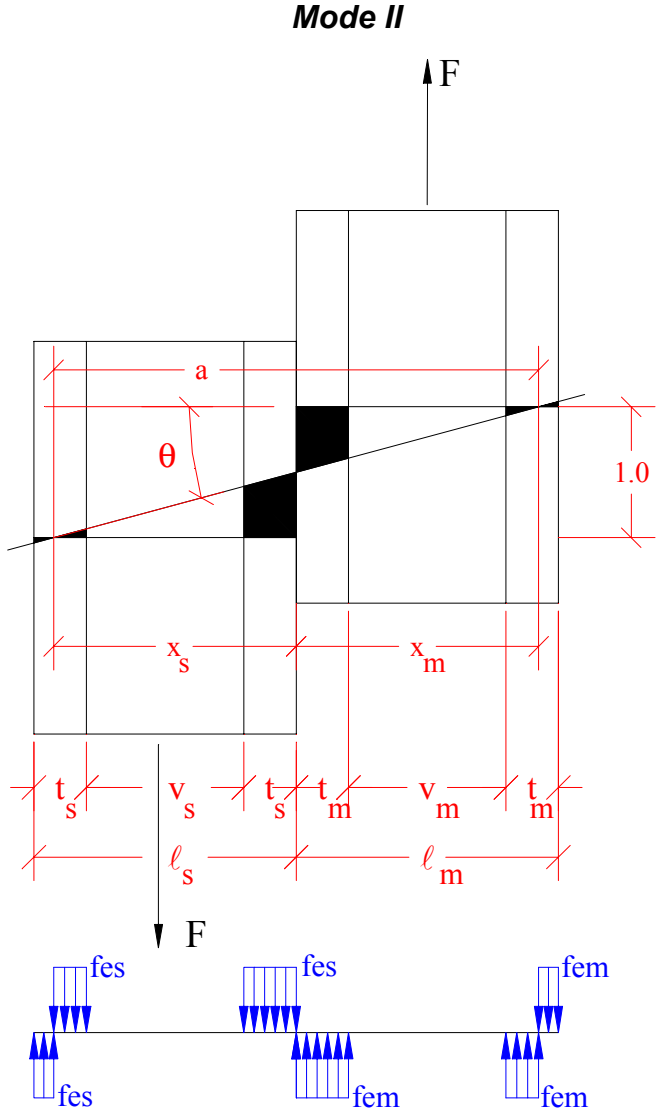

Figure C-4: Mode II: Case 3-3 connection model

General Equation:

$$W = \Sigma\left(f_e \cdot A\right) + \Sigma\left(M_y \cdot \theta\right)$$

Small displacements assumed:

$$\tan(\theta) = \frac{1}{a} = \theta$$

$$a = x_s + x_m$$

$\Sigma\left(M_y \cdot \theta\right)$ term:

For Mode II there is no yielding in the bolt. Therefore, M_y equals 0.

$\Sigma\left(f_e \cdot A\right)$ term:

$$\Sigma\left(f_e \cdot A\right) = \frac{f_{es}}{2 \cdot a} \cdot \left[\left(l_s - x_s\right)^2 + \left(x_s - t_s - v_s\right)^2 + \left(2 \cdot x_s - t_s\right) \cdot t_s\right] + \frac{f_{em}}{2 \cdot a} \cdot \left[\left(2 \cdot x_m - t_m\right) \cdot t_m + \left(x_m - t_m - v_m\right)^2 + \left(l_m - x_m\right)^2\right]$$

Bearing Stress:

$$f_{es} \cdot \left(l_s - x_s\right) + f_{em} \cdot t_m + f_{em} \cdot \left(x_m - t_m - v_m\right) = f_{es} \cdot \left(x_s - t_s - v_s\right) + f_{es} \cdot t_s + f_{em} \cdot \left(l_m - x_m\right)$$

Solve for x_m:

$$x_m = \frac{-1}{2} \cdot \frac{\left(f_{es} \cdot l_s - 2 \cdot f_{es} \cdot x_s - f_{em} \cdot v_m + f_{es} \cdot v_s - f_{em} \cdot l_m\right)}{f_{em}}$$

Substituting into the general equation:

$$W = \Sigma\left(f_e \cdot A\right) + \Sigma\left(M_y \cdot \theta\right)$$

$$W = F \cdot 1 = \frac{f_{es}}{2 \cdot a} \cdot \left[\left(l_s - x_s\right)^2 + \left(x_s - t_s - v_s\right)^2 + \left(2 \cdot x_s - t_s\right) \cdot t_s\right] + \frac{f_{em}}{2 \cdot a} \cdot \left[\left(2 \cdot x_m - t_m\right) \cdot t_m + \left(x_m - t_m - v_m\right)^2 + \left(l_m - x_m\right)^2\right]$$

Substituting for a:

$$F = \frac{f_{es}}{2\cdot(x_s + x_m)}\cdot\left[(l_s - x_s)^2 + (x_s - t_s - v_s)^2 + (2\cdot x_s - t_s)\cdot t_s\right] + \frac{f_{em}}{2\cdot(x_s + x_m)}\cdot\left[(2\cdot x_m - t_m)\cdot t_m + (x_m - t_m - v_m)^2 + (l_m - x_m\right.$$

Substituting for x_m and simplifying:

$$F = \frac{1}{2}\cdot\frac{\left(\begin{array}{l}2\cdot f_{es}\cdot f_{em}\cdot l_s^2 - 4\cdot f_{es}\cdot f_{em}\cdot l_s\cdot x_s + 4\cdot f_{es}\cdot f_{em}\cdot x_s^2 - 4\cdot f_{es}\cdot f_{em}\cdot x_s\cdot v_s + 4\cdot f_{es}\cdot f_{em}\cdot t_s\cdot v_s + 2\cdot f_{es}\cdot f_{em}\cdot v_s^2 - 2\cdot f_{em}^2\cdot v_m\cdot l_m - \blacksquare\ \ldots \\ + 4\cdot f_{es}^2\cdot x_s\cdot v_s + 2\cdot f_{es}^2\cdot l_s\cdot v_s - 4\cdot f_{es}^2\cdot l_s\cdot x_s + 4\cdot f_{em}^2\cdot t_m\cdot v_m + f_{es}^2\cdot l_s^2 + f_{em}^2\cdot v_m^2 + f_{es}^2\cdot v_s^2 + f_{em}^2\cdot l_m^2 + 4\cdot f_{es}^2\cdot x_s^2\end{array}\right)}{\left(2\cdot x_s\cdot f_{em} - f_{es}\cdot l_s + 2\cdot f_{es}\cdot x_s + f_{em}\cdot v_m - f_{es}\cdot v_s + f_{em}\cdot l_m\right)}$$

Substituting $l_s = 2\cdot t_s + v_s$ and $l_m = 2\cdot t_m + v_m$. Then, simplifying:

$$F = \frac{-\left(\begin{array}{l}3\cdot f_{es}\cdot f_{em}\cdot t_s\cdot v_s - 2\cdot f_{es}\cdot f_{em}\cdot x_s\cdot v_s + f_{es}\cdot f_{em}\cdot x_s^2 - 2\cdot f_{es}\cdot f_{em}\cdot x_s\cdot t_s - 2\cdot f_{es}^2\cdot x_s\cdot v_s + f_{em}^2\cdot t_m\cdot v_m - 2\cdot f_{es}^2\cdot x_s\cdot t_s + \blacksquare\ \ldots \\ + 2\cdot f_{es}^2\cdot v_s\cdot t_s + 2\cdot f_{es}\cdot f_{em}\cdot t_s^2 + f_{es}\cdot f_{em}\cdot v_s^2 + f_{es}^2\cdot v_s^2 + f_{es}^2\cdot x_s^2 + f_{em}^2\cdot t_m^2 + f_{es}^2\cdot t_s^2\end{array}\right)}{\left(-x_s\cdot f_{em} + f_{es}\cdot t_s + f_{es}\cdot v_s - f_{es}\cdot x_s - f_{em}\cdot v_m - f_{em}\cdot t_m\right)}$$

Evaluating $\frac{d}{dx_s}(F) = 0$:

$$\frac{d}{dx_s}(F) = 0 = \frac{\left[-(f_{em} + f_{es})\cdot\left[\begin{array}{l}f_{em}^2\cdot t_m\cdot v_m + f_{em}^2\cdot t_m^2 + f_{es}\cdot f_{em}\cdot v_s^2 - f_{es}\cdot f_{em}\cdot x_s^2 + 2\cdot f_{em}\cdot f_{es}\cdot t_s\cdot v_m + 3\cdot f_{es}\cdot f_{em}\cdot t_s\cdot v_s + \blacksquare\ \ldots \\ + 2\cdot f_{em}\cdot f_{es}\cdot v_s\cdot t_m - 2\cdot f_{em}\cdot f_{es}\cdot x_s\cdot v_m + 2\cdot f_{em}\cdot f_{es}\cdot t_s\cdot t_m - 2\cdot f_{em}\cdot f_{es}\cdot x_s\cdot t_m + 2\cdot f_{es}\cdot f_{em}\cdot t_s^2 + \blacksquare\ \ldots \\ + 2\cdot f_{em}\cdot f_{es}\cdot v_s\cdot v_m - f_{es}^2\cdot t_s^2 + 2\cdot f_{es}^2\cdot x_s\cdot v_s - f_{es}^2\cdot x_s^2 + 2\cdot f_{es}^2\cdot x_s\cdot t_s - 2\cdot f_{es}^2\cdot v_s\cdot t_s - f_{es}^2\cdot v_s^2\end{array}\right]\right]}{\left(-x_s\cdot f_{em} + f_{es}\cdot t_s + f_{es}\cdot v_s - f_{es}\cdot x_s - f_{em}\cdot v_m - f_{em}\cdot t_m\right)^2}$$

Solving for x_s and simplifying:

$$x_s = \left[\frac{\left[-f_{es}\cdot\left[f_{em}\cdot\left(t_m + v_m\right) - f_{es}\cdot\left(v_s + t_s\right)\right] - \sqrt{f_{es}\cdot f_{em}\cdot\left[\begin{array}{l}\left(t_m\cdot v_m + t_m^{\,2}\right)\cdot f_{em}^{\,2} + \blacksquare\ \ldots \\ + \left(t_s^{\,2} + t_s\cdot v_s\right)\cdot f_{es}^{\,2} + \blacksquare\ \ldots \\ + \left[\begin{array}{l}2\cdot t_s\cdot v_m + 3\cdot t_m\cdot v_m + 3\cdot t_s\cdot v_s + 2\cdot t_s\cdot t_m + \blacksquare\ \ldots \\ + 2\cdot v_s\cdot t_m + \left(v_s + v_m\right)^2 + 2\cdot t_m^{\,2} + 2\cdot t_s^{\,2}\end{array}\right]\cdot f_{em}\cdot f_{es}\end{array}\right]}\right]}{\left[f_{es}\cdot\left(f_{em} + f_{es}\right)\right]} \right.$$

$$\left. \frac{\left[-f_{es}\cdot\left[f_{em}\cdot\left(t_m + v_m\right) - f_{es}\cdot\left(v_s + t_s\right)\right] + \sqrt{f_{es}\cdot f_{em}\cdot\left[\begin{array}{l}\left(t_m\cdot v_m + t_m^{\,2}\right)\cdot f_{em}^{\,2} + \blacksquare\ \ldots \\ + \left(t_s^{\,2} + t_s\cdot v_s\right)\cdot f_{es}^{\,2} + \blacksquare\ \ldots \\ + \left[\begin{array}{l}2\cdot t_s\cdot v_m + 3\cdot t_m\cdot v_m + 3\cdot t_s\cdot v_s + 2\cdot t_s\cdot t_m + \blacksquare\ \ldots \\ + 2\cdot v_s\cdot t_m + \left(v_s + v_m\right)^2 + 2\cdot t_m^{\,2} + 2\cdot t_s^{\,2}\end{array}\right]\cdot f_{em}\cdot f_{es}\end{array}\right]}\right]}{\left[f_{es}\cdot\left(f_{em} + f_{es}\right)\right]} \right]$$

To pick which root to use, look at the second derivative. The second derivative must be greater than zero for a minimum.

Taking the second derivative and simplifying:

$$\frac{d}{dx_s}(F') = \frac{-2\cdot\left(f_{em} + f_{es}\right)\cdot f_{em}\cdot\left[\begin{array}{l}2\cdot f_{em}\cdot t_m^{\,2}\cdot f_{es} + f_{es}^{\,2}\cdot v_s\cdot t_s + 2\cdot f_{em}\cdot f_{es}\cdot t_s\cdot t_m + f_{es}\cdot f_{em}\cdot v_s^{\,2} + 2\cdot f_{es}\cdot f_{em}\cdot t_s^{\,2} + f_{em}^{\,2}\cdot t_m\cdot v_m + \blacksquare\ \ldots \\ + f_{es}^{\,2}\cdot t_s^{\,2} + 2\cdot f_{em}\cdot f_{es}\cdot v_s\cdot t_m + 3\cdot f_{es}\cdot f_{em}\cdot t_s\cdot v_s + 2\cdot f_{es}\cdot t_s\cdot f_{em}\cdot v_m + 2\cdot f_{es}\cdot v_s\cdot f_{em}\cdot v_m + f_{em}\cdot f_{es}\cdot v_m^{\,2} + \blacksquare\ \ldots \\ + 3\cdot t_m\cdot f_{em}\cdot v_m\cdot f_{es} + f_{em}^{\,2}\cdot t_m^{\,2}\end{array}\right]}{\left[\left(-f_{es} - f_{em}\right)\cdot x_s - f_{em}\cdot v_m + f_{es}\cdot t_s + f_{es}\cdot v_s - t_m\cdot f_{em}\right]^3}$$

x_s must be greater than zero (i.e. use the x_s expression with the positive root.)

Take the positive x_s:

$$x_s = \frac{\left[-f_{es}\cdot\left[f_{em}\cdot\left(t_m+v_m\right)-f_{es}\cdot\left(v_s+t_s\right)\right]+\blacksquare\ldots\right.}{\left[f_{es}\cdot\left(f_{em}+f_{es}\right)\right]}$$
$$\left.+\sqrt{f_{es}\cdot f_{em}\cdot\left[\left(t_m\cdot v_m+t_m^{\,2}\right)\cdot f_{em}^{\,2}+\left(t_s^{\,2}+t_s\cdot v_s\right)\cdot f_{es}^{\,2}+\blacksquare\ldots\right.}\right]$$
$$\left.\left.+\left[2\cdot t_s\cdot v_m+3\cdot t_m\cdot v_m+3\cdot t_s\cdot v_s+2\cdot t_s\cdot t_m+2\cdot v_s\cdot t_m+\left(v_s+v_m\right)^2+2\cdot t_m^{\,2}+2\cdot t_s^{\,2}\right]\cdot f_{em}\cdot f_{es}\right]\right]$$

Let $R = \sqrt{f_{es}\cdot f_{em}\cdot\left[\left(t_m\cdot v_m+t_m^{\,2}\right)\cdot f_{em}^{\,2}+\left(t_s^{\,2}+t_s\cdot v_s\right)\cdot f_{es}^{\,2}+\blacksquare\ldots\right.}$
$$\left.+\left[2\cdot t_s\cdot v_m+3\cdot t_m\cdot v_m+3\cdot t_s\cdot v_s+2\cdot t_s\cdot t_m+2\cdot v_s\cdot t_m+\left(v_s+v_m\right)^2+2\cdot t_m^{\,2}+2\cdot t_s^{\,2}\right]\cdot f_{em}\cdot f_{es}\right]$$

$$x_s = \frac{\left[-f_{es}\cdot\left[f_{em}\cdot\left(t_m+v_m\right)-f_{es}\cdot\left(v_s+t_s\right)\right]+R\right]}{\left[f_{es}\cdot\left(f_{em}+f_{es}\right)\right]}$$

Substituting x_s into the expression for F and reducing:

$$F = \frac{-\left(3\cdot f_{es}\cdot f_{em}\cdot t_s\cdot v_s-2\cdot f_{es}\cdot f_{em}\cdot x_s\cdot v_s+f_{es}\cdot f_{em}\cdot x_s^{\,2}-2\cdot f_{es}\cdot f_{em}\cdot x_s\cdot t_s-2\cdot f_{es}^{\,2}\cdot x_s\cdot v_s+f_{em}^{\,2}\cdot t_m\cdot v_m-2\cdot f_{es}^{\,2}\cdot x_s\cdot t_s+\blacksquare\ldots\right.}{\left(-x_s\cdot f_{em}+f_{es}\cdot t_s+f_{es}\cdot v_s-f_{es}\cdot x_s-f_{em}\cdot v_m-f_{em}\cdot t_m\right)}$$
$$\left.+2\cdot f_{es}^{\,2}\cdot v_s\cdot t_s+2\cdot f_{es}\cdot f_{em}\cdot t_s^{\,2}+f_{es}\cdot f_{em}\cdot v_s^{\,2}+f_{es}^{\,2}\cdot v_s^{\,2}+f_{es}^{\,2}\cdot x_s^{\,2}+f_{em}^{\,2}\cdot t_m^{\,2}+f_{es}^{\,2}\cdot t_s^{\,2}\right)$$

$$F = \frac{1}{\left(f_{em}+f_{es}\right)}\cdot R+\frac{\left[-2\cdot f_{es}\cdot f_{em}\cdot\left(v_m+t_m+v_s+t_s\right)\right]}{\left(f_{em}+f_{es}\right)}+\blacksquare\ldots$$
$$+\frac{\left[f_{es}\cdot f_{em}\cdot\left[\left(t_m\cdot v_m+t_m^{\,2}\right)\cdot f_{em}^{\,2}+\left(t_s^{\,2}+t_s\cdot v_s\right)\cdot f_{es}^{\,2}+\blacksquare\ldots\right.\right.}{\left[\left(f_{em}+f_{es}\right)\cdot R\right]}$$
$$\left.\left.+\left[2\cdot t_s\cdot v_m+3\cdot t_m\cdot v_m+3\cdot t_s\cdot v_s+2\cdot t_s\cdot t_m+2\cdot v_s\cdot t_m+\left(v_s+v_m\right)^2+2\cdot t_m^{\,2}+2\cdot t_s^{\,2}\right]\cdot f_{em}\cdot f_{es}\right]\right]$$

$$F = \frac{1}{\left(f_{em} + f_{es}\right)} \cdot R + \frac{\left[-2 \cdot f_{es} \cdot f_{em} \cdot \left(v_m + t_m + v_s + t_s\right)\right]}{\left(f_{em} + f_{es}\right)} + \frac{R^2}{\left[\left(f_{em} + f_{es}\right) \cdot R\right]}$$

$$F = \frac{2}{\left(f_{em} + f_{es}\right)} \cdot R - 2 \cdot f_{es} \cdot f_{em} \cdot \frac{\left(v_m + t_m + v_s + t_s\right)}{\left(f_{em} + f_{es}\right)}$$

$$F = \frac{2}{\left(f_{em} + f_{es}\right)} \cdot \left[-f_{es} \cdot f_{em} \cdot \left(v_m + t_m + v_s + t_s\right) + R\right]$$

Substituting for R produces the general equation:

$$F = \frac{2}{\left(f_{em} + f_{es}\right)} \cdot \left[-f_{es} \cdot f_{em} \cdot \left(v_m + t_m + v_s + t_s\right) + \blacksquare \ldots + \sqrt{f_{es} \cdot f_{em} \cdot \left[\left(t_m \cdot v_m + t_m^{\,2}\right) \cdot f_{em}^{\,2} + \left(t_s^{\,2} + t_s \cdot v_s\right) \cdot f_{es}^{\,2} + \blacksquare \ldots + \left[2 \cdot t_s \cdot v_m + 3 \cdot t_m \cdot v_m + 3 \cdot t_s \cdot v_s + 2 \cdot t_s \cdot t_m + 2 \cdot v_s \cdot t_m + \left(v_s + v_m\right)^2 + 2 \cdot t_m^{\,2} + 2 \cdot t_s^{\,2}\right] \cdot f_{em} \cdot f_{es}\right]}\right]$$

A simpler method to evaluate this equation would be to use the quadratic formula:

$$F = \frac{-B + \sqrt{B^2 - 4 \cdot A \cdot C}}{2 \cdot A}$$

Terms A and B can be found by inspection:

$$A = \frac{f_{em} + f_{es}}{4} \qquad B = \left(t_m + t_s + v_s + v_m\right) \cdot f_{em} \cdot f_{es}$$

Using the previously defined R to represent the radical:

$$R = \sqrt{B^2 - 4 \cdot A \cdot C}$$

$$0 = B^2 - 4 \cdot A \cdot C - R^2$$

$$C = \frac{1}{4} \cdot \frac{B^2 - R^2}{A}$$

Substituting and simplifying produces:

$$C = -\left[f_{es} \cdot t_s \cdot \left(t_s + v_s\right) + f_{em} \cdot t_m \cdot \left(t_m + v_m\right)\right] \cdot f_{es} \cdot f_{em}$$

The terms A, B, and C can now be reduced further. Since $A \cdot P^2 + B \cdot P + C = 0$

The results of this last simplification will be shown in the equation summary.

$$A = \frac{f_{em} + f_{es}}{4} = \frac{f_{em} + f_{es}}{4 \cdot \left(f_{em} \cdot f_{es}\right)} = \boxed{\frac{1}{4 \cdot f_{es}} + \frac{1}{4 \cdot f_{em}}}$$

$$B = \left(t_m + t_s + v_s + v_m\right) \cdot f_{em} \cdot f_{es} = \boxed{\left(t_m + t_s + v_s + v_m\right)}$$

$$C = -\left[f_{es} \cdot t_s \cdot \left(t_s + v_s\right) + f_{em} \cdot t_m \cdot \left(t_m + v_m\right)\right] \cdot f_{es} \cdot f_{em} = \boxed{-\left[f_{es} \cdot t_s \cdot \left(t_s + v_s\right) + f_{em} \cdot t_m \cdot \left(t_m + v_m\right)\right]}$$

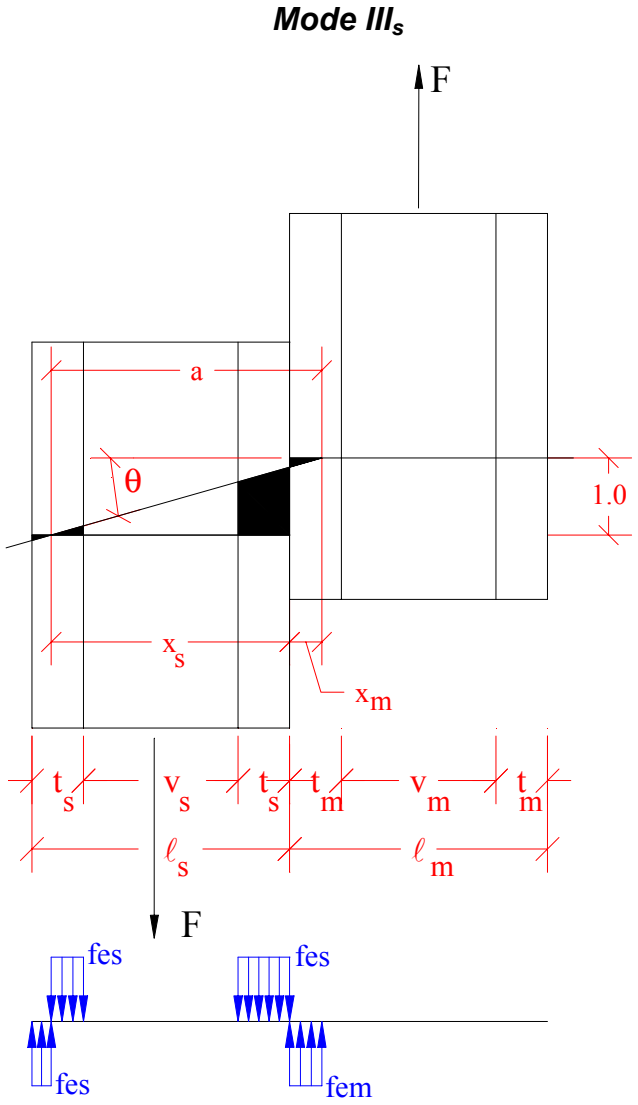

Figure C-5: Mode III$_s$: Case 3-1 connection model

General Equation:

$$W = \Sigma\left(f_e \cdot A\right) + \Sigma\left(M_y \cdot \theta\right)$$

Small displacements assumed:

$$\tan(\theta) = \frac{1}{a} = \theta$$

$$a = x_s + x_m$$

$\Sigma\left(M_y \cdot \theta\right)$ term:

$$\Sigma\left(M_y \cdot \theta\right) = \frac{M_y}{a}$$

$\Sigma\left(f_e \cdot A\right)$ term:

$$\Sigma\left(f_e \cdot A\right) = \frac{f_{es}}{2 \cdot a} \cdot \left[\left(l_s - x_s\right)^2 + \left(x_s - t_s - v_s\right)^2 + \left(2 \cdot x_s - t_s\right) \cdot t_s\right] + \frac{f_{em}}{2 \cdot a} \cdot \left(x_m{}^2\right)$$

Bearing Stress:

$$f_{es} \cdot \left(l_s - x_s\right) + f_{em} \cdot x_m = f_{es} \cdot \left(x_s - t_s - v_s\right) + f_{es} \cdot t_s$$

Solve for x_m:

$$x_m = \frac{-\left(f_{es} \cdot l_s - 2 \cdot f_{es} \cdot x_s + f_{es} \cdot v_s\right)}{f_{em}}$$

Substituting into the general equation:

$$W = \Sigma\left(f_e \cdot A\right) + \Sigma\left(M_y \cdot \theta\right)$$

$$W = F \cdot 1 = \frac{f_{es}}{2 \cdot a} \cdot \left[\left(l_s - x_s\right)^2 + \left(x_s - t_s - v_s\right)^2 + \left(2 \cdot x_s - t_s\right) \cdot t_s\right] + \frac{f_{em}}{2 \cdot a} \cdot \left(x_m{}^2\right) + \frac{M_y}{a}$$

Substituting for a:

$$F = \frac{f_{es}}{\left(2\cdot x_s + 2\cdot x_m\right)}\cdot\left[\left(l_s - x_s\right)^2 + \left(x_s - t_s - v_s\right)^2 + \left(2\cdot x_s - t_s\right)\cdot t_s\right] + \frac{f_{em}}{\left(2\cdot x_s + 2\cdot x_m\right)}\cdot x_m{}^2 + \frac{M_y}{\left(x_s + x_m\right)}$$

Substituting for x_m and simplifying:

$$F = \frac{1}{2}\cdot\frac{\left(\begin{array}{l} f_{em}\cdot f_{es}\cdot l_s{}^2 - 2\cdot f_{em}\cdot f_{es}\cdot l_s\cdot x_s + 2\cdot f_{em}\cdot f_{es}\cdot x_s{}^2 - 2\cdot f_{em}\cdot f_{es}\cdot x_s\cdot v_s + 2\cdot f_{em}\cdot f_{es}\cdot t_s\cdot v_s + f_{em}\cdot f_{es}\cdot v_s{}^2 + f_{es}{}^2\cdot l_s{}^2 - 4\cdot f_{es}{}^2\cdot l_s\cdot x_s + \blacksquare\ \ldots \\ + 2\cdot f_{es}{}^2\cdot l_s\cdot v_s + 4\cdot f_{es}{}^2\cdot x_s{}^2 - 4\cdot f_{es}{}^2\cdot x_s\cdot v_s + f_{es}{}^2\cdot v_s{}^2 + 2\cdot M_y\cdot f_{em} \end{array}\right)}{\left(x_s\cdot f_{em} - f_{es}\cdot l_s + 2\cdot f_{es}\cdot x_s - f_{es}\cdot v_s\right)}$$

Substituting $l_s = 2\cdot t_s + v_s$ and $l_m = 2\cdot t_m + v_m$. Then, simplifying:

$$F = \frac{\left(\begin{array}{l} 2\cdot f_{es}\cdot f_{em}\cdot t_s{}^2 + 3\cdot f_{es}\cdot f_{em}\cdot t_s\cdot v_s - 2\cdot f_{em}\cdot f_{es}\cdot t_s\cdot x_s + f_{em}\cdot f_{es}\cdot v_s{}^2 - 2\cdot f_{em}\cdot f_{es}\cdot v_s\cdot x_s + f_{em}\cdot f_{es}\cdot x_s{}^2 + 2\cdot f_{es}{}^2\cdot x_s{}^2 - \blacksquare\ \ldots \\ + 4\cdot f_{es}{}^2\cdot t_s\cdot x_s - 4\cdot f_{es}{}^2\cdot v_s\cdot x_s + 2\cdot f_{es}{}^2\cdot t_s{}^2 + 4\cdot f_{es}{}^2\cdot t_s\cdot v_s + 2\cdot f_{es}{}^2\cdot v_s{}^2 + M_y\cdot f_{em} \end{array}\right)}{\left(x_s\cdot f_{em} - 2\cdot f_{es}\cdot t_s - 2\cdot f_{es}\cdot v_s + 2\cdot f_{es}\cdot x_s\right)}$$

Evaluating $\frac{d}{dx_s}(F) = 0$:

$$\frac{d}{dx_s}(F) = 0 = \frac{-\left[\begin{array}{l} -4\cdot f_{es}{}^3\cdot v_s{}^2 - 4\cdot f_{es}{}^3\cdot t_s{}^2 - 4\cdot f_{es}{}^3\cdot x_s{}^2 + M_y\cdot f_{em}{}^2 + 4\cdot f_{em}\cdot f_{es}{}^2\cdot v_s\cdot x_s + 4\cdot f_{em}\cdot f_{es}{}^2\cdot t_s\cdot x_s + 2\cdot f_{es}{}^2\cdot f_{em}\cdot t_s\cdot v_s - \blacksquare\ \ldots \\ + 4\cdot f_{em}\cdot f_{es}{}^2\cdot x_s{}^2 + 2\cdot f_{es}{}^2\cdot f_{em}\cdot t_s{}^2 + 8\cdot f_{es}{}^3\cdot t_s\cdot x_s + 8\cdot f_{es}{}^3\cdot v_s\cdot x_s + 2\cdot f_{es}\cdot f_{em}{}^2\cdot t_s{}^2 - f_{es}\cdot x_s{}^2\cdot f_{em}{}^2 - \blacksquare\ \ldots \\ + 8\cdot f_{es}{}^3\cdot t_s\cdot v_s + f_{em}{}^2\cdot f_{es}\cdot v_s{}^2 + 3\cdot f_{es}\cdot f_{em}{}^2\cdot t_s\cdot v_s + 2\cdot M_y\cdot f_{em}\cdot f_{es} \end{array}\right]}{\left(x_s\cdot f_{em} - 2\cdot f_{es}\cdot t_s - 2\cdot f_{es}\cdot v_s + 2\cdot f_{es}\cdot x_s\right)^2}$$

Solving for x_s and simplifying:

$$x_s = \begin{bmatrix} \dfrac{\left[2\cdot f_{es}^{\,2}\cdot\left(v_s+t_s\right)-\sqrt{f_{em}\cdot f_{es}\cdot\left[\left(2\cdot t_s^{\,2}+2\cdot t_s\cdot v_s\right)\cdot f_{es}^{\,2}+\left(f_{em}+2\cdot f_{es}\right)\cdot M_y+\left(t_s+v_s\right)\cdot\left(2\cdot t_s+v_s\right)\cdot f_{es}\cdot f_{em}\right]}\right]}{\left[f_{es}\cdot\left(f_{em}+2\cdot f_{es}\right)\right]} \\ \dfrac{\left[2\cdot f_{es}^{\,2}\cdot\left(v_s+t_s\right)+\sqrt{f_{em}\cdot f_{es}\cdot\left[\left(2\cdot t_s^{\,2}+2\cdot t_s\cdot v_s\right)\cdot f_{es}^{\,2}+\left(f_{em}+2\cdot f_{es}\right)\cdot M_y+\left(t_s+v_s\right)\cdot\left(2\cdot t_s+v_s\right)\cdot f_{es}\cdot f_{em}\right]}\right]}{\left[f_{es}\cdot\left(f_{em}+2\cdot f_{es}\right)\right]} \end{bmatrix}$$

To pick which root to use, look at the second derivative. The second derivative must be greater than zero for a minimum.

Taking the second derivative and simplifying:

$$\frac{d}{dx_s}(F') = 2\cdot\left(f_{em}+2\cdot f_{es}\right)\cdot f_{em}\cdot\frac{\left(M_y\cdot f_{em}+2\cdot f_{es}^{\,2}\cdot t_s\cdot v_s+2\cdot f_{es}^{\,2}\cdot t_s^{\,2}+2\cdot f_{es}\cdot f_{em}\cdot t_s^{\,2}+f_{em}\cdot f_{es}\cdot v_s^{\,2}+3\cdot f_{es}\cdot f_{em}\cdot t_s\cdot v_s+2\cdot M_y\cdot f_{es}\right)}{\left(x_s\cdot f_{em}-2\cdot f_{es}\cdot t_s-2\cdot f_{es}\cdot v_s+2\cdot f_{es}\cdot x_s\right)^3}$$

x_s must be greater than zero (i.e. use the x_s expression with the positive root.)

Take the positive x_s:

$$x_s = \frac{\left[2\cdot f_{es}^{\,2}\cdot\left(v_s+t_s\right)+\sqrt{f_{em}\cdot f_{es}\cdot\left[\left(2\cdot t_s^{\,2}+2\cdot t_s\cdot v_s\right)\cdot f_{es}^{\,2}+\left(f_{em}+2\cdot f_{es}\right)\cdot M_y+\left(t_s+v_s\right)\cdot\left(2\cdot t_s+v_s\right)\cdot f_{es}\cdot f_{em}\right]}\right]}{\left[f_{es}\cdot\left(f_{em}+2\cdot f_{es}\right)\right]}$$

Let $R = \sqrt{f_{em}\cdot f_{es}\cdot\left[\left(2\cdot t_s^{\,2}+2\cdot t_s\cdot v_s\right)\cdot f_{es}^{\,2}+\left(f_{em}+2\cdot f_{es}\right)\cdot M_y+\left(t_s+v_s\right)\cdot\left(2\cdot t_s+v_s\right)\cdot f_{es}\cdot f_{em}\right]}$

$$x_s = \frac{\left[2\cdot f_{es}^{\,2}\cdot\left(v_s+t_s\right)+R\right]}{\left[f_{es}\cdot\left(f_{em}+2\cdot f_{es}\right)\right]}$$

Substituting x_s into the expression for F and reducing:

$$F = \frac{\left(\begin{array}{l} 2\cdot f_{es}\cdot f_{em}\cdot t_s^{\,2} + 3\cdot f_{es}\cdot f_{em}\cdot t_s\cdot v_s - 2\cdot f_{em}\cdot f_{es}\cdot t_s\cdot x_s + f_{em}\cdot f_{es}\cdot v_s^{\,2} - 2\cdot f_{em}\cdot f_{es}\cdot v_s\cdot x_s + f_{em}\cdot f_{es}\cdot x_s^{\,2} + 2\cdot f_{es}^{\,2}\cdot x_s^{\,2} - \blacksquare \ \ldots \\ + 4\cdot f_{es}^{\,2}\cdot t_s\cdot x_s - 4\cdot f_{es}^{\,2}\cdot v_s\cdot x_s + 2\cdot f_{es}^{\,2}\cdot t_s^{\,2} + 4\cdot f_{es}^{\,2}\cdot t_s\cdot v_s + 2\cdot f_{es}^{\,2}\cdot v_s^{\,2} + M_y\cdot f_{em} \end{array}\right)}{\left(x_s\cdot f_{em} - 2\cdot f_{es}\cdot t_s - 2\cdot f_{es}\cdot v_s + 2\cdot f_{es}\cdot x_s\right)}$$

$$F = \frac{1}{\left(f_{em}+2\cdot f_{es}\right)}\cdot R + \frac{\left[-2\cdot f_{em}\cdot f_{es}\cdot\left(t_s+v_s\right)\right]}{\left(f_{em}+2\cdot f_{es}\right)} + \frac{\left[f_{em}\cdot f_{es}\cdot\left[\left(2\cdot t_s^{\,2}+2\cdot t_s\cdot v_s\right)\cdot f_{es}^{\,2}+\left(f_{em}+2\cdot f_{es}\right)\cdot M_y+\left(t_s+v_s\right)\cdot\left(2\cdot t_s+v_s\right)\cdot f_{es}\cdot f_{em}\right]\right]}{\left[\left(f_{em}+2\cdot f_{es}\right)\cdot R\right]}$$

$$F = \frac{1}{\left(f_{em}+2\cdot f_{es}\right)}\cdot R + \frac{\left[-2\cdot f_{em}\cdot f_{es}\cdot\left(t_s+v_s\right)\right]}{\left(f_{em}+2\cdot f_{es}\right)} + \frac{R^2}{\left[\left(f_{em}+2\cdot f_{es}\right)\cdot R\right]}$$

$$F = \frac{2}{\left(f_{em}+2\cdot f_{es}\right)}\cdot R + \frac{\left[-2\cdot f_{em}\cdot f_{es}\cdot\left(t_s+v_s\right)\right]}{\left(f_{em}+2\cdot f_{es}\right)}$$

$$F = \frac{2}{\left(f_{em}+2\cdot f_{es}\right)}\cdot\left[\left(-1\cdot f_{em}\cdot f_{es}\cdot t_s - 1\cdot f_{em}\cdot f_{es}\cdot v_s\right)+R\right]$$

$$F = \frac{2}{\left(f_{em}+2\cdot f_{es}\right)}\cdot\left[-f_{em}\cdot f_{es}\cdot\left(t_s+v_s\right)+R\right]$$

Substituting for R produces the general equation:

$$F = \frac{2}{\left(f_{em}+2\cdot f_{es}\right)}\cdot\left[-f_{em}\cdot f_{es}\cdot\left(t_s+v_s\right)+\sqrt{f_{em}\cdot f_{es}\cdot\left[\left(2\cdot t_s^{\,2}+2\cdot t_s\cdot v_s\right)\cdot f_{es}^{\,2}+\left(f_{em}+2\cdot f_{es}\right)\cdot M_y+\left(t_s+v_s\right)\cdot\left(2\cdot t_s+v_s\right)\cdot f_{es}\cdot f_{em}\right]}\right]$$

A simpler method to evaluate this equation would be to use the quadratic formula:

$$F = \frac{-B + \sqrt{B^2 - 4 \cdot A \cdot C}}{2 \cdot A}$$

Terms A and B can be found by inspection:

$$A = \frac{f_{em} + 2 \cdot f_{es}}{4} \qquad B = f_{em} \cdot f_{es} \cdot \left(t_s + v_s\right)$$

Using the previously defined R to represent the radical:

$$R = \sqrt{B^2 - 4 \cdot A \cdot C}$$

$$0 = B^2 - 4 \cdot A \cdot C - R^2$$

$$C = \frac{1}{4} \cdot \frac{B^2 - R^2}{A}$$

Substituting and simplifying produces:

$$C = \frac{-1}{2} \cdot \left(f_{es} \cdot l_s^{\,2} + 4 \cdot M_y\right) \cdot f_{em} \cdot f_{es}$$

The terms A, B, and C can now be reduced further. Since $A \cdot P^2 + B \cdot P + C = 0$

The results of this last simplification will be shown in the equation summary.

$$A = \frac{f_{em} + 2 \cdot f_{es}}{4} = \frac{f_{em} + 2 \cdot f_{es}}{4 \cdot \left(f_{em} \cdot f_{es}\right)} = \boxed{\frac{1}{4 \cdot f_{es}} + \frac{1}{2 \cdot f_{em}}}$$

$$B = f_{em} \cdot f_{es} \cdot \left(t_s + v_s\right) = \left(t_s + v_s\right) = \boxed{\left(t_s + v_s\right)}$$

$$C = -\left[M_y + f_{es} \cdot t_s \cdot \left(t_s + v_s\right)\right] \cdot f_{es} \cdot f_{em} = -\left[f_{es} \cdot t_s \cdot \left(t_s + v_s\right) + M_y\right] = \boxed{-\left[f_{es} \cdot t_s \cdot \left(t_s + v_s\right) + M_y\right]}$$

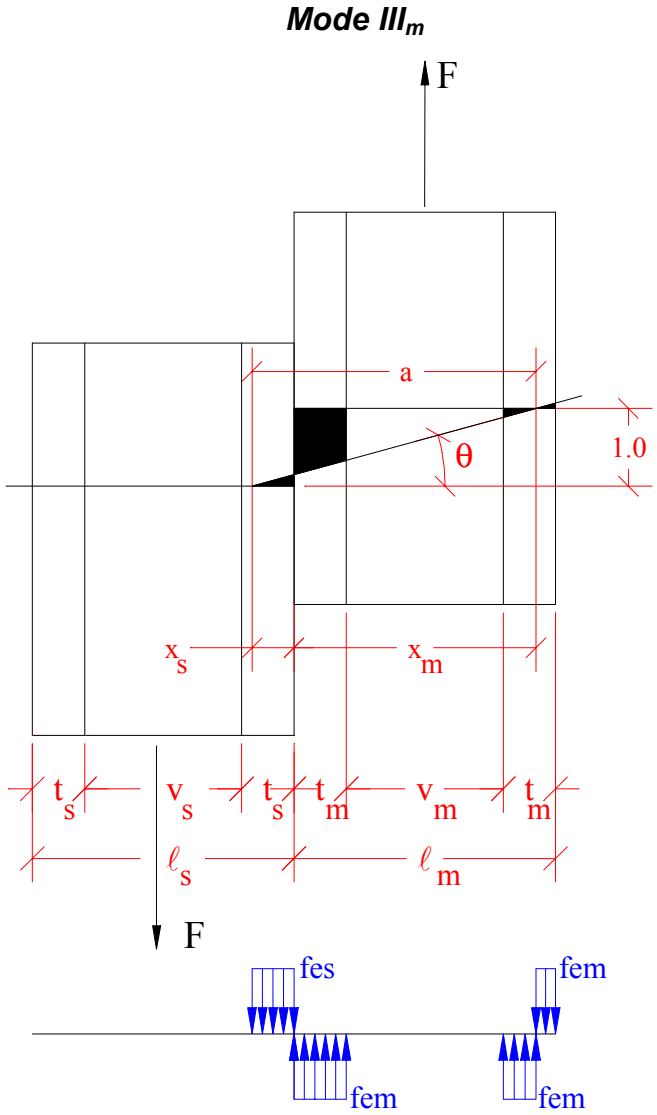

Figure C-6: Mode III$_m$: Case 1-3 connection model

The derivation of the Mode III_m equations is identical to the derivation of the Mode III_s equations with the s and m subscripts reversed. Therefore, only the results for Mode III_m will be given.

Location of dowel rotaion and dowel yielding:

$$x_s = \frac{-\left(f_{em} \cdot l_m - 2 \cdot f_{em} \cdot x_m + f_{em} \cdot v_m\right)}{f_{es}}$$

$$x_m = \frac{\left[2 \cdot f_{em}^2 \cdot \left(v_m + t_m\right) + \sqrt{f_{es} \cdot f_{em} \cdot \left[\left(2 \cdot t_m^2 + 2 \cdot t_m \cdot v_m\right) \cdot f_{em}^2 + \left(f_{es} + 2 \cdot f_{em}\right) \cdot M_y + \left(t_m + v_m\right) \cdot \left(2 \cdot t_m + v_m\right) \cdot f_{em} \cdot f_{es}\right]}\right]}{\left[f_{em} \cdot \left(f_{es} + 2 \cdot f_{em}\right)\right]}$$

General equation:

$$F = \frac{2}{\left(f_{es} + 2 \cdot f_{em}\right)} \cdot \left[-f_{es} \cdot f_{em} \cdot \left(t_m + v_m\right) + \sqrt{f_{es} \cdot f_{em} \cdot \left[\left(2 \cdot t_m^2 + 2 \cdot t_m \cdot v_m\right) \cdot f_{em}^2 + \left(f_{es} + 2 \cdot f_{em}\right) \cdot M_y + \left(t_m + v_m\right) \cdot \left(2 \cdot t_m + v_m\right) \cdot f_{em} \cdot f_{es}\right]}\right]$$

Reduced quadratic formula terms:

$$A = \frac{1}{4 \cdot f_{em}} + \frac{1}{2 \cdot f_{es}}$$

$$B = \left(t_m + v_m\right)$$

$$C = -\left[f_{em} \cdot t_m \cdot \left(t_m + v_m\right) + M_y\right]$$

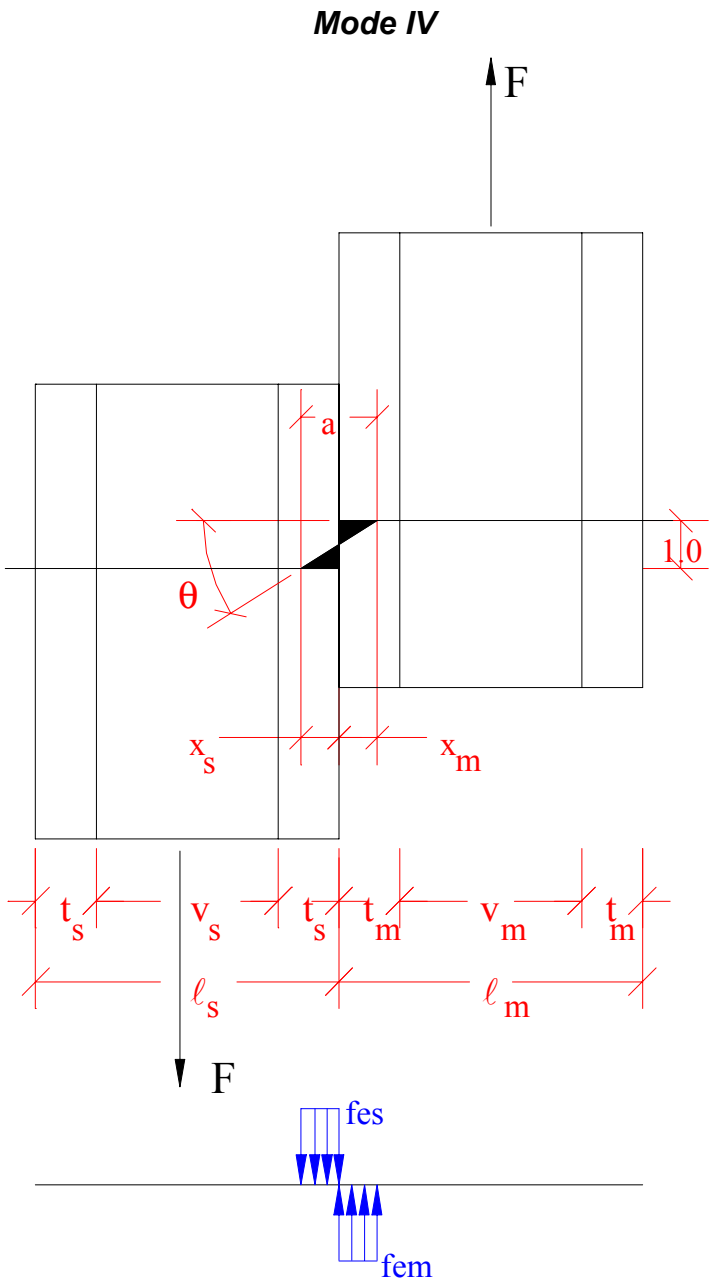

Figure C-7: Mode IV: Case 1-1 connection model

General Equation:

$$W = \Sigma\left(f_e \cdot A\right) + \Sigma\left(M_y \cdot \theta\right)$$

Small displacements assumed:

$$\tan(\theta) = \frac{1}{a} = \theta$$

$$a = x_s + x_m$$

$\Sigma\left(M_y \cdot \theta\right)$ term:

$$\Sigma\left(M_y \cdot \theta\right) = \frac{2 \cdot M_y}{a}$$

$\Sigma\left(f_e \cdot A\right)$ term:

$$\Sigma\left(f_e \cdot A\right) = \frac{f_{es}}{2 \cdot a} \cdot \left(x_s^{\,2}\right) + \frac{f_{em}}{2 \cdot a} \cdot \left(x_m^{\,2}\right)$$

Bearing Stress:

$$f_{es} \cdot x_s = f_{em} \cdot x_m$$

Solve for x_m:

$$x_m = f_{es} \cdot \frac{x_s}{f_{em}}$$

Substituting into the general equation:

$$W = \Sigma\left(f_e \cdot A\right) + \Sigma\left(M_y \cdot \theta\right)$$

$$W = F \cdot 1 = \frac{f_{es}}{2 \cdot a} \cdot \left(x_s^{\,2}\right) + \frac{f_{em}}{2 \cdot a} \cdot \left(x_m^{\,2}\right) + \frac{2 \cdot M_y}{a}$$

Substituting for a:

$$F = \frac{f_{es}}{\left(2 \cdot x_s + 2 \cdot x_m\right)} \cdot x_s^{\,2} + \frac{f_{em}}{\left(2 \cdot x_s + 2 \cdot x_m\right)} \cdot x_m^{\,2} + 2 \cdot \frac{M_y}{\left(x_s + x_m\right)}$$

Substituting for x_m and simplifying:

$$F = \frac{1}{2} \cdot \frac{\left(f_{es} \cdot f_{em} \cdot x_s^{\,2} + f_{es}^{\,2} \cdot x_s^{\,2} + 4 \cdot M_y \cdot f_{em}\right)}{\left[x_s \cdot \left(f_{em} + f_{es}\right)\right]}$$

Evaluating $\frac{d}{dx_s}(F) = 0$:

$$\frac{d}{dx_s}(F) = 0 = \frac{1}{2} \cdot \frac{\left(f_{es} \cdot f_{em} \cdot x_s^{\,2} + f_{es}^{\,2} \cdot x_s^{\,2} - 4 \cdot M_y \cdot f_{em}\right)}{\left[x_s^{\,2} \cdot \left(f_{em} + f_{es}\right)\right]}$$

Solving for x_s and simplifying:

$$x_s = \begin{bmatrix} \frac{2}{\left(f_{es} \cdot f_{em} + f_{es}^2\right)} \cdot \sqrt{f_{es} \cdot \left(f_{em} + f_{es}\right) \cdot M_y \cdot f_{em}} \\ \frac{-2}{\left(f_{es} \cdot f_{em} + f_{es}^2\right)} \cdot \sqrt{f_{es} \cdot \left(f_{em} + f_{es}\right) \cdot M_y \cdot f_{em}} \end{bmatrix}$$

To pick which root to use, look at the second derivative.
The second derivative must be greater than zero for a minimum.

Taking the second derivative and simplifying:

$$\frac{d}{dx_s}(F') = 4 \cdot M_y \cdot \frac{f_{em}}{\left[x_s^3 \cdot \left(f_{em} + f_{es}\right)\right]}$$

x_s must be greater than zero (i.e. use the x_s expression with the positive root.)

Take the positive x_s:

$$x_s = \frac{2}{\left(f_{es} \cdot f_{em} + f_{es}^2\right)} \cdot \sqrt{f_{es} \cdot \left(f_{em} + f_{es}\right) \cdot M_y \cdot f_{em}}$$

:

Substituting x_s into the expression for F and reducing:

$$F = \frac{1}{2} \cdot \frac{\left(f_{es} \cdot f_{em} \cdot x_s^2 + f_{es}^2 \cdot x_s^2 + 4 \cdot M_y \cdot f_{em}\right)}{\left[x_s \cdot \left(f_{em} + f_{es}\right)\right]}$$

$$F = \frac{1}{4} \cdot \begin{bmatrix} \frac{4 \cdot f_{es}^2 \cdot f_{em}^2 \cdot \left(f_{em} + f_{es}\right) \cdot M_y}{\left(f_{es} \cdot f_{em} + f_{es}^2\right)^2} + \blacksquare \ldots \\ + \frac{4 \cdot f_{es}^3 \cdot \left(f_{em} + f_{es}\right) \cdot M_y \cdot f_{em}}{\left(f_{es} \cdot f_{em} + f_{es}^2\right)^2} + 4 \cdot M_y \cdot f_{em} \end{bmatrix} \cdot \frac{\left(f_{es} \cdot f_{em} + f_{es}^2\right)}{\left[\sqrt{f_{es} \cdot \left(f_{em} + f_{es}\right) \cdot M_y \cdot f_{em}} \cdot \left(f_{em} + f_{es}\right)\right]}$$

$$F = 2 \cdot f_{em} \cdot f_{es} \cdot \frac{M_y}{\sqrt{f_{es} \cdot \left(f_{em} + f_{es}\right) \cdot M_y \cdot f_{em}}}$$

$$F = \frac{\sqrt{\left(4 \cdot f_{em}^{\,2} \cdot f_{es}^{\,2} \cdot M_y\right)}}{\sqrt{f_{es} \cdot \left(f_{em} + f_{es}\right) \cdot M_y \cdot f_{em}}}$$

Combining the radicals produces the general equation:

$$F = \sqrt{\frac{\left(4 \cdot f_{em} \cdot f_{es} \cdot M_y\right)}{\left(f_{em} + f_{es}\right)}}$$

A simpler method to evaluate this equation would be to use the quadratic formula:

$$F = \frac{-B + \sqrt{B^2 - 4 \cdot A \cdot C}}{2 \cdot A}$$

The term B can be found by inspection:

$$B = 0$$

The quadratic formula can now be reduced in the following manner:

$$F = \frac{\sqrt{-4 \cdot A \cdot C}}{2 \cdot A} = \frac{\sqrt{-4 \cdot A \cdot C}}{\sqrt{4 \cdot A^2}} = \sqrt{\frac{-C}{A}}$$

Therefore:

$$A = f_{em} + f_{es}$$

$$C = -\left(4 \cdot f_{em} \cdot f_{es} \cdot M_y\right)$$

The terms A, B, and C can now be reduced further. Since $A \cdot P^2 + B \cdot P + C = 0$

The results of this last simplification will be shown in the equation summary.

$$A = f_{em} + f_{es} = \frac{f_{em} + f_{es}}{f_{em} \cdot f_{es}} = \frac{1}{4 \cdot f_{es}} + \frac{1}{4 \cdot f_{em}}$$

$$B = 0 = 0 = 0$$

$$C = -\left(4 \cdot f_{em} \cdot f_{es} \cdot M_y\right) = -M_y = -M_y$$

Double Shear in Hollow Sections

The hollow section yield equations have been derived in single shear. Table C-3 describes the conversion of the single shear equations to double shear. Mode I_s in double shear is two times the single shear connection capacity. However, double shear Mode I_m remains the same as the single shear equation. The double shear yield mode cannot solely consist of dowel rotation in the main member. Therefore, all cases of Mode II and Mode III_m; Mode III_s: Case 1-3 and Case 3-3; and Mode IV: Case 1-3 and Case 3-3 are not physically possible in double shear. The double shear equations for Mode III_s and Mode IV for Cases 3-1 and 1-1 are twice the single shear equations.

Table C-3: Double Shear Equations

Mode	Case	Double Shear Equation
Mode I_m	-	Same as single shear
Mode I_s	-	Two times single shear
Mode II	1-1	N/A
	3-3	
	3-1	
	1-3	
Mode III_m	3-3	N/A
	3-1	
	1-1	
	1-3	
Mode III_s	3-3	N/A
	1-3	N/A
	1-1	Two times single shear
	3-1	Two times single shear
Mode IV	1-1	Two times single shear
	3-3	N/A
	3-1	Two times single shear
	1-3	N/A

In addition to the single shear yield modes considered, four yield modes specific to double shear equations with hollow members must be considered (Figure C-8). These four yield modes are a result of an additional location of dowel yielding due to the symmetry of the double shear problem. Yield load equations were derived of each yield equation (Table C-4). The resulting equations were in a different form from the rest of the equations. Because the equations are for

strictly hollow sections, the EYM equations are not produced when the void spaces are set to zero. Even though theoretically these cases may occur, the derivation of the equations limits there governing. In order to satisfy equilibrium, both the points of dowel yielding and dowel rotation in the side and main members (x_s and x_m) are restricted to specific locations. Since the locations of dowel yielding and dowel rotation are already determined, energy is no longer minimized during the derivation procedure. This results in the equations failing to ever control connection capacity.

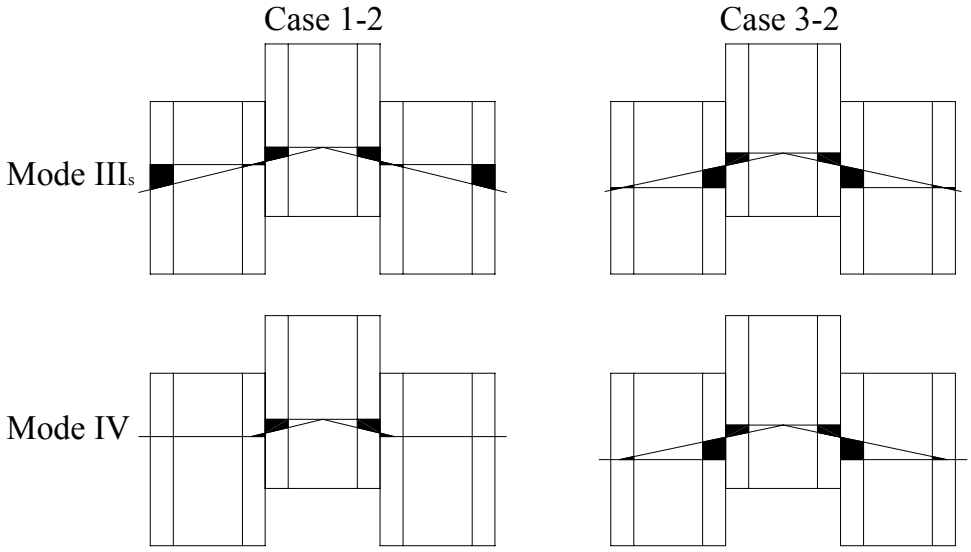

Figure C-8: Double shear yield modes due to symmetry

Table C-4: Double Shear Equations For Symmetric Yield Modes

Yield Mode	Case	Yield Equation
Mode III$_s$	1-2	$F = \frac{\left(4\cdot t_s\cdot l_s - 4\cdot t_s^2\right)\cdot f_{es}^2 + \left(2\cdot t_m\cdot v_m + 2\cdot t_m^2\right)\cdot f_{es}\cdot f_{em} + f_{em}^2\cdot t_m^2 + 4\cdot M_y\cdot f_{es}}{\left[\left(2\cdot t_s + 2\cdot t_m + v_m\right)\cdot f_{es} + f_{em}\cdot t_m\right]}$
	3-2	$F = \frac{\left[\left(v_s - l_s\right)^2 + 4\cdot v_s\cdot t_s\right]\cdot f_{es}^2 + \left(2\cdot t_m^2 + 2\cdot t_m\cdot v_m\right)\cdot f_{es}\cdot f_{em} + f_{em}^2\cdot t_m^2 + 4\cdot M_y\cdot f_{es}}{\left(l_s + v_s + 2\cdot t_m + v_m\right)\cdot f_{es} + f_{em}\cdot t_m}$
Mode IV	1-2	$F = \frac{2\cdot\left[\left[\left(t_m^2 + v_m\cdot t_m\right)\cdot f_{em} + 4\cdot M_y\right]\cdot f_{es} + f_{em}^2\cdot t_m^2\right]}{\left[\left(2\cdot t_m + v_m\right)\cdot f_{es} + 2\cdot f_{em}\cdot t_m\right]}$
	3-2	$F = \frac{2\cdot\left[2\cdot t_s\cdot v_s\cdot f_{es}^2 + \left[f_{em}\cdot\left(t_m^2 + v_m\cdot t_m\right) + 4\cdot M_y\right]\cdot f_{es} + f_{em}^2\cdot t_m^2\right]}{\left[\left(2\cdot v_s + 2\cdot t_m + v_m\right)\cdot f_{es} + 2\cdot f_{em}\cdot t_m\right]}$

Summary of Derived Equations for the Hollow Section Yield Model

Table C-5: Hollow Section Yield Model Equations

Yield Mode	Single Shear	Double Shear
I_m	$F = 2 \cdot t_m \cdot f_{em}$	$F = 2 \cdot t_m \cdot f_{em}$
I_s	$F = 2 \cdot t_s \cdot f_{es}$	$F = 4 \cdot t_s \cdot f_{es}$
II-IV	$F = \frac{-B + \sqrt{B^2 - 4 \cdot A \cdot C}}{2 \cdot A}$	$F = \frac{-B + \sqrt{B^2 - 4 \cdot A \cdot C}}{A}$

Table C-6: Factors for Hollow Section Yield Model

Mode	Case	A	B	C
Mode II	1-1	$\frac{1}{4 \cdot f_{em}} + \frac{1}{4 \cdot f_{es}}$	$t_s + t_m$	$-\left[f_{es} \cdot t_s \cdot \left(t_s + v_s\right) + f_{em} \cdot t_m \cdot \left(t_m + v_m\right)\right]$
	3-3		$t_s + v_s + t_m + v_m$	
	3-1		$t_s + v_s + t_m$	
	1-3		$t_s + t_m + v_m$	
Mode III_m	3-3	$\frac{1}{4 \cdot f_{em}} + \frac{1}{2 \cdot f_{es}}$	$t_m + v_m + v_s$	$-\left[f_{em} \cdot t_m \cdot \left(t_m + v_m\right) + f_{es} \cdot t_s \cdot v_s + M_y\right]$
	3-1		$t_m + v_s$	
	1-1		t_m	$-\left[f_{em} \cdot t_m \cdot \left(t_m + v_m\right) + M_y\right]$
	1-3		$t_m + v_m$	
Mode III_s	3-3	$\frac{1}{2 \cdot f_{em}} + \frac{1}{4 \cdot f_{es}}$	$t_s + v_s + v_m$	$-\left[f_{es} \cdot t_s \cdot \left(t_s + v_s\right) + f_{em} \cdot t_m \cdot v_m + M_y\right]$
	1-3		$t_s + v_m$	
	1-1		t_s	$-\left[f_{es} \cdot t_s \cdot \left(t_s + v_s\right) + M_y\right]$
	3-1		$t_s + v_s$	
Mode IV	1-1	$\frac{1}{4 \cdot f_{em}} + \frac{1}{4 \cdot f_{es}}$	0	$-M_y$
	3-3	$\frac{1}{2 \cdot f_{em}} + \frac{1}{2 \cdot f_{es}}$	$v_m + v_s$	$-\left(v_m \cdot t_m \cdot f_{em} + v_s \cdot t_s \cdot f_{es} + 2 \cdot M_y\right)$
	3-1		v_s	$-\left(v_s \cdot t_s \cdot f_{es} + 2 \cdot M_y\right)$
	1-3		v_m	$-\left(v_m \cdot t_m \cdot f_{em} + 2 \cdot M_y\right)$

APPENDIX D: COMPUTER PROGRAM TO SIMPLIFY HSYM

Overview

This appendix provides information about the computer program utilized to simplify the hollow section yield model. The Fortran program loops over a selected range of input parameters and section geometries and evaluates the yield model. The program can output the results two ways: 1) the values for the independent variables followed by the yield load, yield mode, and yield case (results.txt) and/or 2) only names of the yield modes and cases followed by the number of times that the mode and case controlled (count.txt). The most useful information is the output with the number of times each mode and case controlled. The file of controlling yield loads for each loop becomes unmanageably large with even a small range of input parameters and section geometries. Therefore, the lines that output the entire results have been commented out in the "Program Code" section below (i.e. lines 36, 40, 44, 48, 57, 61, 65, 69,189, 193, 197, 201, 205, 209, 213, 217, 221, 225, 229, 233, 237, 241, 245 ,249, 253, and 257).

Range of Strength and Section Properties

Table D-1: Range of Strength and Section Properties Used

Variable	Initial Value	Final Value	Step
Fb	1,000 psi	200,000 psi	50,000 psi
Fes1	1,000 psi	50,000 psi	5,000 psi
Fem1	1,000 psi	50,000 psi	5,000 psi
D	0.05 in	1.10 in	0.15 in
ts	0.05 in	1.55 in	0.15 in
tm	0.05 in	1.55 in	0.15 in
vs	0.05 in	12.55 in	0.5 in
vm	0.05 in	12.55 in	0.5 in

Several other intermediate ranges were also evaluated using smaller steps and produced the same controlling yield modes. Table D-1 contains the broadest range of strength values and geometries of the program variables evaluated.

Program Variables

Table D-2: Program Variables

Variable	Description
nIs, nIm	Counter for Mode I_s and Mode I_m; respectively
nII11, nII33, nII13, nII31	Counter for Mode II: Case 1-1, Case 3-3, Case 1-3, Case 3-1; respectively
nIIIm11, nIIIm33, nIIIm13, nIIIm31	Counter for Mode III_m: Case 1-1, Case 3-3, Case 1-3, Case 3-1; respectively
nIIIs11, nIIIs33, nIIIs13, nIIIs31	Counter for Mode III_s: Case 1-1, Case 3-3, Case 1-3, Case 3-1; respectively
nIV11, nIV33, nIV13, nIV31	Counter for Mode IV: Case 1-1, Case 3-3, Case 1-3, Case 3-1; respectively
Fb	Bending yield strength (user input)
Fes1	Dowel bearing strength of the side member (user input)
Fem1	Dowel bearing strength of the main member (user input)
D	Dowel diameter (user input)
fes	Dowel bearing resistance of the side member
fem	Dowel bearing resistance of the main member
My	Moment resistance of the dowel
ts	Thickness of the side member (user input)
tm	Thickness of the main member (user input)
vs	Void width in the side member (user input)
vm	Void width in the main member (user input)
fIs, fIm	Calculated yield strength for Mode I_s and Mode I_m; respectively
fII11, fII33, fII13, fII31	Calculated yield strength for Mode II: Case 1-1, Case 3-3, Case 1-3, Case 3-1; respectively
fIIIm11, fIIIm33, fIIIm13, fIIIm31	Calculated yield strength for Mode III_m: Case 1-1, Case 3-3, Case 1-3, Case 3-1; respectively
fIIIs11, fIIIs33, fIIIs13, fIIIs31	Calculated yield strength for Mode III_s: Case 1-1, Case 3-3, Case 1-3, Case 3-1; respectively
fIV11, fIV33, fIV13, fIV31	Calculated yield strength for Mode IV: Case 1-1, Case 3-3, Case 1-3, Case 3-1; respectively
A, B, C	Terms for calculation of the yield strength using the quadratic formula
iresults	Internal variable to write data to results.txt
icount	Internal variable to write data to count.txt

Program Code

```
1         program hsym
2         implicit double precision (a-h,o-z), integer(i-n)
3         real My
4   c
5   c---- This program evaluates the HSYM for single shear
6   c----
7         icount=10
8   c     iresults=11
9         open (unit=10,status='new',file='count.txt')
10  c     open (unit=11,status='new',file='results.txt')
11  c
12  c---- initialize counters
13        nIs=0
14        nIm=0
15        nII11=0
16        nII33=0
17        nII13=0
18        nII31=0
19        nIIIm11=0
20        nIIIm33=0
21        nIIIm13=0
22        nIIIm31=0
23        nIIIs11=0
24        nIIIs33=0
25        nIIIs13=0
26        nIIIs31=0
27        nIV11=0
28        nIV33=0
29        nIV13=0
30        nIV31=0
31        ntotal=0
32  c
33  c---- Given Loop
34        Do 10 i=0,200000,50000
35        Fb=i
36  c     write(iresults,900)'Fb =  ',Fb
37  c
38        Do 20 j=0, 50000, 5000
39        Fes1=j
40  c     write(iresults,900)'Fes = ',Fes1
41  c
42        Do 30 k=0, 50000, 5000
43        Fem1=k
44  c     write(iresults,900)'Fem = ',Fem1
45  c
46        Do 40 r=0.05, 1.051, 0.15
47        d=r
48  c     write(iresults,900)'Dia = ',d
49  c
50        fes=Fes1*d
51        fem=Fem1*d
52        My=Fb*(D**3)/6
53  c
```

```
c
      Do 50 s=0.05, 1.56, 0.15
      ts=s
c     write(iresults,900)'ts =  ',ts
c
      Do 60 t=0.05, 1.56, 0.15
      tm=t
c     write(iresults,900)'tm =  ',tm
c
      Do 70 u=0.05, 12.51, 0.5
      vs=u
c     write(iresults,900)'vs =  ',vs
c
      Do 80 v=0.05, 12.51, 0.5
      vm=v
c     write(iresults,900)'vm =  ',vm
c
c
c---- This section is repeated inside the loop every
time~~~~~~~~~~~~
c
c---- Mode Im ----------------------------------------
      fIm=2*tm*fem
c
c---- Mode Is ----------------------------------------
      fIs=2*ts*fes
c
c---- Mode II ----------------------------------------
c
      A=(1/(4*fem))+(1/(4*fes))
      C=-1*(fes*ts*(ts+vs)+fem*tm*(tm+vm))
c
c---- Case 1-1
      B=ts+tm
      fII11=(-1*B+sqrt(B**2-4*A*C))/(2*A)
c
c---- Case 3-3
      B=ts+vs+tm+vm
      fII33=(-1*B+sqrt(B**2-4*A*C))/(2*A)
c
c---- Case 3-1
      B=ts+vs+tm
      fII31=(-1*B+sqrt(B**2-4*A*C))/(2*A)
c
c---- Case 1-3
      B=ts+tm+vm
      fII13=(-1*B+sqrt(B**2-4*A*C))/(2*A)
c---- ------------------------------------------------
c
c
c---- Mode IIIm ---------------------------------------
c
      A=(1/(4*fem))+(1/(2*fes))
      C=-1*(fes*ts*vs+fem*tm*(tm+vm)+My)
c
c---- Case 3-3
      B=vs+tm+vm
```

```
111         fIIIm33=(-1*B+sqrt(B**2-4*A*C))/(2*A)
112   c
113   c---- Case 3-1
114         B=vs+tm
115         fIIIm31=(-1*B+sqrt(B**2-4*A*C))/(2*A)
116   c
117         C=-1*(fem*tm*(tm+vm)+My)
118   c
119   c---- Case 1-1
120         B=tm
121         fIIIm11=(-1*B+sqrt(B**2-4*A*C))/(2*A)
122   c
123   c---- Case 1-3
124         B=tm+vm
125         fIIIm13=(-1*B+sqrt(B**2-4*A*C))/(2*A)
126   c---- ------------------------------------------------
127   c
128   c
129   c---- Mode IIIs -------------------------------------
130   c
131         A=(1/(2*fem))+(1/(4*fes))
132         C=-1*(fes*ts*(ts+vs)+fem*tm*vm+My)
133   c
134   c---- Case 3-3
135         B=vs+ts+vm
136         fIIIs33=(-1*B+sqrt(B**2-4*A*C))/(2*A)
137   c
138   c---- Case 1-3
139         B=ts+vm
140         fIIIs13=(-1*B+sqrt(B**2-4*A*C))/(2*A)
141   c
142         C=-1*(fes*ts*(ts+vs)+My)
143   c
144   c---- Case 1-1
145         B=ts
146         fIIIs11=(-1*B+sqrt(B**2-4*A*C))/(2*A)
147   c
148   c---- Case 3-1
149         B=vs+ts
150         fIIIs31=(-1*B+sqrt(B**2-4*A*C))/(2*A)
151   c---- ------------------------------------------------
152   c
153   c
154   c---- Mode IV ---------------------------------------
155   c
156   c
157   c---- Case 1-1
158         A=(1/(4*fem))+(1/(4*fes))
159         B=0
160         C=-1*My
161         fIV11=(-1*B+sqrt(B**2-4*A*C))/(2*A)
162   c
163         A=(1/(2*fem))+(1/(2*fes))
164   c
165   c---- Case 3-3
166         B=vs+vm
167         C=-1*(fes*ts*vs+fem*tm*vm+2*My)
```

```
168         fIV33=(-1*B+sqrt(B**2-4*A*C))/(2*A)
169   c
170   c---- Case 3-1
171         B=vs
172         C=-1*(fes*ts*vs+2*My)
173         fIV31=(-1*B+sqrt(B**2-4*A*C))/(2*A)
174   c
175   c---- Case 1-3
176         B=vm
177         C=-1*(fem*tm*vm+2*My)
178         fIV13=(-1*B+sqrt(B**2-4*A*C))/(2*A)
179   c---- ------------------------------------------------
180   c
181   c---- Find yield load and yield mode
182
183   yload=min(fIm,fIs,fII11,fII13,fII33,fII31,fIV11,fIV13,fIV33,fIV31
184         .
185   ,fIIIs11,fIIIs13,fIIIs33,fIIIs31,fIIIm11,fIIIm13,fIIIm33
186         .          ,fIIIm31)
187   c
188         if (fIm.eq.yload) then
189   c         write(iresults,1000)'Mode Im          ',yload
190            nIm=nIm+1
191         endif
192         if (fIs.eq.yload) then
193   c        write(iresults,1000)'Mode Is          ',yload
194            nIs=nIs+1
195         endif
196         if (fII11.eq.yload) then
197   c         write(iresults,1000)'Mode II - 1-1    ',yload
198            nII11=nII11+1
199         endif
200         if (fII33.eq.yload) then
201   c         write(iresults,1000)'Mode II - 3-3    ',yload
202            nII33=nII33+1
203         endif
204         if (fII31.eq.yload) then
205   c         write(iresults,1000)'Mode II - 3-1    ',yload
206            nII31=nII31+1
207         endif
208         if (fII13.eq.yload) then
209   c         write(iresults,1000)'Mode II - 1-3    ',yload
210            nII13=nII13+1
211         endif
212         if (fIIIm11.eq.yload) then
213   c         write(iresults,1000)'Mode IIIm - 1-1  ',yload
214            nIIIm11=nIIIm11+1
215         endif
216         if (fIIIm33.eq.yload) then
217   c         write(iresults,1000)'Mode IIIm - 3-3  ',yload
218            nIIIm33=nIIIm33+1
219         endif
220         if (fIIIm31.eq.yload) then
221   c         write(iresults,1000)'Mode IIIm - 3-1  ',yload
222            nIIIm31=nIIIm31+1
223         endif
224         if (fIIIm13.eq.yload) then
```

```
225   c         write(iresults,1000)'Mode IIIm - 1-3  ',yload
226             nIIIm13=nIIIm13+1
227           endif
228           if (fIIIs11.eq.yload) then
229   c         write(iresults,1000)'Mode IIIs - 1-1  ',yload
230             nIIIs11=nIIIs11+1
231           endif
232           if (fIIIs33.eq.yload) then
233   c         write(iresults,1000)'Mode IIIs - 3-3  ',yload
234             nIIIs33=nIIIs33+1
235           endif
236           if (fIIIs31.eq.yload) then
237   c         write(iresults,1000)'Mode IIIs - 3-1  ',yload
238             nIIIs31=nIIIs31+1
239           endif
240           if (fIIIs13.eq.yload) then
241   c         write(iresults,1000)'Mode IIIs - 1-3  ',yload
242             nIIIs13=nIIIs13+1
243           endif
244           if (fIV11.eq.yload) then
245   c         write(iresults,1000)'Mode IV - 1-1    ',yload
246             nIV11=nIV11+1
247           endif
248           if (fIV33.eq.yload) then
249   c         write(iresults,1000)'Mode IV - 3-3    ',yload
250             nIV33=nIV33+1
251           endif
252           if (fIV31.eq.yload) then
253   c         write(iresults,1000)'Mode IV - 3-1    ',yload
254             nIV31=nIV31+1
255           endif
256           if (fIV13.eq.yload) then
257   c         write(iresults,1000)'Mode IV - 1-3    ',yload
258             nIV13=nIV13+1
259           endif
260   c
261           ntotal=ntotal+1
262   c---- This ends the section of repeated eqn evaluation~~~~~~~~~~~~
263   80    continue
264   70    continue
265   60    continue
266   50    continue
267   40    continue
268   30    continue
269   20    continue
270   10    continue
271   c
272   c---- Report the number of each mode
273           write(icount,2000)'Mode Im          ',nIm
274           write(icount,2000)'Mode Is          ',nIs
275           write(icount,2000)'Mode II - 1-1    ',nII11
276           write(icount,2000)'Mode II - 3-3    ',nII33
277           write(icount,2000)'Mode II - 3-1    ',nII31
278           write(icount,2000)'Mode II - 1-3    ',nII13
279           write(icount,2000)'Mode IIIm - 1-1  ',nIIIm11
280           write(icount,2000)'Mode IIIm - 3-3  ',nIIIm33
281           write(icount,2000)'Mode IIIm - 3-1  ',nIIIm31
```

```
282         write(icount,2000)'Mode IIIm - 1-3  ',nIIIm13
283         write(icount,2000)'Mode IIIs - 1-1  ',nIIIs11
284         write(icount,2000)'Mode IIIs - 3-3  ',nIIIs33
285         write(icount,2000)'Mode IIIs - 3-1  ',nIIIs31
286         write(icount,2000)'Mode IIIs - 1-3  ',nIIIs13
287         write(icount,2000)'Mode IV - 1-1    ',nIV11
288         write(icount,2000)'Mode IV - 3-3    ',nIV33
289         write(icount,2000)'Mode IV - 3-1    ',nIV31
290         write(icount,2000)'Mode IV - 1-3    ',nIV13
291         write(icount,2000)'Total            ',ntotal
292   c
293   900   format(a6,f12.3)
294   1000  format(a17,f10.2)
295   2000  format(a17,i15.1)
296   c
297         end
298   c
299   c
300   c
```

APPENDIX E: DERIVATION OF THE LOAD-DISPLACEMENT BEHAVIOR MODEL

Overview

This appendix provides the derivation of the equations that predict the load-displacement curve of a laterally-loaded connection with hollow sections. The goal was to develop a set of equations that would enable a designer to predict the load-displacement behavior of a connection after only conducting dowel bearing tests and bending yield strength tests. The input to the model will be the coefficients of the curves fit to the test data and the dimensions of the dowel and members. Equations have been developed for only the controlling modes of the hollow section yield model (Mode I_m, Mode I_s, Mode II: Case 3-3, Mode III_s: Case 3-1, Mode III_m: Case 1-3, and Mode IV: Case 1-1).

General Procedure

The Mode I_s and I_m load-displacement model equations are simply the curves fit to the dowel resistance data times the sum of the wall thicknesses. Modes II, III, and IV utilize the method of virtual displacements. In the hollow section yield model development the virtual displacement method was used; external work and internal work are set equal to each other as a connection undergoes a unit slip. To produce the load-displacement equations, energy is conserved as the connection displaced a finite distance. The resulting equation for the yield load is a function of the connection displacement, δ. The general equation becomes Equation E-1. Derivation of load-displacement behavior expressions requires evaluating the integral and simplifying. However, due to the number of terms introduced from the geometry of the hollow section problem, a closed form solution to the problem is impractical.

$$W = F \cdot \delta = \int f_e \cdot \eta \cdot d\xi + \sum \left(M_y \theta \right)$$ Equation E-1

where:
$F =$ *yield load*
$D =$ *dowel diameter*
$f_e =$ *dowel bearing resistance* $= C_1\delta + C_2\delta^2 + C_3\delta^3 + C_4\delta^4 + C_5\delta^5 + C_6\delta^6$
$M_y =$ *moment resistance of the dowel*
$\theta =$ *angle of rotation of the dowel*
$\eta, \xi =$ *integration variables*

The dowel bearing resistance is obtained in this research by fitting sixth-order polynomials (restricted to pass through the origin) to the dowel bearing curves divided by the wall thickness (dowel bearing resistance curves). For derivation purposes, the moment resistance will be assumed to be constant. In the final step to of the derivation, a function for the bending moment in terms of connection displacement may be substituted.

Derivation Steps:

1) Substitute known expressions into Equation E-1 (f_{es}, f_{em}, and θ)
2) Simplify with known relationships for η and evaluate integral.
3) Substitute for x_m. Leaving the function with only one unknown variable, x_s.
4) Reduce equation to smallest possible form. Divide by δ to leave *F* only on the left side of the expression.
5) Take the derivative of *F* with respect to x_s and set to zero.
6) Solve for x_s to find the location where energy is minimized. Reduce x_s expression.
7) Substitute the reduced x_s expression back into *F*. Reduce expression for *F* to final usable form.

The above procedure was attempted for each of the yield modes. Steps 1 through 5 were completed successfully. However, once the derivative with respect to x_s was computed and set

to zero, it was unfeasible to solve for x_s. Numerical methods of minimizing the functions were attempted, but proved to be too computationally demanding. Therefore, the load-displacement equations were developed as functions of x_s, x_m, and δ. An approximate values for x_s and x_m were found using the expressions found during the derivation of the hollow section yield model. Incorporated into the x_s and x_m expressions is the dowel bearing strength of the members and bending yield strength of the dowel. Using these terms appears to be contradictory to the objective of predicting the entire load-displacement curve (i.e. no longer relying on one arbitrary point from the input curves), but only the ratios of the strength properties to each other is important. For example, using a 5% offset basis to determine these properties would provide a ratio of the strength properties at that location. The assumption is that the x_s and x_m remain constant. Therefore, the values obtained from the yield model equations are sound enough to produce approximate x_s and x_m locations.

Equation E-1 will be evaluated as separate terms because a closed form solution was impossible. The external energy consists of the yield load, F, times the displacement, δ. The internal energy depends on the yield mode which is a combination of dowel rotation and dowel yielding. Five general types of internal energy have been defined (Figure E-1). E1, E2, E3, and E4 relate to energy of material crushing. E1, E2, and E3 relate to energy of material crushing when the dowel rotates about a point in the wall farthest from the shear plane. E4 relates to energy of material crushing when a hinge forms within the wall closest to the shear plane. E5 corresponds the energy of forming a hinge in the dowel. Table E-2 defines the types of internal energy present in each yield mode. The total internal energy is the sum of all the applicable E-terms to the side and main members. For example, for Mode III_s: Case 3-1, the internal energy equals $E_{1s}+E_{2s}+E_{3s}+E_{4m}+E_{5m}$.

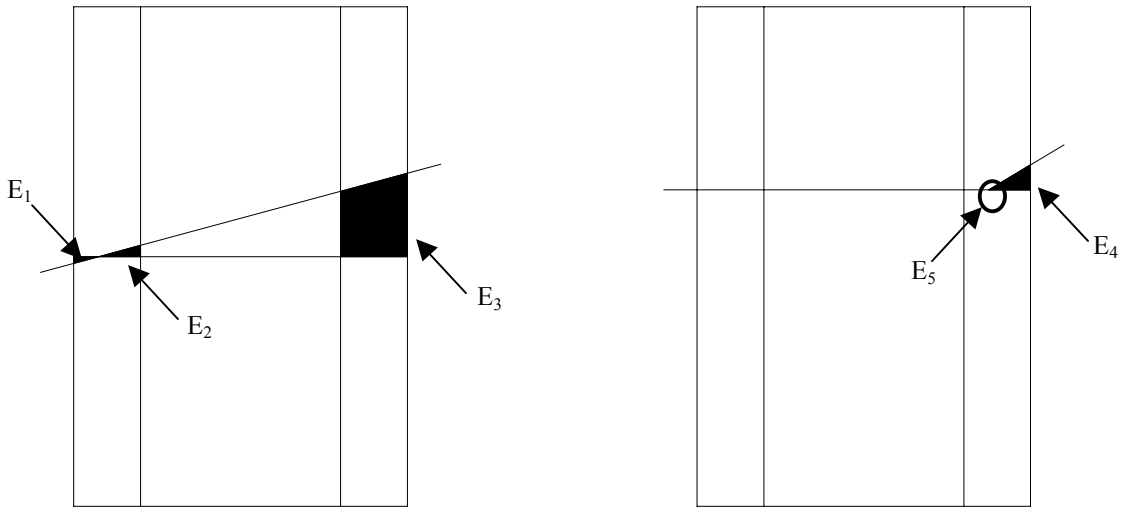

Figure E-1: General internal energy conditions.

Table E-1: Energy Terms by Mode

Yield Mode	Applicable Internal Energy Terms	
	Side Member	Main Member
Mode II: Case 3-3	E_1, E_2, E_3	E_1, E_2, E_3
Mode III_m: Case 1-3	E_4, E_5	E_1, E_2, E_3
Mode III_s: Case 3-1	E_1, E_2, E_3	E_4, E_5
Mode IV: Case 1-1	E_4, E_5	E_4, E_5

Predicting an entire load-displacement curve is mathematically intensive and hence a spreadsheet was used. Derived equations are evaluated at specific displacements to produce ordered pairs of displacement and load. Separate equations were developed for each component of the internal energy in order to utilize a spreadsheet more effectively and account for the lack of a closed form solution.

Derivation of Mode III$_s$

Mode III connections contain all five internal energy types. The derivation of Mode III$_s$ will be shown in detail. The general equations for each energy type were developed from this one derivation.

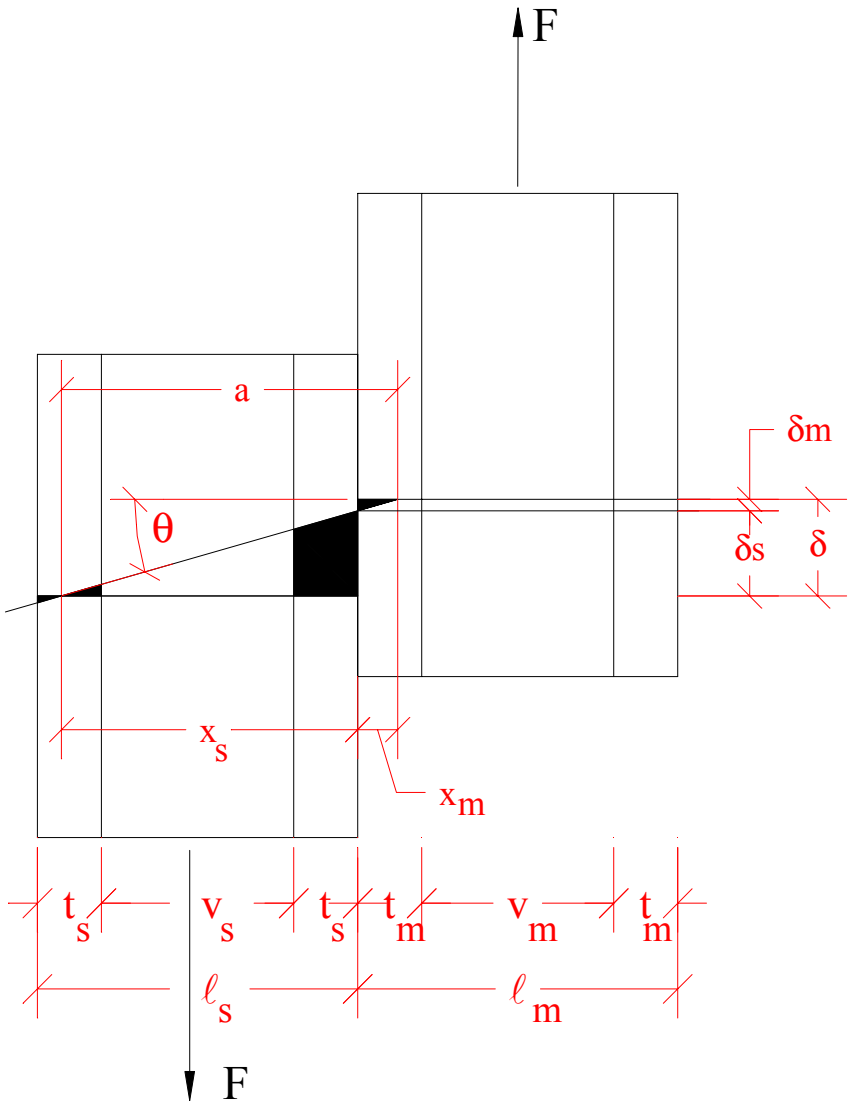

Figure E-2: Mode III$_s$ connection model.

Useful relationships from the geometry of the problem:

$$\tan\theta = \theta = \frac{\delta}{a} = \frac{\delta_m + \delta_s}{x_s + x_m} \qquad \tan\theta = \frac{\delta_m}{x_m} \qquad \tan\theta = \frac{\delta_s}{x_s}$$

Therefore:

$$\frac{\delta_m}{x_m} = \frac{\delta_s}{x_s} \qquad \text{so} \qquad \delta_m = \frac{\delta_s}{x_s} \cdot x_m$$

Also,

$$\delta = \delta_m + \delta_s \qquad \text{so} \qquad \delta = \delta_s \cdot \left(\frac{x_m}{x_s} + 1 \right) \qquad \text{and} \qquad \delta_s = \frac{\delta}{\left(\frac{x_m}{x_s} + 1 \right)}$$

From Figure E-3, the following relationships can be developed:

For the side member:

$$\frac{\eta_s}{\delta_s} = \frac{\xi_s}{x_s}$$

$$\eta_s = \frac{\xi_s}{x_s} \cdot \delta_s$$

For the main member:

$$\frac{\eta_m}{\delta_m} = \frac{\xi_m}{x_m}$$

$$\eta_m = \frac{\xi_m}{x_m} \cdot \delta_m$$

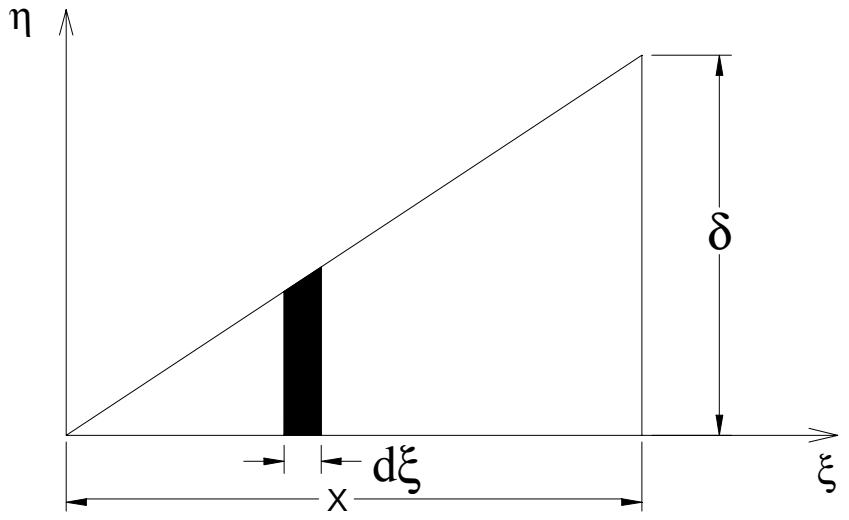

Figure E-3: Relationship of integration variables.

From the general equation:

$$F * \delta = E1 + E2 + E3 + E4 + E5$$

Each energy term (E1 through E5) is an intergral that uses the following inputs:

$$fes = a\,\eta s + b\,\eta s^2 + c\,\eta s^3 + d\,\eta s^4 + e\,\eta s^5 + f\,\eta s^6$$

$$fem = l\,\eta m + m\,\eta m^2 + n\,\eta m^3 + o\,\eta m^4 + p\,\eta m^5 + q\,\eta m^6$$

The relationships from Figure E-3 can now be substitude:

$$\eta s = \frac{\xi s}{xs} * \delta s$$

$$\eta m = \frac{\xi m}{xm} * \delta m$$

The general energy terms are now defined and evaluated.

$$E1 = \int_0^{2t+v-xs} fes * \eta s \, d\xi s$$

Substituting and reducing E1 produces:

$$\frac{1}{xs}\left(\delta s\left(-\frac{a\,(2t+v-xs)^3\,\delta s}{3\,xs} - \frac{b\,(2t+v-xs)^4\,\delta s^2}{4\,xs^2} - \frac{c\,(2t+v-xs)^5\,\delta s^3}{5\,xs^3} - \frac{d\,(2t+v-xs)^6\,\delta s^4}{6\,xs^4} - \frac{e\,(2t+v-xs)^7\,\delta s^5}{7\,xs^5} - \frac{f\,(2t+v-xs)^8\,\delta s^6}{8\,xs^6}\right)\right)$$

$$E2 = \int_0^{xs-t-v} fes * \eta s \, d\xi s$$

Substituting and reducing E2 produces:

$$\frac{1}{xs}\left(\delta s\left(\frac{a\,(-t-v+xs)^3\,\delta s}{3\,xs} + \frac{b\,(-t-v+xs)^4\,\delta s^2}{4\,xs^2} + \frac{c\,(-t-v+xs)^5\,\delta s^3}{5\,xs^3} + \frac{d\,(-t-v+xs)^6\,\delta s^4}{6\,xs^4} + \frac{e\,(-t-v+xs)^7\,\delta s^5}{7\,xs^5} + \frac{f\,(-t-v+xs)^8\,\delta s^6}{8\,xs^6}\right)\right)$$

$$E3 = \int_{xs-t}^{xs} fes * \eta s \, d\xi s$$

Substituting and reducing E3 produces:

$$\frac{1}{xs}\left(\delta s\left(\frac{1}{3}\, a\, xs^2\, \delta s - \frac{a\,(-t+xs)^3\,\delta s}{3\,xs} + \frac{1}{4}\, b\, xs^2\, \delta s^2 - \frac{b\,(-t+xs)^4\,\delta s^2}{4\,xs^2} + \frac{1}{5}\, c\, xs^2\, \delta s^3 - \frac{c\,(-t+xs)^5\,\delta s^3}{5\,xs^3} + \frac{1}{6}\, d\, xs^2\, \delta s^4 - \frac{d\,(-t+xs)^6\,\delta s^4}{6\,xs^4} + \frac{1}{7}\, g\, xs^2\, \delta s^5 - \frac{e\,(-t+xs)^7\,\delta s^5}{7\,xs^5} + \frac{1}{8}\, f\, xs^2\, \delta s^6 - \frac{f\,(-t+xs)^8\,\delta s^6}{8\,xs^6}\right)\right)$$

$$E4 = \int_{0}^{xm} fem * \eta m \, d\xi m$$

Substituting and reducing E4 produces:

$$\frac{1}{xm}\left(\delta m\left(\frac{1}{3}\, l\, xm^2\, \delta m + \frac{1}{4}\, m\, xm^2\, \delta m^2 + \frac{1}{5}\, n\, xm^2\, \delta m^3 + \frac{1}{6}\, o\, xm^2\, \delta m^4 + \frac{1}{7}\, p\, xm^2\, \delta m^5 + \frac{1}{8}\, q\, xm^2\, \delta m^6\right)\right)$$

$$E5 = \frac{My\,\delta s}{xs}$$

The above expressions can now be written in terms of δ only by substituting:

$$\delta m = \frac{xm\,\delta s}{xs}$$

and then substituting:

$$\delta s = \frac{\delta}{\left(1 + \frac{xm}{xs}\right)}$$

The equations can be simplified further by dividing each term by δ. The summation of the primed terms will now be equal to the load directly.

$$F = \frac{E1 + E2 + E3 + E4 + E5}{\delta} = E1' + E2' + E3' + E4' + E5'$$

Simplified forms:

$$E1' = \frac{a\,(2t+v-xs)^3\,\delta}{3\,(xm+xs)^2} + \frac{b\,(2t+v-xs)^4\,\delta^2}{4\,(xm+xs)^3} + \frac{c\,(2t+v-xs)^5\,\delta^3}{5\,(xm+xs)^4} + \frac{d\,(2t+v-xs)^6\,\delta^4}{6\,(xm+xs)^5} + \frac{e\,(2t+v-xs)^7\,\delta^5}{7\,(xm+xs)^6} + \frac{f\,(2t+v-xs)^8\,\delta^6}{8\,(xm+xs)^7}$$

$$E2' = -\frac{a\,(t+v-xs)^3\,\delta}{3\,(xm+xs)^2} + \frac{b\,(t+v-xs)^4\,\delta^2}{4\,(xm+xs)^3} - \frac{c\,(t+v-xs)^5\,\delta^3}{5\,(xm+xs)^4} + \frac{d\,(t+v-xs)^6\,\delta^4}{6\,(xm+xs)^5} - \frac{e\,(t+v-xs)^7\,\delta^5}{7\,(xm+xs)^6} + \frac{f\,(t+v-xs)^8\,\delta^6}{8\,(xm+xs)^7}$$

$$E3' = \frac{a\,((t-xs)^3+xs^3)\,\delta}{3\,(xm+xs)^2} + \frac{b\,(-(t-xs)^4+xs^4)\,\delta^2}{4\,(xm+xs)^3} + \frac{c\,((t-xs)^5+xs^5)\,\delta^3}{5\,(xm+xs)^4} + \frac{d\,(-(t-xs)^6+xs^6)\,\delta^4}{6\,(xm+xs)^5} + \frac{e\,((t-xs)^7+xs^7)\,\delta^5}{7\,(xm+xs)^6} + \frac{f\,(-(t-xs)^8+xs^8)\,\delta^6}{8\,(xm+xs)^7}$$

$$E4' = \frac{l\,xm^3\,\delta}{3\,(xm+xs)^2} + \frac{m\,xm^4\,\delta^2}{4\,(xm+xs)^3} + \frac{n\,xm^5\,\delta^3}{5\,(xm+xs)^4} + \frac{o\,xm^6\,\delta^4}{6\,(xm+xs)^5} + \frac{p\,xm^7\,\delta^5}{7\,(xm+xs)^6} + \frac{q\,xm^8\,\delta^6}{8\,(xm+xs)^7}$$

$$E5' = \frac{My}{xm+xs}$$

A general equation for E′ can be found by inspection of the E1′, E2′, E3′, and E4′ equations:

$$E' = \frac{c1\,(i^3-j^3)\,\delta}{3a^2} + \frac{c2\,(i^4-j^4)\,\delta^2}{4a^3} + \frac{c3\,(i^5-j^5)\,\delta^3}{5a^4} + \frac{c4\,(i^6-j^6)\,\delta^4}{6a^5} + \frac{c5\,(i^7-j^7)\,\delta^5}{7a^6} + \frac{c6\,(i^8-j^8)\,\delta^6}{8a^7}$$

Equation E-2

where :

$a = x_s + x_m$

$C_1, C_2, C_3, C_4, C_5,$ *and* C_6 *are the coefficien ts from the fit dowel resistance curves*

i and j depend on the type of energy (Table E - 2)

Table E-2: Coefficients for Equation E-2

Internal Energy Type	i	j
E_1	$2t+v-x$	0
E_2	$x-t-v$	0
E_3	x	$x-t$
E_4	x	0
Note: x will either be x_s or x_m depending on the mode and member being considered		

Also note: the *i* and *j* terms are the integration limits used at the beginning of the derivation for each energy type.

As stated earlier, during the derivation the dowel bending resistance, M_y, was assumed constant. A function for the dowel bending resistance in terms of connection slip, $M_y(\delta)$, may be used when actually evaluating the E_5 equation. For this research, a sixth-order polynomial curve was fit to the bending yield strength load-displacement data (Equation E-4). Due to the configuration of the bending yield strength test apparatus, the load was equal to the dowel bending resistance, M_y (see Equation E-3).

$$M_y = \frac{PL}{4} = \frac{P(4)}{4} = P \qquad \text{Equation E-3}$$

The curve fit to the load-displacement data cannot be used directly in the E_5 equation because the displacement in the bending yield test is different than the displacement in a connection test. The angle of rotation of the dowel was used to relate the two tests and produce Equation E-5.

$$M_y(\Delta) = A_m\Delta + B_m\Delta^2 + C_m\Delta^3 + D_m\Delta^4 + E_m\Delta^5 + F_m\Delta^6 \quad \text{Equation E-4}$$

$$M_y(\delta) = A_m\left[2\tan\left(\frac{\delta}{2(x_s+x_m)}\right)\right] + B_m\left[2\tan\left(\frac{\delta}{2(x_s+x_m)}\right)\right]^2 + C_m\left[2\tan\left(\frac{\delta}{2(x_s+x_m)}\right)\right]^3 + D_m\left[2\tan\left(\frac{\delta}{2(x_s+x_m)}\right)\right]^4 + E_m\left[2\tan\left(\frac{\delta}{2(x_s+x_m)}\right)\right]^5 + F_m\left[2\tan\left(\frac{\delta}{2(x_s+x_m)}\right)\right]^6 \quad \text{Equation E-5}$$

where :

Δ = *displacement in bending yield strength test*

δ = *displacement in connection test*

Equation Summary

Table 3-4 summarizes the load-displacement predicting equations for single shear connections. The double shear equations are produced by multiplying the single shear equations by two; except in Mode I_m where the single shear and double shear equations are identical.

Table E-3: Load-Displacement Equations for Single Shear Connections

Mode	Load-Displacement Equation
I_s	$F(\delta) = 2t_s\left(A\delta + B\delta^2 + C\delta^3 + D\delta^4 + E\delta^5 + F\delta^6\right)$
I_m	$F(\delta) = 2t_m\left(L\delta + M\delta^2 + N\delta^3 + O\delta^4 + P\delta^5 + Q\delta^6\right)$
II: Case 3-3	$F(\delta) = \left(E_{1s}' + E_{2s}' + E_{3s}' + E_{1m}' + E_{2m}' + E_{3m}'\right)$
III_s: Case 3-1	$F(\delta) = \left(E_{1s}' + E_{2s}' + E_{3s}' + E_{4m}' + E_5'\right)$
III_m: Case 1-3	$F(\delta) = \left(E_{4s}' + E_5' + E_{1m}' + E_{2m}' + E_{3m}'\right)$
IV: Case 1-1	$F(\delta) = \left(E_{4s}' + E_5' + E_{4m}' + E_5'\right)$

In the Mode IV connections used in this research, the side member and the main member are made of the same material. Therefore, only one set of coefficients are needed and the Mode IV equation may be simplified to Equation E-6 (single shear).

$$F(\delta) = \sqrt{\left[M_y(\delta)\right]\left[\frac{2}{3}A\delta + \frac{1}{4}B\delta^2 + \frac{1}{10}C\delta^3 + \frac{1}{24}D\delta^4 + \frac{1}{56}E\delta^5 + \frac{1}{128}F\delta^6\right]} \quad \text{Equation E-6}$$

Mode IV Closed-Form Derivation

Equation E-6 was derived using the closed-form solution outlined above. The noteworthy steps are summarized below.

Using the general equations for the internal energy for Mode IV:

$$F = 2 * E4' + 2 * E5'$$

Substituting the terms:

$$F = \frac{2\,My}{xm + xs} + 2\left(\frac{l\,xm^3\,\delta}{3\,(xm+xs)^2} + \frac{m\,xm^4\,\delta^2}{4\,(xm+xs)^3} + \frac{n\,xm^5\,\delta^3}{5\,(xm+xs)^4} + \frac{o\,xm^6\,\delta^4}{6\,(xm+xs)^5} + \frac{p\,xm^7\,\delta^5}{7\,(xm+xs)^6} + \frac{q\,xm^8\,\delta^6}{8\,(xm+xs)^7}\right)$$

Since the problem is symmetric, xm = xs. Substituting and simplifying:

$$F = \frac{My}{xs} + 2\,\frac{xs\,\delta\,(8960\,l + 3360\,m\,\delta + 1344\,n\,\delta^2 + 560\,o\,\delta^3 + 240\,p\,\delta^4 + 105\,q\,\delta^5)}{107520}$$

Taking the derivative with respect to xs:

$$F' = -\frac{My}{xs^2} + 2\left(\frac{l\,\delta}{12} + \frac{m\,\delta^2}{32} + \frac{n\,\delta^3}{80} + \frac{o\,\delta^4}{192} + \frac{p\,\delta^5}{448} + \frac{q\,\delta^6}{1024}\right)$$

Setting F′ equal to zero and solving for xs produces:

$$\left\{xs \to \frac{\sqrt{My}}{\sqrt{2}\,\sqrt{\left(\frac{l\,\delta}{12} + \frac{m\,\delta^2}{32} + \frac{n\,\delta^3}{80} + \frac{o\,\delta^4}{192} + \frac{p\,\delta^5}{448} + \frac{q\,\delta^6}{1024}\right)}}\right\}$$

Substituting xs back into F and reducting:

$$F = \frac{\sqrt{My}\,\sqrt{\delta\,(8960\,l + \delta\,(3360\,m + \delta\,(1344\,n + 5\,\delta\,(112\,o + 48\,p\,\delta + 21\,q\,\delta^2))))}}{8\sqrt{210}}$$

$$F = \sqrt{My\left(\frac{2\,l\,\delta}{3} + \frac{m\,\delta^2}{4} + \frac{n\,\delta^3}{10} + \frac{o\,\delta^4}{24} + \frac{p\,\delta^5}{56} + \frac{q\,\delta^6}{128}\right)}$$

APPENDIX F: TEST DATA

Dowel Bearing Strength Data

HDPE 0.2" wall thickness - 1/4" hole				wall thicknesses		5% offset	Max
Sample	Max Load	Int Load	Yield Load	wall 1	wall 2	DBS	DBS
15L	480.8	480.8	480.8	0.192	0.212	4821.34	4821.34
17L	476.0	475.4	475.4	0.194	0.211	4755.42	4761.42
16L	473.3	470.9	470.9	0.193	0.210	4733.78	4757.91
10R	471.9	471.7	471.9	0.195	0.215	4662.84	4662.84
16R	469.5	469.3	469.3	0.193	0.211	4706.02	4708.02
12R	476.2	476.2	476.2	0.196	0.212	4728.39	4728.39
8R	452.1	450.7	450.7	0.198	0.214	4431.75	4445.51
9L	465.8	464.7	464.7	0.198	0.214	4569.41	4580.22
14R	471.4	471.1	471.1	0.194	0.214	4677.75	4680.73
11R	482.4	482.1	482.1	0.194	0.212	4810.56	4813.55
17R	463.6	463.1	463.1	0.194	0.214	4598.32	4603.28
15R	484.8	484.3	484.8	0.194	0.213	4825.61	4825.61
13L	447.2	447.0	447.2	0.194	0.212	4462.31	4462.31
		average =	469.9	0.195	0.213	4675.7	4680.9
		standard devation =	11.27	0.2038		128.39	126.93
		COV =	2.4%			2.7%	2.7%
		min	447.20		min	4431.75	4445.51
		max	484.80		max	4825.61	4825.61

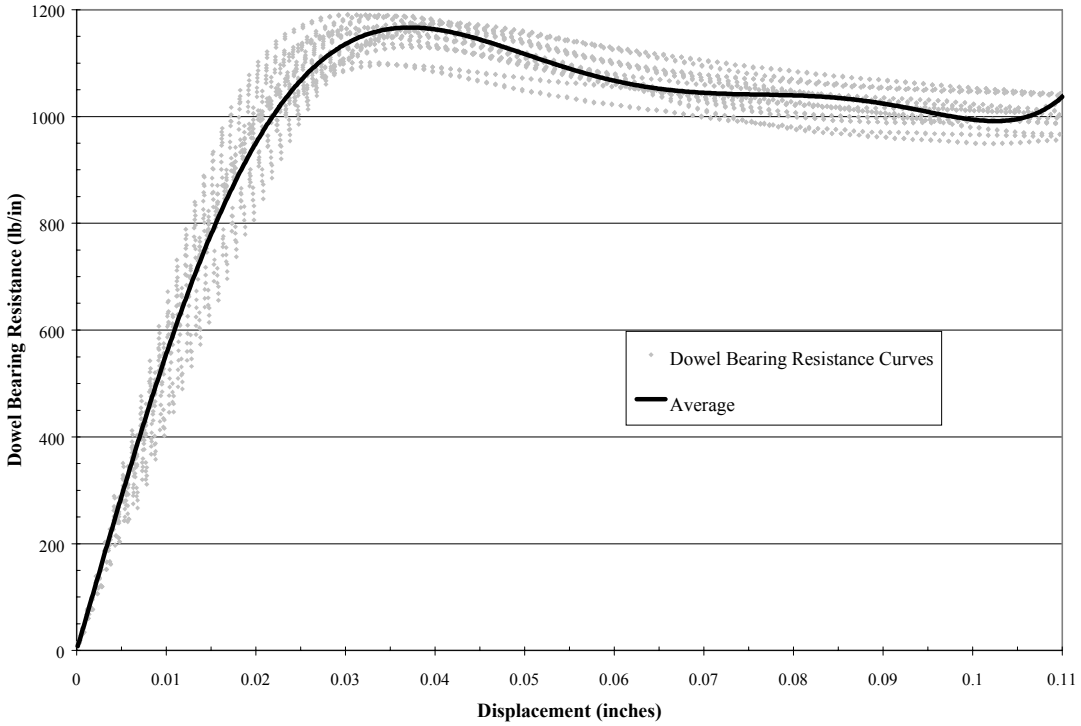

HDPE 0.2" wall thickness - 3/8" hole				wall thicknesses		5% offset	Max
Sample	Max Load	Int Load	Yield Load	wall 1	wall 2	DBS	DBS
7a	656.4	653.7	656.4	0.198	0.214	4296.20	4296.20
7c	643.8	639.7	643.8	0.196	0.215	4223.99	4223.99
5	665.0	663.4	665.0	0.195	0.211	4416.81	4416.81
6	646.4	641.9	646.4	0.199	0.214	4220.51	4220.51
5b	654.0	652.3	654.0	0.199	0.211	4301.38	4301.38
7	617.4	614.2	617.4	0.199	0.215	4021.42	4021.42
		average =	647.2	0.198	0.213	4246.7	4246.7
		standard devation =	16.42	0.2055		131.40	131.40
		COV =	2.5%			3.1%	3.1%
		min	617.40		min	4021.42	4021.42
		max	665.00		max	4416.81	4416.81

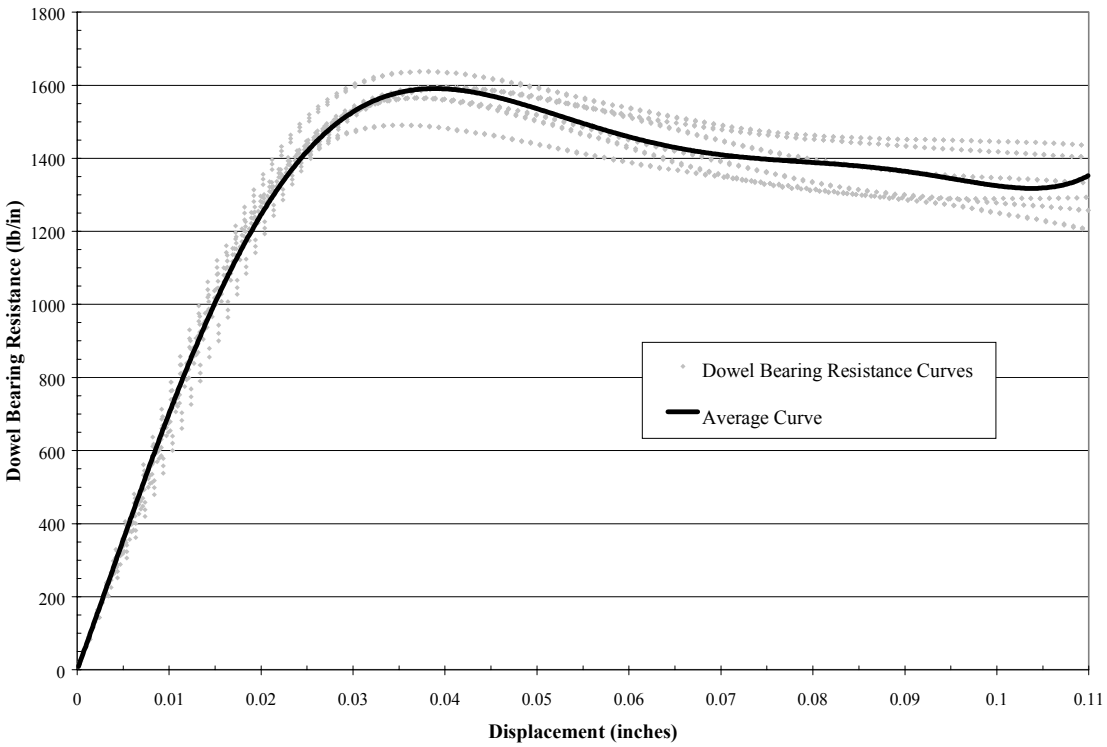

HDPE 0.3" wall thickness - 1/4" hole				wall thicknesses		5% offset	Max
Sample	Max Load	Int Load	Yield Load	wall 1	wall 2	DBS	DBS
9a	786.6	773.2	773.2	0.323	0.296	5060.41	5148.11
9a4	796.8	776.9	776.9	0.324	0.297	5068.25	5198.07
9b	786.0	771.8	771.8	0.325	0.296	5034.98	5127.61
9b2	767.5	762.4	762.4	0.324	0.297	4973.66	5006.93
9b3	797.0	776.4	776.4	0.322	0.298	5073.16	5207.76
9b4	793.0	788.5	788.5	0.322	0.296	5168.89	5198.39
8a	797.3	794.4	794.4	0.323	0.295	5207.57	5226.58
8a2	796.5	785.0	785.0	0.324	0.296	5129.35	5204.49
8a3	817.2	807.8	807.8	0.322	0.298	5278.33	5339.75
8b	766.2	753.3	753.3	0.322	0.296	4938.15	5022.71
		average =	779.0	0.323	0.297	5093.3	5168.0
		standard devation =	15.73	0.3098		104.46	98.18
		COV =	2.0%			2.1%	1.9%
		min	753.30		min	4938.15	5006.93
		max	807.80		max	5278.33	5339.75

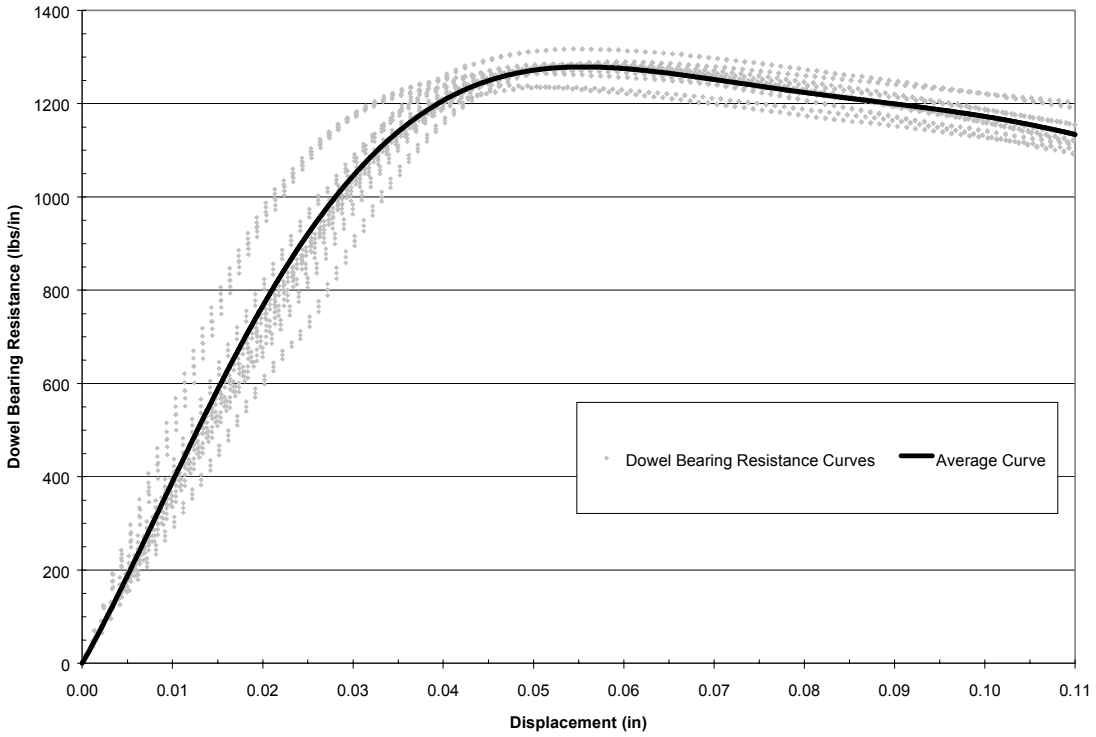

HDPE 0.3" wall thickness - 3/8" hole				wall thicknesses		5% offset	Max
Sample	Max Load	Int Load	Yield Load	wall 1	wall 2	DBS	DBS
6L	1096.0	1090.0	1090.0	0.325	0.298	4717.93	4743.90
6R	1093.0	1089.0	1089.0	0.323	0.296	4744.07	4761.49
25L	1073.0	1071.0	1071.0	0.322	0.295	4680.77	4689.52
23R	1086.0	1084.0	1084.0	0.323	0.294	4737.59	4746.33
11R	1059.0	1058.0	1058.0	0.326	0.296	4586.79	4591.12
11L	1078.0	1074.0	1074.0	0.321	0.298	4678.72	4696.15
17R	1077.0	1075.0	1075.0	0.325	0.297	4660.49	4669.16
17L	1074.0	1068.0	1068.0	0.323	0.296	4652.58	4678.72
25R	1077.0	1075.0	1075.0	0.322	0.292	4721.21	4730.00
		average =	1076.0	0.323	0.296	4686.7	4700.7
		standard devation =	10.30	0.3096		49.97	52.60
		COV =	1.0%			1.1%	1.1%
		min	1058.00		min	4586.79	4591.12
		max	1090.00		max	4744.07	4761.49

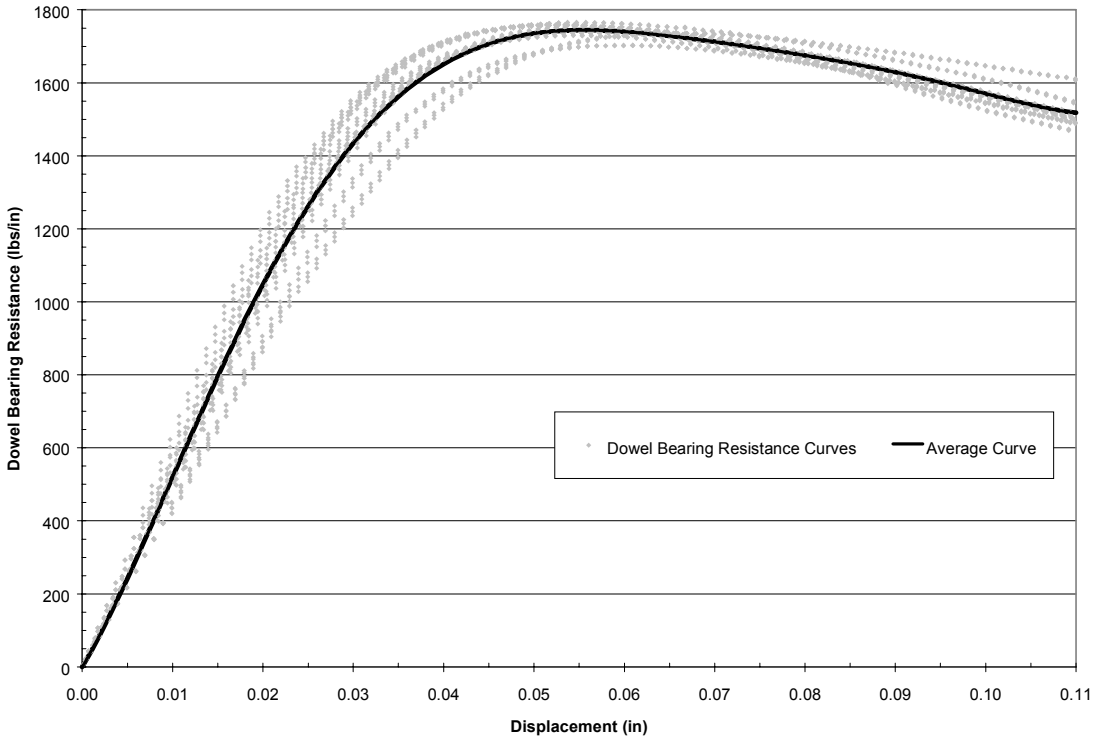

HDPE 0.4" wall thickness - 3/16" hole				wall thicknesses		5% offset	Max
Sample	Max Load	Int Load	Yield Load	wall 1	wall 2	DBS	DBS
19	1048.0	967.5	967.5	0.411	0.410	6326.52	6852.91
20	1065.0	1020.0	1020.0	0.409	0.413	6661.71	6955.60
15	1027.0	970.7	970.7	0.409	0.409	6370.72	6740.22
16L	1057.0	962.7	962.7	0.409	0.410	6310.51	6928.64
8R	1104.0	990.1	990.1	0.409	0.411	6482.20	7227.90
25R	1042.0	983.6	983.6	0.410	0.410	6439.64	6821.99
10R	1026.0	956.2	956.2	0.412	0.413	6222.31	6676.53
27	1013.0	956.2	956.2	0.409	0.413	6245.02	6615.99
14R	1021.0	951.4	951.4	0.411	0.413	6198.59	6652.05
18R	1046.0	978.3	978.3	0.410	0.411	6397.14	6839.83
21R	1031.0	979.3	979.3	0.407	0.410	6435.03	6774.76
26L	1030.0	966.4	966.4	0.410	0.411	6319.33	6735.21
23L	1033.0	966.4	966.4	0.409	0.409	6342.50	6779.60
11L	1026.0	929.7	929.7	0.411	0.410	6079.34	6709.05
13L	1020.0	932.3	932.3	0.413	0.413	6059.44	6629.45
17	1047.0	930.2	930.2	0.408	0.410	6104.92	6871.48
		average =	965.1	0.410	0.411	6312.2	6800.7
		standard devation =	23.52	0.4104		159.33	152.97
		COV =	2.4%			2.5%	2.2%
		min	929.70		min	6059.44	6615.99
		max	1020.00		max	6661.71	7227.90

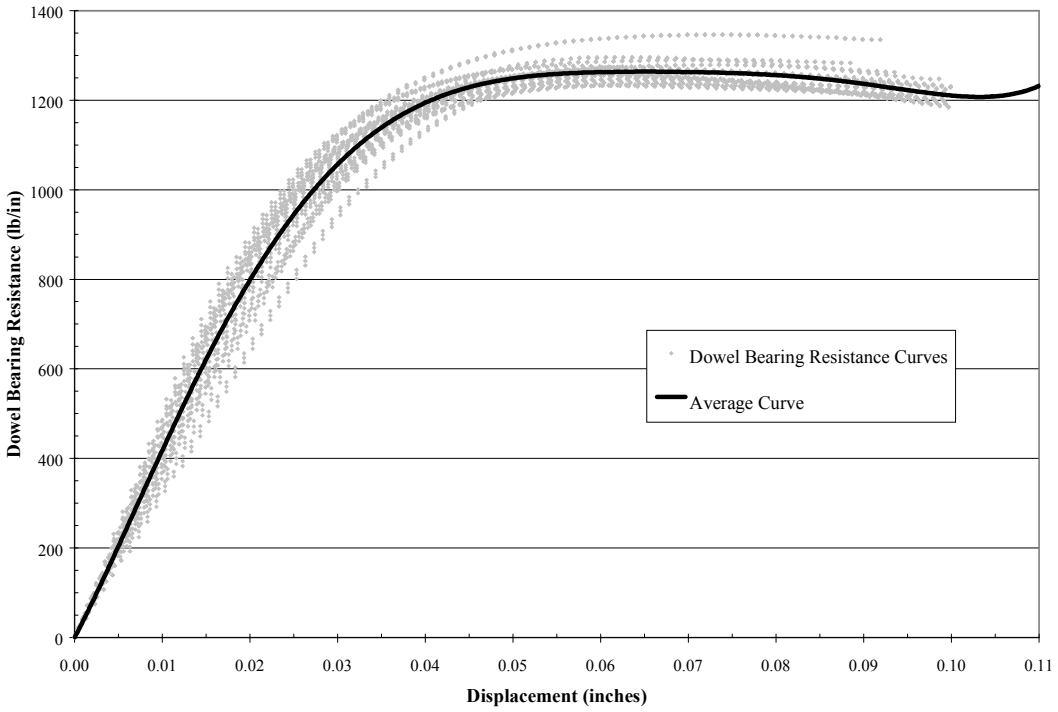

HDPE 0.4" wall thickness - 1/4" hole				wall thicknesses		5% offset	Max
Sample	Max Load	Int Load	Yield Load	wall 1	wall 2	DBS	DBS
5	1155.0	1073.0	1073.0	0.412	0.415	5256.28	5657.97
7	1159.0	1111.0	1111.0	0.409	0.412	5482.21	5719.06
2	1098.0	1036.0	1036.0	0.414	0.409	5099.70	5404.89
4	1138.0	1076.0	1076.0	0.414	0.412	5277.36	5581.45
16R	1129.0	1071.0	1071.0	0.412	0.410	5278.40	5564.25
7b	1158.0	1080.0	1080.0	0.410	0.409	5342.25	5728.08
12	1083.0	1035.0	1035.0	0.415	0.414	5057.90	5292.47
5b	1127.0	1067.0	1067.0	0.410	0.411	5265.09	5561.16
15	1140.0	1087.0	1087.0	0.409	0.410	5376.88	5639.04
6b	1149.0	1086.0	1086.0	0.410	0.412	5352.32	5662.82
21L	1178.0	1108.0	1108.0	0.407	0.408	5507.65	5855.61
4b	1153.0	1108.0	1108.0	0.411	0.410	5467.40	5689.45
	average =	1078.2		0.411	0.411	5313.6	5613.0
	standard devation =	24.95		0.4110		139.93	149.69
	COV =	2.3%				2.6%	2.7%
	min	1035.00			min	5057.90	5292.47
	max	1111.00			max	5507.65	5855.61

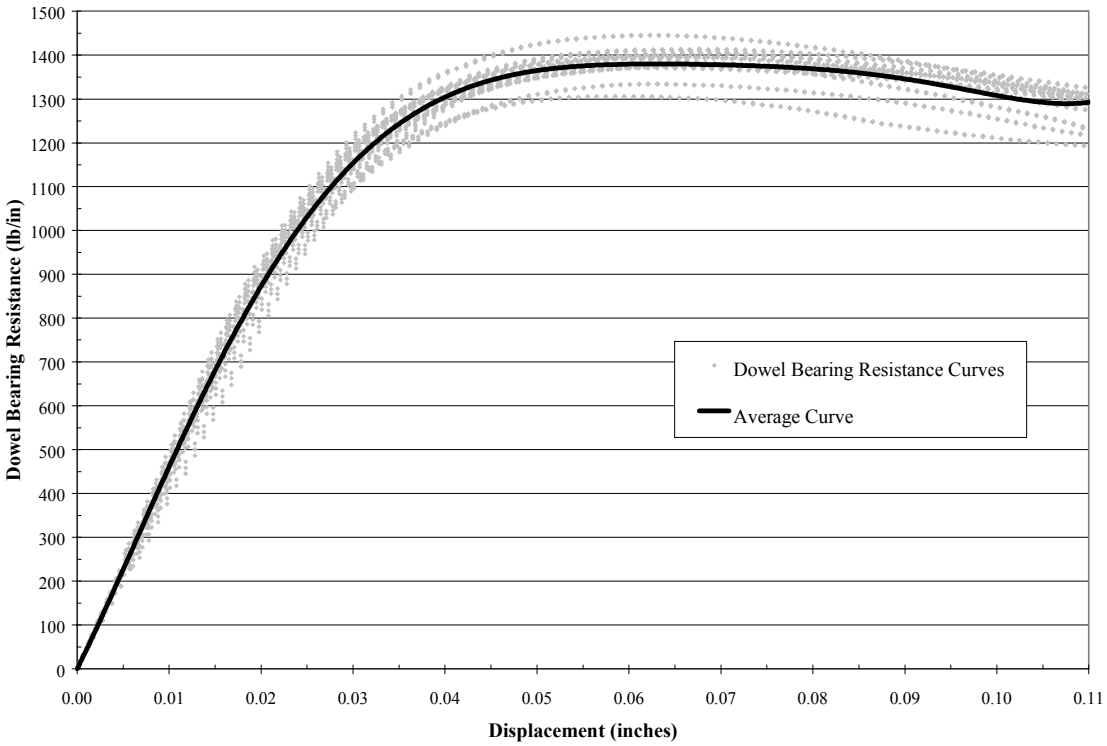

HDPE 0.4" wall thickness - 3/8" hole				wall thicknesses		5% offset	Max
Sample	Max Load	Int Load	Yield Load	wall 1	wall 2	DBS	DBS
11R	1536.0	1520.0	1520.0	0.415	0.412	4954.09	5006.24
9	1545.0	1517.0	1517.0	0.412	0.413	4956.30	5047.78
24L	1569.0	1534.0	1534.0	0.409	0.410	5048.56	5163.75
13R	1529.0	1504.0	1504.0	0.412	0.412	4919.79	5001.57
12	1537.0	1518.0	1518.0	0.415	0.412	4947.57	5009.50
22	1516.0	1481.0	1481.0	0.406	0.410	4892.05	5007.66
8L	1511.0	1471.0	1471.0	0.413	0.412	4806.01	4936.70
22R	1590.0	1563.0	1563.0	0.409	0.411	5137.73	5226.48
10L	1545.0	1519.0	1519.0	0.410	0.413	4974.90	5060.05
23	1529.0	1513.0	1513.0	0.410	0.411	4967.32	5019.85
	average =	1514.0		0.411	0.412	4960.4	5048.0
	standard devation =	25.66		0.4114		88.10	85.37
	COV =	1.7%				1.8%	1.7%
	min	1471.00			min	4806.01	4936.70
	max	1563.00			max	5137.73	5226.48

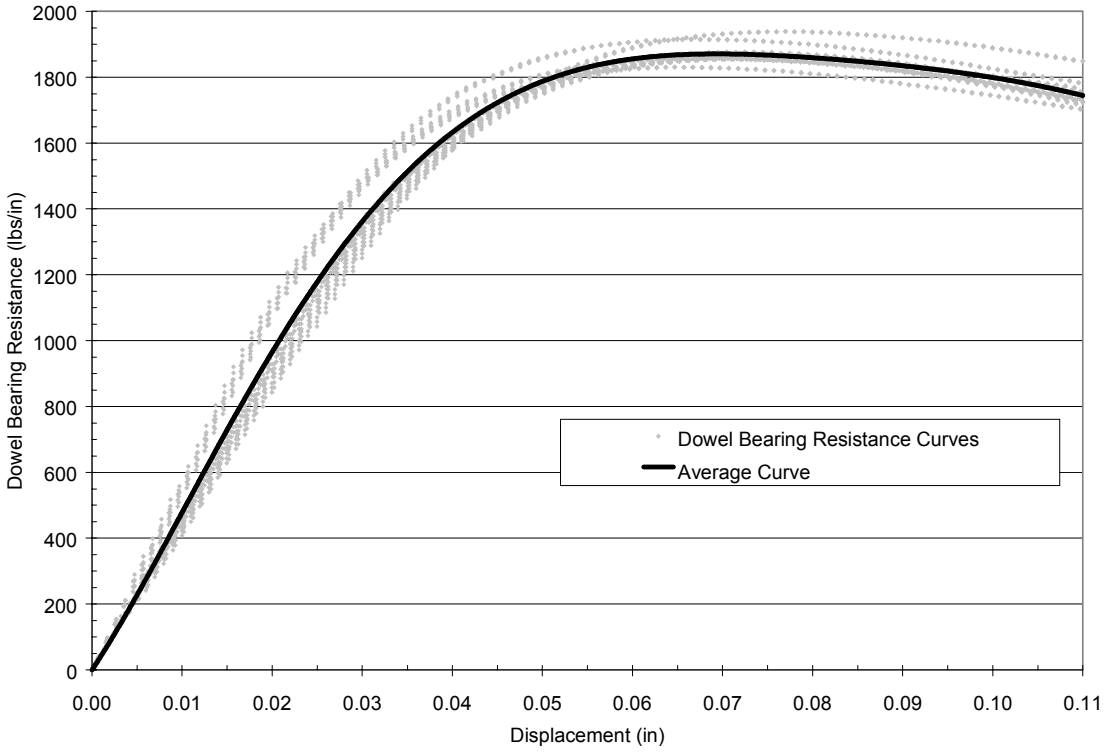

PVC 0.2" wall thickness - 1/4" hole				wall thicknesses		5% offset	Max
Sample	Max Load	Int Load	Yield Load	wall 1	wall 2	DBS	DBS
9a	1608.1	1556.7	1608.1	0.192	0.207	16327.20	16327.20
9a2	1713.1	1686.3	1713.1	0.195	0.208	17221.52	17221.52
9b	1605.6	1559.2	1605.6	0.195	0.209	16100.62	16100.62
9a3	1740.0	1674.0	1740.0	0.195	0.210	17405.38	17405.38
9b3	1698.5	1652.0	1698.5	0.195	0.210	16989.80	16989.80
		average =	1673.1	0.194	0.209	16808.9	16808.9
		standard devation =	62.27	0.2016		568.44	568.44
		COV =	3.7%			3.4%	3.4%
		min	1605.61		min	16100.62	16100.62
		max	1740.02		max	17405.38	17405.38

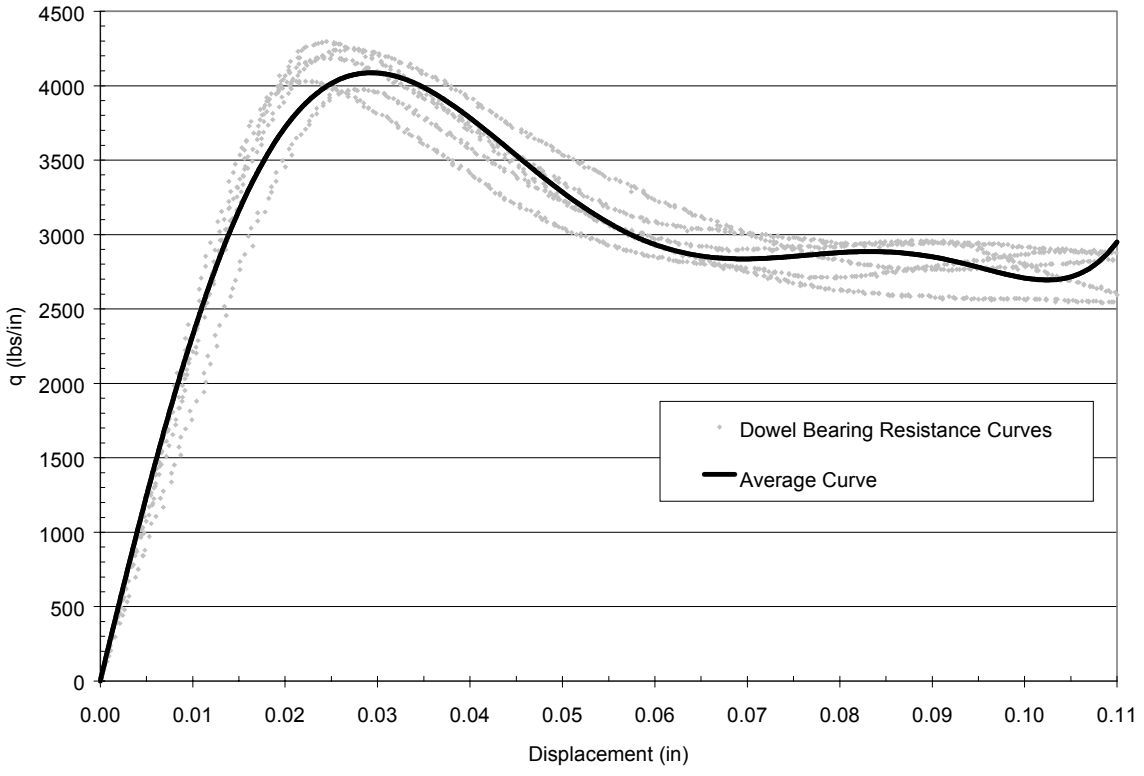

PVC 0.2" wall thickness - 3/8" hole				wall thicknesses		5% offset	Max
Sample	Max Load	Int Load	Yield Load	wall 1	wall 2	DBS	DBS
11L	1979.5	1935.5	1979.5	0.193	0.210	13245.47	13245.47
12R	2155.5	2089.5	2155.5	0.194	0.205	14567.44	14567.44
15R	2236.1	2157.9	2236.1	0.193	0.212	14888.59	14888.59
17L	2094.4	1986.8	2094.4	0.192	0.208	14119.14	14119.14
4	1940.4	1901.3	1940.4	0.195	0.208	12983.84	12983.84
16L	2106.6	2038.2	2106.6	0.193	0.203	14344.97	14344.97
7	1930.6	1884.2	1930.6	0.192	0.205	13113.67	13113.67
18L	2028.4	1942.9	2028.4	0.193	0.210	13572.52	13572.52
14R	1957.5	1920.9	1957.5	0.192	0.207	13229.61	13229.61
19L	2040.6	2006.4	2040.6	0.191	0.206	13860.65	13860.65
5	2028.4	1938.0	2028.4	0.192	0.209	13640.22	13640.22
13L	2101.7	2067.5	2101.7	0.192	0.211	14063.10	14063.10
5b	1999.1	1913.5	1999.1	0.191	0.208	13510.39	13510.39
7b	2087.0	2047.9	2087.0	0.197	0.207	13930.42	13930.42
		average =	2049.0	0.193	0.208	13790.7	13790.7
		standard devation =	86.98	0.2003		567.90	567.90
		COV =	4.2%			4.1%	4.1%
		min	1930.64		min	12983.84	12983.84
		max	2236.12		max	14888.59	14888.59

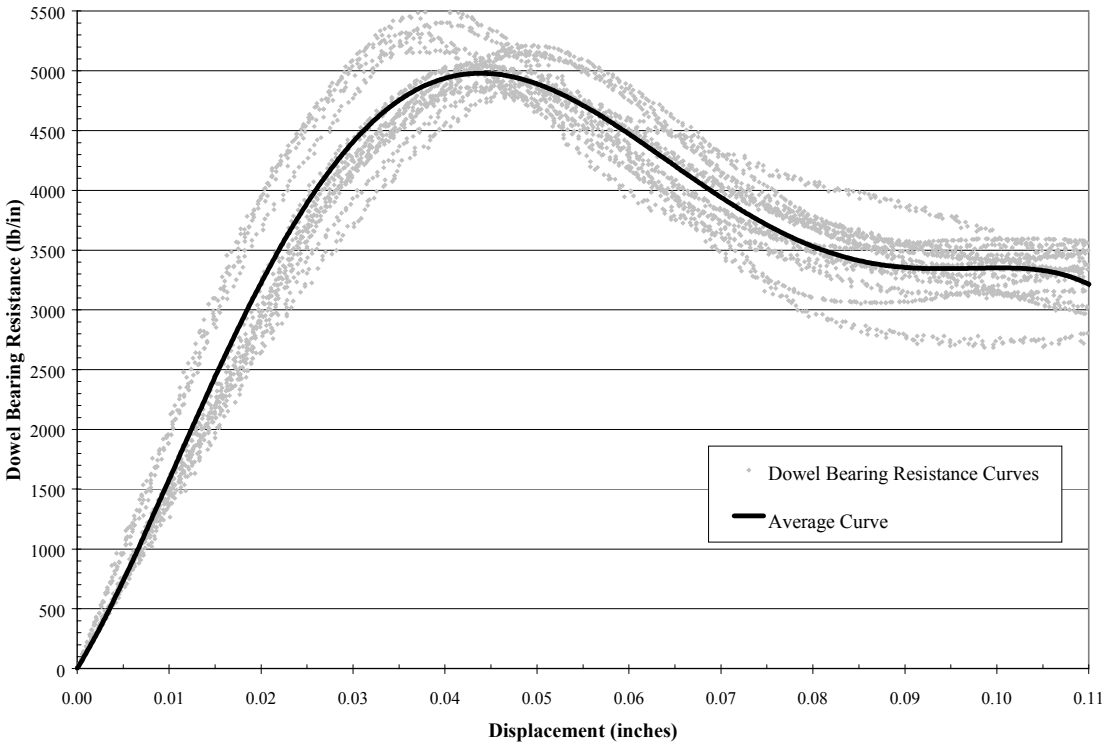

PVC 0.3" wall thickness - 1/4" hole				wall thicknesses		5% offset	Max
Sample	Max Load	Int Load	Yield Load	wall 1	wall 2	DBS	DBS
6a	2837.3	2798.2	2837.3	0.314	0.294	18905.46	18905.46
7a2	2854.4	2825.1	2854.4	0.316	0.295	18926.06	18926.06
6a3	2876.4	2861.7	2876.4	0.315	0.294	19134.53	19134.53
7a3	2781.1	2776.2	2776.2	0.314	0.295	18467.99	18500.50
7b3	2837.3	2773.8	2837.3	0.314	0.296	18843.47	18843.47
6b2	2812.9	2793.3	2812.9	0.314	0.292	18804.48	18804.48
6b4	2844.6	2815.3	2844.6	0.316	0.296	18830.43	18830.43
7b4	2810.4	2778.7	2810.4	0.313	0.295	18726.34	18726.34
		average =	2831.2	0.315	0.295	18829.8	18833.9
		standard devation =	30.77	0.3046		189.09	180.35
		COV =	1.1%			1.0%	1.0%
		min	2776.21		min	18467.99	18500.50
		max	2876.41		max	19134.53	19134.53

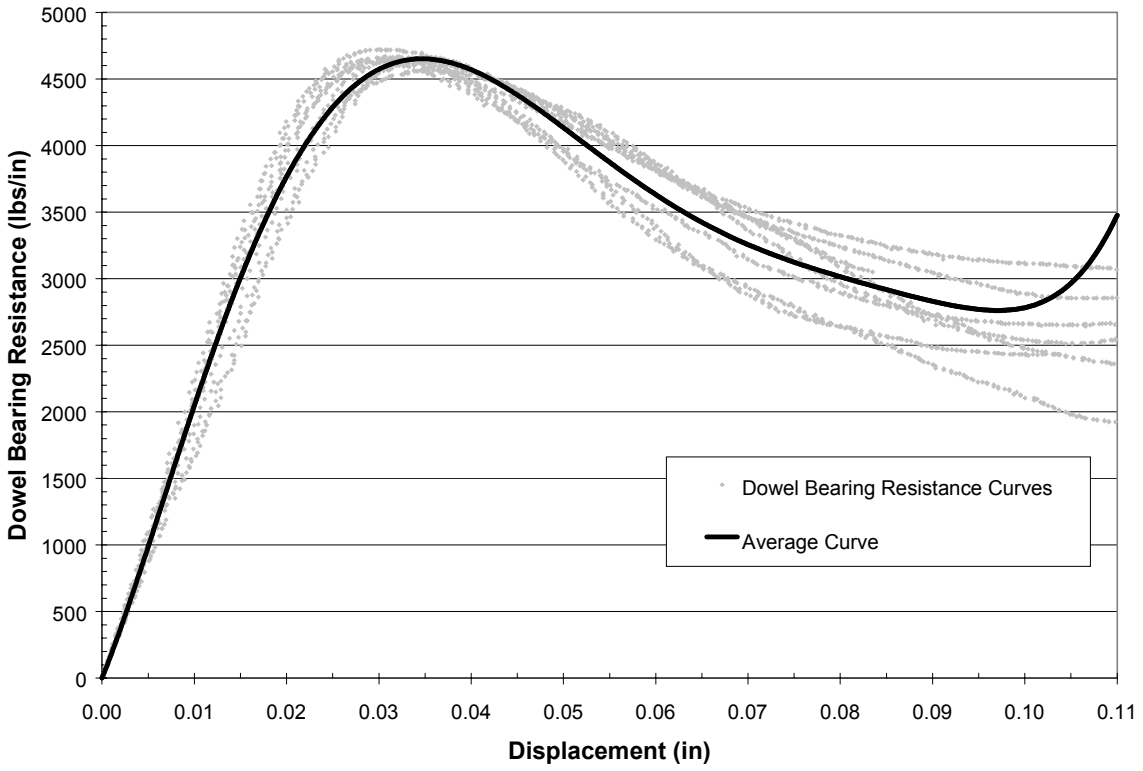

PVC 0.3" wall thickness - 3/8" hole				wall thicknesses		5% offset	Max
Sample	Max Load	Int Load	Yield Load	wall 1	wall 2	DBS	DBS
8R	3863.7	3729.3	3863.7	0.316	0.294	17080.07	17080.07
18L	3797.7	3704.9	3797.7	0.314	0.296	16788.38	16788.38
8L	3836.8	3753.8	3836.8	0.311	0.292	17158.13	17158.13
1L	3788.0	3685.3	3788.0	0.313	0.293	16855.69	16855.69
9R	3902.8	3790.4	3902.8	0.314	0.294	17309.67	17309.67
1R	3827.1	3682.9	3827.1	0.315	0.294	16945.80	16945.80
9L	3878.4	3802.6	3878.4	0.312	0.294	17258.06	17258.06
2L	3731.8	3680.4	3731.8	0.315	0.291	16605.58	16605.58
2R	3748.9	3653.6	3748.9	0.314	0.293	16654.22	16654.22
18R	3863.7	3734.2	3863.7	0.314	0.290	17249.74	17249.74
		average =	3823.9	0.314	0.293	16990.5	16990.5
		standard devation =	56.42	0.3035		258.00	258.00
		COV =	1.5%			1.5%	1.5%
		min	3731.76		min	16605.58	16605.58
		max	3902.82		max	17309.67	17309.67

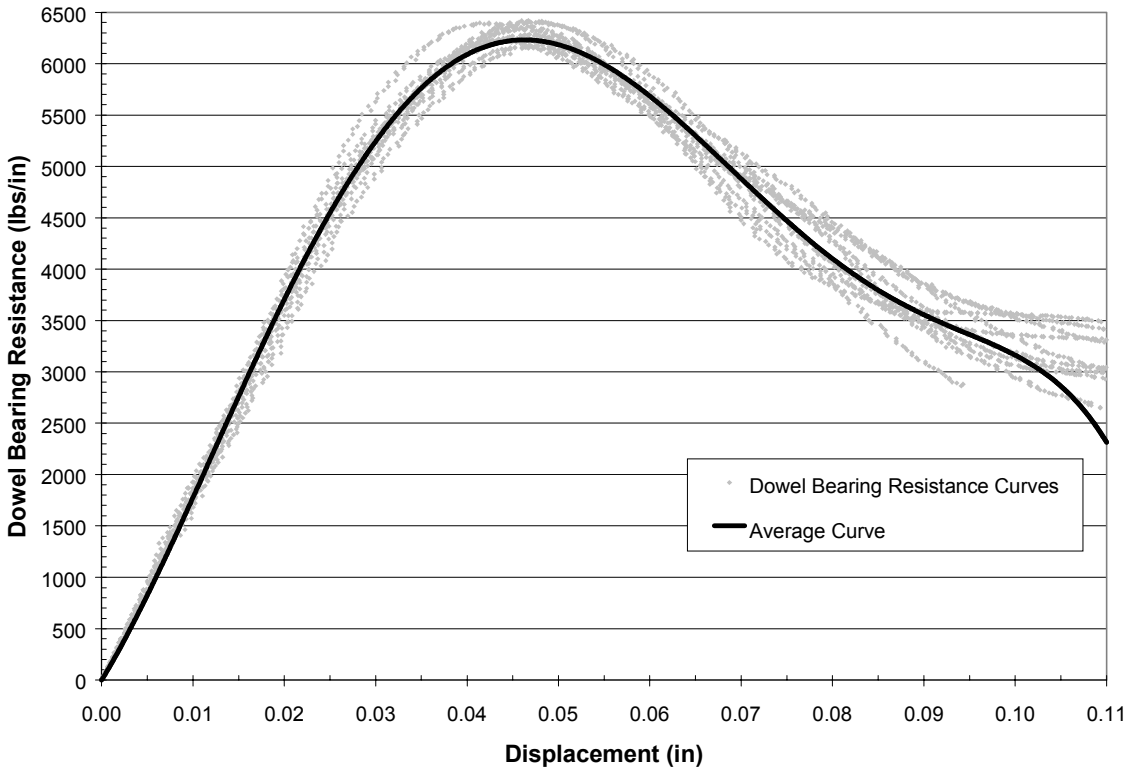

PVC 0.4" wall thickness - 1/4" hole				wall thicknesses		5% offset	Max
Sample	Max Load	Int Load	Yield Load	wall 1	wall 2	DBS	DBS
6	3935.6	3906.2	3935.6	0.390	0.410	19929.89	19929.89
24L	4121.6	4053.1	4121.6	0.391	0.410	20845.79	20845.79
7L	4004.1	3945.4	4004.1	0.390	0.410	20276.93	20276.93
22	4141.2	4053.1	4141.2	0.390	0.409	20997.25	20997.25
23R	3769.2	3730.0	3769.2	0.389	0.411	19087.09	19087.09
25	3955.2	3925.8	3955.2	0.391	0.410	20004.04	20004.04
20R	4013.9	3974.8	4013.9	0.391	0.410	20301.13	20301.13
26L	3886.6	3867.1	3886.6	0.391	0.410	19657.44	19657.44
3	3945.4	3925.8	3945.4	0.391	0.413	19880.07	19880.07
19R	3935.6	3876.9	3935.6	0.391	0.411	19880.19	19880.19
4L	4004.1	3965.0	4004.1	0.393	0.412	20150.99	20150.99
18	4013.9	3965.0	4013.9	0.391	0.410	20301.13	20301.13
21R	4092.2	4033.5	4092.2	0.392	0.411	20645.70	20645.70
17	3925.8	3896.4	3925.8	0.392	0.410	19830.74	19830.74
5R	3965.0	3935.6	3965.0	0.390	0.410	20078.62	20078.62
2R	3788.7	3739.8	3788.7	0.390	0.411	19162.29	19162.29
	average =		3968.6	0.391	0.411	20064.3	20064.3
	standard devation =		102.86	0.4007		520.41	520.41
	COV =		2.6%			2.6%	2.6%
		min	3769.17		min	19087.09	19087.09
		max	4141.19		max	20997.25	20997.25

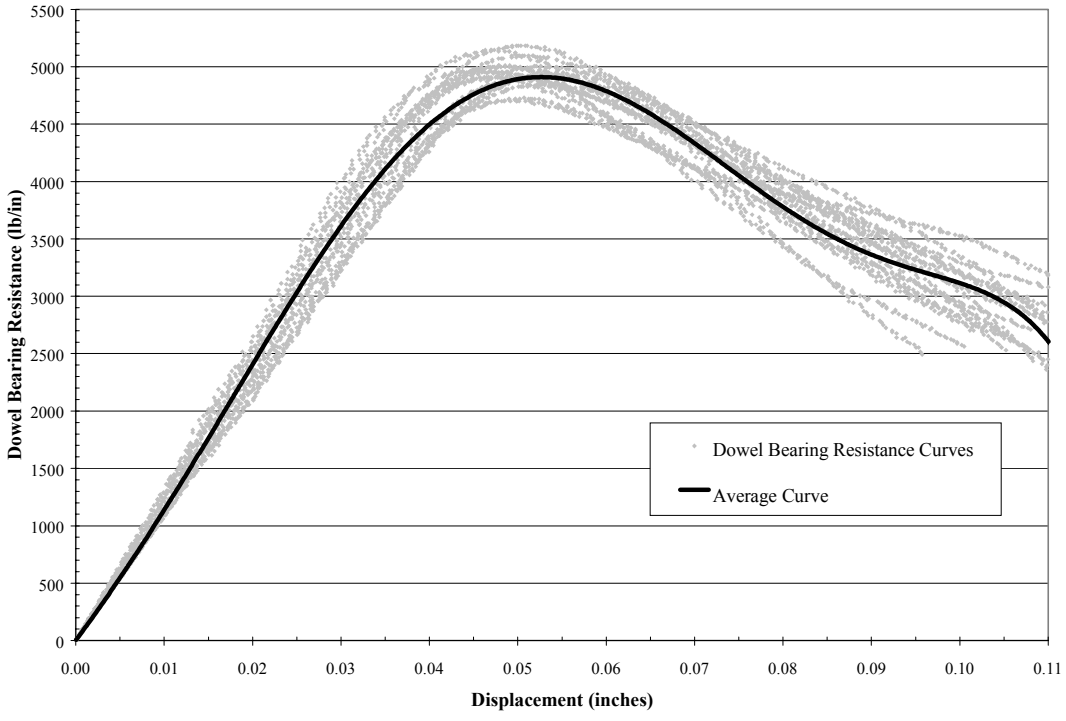

PVC 0.4" wall thickness - 3/8" hole				wall thicknesses		5% offset	Max
Sample	Max Load	Int Load	Yield Load	wall 1	wall 2	DBS	DBS
11	5482.4	5247.5	5482.4	0.392	0.412	18387.80	18387.80
13	5453.1	5267.0	5453.1	0.393	0.410	18312.07	18312.07
11b	5472.6	5237.7	5472.6	0.391	0.411	18400.74	18400.74
14	5619.5	5433.5	5619.5	0.392	0.410	18894.50	18894.50
17	5639.1	5413.9	5639.1	0.392	0.413	18889.67	18889.67
15	5599.9	5472.6	5599.9	0.391	0.411	18828.66	18828.66
12	5619.5	5492.2	5619.5	0.392	0.411	18870.97	18870.97
14b	5462.8	5208.3	5462.8	0.393	0.410	18344.95	18344.95
12b	5599.9	5482.4	5599.9	0.391	0.411	18828.66	18828.66
13b	5551.0	5364.9	5551.0	0.390	0.410	18710.74	18710.74
	average =		5550.0	0.392	0.411	18646.9	18646.9
	standard devation =		74.62	0.4013		252.02	252.02
	COV =		1.3%			1.4%	1.4%
		min	5453.05		min	18312.07	18312.07
		max	5639.06		max	18894.50	18894.50

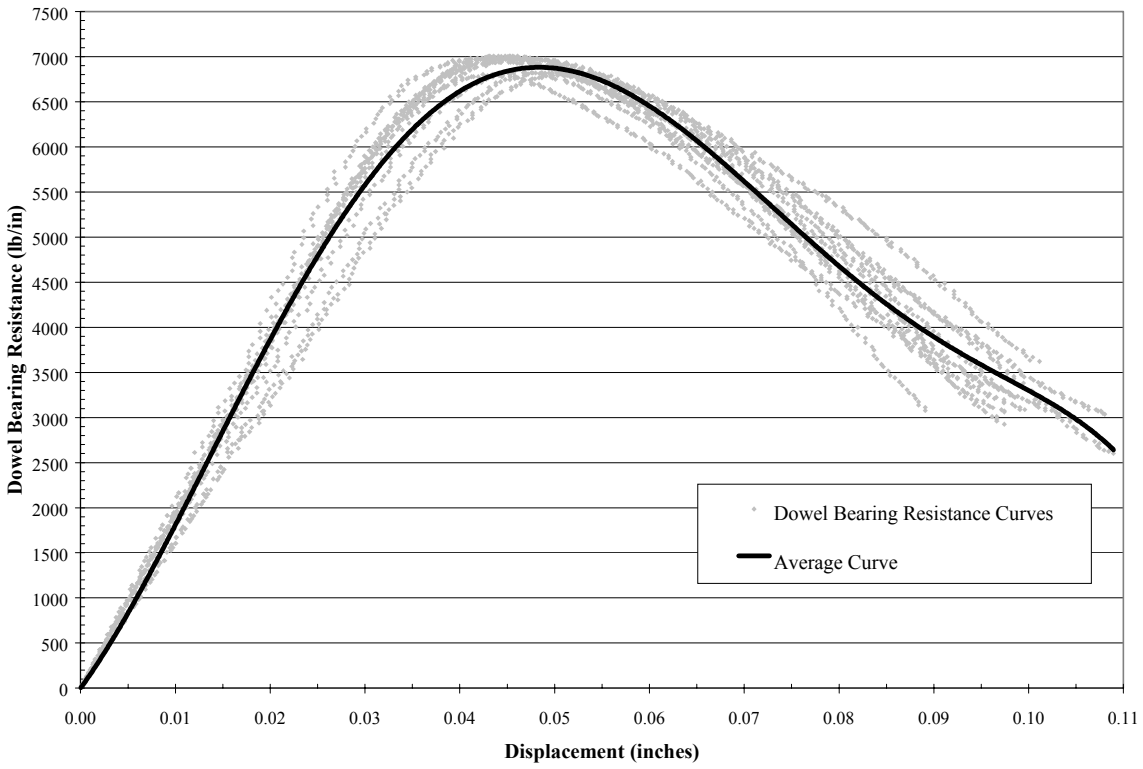

Bending Yield Strength Data

3/8" Diameter A307 Bolts							5% offset	Max Load
Sample	d1	d2	d3	ave dia	Max Load	Yield Load	Fyb	Fyb
1-1	0.371	0.374	0.373	0.373	861.52	744.04	86255.7	99875.0
1-2	0.370	0.371	0.370	0.370	841.94	734.25	86739.8	99461.7
1-3	0.371	0.371	0.371	0.371	832.15	724.46	85122.8	97776.1
1-4	0.371	0.371	0.370	0.371	837.47	742.19	87440.8	98666.0
1-5	0.372	0.371	0.372	0.372	849.40	748.20	87439.6	99266.5
1-6	0.371	0.371	0.371	0.371	845.60	746.80	87747.3	99356.1
1-7	0.371	0.371	0.371	0.371	899.90	748.20	87911.8	105736.2
1-8	0.372	0.371	0.372	0.372	860.40	754.10	88129.1	100552.0
1-9	0.372	0.370	0.371	0.371	841.60	747.10	87782.6	98886.1
2-1	0.372	0.371	0.372	0.372	851.73	744.04	86953.8	99539.2
2-2	0.371	0.372	0.373	0.372	861.52	744.04	86720.2	100412.9
2-3	0.370	0.371	0.370	0.370	890.89	734.25	86739.8	105244.3
2-4	0.370	0.371	0.371	0.371	861.50	764.30	90046.0	101497.6
2-5	0.371	0.372	0.371	0.371	852.30	754.10	88366.6	99873.9
2-6	0.370	0.371	0.370	0.370	849.10	747.40	88292.9	100307.1
2-7	0.370	0.371	0.370	0.370	827.60	734.50	86769.0	97767.2
2-8	0.370	0.371	0.370	0.370	842.10	746.00	88127.5	99480.2
3-1	0.370	0.370	0.370	0.370	900.68	734.25	86974.5	106688.7
3-2	0.370	0.371	0.371	0.371	910.47	744.04	87659.4	107267.5
3-3	0.372	0.370	0.370	0.371	832.15	734.25	86506.0	98040.2
3-5	0.370	0.371	0.370	0.370	833.30	738.30	87217.9	98440.6
3-7	0.371	0.371	0.371	0.371	845.60	751.10	88252.6	99356.1
3-8	0.370	0.371	0.370	0.370	897.20	745.00	88009.4	105989.3

overall average =	0.37091	inches	743.69	**87443.71**	**100846.98** psi
standard deviation =	0.000853		8.58	974.39	3026.71
COV =	0.23%		1.15%	1.11%	3.00%
			Min =	85122.8	97767.2
			Max =	90046.0	107267.5

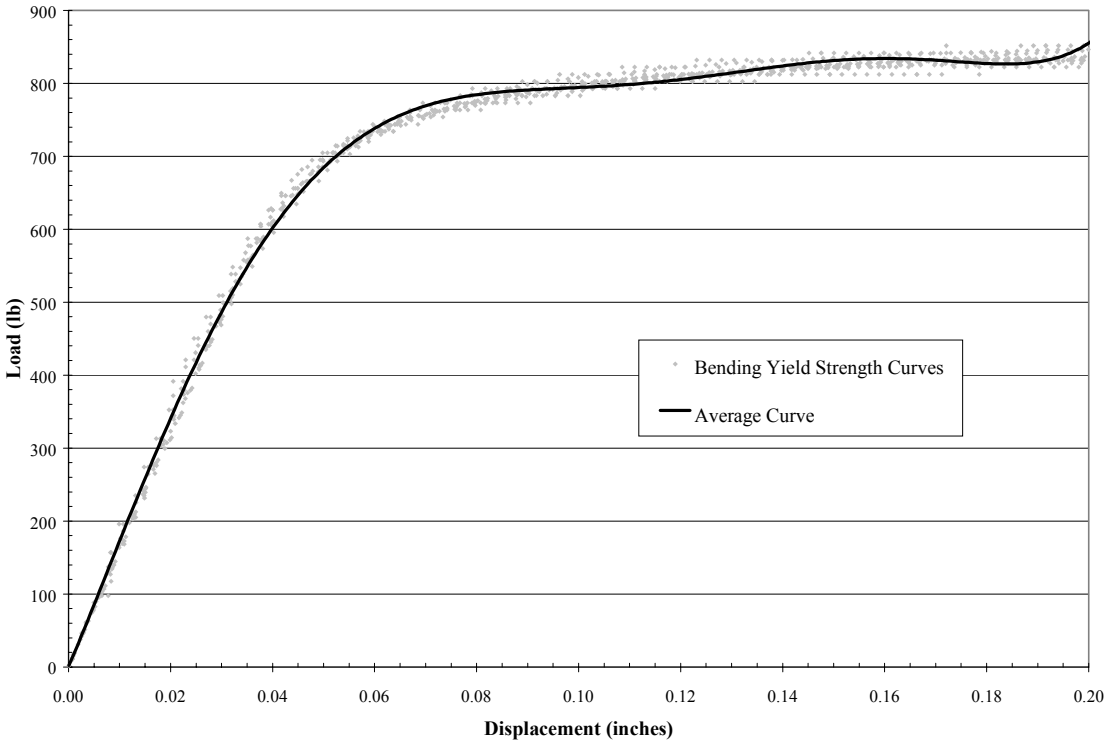
900
800
700
600
500
400
300
200
100
0
Load (lb)
0.00
0.02
0.04
0.06
0.08
0.10
0.12
0.14
0.16
0.18
0.20
Displacement (inches)
Bending Yield Strength Curves
Average Curve

1/4" bolts - Blank - 8" long							5% offset	Max Load
Sample	d1	d2	d3	ave dia	Max Load	Yield Load	Fyb	Fyb
b8-1	0.247	0.248	0.248	0.248	271.27	224.83	88799.5	107138.5
b8-2	0.247	0.247	0.247	0.247	261.49	215.06	85628.3	104116.2
b8-3	0.247	0.247	0.247	0.247	261.49	210.17	83682.2	104116.2
b8-4	0.246	0.247	0.247	0.247	261.49	215.06	85975.9	104538.9
b8-5	0.247	0.247	0.246	0.247	261.49	217.50	86952.9	104538.9
b8-6	0.247	0.247	0.247	0.247	270.00	218.40	86958.7	107503.9
b8-7	0.247	0.247	0.247	0.247	269.00	225.40	89745.8	107105.7
b8-8	0.247	0.246	0.247	0.247	259.90	215.40	86112.4	103902.5
b8-9	0.247	0.247	0.246	0.247	261.50	218.00	87151.8	104542.2
b8-10	0.247	0.247	0.247	0.247	263.60	224.30	89307.9	104955.6
b8-11	0.247	0.246	0.247	0.247	265.80	219.30	87671.5	106261.2
b8-12	0.246	0.247	0.247	0.247	262.80	210.60	84193.4	105061.9
b8-13	0.247	0.246	0.247	0.247	261.20	215.00	85952.5	104422.2
b8-14	0.246	0.246	0.247	0.246	263.70	221.00	88710.3	105850.2
b8-15	0.247	0.247	0.247	0.247	261.00	214.20	85286.4	103920.4

overall average =	0.24684	inches	217.61	**86808.63**	**105198.31** psi
standard deviation =	0.000475		4.73	1804.65	1250.92
COV =	0.19%		2.17%	2.08%	1.19%
			Min =	83682.2	103902.5
			Max =	89745.8	107503.9

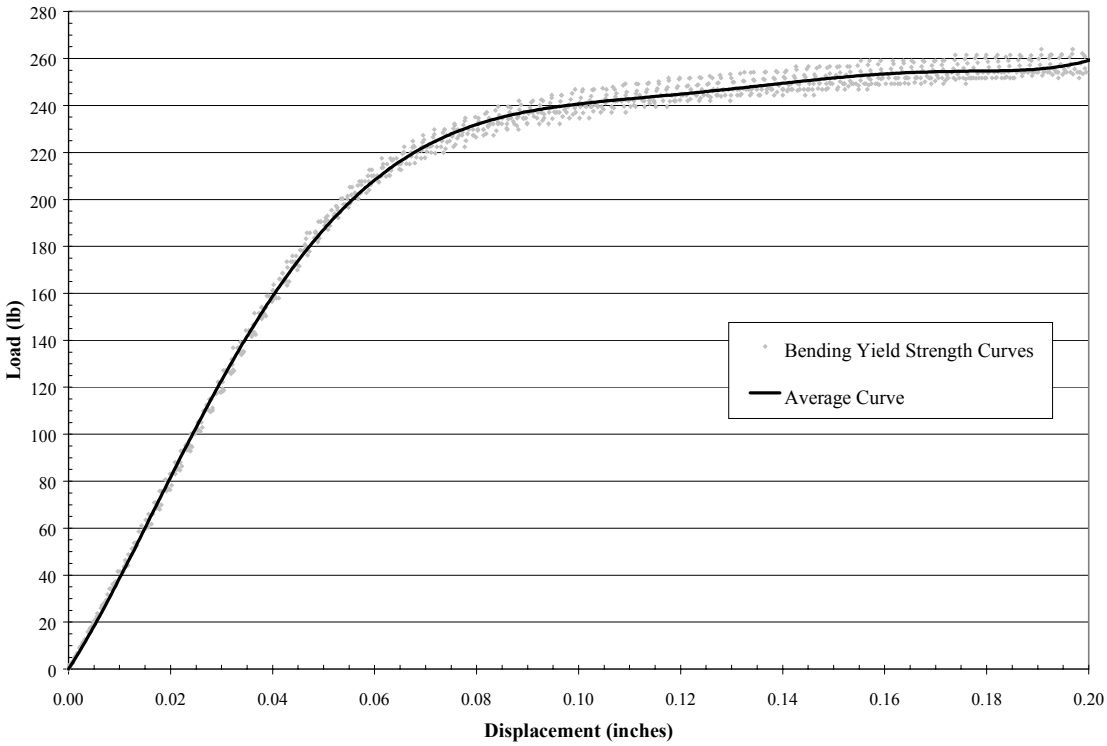

3/16" Diameter Rods							5% offset	Max Load
Sample	d1	d2	d3	ave dia	Max Load	Yield Load	Fyb	Fyb
2-1	0.186	0.187	0.186	0.186	83.09	63.54	58928.7	77060.6
2-2	0.187	0.186	0.186	0.186	83.09	61.10	56662.2	77060.6
2-3	0.186	0.187	0.187	0.187	83.27	60.13	55468.0	76813.8
2-4	0.186	0.186	0.186	0.186	85.69	62.93	58677.3	79899.2
4-1	0.186	0.186	0.186	0.186	83.92	61.21	57073.5	78248.8
4-2	0.186	0.187	0.187	0.187	85.42	63.25	58346.1	78797.1
4-3	0.186	0.186	0.186	0.186	84.08	61.69	57521.1	78398.0
4-4	0.186	0.186	0.186	0.186	83.70	60.13	56066.5	78043.7
5-1	0.186	0.186	0.186	0.186	81.02	54.12	50462.7	75544.8
5-2	0.186	0.187	0.187	0.187	81.07	56.05	51704.3	74784.4
5-3	0.186	0.186	0.186	0.186	80.91	52.24	48709.7	75442.2
5-4	0.186	0.186	0.186	0.186	79.84	51.76	48262.2	74444.6
6-1	0.186	0.186	0.186	0.186	81.77	62.23	58024.6	76244.1
6-2	0.186	0.187	0.187	0.187	83.60	64.05	59084.0	77118.3
6-3	0.186	0.186	0.186	0.186	84.03	64.59	60225.1	78351.4
6-4	0.186	0.186	0.186	0.186	84.08	64.43	60075.9	78398.0
9-1	0.186	0.186	0.186	0.186	81.50	58.63	54667.9	75992.4
9-2	0.186	0.187	0.187	0.187	83.81	62.17	57349.8	77312.0
9-3	0.186	0.186	0.186	0.186	82.74	59.44	55423.2	77148.6
9-4	0.186	0.186	0.186	0.186	82.58	58.15	54220.3	76999.4
overall average =		0.18620	inches			60.09	**55847.65**	**77105.11** psi
standard deviation =		0.0004034				3.89	3570.98	1405.70
COV =		0.22%				6.48%	6.39%	1.82%
					Min =		48262.2	74444.6
					Max =		60225.1	79899.2

Sample	5% Offset			Max Load		
	Average Fyb	Std Dev	COV	Average Fyb	Std Dev	COV
2-1	57361.9	1657.4	2.89%	77708.6	1465.1	1.89%
2-2						
2-3						
2-4						
4-1	57251.8	949.8	1.66%	78371.9	318.5	0.41%
4-2						
4-3						
4-4						
5-1	49784.7	1593.5	3.20%	75054.0	527.8	0.70%
5-2						
5-3						
5-4						
6-1	59352.4	1019.8	1.72%	77528.0	1041.0	1.34%
6-2						
6-3						
6-4						
9-1	55415.3	1381.9	2.49%	76863.1	594.3	0.77%
9-2						
9-3						
9-4						

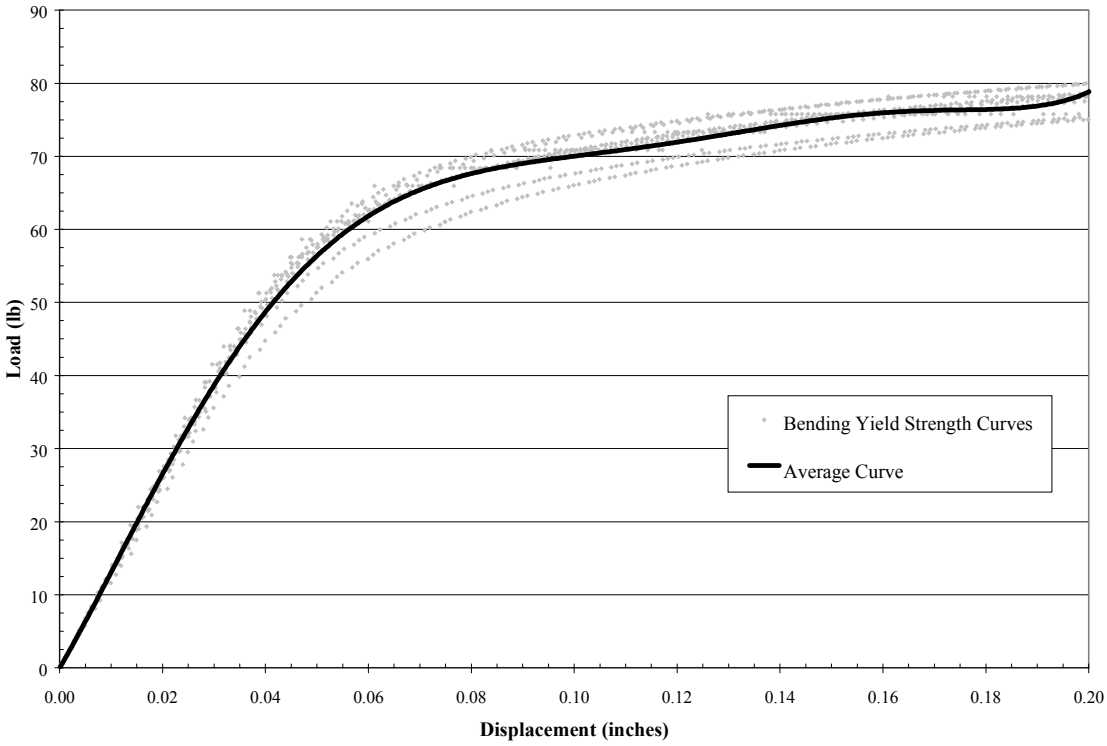
90
80
70
60
50
40
30
20
10
0
Load (lb)
0.00
0.02
0.04
0.06
0.08
0.10
0.12
0.14
0.16
0.18
0.20
Displacement (inches)
Bending Yield Strength Curves
Average Curve

Connection Test Data

HDPE - Mode Im

sample	Intersection Load	Yield Load	Max Load
17-6-17	666.7	666.7	679.0
23-6-23	647.1	647.1	666.7
11-7-11	634.9	634.9	652.0
25-5-25	674.1	674.1	679.0
	average =	655.7	669.2
	standard deviation =	17.94584446	12.83442636
	COV =	2.7%	1.9%
	min	634.90	652.00
	max	674.10	679.00

PVC - Mode Im

Sample	Intersection Load	Yield Load	Max Load
1-7-1	1991.7	1991.7	1994.2
2-5-2	2030.8	2055.3	2055.3
9-7-9	2038.2	2038.2	2055.3
18-4-18	1881.8	1881.8	1884.2
	average =	1991.8	1997.3
	standard deviation =	78.07092929	80.7
	COV =	3.9%	4.0%
	min	1881.80	1884.20
	max	2055.30	2055.30

HDPE - Mode IIIs

sample	Intersection Load	Yield Load	Max Load
9-2-9	520.5	520.5	640.3
12-5-12	508.3	508.3	652.5
14-6-14	493.7	493.7	628.1
10-4-10	501.0	501.0	652.5
8-3-8	505.9	505.9	633.0
11-4-11	515.7	515.7	637.8
16-7-16	503.4	503.4	618.3
17-7-17	505.9	505.9	635.4
15-6-15	481.4	481.4	620.7
	average =	504.0	635.4
	standard deviation =	11.52	12.16
	COV =	2.3%	1.9%
	min =	481.40	618.30
	max =	520.50	652.50

PVC - Mode IIIs

sample	Max Load	Intersection Load	Yield Load
18-17-18	2363.2	2292.3	2292.3
17-15-17	2412.1	2397.4	2412.1
15-11-15	2380.3	2338.8	2338.8
19-13-19	2404.7	2177.5	2177.5
16-11-16	2453.6	2448.7	2448.7
11-12-11	2333.9	2331.4	2333.9
14-13-14	2358.3	2351.0	2358.3
10-14-10	2485.4	2485.4	2485.4
12-14-12	2368.1	2282.6	2282.6
13-12-13	2385.2	2170.1	2170.1
average =	2394.5	2327.5	2330.0
standard deviation =	46.0880751	103.1357337	104.544037
COV =	1.9%	4.4%	4.5%
min =	2333.90	2170.10	2170.10
max =	2485.40	2485.40	2485.40

HDPE - Mode IV

sample	Intersection Load	Yield Load	Max Load
11-12-11	615.8	615.8	862.7
13-12-13	620.7	620.7	862.7
10-9-10	606.1	606.1	870.0
8-9-8	601.2	601.2	865.1
14-15-14	620.7	620.7	879.8
16-15-16	640.3	640.3	877.3
23-19-22	637.8	637.8	833.4
26-27-25	637.8	637.8	874.9
21-20-21	593.9	593.9	860.2
18-17-18	593.9	593.9	852.9
	average =	616.8	863.9
	standard deviation =	17.9	13.6
	COV =	2.9%	1.6%
	min =	593.90	833.40
	max =	640.30	879.80

sample	Rod Type	5% offset			Max Load Based		
		ave	stdev	cov	ave	stdev	cov
11-12-11 13-12-13	6	618.3	3.5	0.6%	862.7	0.0	0.0%
10-9-10 8-9-8	5	603.7	3.5	0.6%	867.6	3.5	0.4%
14-15-14 16-15-16	2	630.5	13.9	2.2%	878.6	1.8	0.2%
23-19-22 26-27-25	9	637.8	0.0	0.0%	854.2	29.3	3.4%
21-20-21 18-17-18	4	593.9	0.0	0.0%	856.6	5.2	0.6%

PVC - Mode IV

sample	Max Load	Intersection Load	Yield Load
24-25-24	2874.0	2610.0	2610.0
7-6-7	2764.0	2519.6	2519.6
26-25-26	2959.5	2614.9	2614.9
23-22-23	2930.2	2673.6	2673.6
21-22-21	2842.2	2548.9	2548.9
4-3-4	2952.2	2651.6	2651.6
2-3-2	2771.3	2502.5	2502.5
20-18-20	2837.3	2514.7	2514.7
19-17-19	2820.2	2561.2	2561.2
5-6-5	2832.4	2504.9	2504.9
average =	2858.3	2570.2	2570.2
standard deviation =	69.7	63.2	63.2
COV =	2.4%	2.5%	2.5%
min =	2764.00	2502.50	2502.50
max =	2959.50	2673.60	2673.60